MASTER

Fatigue in adhesively bonded aluminium joints

experimental and numerical research on adhesively bonded aluminum lap and tubular joints

Strik, Jaap H.A.

Award date:
2005

Artikel voor afstudeer syllabus

Titel:
Voorspellingsmodellen voor de vermoeiingslevensduur van gelijmde aluminium verbindingen

Afstudeerder:
J.H.A. Strik
S448826

Afstudeerrichting:
Constructief Ontwerpen

Afstudeercommissie:
Prof ir Frans Soetens (TNO Bouw/TUE)
Ir Dianne van Hove (TNO Bouw/TUE)
Dr ir IJsbrand van Straalen (TNO Bouw)

Zitting examencommissie:
26 april 2005

Het voorspellingsmodel dat hier onderzocht is combineert materiaal afhankelijke en geometrie afhankelijke informatie in een rekenmodel voor een gelijmde aluminium verbinding, belast met een cyclische belasting. Met het rekenmodel kan een levensduur voorspelling worden gemaakt. Het betreft een fundamenteel onderzoek naar het scheuren van gelijmde verbindingen onder een wisselende belasting. Hierbij wordt experimenteel scheurgroei onderzoek gecombineerd met eindige elementen onderzoek. Met dit rekenmodel kan een ondergrens voorspelling worden gedaan over de vermoeiingslevensduur van gelijmde aluminium verbindingen. De berekende voorspellingen zijn vervolgens experimenteel gevalideerd.

Trefwoorden:
Vermoeiing; aluminium; lijmen; voorspellingsmodel; breukmechanica

Voorspellingsmodellen voor de vermoeiingslevensduur van gelijmde aluminium verbindingen

Inleiding

Wanneer gelijmde verbindingen worden toegepaste in constructies als primaire verbindingstechniek, dan is één van de vragen die gesteld wordt: Hoe lang gaat de verbinding mee? Duurzaamheid is een belangrijk aandachtspunt binnen lijm technologie. Echt interessant wordt het wanneer het duurzaamheids aspect wordt gecombineerd met de constructieve mogelijkheden van gelijmde verbindingen. Eén van de aspecten van het constructieve gedrag en duurzaamheid is vermoeiing. Vermoeiing is het bezwijken door inscheuring onder een cyclische belasting, waarbij de maximale nominale spanning in het betreffende bouwdeel in een cyclus onder de vloeigrens van het materiaal blijft. In verband met constructieve veiligheid is het belangrijk te weten na hoeveel wisselingen een constructie niet meer veilig is en wanneer men controles naar eventuele vermoeiingsscheuren dient uit te voeren.

Voorspellingsmodellen

Om een uitspraak te kunnen doen over de vermoeiingslevensduur, kan een voorspellingsmodel gebaseerd op breukmechanica uitkomst bieden. Het maken van het vermoeiingsmodel en de experimentele validatie is het hoofdonderwerp van mijn afstudeerwerk. Dit voorspellingsmodel is onder te verdelen in drie delen (figuur 1): een rekenmodel, scheurgroei informatie wat betreft de geometrie en scheurgroei informatie wat betreft materialen. Het experimenteel valideren van de gemaakte voorspellingen is het vierde deel voor het model.

Geometrie

Onderwerp voor de voorspellingsmodellen zijn twee soorten geometriën, namelijk een dubbele overlap verbinding en een buisverbinding. De dubbele overlap verbinding is uitgevoerd met twee verschillende lijmen, namelijk een één component MS polymer en een twee componenten epoxy (respectievelijk figuur 2a en 2b) . De MS polymer is een erg flexibele en taaie lijm, die eigenlijk het midden houdt tussen een lijm en een kit. De epoxy is een vrij stijve, sterke lijm. De gelijmde buisverbinding is slechts uitgevoerd in epoxy (figuur 2c). Alledrie de gelijmde verbindingen zullen bekeken worden voor twee belastingsgevallen. De belastingsgevallen worden gekenmerkt door de verhouding tussen de minimale en de maximale belasting binnen één belastingscyclus, R. De twee gevallen die bekeken zullen worden zijn R=0.1 en R=0.5. Vooraf is een aangenomen dat de lijmnaden vanaf beiden kanten tegelijk in zullen scheuren. Verwacht wordt dat de scheur over de hele breedte of over de hele omtrek gelijkmatig in zal scheuren.
Voor elke van de drie gelijmde verbindingen is een scheurgroeicurve ontwikkeld met behulp van het eindige elementenpakket DIANA 8.2. Per scheur zijn een aantal berekeningen gemaakt, waarbij de scheurdiepte steeds toenam. Hierbij is de energy release rate G een belangrijke parameter. De energy release rate is een grootheid die voortkomt uit de breukmechanica en geeft aan hoeveel energie er vrijkomt per lengte eenheid bij de groei van een scheur. Vervolgens is er met behulp van een curve fitting programma een wiskundige vergelijking afgeleid voor het verband tussen de scheurdiepte en de energy release rate. Deze wiskundige uitdrukking is de ene helft van de invoer voor het rekenmodel.

Materiaal

De andere helft van het scheurgroeimodel is de scheurgroei data van de twee gebruikte lijmen. De scheurgroei data wordt verzameld met behulp van een speciaal proefstuk, het zogenaamde double cantilever beam (DCB) proefstuk. Dit proefstuk bestaat uit twee strips die op elkaar gelijmd worden. In de lijmlaag tussen de strips wordt een stukje folie aangebracht. Nadat de lijm is uitgehard, wordt het proefstuk uit elkaar getrokken onder een cyclische belasting. Vervolgens is de verwachting dat de lijmnaad in zal scheuren. De snelheid van het inscheuren hangt af van de scheurdiepte en van het niveau van de belasting. Door middel van het opmeten van de verplaatsingen aan de uiteinden van het proefstuk aan de kant waar het ook belast wordt, kan met behulp van een simulatie in DIANA berekend worden hoe diep de scheur is en hoeveel energie er vrij komt. Aan de hand van de resultaten van dit experiment kan een scheurgroei curve worden bepaald. Wanneer alle gegevens worden gecombineerd in het rekenmodel kan er een voorspelling worden gedaan. Eén van de aandachtspunten bij deze manier van voorspellen is de wijze waarop de scheurtip belast wordt. Er kunnen namelijk drie soorten van belasting onderscheiden worden, namelijk mode I trek, mode II afschuiving en mode III verscheuring uit het vlak. Over het algemeen wordt aangenomen dat trek de meest ernstige vorm van belasting is voor een scheurtip. De scheurgroei data die gevonden is met behulp van het DCB proefstuk is informatie over mode I In de onderzochte geometriën zal echter een combinatie optreden tussen trek en afschuiving, mode I en mode II plaatsvinden. De gemaakte voorspellingen zullen daarom onder waarde voorspellingen zijn van de levensduur. Gedurende de scheurgroei proeven gedroeg de epoxy zich volgens de gedane aannames en vertoonde een regelmatig scheurgroei patroon. De MS polymer daarentegen gedroeg zich onregelmatig.

Conclusies

Op basis van het onderzoek en de validatie kunnen vervolgens conclusies worden getrokken betreft de drie stappen in het voorspellingsmodel.

Wat betreft het verzamelen en verwerken van de informatie over de scheurgroei in de geometriën, kan gesteld worden dat met gebruik van breukmechanica in een eindige elementen pakket een goed beeld gevormd kan worden van het scheurgroei gedrag van zowel de dubbele overlap verbinding in epoxy en MS polymer als de buisverbinding in epoxy.

Ten aanzien van het verzamelen van het verzamelen van scheurgroei informatie van een lijmsoort met behulp van het DCB proefstuk kan worden geconcludeerd dat het mogelijk is redelijk nauwkeurige scheurgroei gegevens te verzamelen, indien de onderzochte lijm een regelmatig scheurgroei gedrag vertoont, wat nauwkeurig te simuleren is in een eindige elementen pakket.

Aangaande de voorspellingen kan gesteld worden dat indien nauwkeurige scheurgroei informatie over de lijm verzameld kan worden onder belastingsmode I, er met deze informatie onderwaarde voorspellingen gedaan kunnen worden betreft de levensduur.

Met de verzamelde informatie kan er vervolgens voor elke willekeurige geometrie met dezelfde lijm en vergelijkbare belastingsmode een levensduurvoorspelling gedaan worden, nadat met behulp van een eindige elementen pakket het scheurgroei gedrag gesimuleerd is.

General overview of literature survey on fatigue behaviour

Jaap Strik

February 2004

Preliminary report A
A 2005-13
O 2005-09

1 Introduction

This report is resuming an exploring literature survey on the general aspects of fatigue in metallic joints. It is concerned with the first exploration of the literature on fatigue in (mainly) steel joints and it serves as an introduction of the author's graduation project on fatigue in *aluminium* joints. Although steel and aluminium have different mechanical material properties, the theories and models of the fatigue failure of steel and aluminium connections share the same basics. Because the research and the literature on the fatigue behaviour of steel connections is much more extensive, the kick off of the graduation project will start with fatigue failure of steel joints, in order to obtain a broad view on and some fundamental understanding of the phenomenon fatigue. The next step in this report is a further focus on the fatigue behaviour of aluminium.

First of all, the definition of fatigue failure: the failure of a structural member under cyclic loading that is significantly lower than the static strength of the joint. From a statically design point of view, the failure of this particular part of the structure is totally unexpected, since the stresses under which fatigue failure occur can be really far below the yield stress, especially when a really large number of stress changes have taken place. In this report, the causes of this failure mechanism and the most important aspects of fatigue will be regarded shortly.

At first, the material phenomenon fatigue will be considered in Chapter 2, both crack initiation and crack growth will be considered. Then, three important factors in fatigue engineering will be regarded, stress concentration, stress intensity and the influence of notches. Finally, the high and low cycle fatigue are regarded. In chapter 3, load spectra are categorised and methods to describe the load spectrum are considered. In chapter 5 an important damage prediction tool is described namely the Miner rule. This prediction tool is based on an *empirical* model of fatigue failure. In Chapter 6, an *analytica*l model of crack growth and failure is considered. In Chapter 7, 8and 9 three types of frequently used connection techniques in engineering and their specific fatigue aspects are considered, respectively welded, bolted and adhesive connections.

As pointed out before, this report will be used as an introduction of a graduation project on fatigue, which objective still has to be determined. The purpose of this report is to get a broad scope on the engineering of fatigue failure. Later on in the project, when the final object has been described more precisely, a more specific report will be the follow-up.

The literature used for this report is general oriented literature on fatigue. As the knowledge which has been subtracted is not very specific, the sources are not specifically mentioned. The works which have been used are:

- 'Fatigue of structures and materials' – J.Schijve, 2001
- 'Fatigue strength of welded structures' – S.J.Maddox, 1991
- 'Ontwerp en berekening van op vermoeiing belaste staalconstructies' – J.de Back, 1987
- 'Computational fracture mechanics in the Netherlands'- CIAD project group fracture mechanics, 1986

2 Fatigue as a material phenomenon

2.1 Introduction

If a specimen is subjected to a cyclic load a crack can be nucleated on or near the material surface. This nucleus of the fatigue crack is on a microscopically small scale. Dependent on the circumstances, this micro crack can propagate into the material and grow to a macroscopic scale. Finally, the crack can result in failure of the specimen. Each load cycle can cause damage to the material.

To understand the fatigue mechanism well, both the initiation and the growth of crack period of fatigue have to be evaluated. The fatigue life of a specimen or a structure is usually divided into two periods: the crack initiation period and the crack growth period. These two periods are considered separately because the conditions that largely influence the one period do not or hardly influence the other period. The initiation period again can be split into cyclic slip, crack nucleation and micro crack growth. The crack initiation will be discussed in section 2.2, followed by the crack growth period in section 2.3, which eventually can lead to fatigue failure. The fatigue life cycle is presented in figure 1.

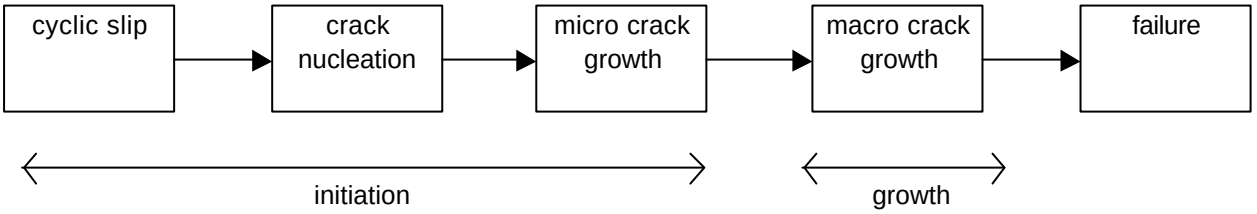

Figure 1: the stages of the fatigue life cycle

2.2 Crack initiation

2.2.1 Crystallographic aspects

The nucleation of fatigue cracks is a consequence of cyclic slip in slip bands. Cyclic slip is the result of very local cyclic plastic deformation. The nucleation occurs on a micro scale, only a small number of grains is included. The plastic behaviour of the grains will occur more easily near the surface, where the material is border on only one side. Shear stress is required to initiate cyclic slip. On a microscopic level, stresses are not distributed homogeneously throughout the material, the shear stresses between the planes of the grains differ from grain to grain depending on shape, crystallographic orientation, size and elastic anisotropy. This shear stress can exceed the yield stress and hence plastic deformation

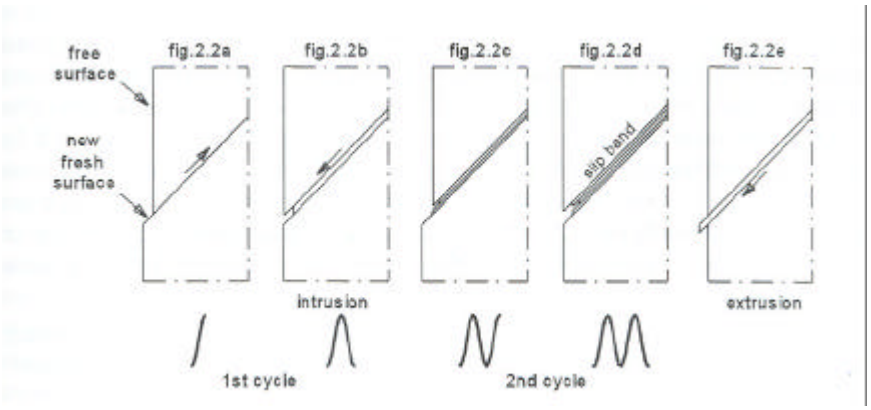

Figure 2: schematic representation of cyclic slip during the first load steps

can occur. The nucleation of cyclic slip is schematically represented in figure 2.

The first slip step will be created and a micro intrusion will occur at the material surface. The surface of this intrusion is immediately covered with an oxide layer and strain hardening will have taken place. Due to this change of the material at the surface of this slip step, the inclusion is irreversible and another cyclic slip will take place on the same band, when the load changes. The next slips will all appear parallel at slip band adjacent to the first one. Decohesion of the material is now a fact and after more loading cycles the crack can grow into the material, if the cyclic load is high enough. If the load is not sufficient, then equilibrium will be established. It has to be stated that crack initiation is a material *surface* phenomenon.

The initiation depends on the crystallographic material characteristics, such as variation of crystal orientation, slip systems, cross slipping, grain size and shape.

Beside crack nucleation caused by high local shear stresses, cracks can also be initiated by inclusions of microscopic size. Macroscopic inclusions are regarded as material defects and should not occur at all. These micro inclusions can affect the stress distribution on a micro-level and hence contribute to crack nucleation at the surface, especially in case of high strength steel. Also, when inclusions are present near the surface, a crack can start in the subsurface and break through to the surface.

The initiation period is supposed to be completed when the micro-crack growth is not longer depending on the conditions of the free surface. The crack initiation of *unnotched* specimen shows very low growth rates.

2.2.2 Surface effects

As stated in section 2.2.1, crack initiation is a surface phenomenon. Various kinds of surface conditions can influence the crack initiation. Examples of surface effects:

- Surface roughness
- Surface damage
  - Scratches
  - Dents
  - Fretting
- Surface treatments
  - Anodising
  - Nitriding
  - Shot peening
  - Machining
  - Spot heating
- Soft Layers
  - Cladding
  - Decarburising
- Environmental effects
  - Pitting

If the surface is not perfectly flat, small stress concentrations can occur. Although these concentrations do not reach to a great depth, they still are able to improve the conditions of crack nucleation. These surface effects only reduce the resistance against initiation and hardly effect the propagation resistance.

In case of a short life (small number of load cycles), initial surface damage can be less important because the high amplitude stresses will generate a crack easily, although the initial damage will accelerate the fatigue failure. Contrary to the long life and lower amplitude stresses, that need a large number of cycles to initiate cracks.

2.3 Crack growth

2.3.1 Crack propagation and striations

The crack growth period starts when the initial crack has past a sufficient amount of grains. The crack growth has become a more or less continuous process. The rate of the crack propagation depends no longer on the surface properties, but on the bulk properties of the material. Usually the crack grows perpendicular to the direction of the main principle stress.

The slip deformations will take place on more than one slip plane. The crack growth mechanism is schematically represented in figure 3. During loading the crack will be opened and some crack extension will occur, during unloading the crack tip will be sharpened. Hence, when the next loading cycle starts, the blunting of crack tip and crack extension will take place. The slip deformation at the crack tip is not reversible due to strain hardening, therefore the crack will not be closed at the minimum loading. Due to the loading and unloading, the slip step surface of the propagating crack will have a very fine texture of small ridges. Every crack extension will generate a ridge, a so-called striation. An example of the fine texture of the striations is given in figure 4. After fatigue failure these striation, visible with an electron microscope can provide information about the crack growth. The size of the each crack extension, i.e. the increment of the fatigue damage, depends on the amplitude of the load cycle. A quantitative approach of crack growth in a specimen will be considered in Chapter 6

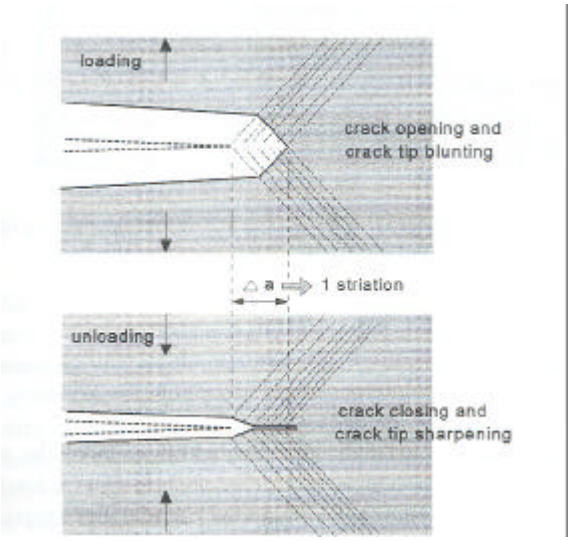

Figure 3: crack propagation mechanism during loading and unloading

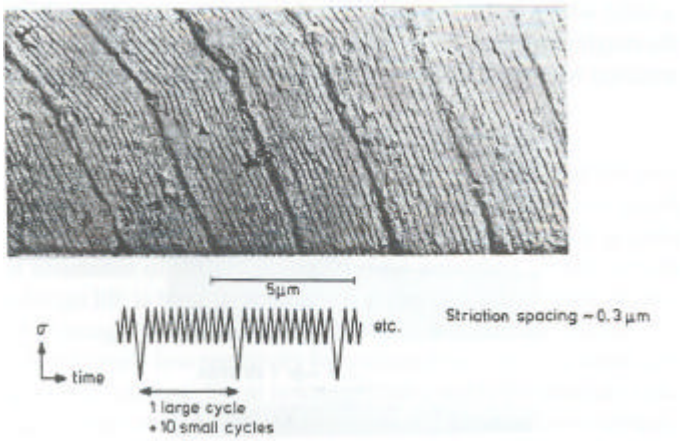

Figure 4: observation of the striation pattern through an electro n microscope.

2.3.2 Environmental aspects

Environmental conditions can cause the corrosion of metallic building materials. In case of statically loaded structures this means a reduction of the applicable section. In case of fatigue, interaction between the corrosion and the fatigue mechanism will occur, especially at the location of peak stresses. Therefore corrosion will have a negative influence on the fatigue resistance. It should be remembered that every time a crack is extended, a very thin layer of oxidation will is established on the fresh crack. Therefore, some researchers say all fatigue is corrosion related. However, in general only corrosion in a largely corrosive environment is regarded as corrosion-fatigue.

Corrosion-fatigue is not just the sum of corrosion and fatigue, interaction between the two systems will occur. Corrosion pits can be the location of the micro initiation. When fatigue cracks propagate, corrosion will increase the crack growth rate.

Also, in a strong corrosive environment, there seems to be no lower value for the stress range, initiating the fatigue mechanism, so even very low cyclic stresses can trigger the process. Also, the frequency of the cyclic load affects the corrosion fatigue, different rates for crack propagation were found for different frequencies, both in corrosive as in non-corrosive environments. This proves that fatigue is a time dependent phenomenon.

2.4 Stress concentration

2.4.1 Definition Kt

In many structures holes and notches are inevitable. These holes and notches cause an inhomogeneous stress distribution in the structure material. Especially near the root of the notches there will be a significant stress concentration.

The relation between the nominal stress in the specimen (figure 5) and the stress peaks at the notch root is expressed in the stress concentration factor K_t:

$$K_t = \frac{s_{peak}}{s_{nominal}}$$

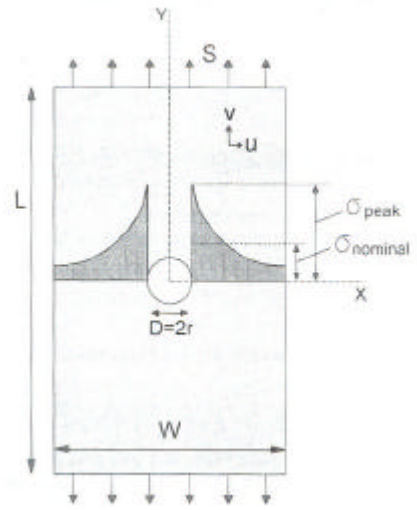

Figure 5: stress concentration near a circular hole

The stress concentration factor is the result of elastic analysis of the stress concentration around the discontinuities in specimen and structures. K_t can be determined analytically for an elliptical hole in an infinite sheet. Other geometries cannot be determined analytically, a numerical approach has to be used. For the elliptical hole in the infinite sheet, the peak stresses and the stress concentration factor are respectively:

$$s_{peak} = S(1+2\frac{a}{b}) = S(1+2\sqrt{\frac{a}{r}})$$

$$K_t = 1+2\frac{a}{b} = 1+2\sqrt{\frac{a}{r}}$$

in which:
S is the nominal stress
a is the length of half the crack
b is the height of half the crack and
ρ is the radius of the root of the notch

Beside the stress peaks near the notch in a specimen, the stress gradient can be of interest as well. In some prediction models these gradients are included. For an elliptical hole in an infinite sheet (figure) the exact solution of σ_y can be computed with:

$$\frac{(s_y)_{y=o}}{S} = 1+\frac{a(a-2b)(x-\sqrt{x^2-c^2})(x^2-c^2)+ab^2(a-b)x}{(a-b)^2(x^2-c^2)\sqrt{x^2-c^2}}$$

in which
$c= \sqrt{(a^2+b^2)}$

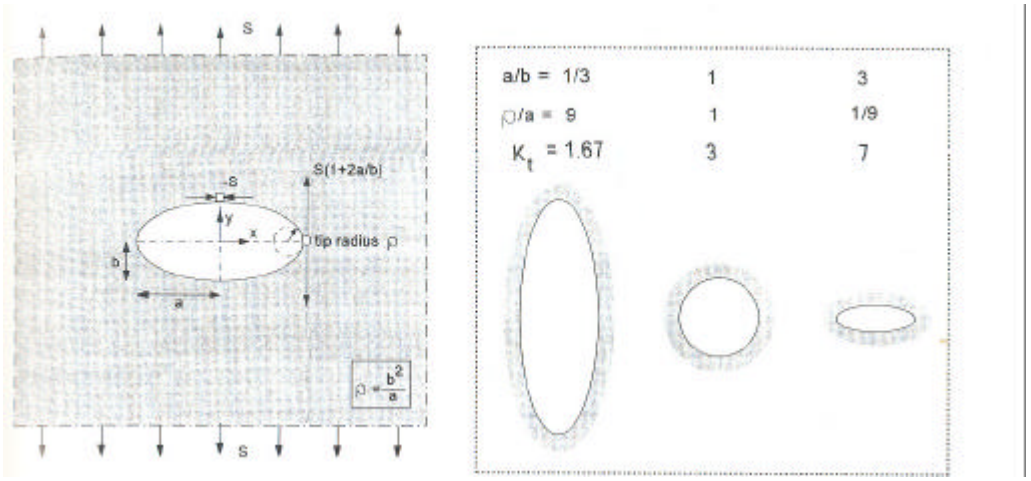

The stress gradient at the root of the notch can be calculated by differentiation of the function above, combined with the expression of K_t:

$$\left(\frac{ds_y}{dx}\right)_{x=a} = -\left(2+\frac{1}{K_t}\right)\frac{s_{peak}}{r} = -a\frac{s_{peak}}{r}$$

so the gradient is linear proportional related to the peak stress.

The stress peak drops off quite fast when the gradient is calculated in the area around the crack tip, along the x-axis. The stress gradient of a circular hole is given in figure 6. In the loading direction, along the height of the hole, the stress drops decrease much slower. So along the edge of the hole there is a high stress peak over a rather large part of the edge. It should be noted that in the initial phase, fatigue is a material surface phenomenon. Hence, it can be concluded that the stress gradient along side the hole's edge is more important than the gradient perpendicular on the loading direction,

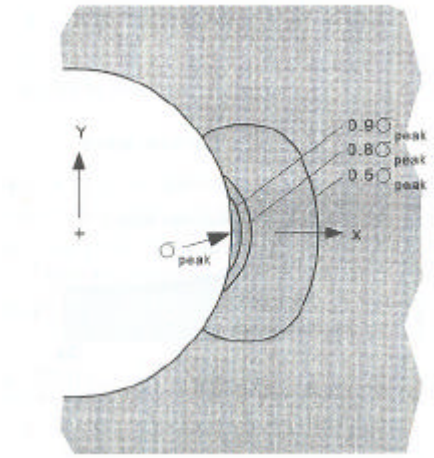

Figure 6: stress gradient at the edge of a circular hole

starting from the notch root. This also points out that the surface quality of the material near a hole is of great importance.

The calculated relations above are obtained for an infinite sheet with an elliptical hole, but more results in literature confirm the same trends with respect to stress gradients with similar notches and the notch radii, which are a point of interest from engineering point of view.

2.4.2 Geometry aspects

As can be seen in the formulae of section 2.4.1, the radius of the root of the discontinuity plays a very important role on the stress distribution near this discontinuity. Therefore, holes with small radii should be avoided in parts of structures designed to resist fatigue failure.

K_t is a dimensionless ratio, it is a scale factor between nominal stresses and peak stresses. Scale effects on the holes do not influence the values of K_t , however larger notches have larger high stress surfaces, which is a significant influence for the size effect of fatigue. A large area is more likely to have a small notch and thus an initiation location. However, accounting the size effect of a specimen in a calculation is not possible in a rational way, it can only be understood in a qualitative way..

2.5 Stress intensity

2.5.1 Introduction

In this section, some of the main characteristics of the crack tip stress and strain behaviour are given. The main stresses and strain characteristics are:

- Stress intensity factor K
- J integral
- Crack tip displacements
- Energy release rate

Next, the plastic stress and strain near the crack tip are regarded. The stress and strain near the crack tip are severe and require some extra attention.

2.5.2 Definition K

In Section 2.4, the stressconcentration factor K_t has been introduced to calculate the severe stresses at the root of a notch. K_t was dependent on the reciprocal value of the square root of the notch root radius. A crack is a notch with a root radius of zero. With the K_t approach, the value of the stress would become infinite, which does not make sense physically. An other concept to calculate the stress near the crack is required.

In an infinite sheet with a crack (figure 7), the stresses s_x s_y and t_{xy} can be calculated with

$$s_x = \frac{S\sqrt{pa}}{\sqrt{2pr}}\cos\frac{J}{2}\left(1-\sin\frac{J}{2}\sin\frac{3J}{2}\right)-S$$

$$s_y = \frac{S\sqrt{pa}}{\sqrt{2pr}}\cos\frac{J}{2}\left(1+\sin\frac{J}{2}\sin\frac{3J}{2}\right)$$

$$t_{xy} = \frac{S\sqrt{pa}}{\sqrt{2pr}}\cos\frac{J}{2}\left(\sin\frac{J}{2}\cos\frac{3J}{2}\right)$$

These formulae can be rewritten as

$$s_{i;j} = \frac{K}{\sqrt{2pr}} f_{i;j}(J)$$

$$K = S\sqrt{pa}$$

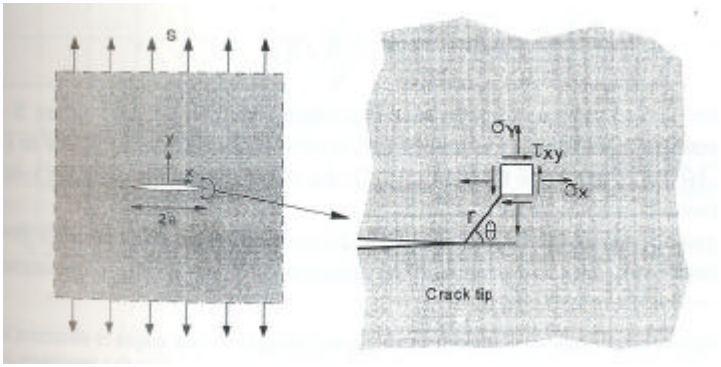

Figure 7: central crack in an infinite sheet

The formulae above can be used *around* the crack tip, where r<<a. Also, if r=0 is used, the stresses will become infinite. However, the whole theory is based on elasticity. If only a small area around the around the crack tip will be exposed to plastic strain, the theory will be sufficient. Also, if the radius is huge, the calculated stresses will approach zero, where the nominal stress should be expected. Again, it should be noted that the theory with the *elastic* concept K is only applicable around the crack tip, where r<<a.

The above formulae can be used for one crack in an infinite sheet. To be able to use the formula on other geometries, a geometry correction factor ß is introduced. ß is a dimensionless factor to account the geometry and the load influences on the stresses. K represents the severity of the stress near the crack tip of a central crack in an infinite sheet.

$$K = S\sqrt{pa}$$

However, K is not similar to K_t on a micro level. K_t is a dimensionless factor, in contrary to K. K_t only accounts the geometry of the specimen, where as K accounts both the geometry and the loads. K is an important parameter factor in the elastic fracture mechanics. In literature, a number of values for ß are published for an enormous variety in geometry.

If it is assumed that the stress field near the crack tip is responsible for the fatigue failure behaviour, it follows that the fatigue failure is directly related to K. Similar cyclic conditions applied to fatigue cracks in different specimens or structures of the same material should have similar consequences, i.e. similar crack extensions per cycle. This principle is known as the similarity concept, also referred to as the similitude principle. When we assume that the stress field near the crack tip is determined for the fatigue failure mechanism of the specimen, a critical stress field or a critical K (K_c) could be indicated. This value K_c would be a material dependent value for the stress field. K_c could be gained by experiments. However, K_c is not strictly material related, it is affected by temperature and the stress situation (plane stress or plane strain) as well.

The effect of K on the extension of a crack depends on the material properties; at a certain K in a material certain crack propagation will occur, largely based on which kind of material is used. However, also the surrounding structure will affect the extension of the crack. In case of a thin specimen, there will be a plane stress situation near the crack tip. In a thicker specimen however, there will be a plane strain and three-dimensional stress situation. For a plane strain situation, the effect on the crack propagation of a certain K will be less than in case of a plane stress situation, as the surrounding material will distribute the stresses better.
For an initial estimation of K, superposition of stress intensity may be used to approach the exact value of K.

$$s_{i;j} = \frac{K}{\sqrt{2pr}} f_{i;j}(J) = \frac{K_1}{\sqrt{2pr}} f_{i;j}(J) + \frac{K_2}{\sqrt{2pr}} f_{i;j}(J)$$

and

$$K = K_1 + K_2$$

Also, similar geometric and load cases can be studied. If more accurate values for K are required, a FEM analysis should be made.

2.5.3 Energy release rate

When a plate is loaded with a tensile load P, causing a homogeneous stress S, it becomes longer. To stretch the material, work has to be done and potential energy is added to the material of the plate. When one side is released, the potential energy will be released again. This will occur only if the plate is deformed elastically. The equation for the elastic energy is

$$U = \frac{1}{2} Pd = \frac{1}{2} SWt \frac{S}{E} H = \frac{1}{2} \frac{S^2}{E} HWt$$

with H being the height of the specimen
W being the width and
t being the thickness
HWt is the volume of the plate and $S^2/2E$ the energy per volume unit (strain energy density). In case the plate has a crack and is exposed to the same elongation, less load is required. Thus, for the same elongation, the plate will absorb less strain energy. With respect to the perfect plate, relaxation occurs in the cracked plate if the crack is extended. If the crack would be extended with Δa, the strain energy U would decrease. The following relation between the strain energy, the stress intensity and the crack extension can be derived:

$$\Delta U = \frac{K^2}{E^*} \Delta a$$

with $E^*=E$ for plane stress and with $E^*=E(1-\nu^2)$ for plane strain
Hence, the so-called energy release rate G can be defined as

$$G = \frac{dU}{da} = \frac{K^2}{E^*}$$

The energy release rate is the amount of strain energy that is released per infinitesimal crack extension. When a cracked specimen is loaded, the applied load will try to extend the crack to minimise the strain energy. The energy release rate is also referred to as the crack driving force.

2.5.4 Crack tip plasticity

According to the relation $s_{i;j} = \frac{K}{\sqrt{2pr}} f_{i;j}(J)$
stress would become infinite when r? 0. Most construction metals do have some ductility. As a result of this ductility, some plastic zone will be created. In this plastic zone K seems no longer useful, as it is based on the assumption of elastic material behaviour. In the plastic zone, the infinite stress peak is levelled off. It is important to know if the plasticity affects the meaning of K. Therefore, two areas are defined: the area in which the estimation of K and s are still correct, A_e with radius r_e, also known as

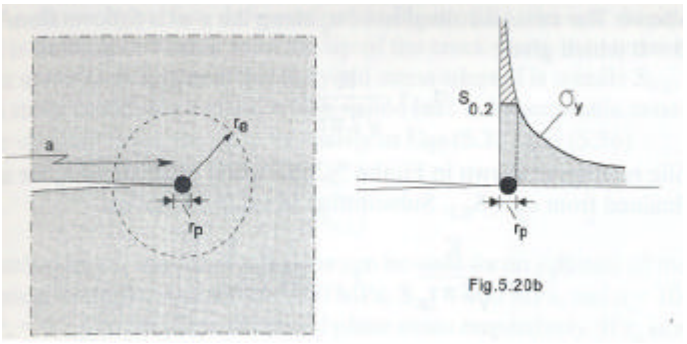

Figure 8: elastic and plastic dominated areas near the crack tip

the K-dominated zone, and the area which is dominated by plasticity, A_p with radius r_p (figure 8). If the ratio r_p/r_e is small, a redistribution of stress will not significantly disturb the area in which K is applied, these types of plastic zones are referred to as small scale yielding. When the ratio r_p/r_e is small, K gives an appropriate indication of the severe stresses in the A_e.
From the requirements $r_p > r_e$ and $r_p < a$ it becomes clear that K will not be valid if large plastic zones occur. The size of the plastic zones depends on the yield level and the state of stress (plane stress or plane strain). r_p Can be estimated by applying the following formula, if $S_{0.2}$ is a adopted as the yield criterion.

$$S_{0.2} = \frac{K}{\sqrt{2pr}}$$

Hence r_p can be estimated with

$$r_p = \frac{1}{2p}\left(\frac{K}{S_{0.2}}\right)^2$$

In case of plane stress, the first approach will be an underestimation, because it ignores the levelled off part, a better estimate can be made with

$$r_p = \frac{1}{p}\left(\frac{K}{S_{0.2}}\right)^2$$

In case of plane strain, for the first approach a yield criterion, like the Von Mises criterion, can be adopted. Because plain strain implies a constraint on lateral contraction, the effective yield stress is substantially higher. To account for this effect, the following estimation can be used.

$$r_p = \frac{1}{3p}\left(\frac{K}{S_{0.2}}\right)^2$$

The shape of area is not considered. In literature, proposals for shapes can be found.

In a plate the lateral contraction can be described by

$$e_z = \frac{s_z}{E} - \frac{n\left(s_x + s_y\right)}{E}$$

In case of plane stress, the $\sigma_z=0$, thus $\varepsilon_z=-\nu(\sigma_x+\sigma_y)/E$. Close to the crack tip, the stresses become very large, hence the lateral strain would be huge. This is not happening, because an area with lower stresses surrounds the area in which the stresses are severe. The contraction in this surrounding area is relative much smaller. Because the material is a continuous field, these extreme differences in contraction cannot occur. The small area with $r\rightarrow 0$ is supported by the surrounding area, and avoids extreme contraction. The state of stress will be close to $\varepsilon_z=0$ i.e. plane strain. Near the edge of the crack a high σ_z will be present, because for $\varepsilon_z=0$, $\sigma_z=\nu(\sigma_x+\sigma_y)$. Then again, at the material surface, $\sigma_z=0$. The singularity of the stresses near the crack tip results in a three-dimensional stress situation. Only in very thin sheets plane stress will occur in the whole sheet, even near the crack tip, as the material will not be able to prevent contraction. In thicker plates, only a small part of the material near the surfaces is in plane stress, the rest of the material is in plain strain.

2.5.5 J-integral

Another fracture mechanics characteristic used in prediction models is the J integral, which takes in account non-linear material behaviour. The J-integral is based on the Griffith energy balance approach. The total energy content U of an elastic, remotely loaded, cracked plate is:

$$U = U_o + U_a + U_g - F$$

With U_o is the elastic energy content of the loaded uncracked plate
U_a is the change in the elastic strain energy caused by introduction of the crack
$U_?$ is is the change in the elastic surface energy by the formation of crack surfaces
F is the work performed by external forces

This energy balance is valid for both linear and non-linear elastic behaviour. However, under certain restrictions, this non-linear elastic behaviour can be used to model plastic behaviour. The main restriction is that no unloading will occur in any part of the body. In case of elastic behaviour deformation is fully reversible, in case of plastic behaviour, the plastic deformation is irreversible.

A non-linear elastic equivalent of G, J can be defined:

$$J = \frac{d}{da}\left(F - U_a\right)$$

The potential energy U_P is can be defined as

$$U_p = U_o + U_a - F$$

And hence U as

$$U = U_p + U_g$$

U_P contains all energy terms that are related to non-linear elasticity, while $U_?$ is in general irreversible. U_o is a constant, hence differentiation of U_p gives

$$\frac{dU_p}{da} = \frac{d}{da}\left(U_a - F\right) = -\frac{d}{da}\left(F - U_a\right)$$

J is defined as

$$J = -\frac{dU_p}{da}$$

The energy provided by the external force per increment of the crack length is described by dF/da and dU_a/da is the increase of elastic energy owing to dF/da, so dU_p/da represents the change in stored energy. A decrease of dU_p/da results in an increase in the crack driving energy J, providing energy for $dU_?/da$ to extend the crack a.

Consider a cracked body with a perimeter G, a surface A and a traction load T, as in the figure 9. The traction force T on the perimeter performs an amount of external work. The potential energy is the sum of U_0, U_a, and –F. These components can by described by

$$U_a + U_o = \iint_A W dx dy$$

$$F = \int_\Gamma \underline{T}\, ds\, \underline{u}$$

with W as the strain energy density
$\underline{T}$ as the traction vector
$\underline{u}$ as the displacement vector and
s as the coordinate along the perimeter

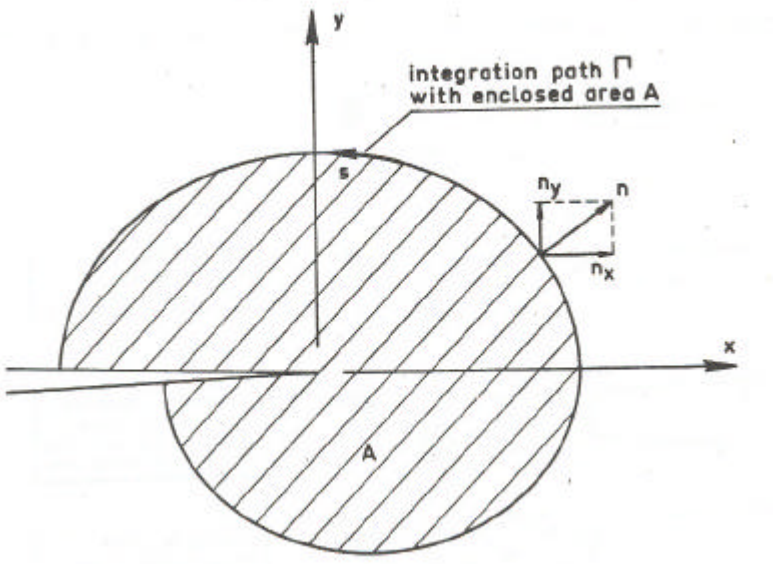

Figure 9: contour for J-integral

thus

$$U_p = \iint_A W dx dy - \int_\Gamma \underline{T} ds \underline{u}$$

If the traction on the body is constant, we may write

$$\frac{dU_p}{da} = \iint_A \frac{\partial W}{\partial a} dx dy - \int_\Gamma \underline{T} \frac{\partial \underline{u}}{\partial a} ds$$

which can be rewritten as, according Green's theorem

$$J = -\int_\Gamma W dy - \int_\Gamma \left(\underline{T} \frac{\partial \underline{u}}{\partial x} \right) ds = \int_\Gamma \left(W n_x - \underline{T} \frac{\partial \underline{u}}{\partial x} \right) ds$$

With
Γ is the contour enclosing the crack tip, starting and ending at the bottom and the top crack surfaces, respectively
$\underline{n}$ is the unit normal on Γ ($\underline{n} = \{n_x, n_y\}$)

For elastic material behaviour, it can be proved that J is equal to the energy release rate. However, J is applied because it is able to characterise path independently the stress/deformation field in the vicinity of the crack tip for inelastic material behaviour, provided that the inelastic deformation history can be approximated by some kind of stress-strain relationship. This excludes situations with unloading,the plastic deformation of the material is irreversible. It can be argued that the best condition to apply J is that loads should grow proportionally to a single load parameter. It is not certain though, that the condition that J should be independent is met. If J is applied, these conditions should always be verified. In the area adjacent to the crack, also referred to as the process zone, these conditions are not met, due to the micro deformations. Anyway, outside the process zone, the intensity of both stress and strain can be characterised accurately.

J can be used for three-dimensional situations as well. In these three-dimensional situations however, J is found to be quite similar to the strain energy release rate.

2.5.6 Crack opening displacements

Elastic

Another fatigue crack characteristic is the opening of the crack. Every time a tensile force loads the specimen, the crack will open. Two types of crack tip openings can be used to describe the crack growth, the displacement of the middle of the crack surfaces and the displacement at the crack tip.
The displacements at the middle of the crack (crack opening displacements, COD) can exactly be calculated in case of a central crack in an infinite sheet loaded by remote tensile stress S:

$$COD_{x=0} = 4\frac{S}{E}a$$

The displacements close to the crack tip, r<<a can be presented by

$$u_i = \frac{K}{G}\sqrt{\frac{r}{2p}}\,f_i(q)$$

with ų representing the displacements u, v, and w in respectively the x, y and z direction. G is the shear modulus. All displacements go to zero if r→0 as could be expected. For large values of r, the equation becomes meaningless.

Considering two stress situations, plane stress and plane strain, we see that plane stress is characterised by $\sigma_z=0$, while plain strain refers to $\varepsilon_z=0$. Because plain strain refers to a deformation constraint in the plane, the material behaves like if it has increased elastic stiffness. Therefore the crack tip opening will be lower, by about 10%.

Plastic

Near the crack tip, the stresses and strains near the crack tip will be responsible for failure. The stresses will exceed the yield stress and plastic deformation will occur. When the yield stresses are exceeded, at a certain point the plastic strains will cross a critical limit and the grain next to the tip fails. It can be argued that the stresses next to the crack tip will always exceed the critical limits and hence it is the plastic strain that dominates the failure behaviour. Hence it can be expected that there is a critical value for crack tip opening displacement, d_t, a material specific value which is applicable as a fracture criterion.

Burdekin and Stone researched the COD concept by using a Dugdale strip and proposed the following expression:

$$d_t = \frac{8s_y a}{pE}\ln\sec\left(\frac{sp}{2s_y}\right)$$

And for the Irwin circular plastic zone analysis this is

$$d_t = \frac{4K^2}{pE}$$

This relation shows that the elastic concept K is compatible with the COD approach.

Unfortunately, the found formulae are only applicable for an infinite sheet, and deriving a formula for practical geometry is not possible.

2.6 High cycle fatigue

High cycle and low cycle fatigue are two different kinds of fatigue behaviour. High and low cycle refers to the respectively high and low number of cycles until fatigue failure. Under high cycle fatigue, the material deformation is mostly elastic. The crack initiation covers the largest part of the fatigue life of the unnotched specimen. The boundary between high cycle and low cycle is not exactly defined, but in general it is about 10^4 cycles.

High cycle fatigue is the more common case in practice and is related to elastic behaviour on a macro scale of the material. In this report, if fatigue is considered, it will mainly concern high cycle fatigue.

High cycle fatigue for unnotched specimens is dominated by crack initiation, thus material surface conditions play an important role. Other 'classic' aspects of high cycle fatigue are

2.7 Low cycle fatigue

Low cycle fatigue is associated with plastic deformation on a macro scale in every load cycle. The structure is only exposed to a rather small number of loads during its life cycle. If it would be required to keep the stresses below the fatigue limit, very heavy structures would occur, without being necessary.

In low cycle fatigue, micro cracks are nucleated in the first loading cycle. Failure will occur while the cracks are still small, which implies that the detection of low cycle fatigue is difficult. Under constant amplitude loading, the deformation in the first loading cycle is high, related to the deformations in the subsequent cycles. For that reason, it is also important to perform constant strain experiments if a good understanding of the low cycle mechanism is desired. The stress amplitude will vary in the successive cycles, depending on the type of material. Both cyclic strain hardening and cyclic strain softening are possible, depending on the type of material. Cyclic strain hardening appears when rather soft materials are tested. The amplitude of the load needs to be increased in the loading sequence. Cyclic strain softening is the reverse effect, the amplitude of the load needs to be decreased in the loading sequence. This behaviour appears mainly when hardened materials are tested. The hardening can be achieved by thermal hardening or by a deformation process. Structural changes in the material arise, leading to relaxation of the potential energy of the material. After a relative low number of cycles (compared to the total fatigue life) these cyclic strain effects stabilise.

3 Loads

3.1 Load Spectra

3.1.1 Different types of load spectra

The total amount of fatigue loads on a structure in service is usually referred to as the load spectrum. The load spectrum for a specific application can be obtained from codes or literature, if the application and the corresponding load spectrum are classified and quantified, or the spectrum can be measured from a similar application. The first fundamental distinction that is made is the constant and the variable amplitude loading. In case of the variable loading, the amount of cyclic loads in the particular stress ranges needs to be quantified.

3.2 Constant Amplitude Loading

For most civil engineering applications, the constant amplitude (CA) loading of a structure is not the most common load case. However, the CA loading is used to obtain the SN-curves for different types of connections. This approach to present the effect of loading amplitudes and the number of cycles comes from the classic experiments of Wöhler. The results obtained by CA loading experiments can be plotted on a double logarithmic scale, resulting in a diagram with three straight lines, as discussed in section 4. In case of CA loading, no damage will occur if $\Delta\sigma<S_f$.
The SN-curves given in the codes are the result of experiments and statistical moderation. The mean line for the experiments can be plotted and the standard deviation can be computed. Hence, the 95% line can be computed. 95% of all experimental results will be above the values of the 95% line. The position of the 95% line with respect to the mean value line depends on the number of experiments and the standard deviation of the results of the experiments.

3.3 Variable Amplitude Loading

3.3.1 Variable Amplitude Loading on structures

Most structures exposed to cyclic loads will carry variable amplitude (VA) loads. The load history of these structures is not very regular most of the time. To be able to predict the effect of the loading history, it would be more favourable to translate the irregular loading pattern to a regular sinus shape loading history. If the load history can be expected to be very simple, the load history can be divided into a number of CA load domains. For each CA load domain, a number of changes can be estimated. Each representative CA load is characterised by the stress interval and the number of changes. Hence, these CA loads and the number of represented by a block scheme, like figure 10.

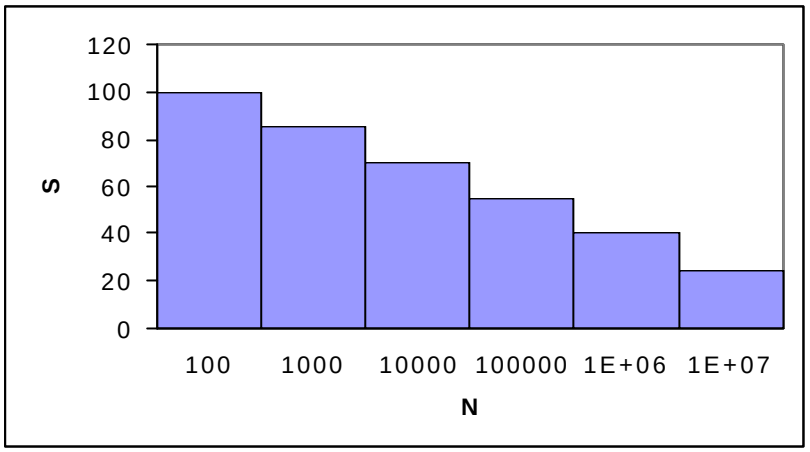

Figure 10: cumulative block scheme

Needless to say, this method is rather inaccurate.

If the load history is more complex, the number and the values of the stress ranges have to be measured. Of course, it is important to measure over a sufficient time span, in order to obtain representative measurement results. When the loads on a structure are rather predictable, like the loads on a railway bridge, the loads are deterministic. If the loads are not very predictable, the loads are referred to as stochastic loads. A stochastic load can only be described appropriate using a statistical notation. Practically, for measuring number and the values of the changes of the loads, the measuring for the stochastic loads requires a longer period, in contrary to the deterministic loads, for which a rather short period is sufficient. The measuring period should be long enough to avoid the missing of measuring of 'rare' high loads, as these high loads will not occur often. In the Dutch codes, this is solved by introducing $\Delta\sigma_v$. The hundred highest loads are levelled off to the value of the hundredth load $\Delta\sigma_v$. Physically, this is no problem, as the first hundred loads hardly add any extra damage then if they are assumed $\Delta\sigma_v$. The boundaries of the load spectrum are $\Delta\sigma_v$ and $0.55\Delta\sigma_f$, as the loads smaller than $0.55\Delta\sigma_f$, are not expected to cause any damage. The load range between $\Delta\sigma_v$ and $0.55\Delta\sigma_f$ is then divided into eight or ten blocks with constant width per block.

If the load history is known, it can be analysed and the number of load changes can be counted and the size of changes can be analysed. The analysis of the stress history can be done by the counting method, discussed in 3.3.2. The result of the analysis can be represented in a block scheme as well.

3.3.2 Description of load history

To describe the load history on a structure, a number of description techniques is available, level crossing count methods, range-counting methods, the rain flow counting method and the range pair counting method. The counting method supported by most codes is the rain flow counting method. The range pair counting method results in the same spectra as the rain flow counting method. In the level crossing count method the numbers of crossings of reference levels is counted. In the range-counting methods, all the stress ranges from one interval to another interval are counted, so two parameters are involved in this counting method.

However, the rain flow is the counting method that is supported the most, because it matches best with the plasticity behaviour of notches. Therefore, this method will be considered a bit closer.

In a loading sequence small and large loads succeed each other. In such a sequel one large load change, with a very little load change half way can occur. The question arises if this should be accounted as two 'average' load steps and one 'small' one, or as one 'large' load step and one 'small' step. The rain flow count method combines all loads between ultimate stresses into different steps as can be seen in figure 11.

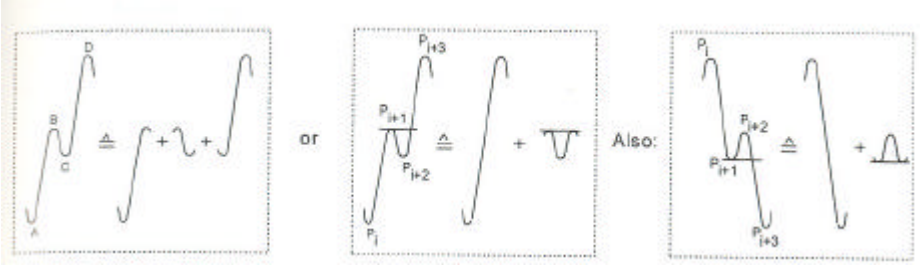

Figure 11: accounting a small and a large load step

The rain flow count method deals with this fundamental question. Because the fatigue damage is related to the load ranges, it should be expected that the fatigue damage of the great load alone is bigger than the sum of damage of the smaller steps. The rain flow method combines the successive load cycles between an absolute maximum and a absolute minimum and counts it as one load cycle, separate of all the smaller load cycles in between. The peak values of the intermediate small load reversal should be inside the range of two larger peak values. As in figure 12, first the smallest load ranges can be counted and removed from the diagram. Hence , the second smallest load ranges are filtered, until there no load peaks surrounding the left over peaks. Hence, the load changes should be categorised in defined load range blocks. Then, the amount of load changes per block can be counted.

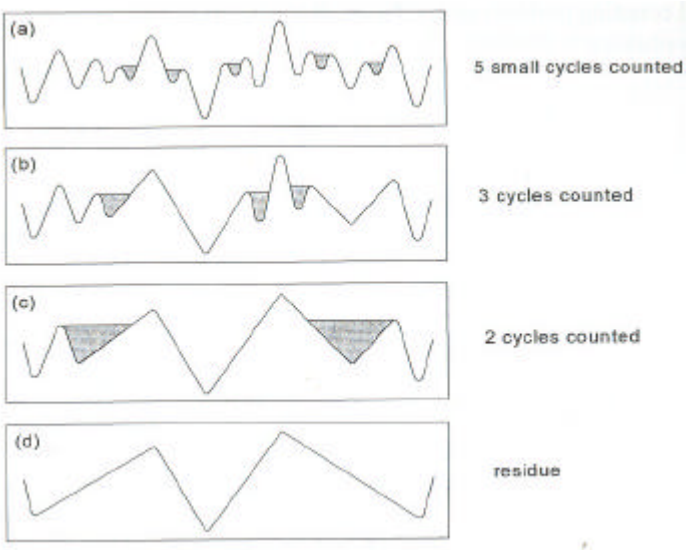

Figure 12: rain flow counting method

In figure 12, a simple example is elaborated.

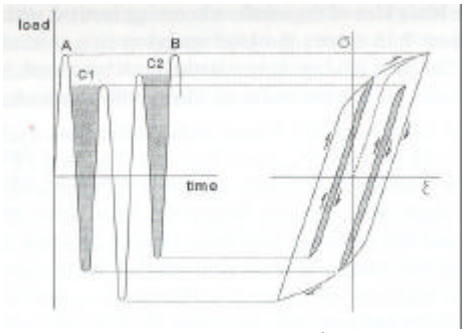

Figure 13: hysteresis loop for a simple load sequence

The mechanic consequence of the rain flow count method can be understood when the plastic deformation of a small load cycle is considered. A small loading sequence is given in figure 13 and the analysis according to the rain flow method, in the left part of the figure. In the right part of the picture the plastic behaviour is indicated schematically. The plastic behaviour can be applied for local plastic

behaviour, like the crack tip plasticity or the plasticity at the surface at the crack initiation. The intermediate load reversals c1 and c2 cause intermediate hysteresis loops inside the major hysteresis loop. It is assumed that these small loops do not affect the major loop. This reasoning gives some plausible support for the rain flow count method.

4 Fatigue strength of unnotched and notched specimen

4.1 Description of fatigue properties of unnotched specimen

The loading of specimen in fatigue failure testing is characterised by the maximum load, the minimum load. From there , the amplitude S_a and the load range ΔS can be determined. Another characteristic is R, figure 14.

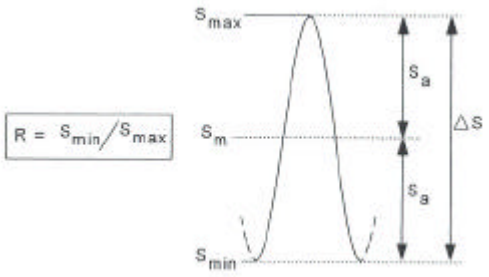

Figure 14: load cycle

Which properties of a load are offered depends on the field of subject giving the load characteristics. From a mechanic fatigue perspective, the maximum and the minimum load could be the most logical, as cyclic crack extension stops at S_{max}. However, when a structure is in service, a certain load is present, namely the dead weight of the structure. The variable load in some configuration is then applied, resulting in a minimum or maximum. From that perspective the mean load and the amplitude might be more logical. Another specific feature of the load is the wave shape of the loading cycles. Also the frequency affects the fatigue mechanism.

Fatigue resistance properties are generally supposed to be material properties. If a series of identical specimen from the same material would be tested by a range of constant cyclic loads until failure, a number of measuring points with a specific number of load changes until failure for each value of load change is obtained. If this data is plotted on a double logarithmic scale, an SN-curve is obtained. On the double logarithmic scale the diagram consists of three straight lines, as in figure 15.

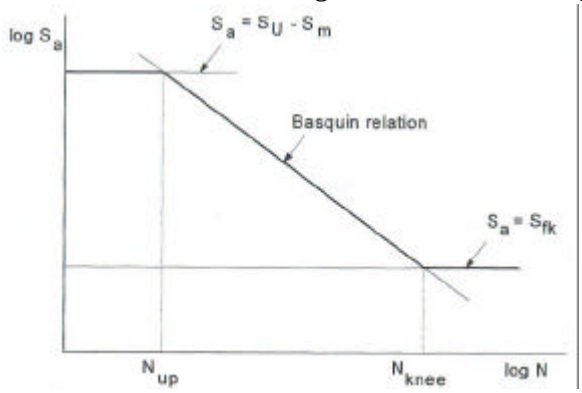

Figure 15: modified SN curve

The stress value at the right asymptote is the stress that is the lower threshold, the knee. For most specimens, this threshold will lay at about 10^7 load cycles. This load level is called the fatigue limit S_f. The threshold limit is the lowest stress that can cause *crack nucleation under constant amplitude loading.* Every unnotched material has its own specific SN curve. At the left side of the curveanother asymptote appears. This left asymptote is related to the low cycle fatigue, which was considered in 2.7.

The specific values of the 'right' boundary of the low cycle fatigue part of the SN curve and the fatigue limit is a characteristic for every unnotched material. Besides the material it also depends on the R-value and the mean stress, and in case of a notched specimen, on the radius of the notch and on the geometry of the specimen. If the mean stress $S_m>0$, the stress levels in a specimen are more likely to reach the yield level. Gerber and Goodman both proposed models to account the effect of the mean stress and the amplitude. However, more recent research has pointed out that the influence of the mean stress is small on sharply notched specimens. The amplitude is much more important for the fatigue life than the mean stresses, especially for long fatigue lives. The effect of the geometry on fatigue under constant amplitude loading can be found in literature and in the Codes. In most codes, most standard joint geometries have their own SN curve.

4.2 Description of fatigue properties of notched specimen

To calculate the influence of a notch on the fatigue life, the following initial estimation was made: if a stress S in an unnotched specimen can initiate a micro crack, it should be possible to initiate the same crack in a notched specimen, if the local stress, calculated with K_t, is equal to the stress S in the unnotched specimen. This is called the similarity principle.

$$S_{f;notched} = \frac{S_{f;unnotched}}{K_t}$$

Unfortunately this is not entirely correct, therefore the factor K_f is introduced, it correlates the fatigue limit of a notched specimen to the fatigue limit of an unnotched specimen:

$$K_f = \frac{S_{f;unnotched}}{S_{f;notched}}$$

Most often $K_f < K_t$, especially for small specimens with high K_t values. Also for low strength materials this is true. For low values of K_t, K_f will approach K_t, although it will be slightly smaller. For high values of K_t, K_f will be much smaller than K_t. When a group of specimen is tested, all with the same K_t, but for different specimen sizes or different geometries, different K_f values are found. Also, K_f is dependent on the grain size and the material quality.

The inequality $K_f < K_t$ limits the applicability of the similarity principle. Nevertheless, this inequality is favourable, if $K_f < K_t$, the material is less notch sensitive than would have been estimated by the similarity principle. Hence, Peterson proposes the notch sensitivity ratio q:

$$q = \frac{K_f - 1}{K_t - 1}$$

A high notch sensitivity is obtained if the similarity principle is correct, then q=1. If there is no sensitivity at all, q=0. Roughly, it can be stated that if the grade of the material is increased, q decreases when K_t is increased. This means that high-grade materials are more notch sensitive, or, K_f will approach more K_t for high-grade materials, than for lower grade materials.
This has the following effects for the fatigue behaviour:

- In unnotched condition, a higher grade material is less notch sensitive than a lower grade material, but this ratio is smaller than the yield stress ratio.
- If specimens have sharp notches and/or a rough surface, the benefits of a high-grade material over a lower grade material can be lost.

Regarding the loading of the specimen, the influence of mean stress on the fatigue mechanism in notched specimens is complicated, because of the local plastic deformation of the specimen. As for the prediction of the influence of the mean stress level and the amplitude, the methods of Gerber and Goodman can be applied, although they both require moderation.

Important variables for the prediction of fatigue strength are K_t, the size of the notch, the surface finish and the mean stress.

5 Damage prediction under variable amplitude loading

5.1 Miner rule

When the load spectrum of a structure is determined the fatigue damage, the fatigue strength can be estimated, by experimental research or by applying prediction models for fatigue damage. The total load spectrum can be divided into a number of blocks, each with their amplitude and predicted number of changes. The Miner rule is a rather simple prediction method, used by most national codes. The Miner rule is an empirical method to estimate the fatigue life. The basic principle behind the Miner rule is the assumption that a specimen or structure can absorb a total work W until failure. W is a constant value for a specific material, geometry and notch, independent from the loads applied. Every subsequent load cycle n_i adds the work quantity w_i. Hence, the following assumption is made:

$$w_i / W_i = n_i / N_i$$

In which:
n_i is the total number of the load changes of a certain load block and
N_i is the number of load changes that causes failure under the load change $\Delta\sigma_i$
The total damage to a structure sums the damage of the different load blocks:

$$D = \sum \frac{n_i}{N_i} \leq 1.0$$

In which:
D is the total damage due to the different loads.
Failure occurs if D>1.0

The use of characteristic SN curves of construction connections is supported by the national codes. Most connections in a structure, exposed to a cyclic variable load, can be classified in a system prescribed by the codes. In 5.2 some additional modifications for the Miner rule, adopted by the codes are included.

5.2 Notes for the Miner rule

Fatigue damage is a complex phenomenon that cannot be covered by a simple (linear) quantitative description. The Miner rule indicates the fatigue damage of a structure using a single parameter to describe the accumulated damage from zero (flawless) to one (failure). This is a fundamental shortcoming of the Miner rule.

Basically, there are three objections against the Miner rule, resulting from the fundamental shortcoming:

- Ignoring the damaging effect of small stresses
- Ignoring the sequence effect
- Estimation of the crack size at failure

These shortcomings will be all reviewed in this section.

Ignoring the damaging effect of small stresses

Small loads with amplitudes below the fatigue limit, $\Delta\sigma<\Delta\sigma_f$, cannot initiate micro cracks and develop them until failure under CA loading. In the Miner rule, these loads are considered as not damaging under VA loading. This is physically incorrect. Some loads stresses smaller than the fatigue limit are able to propagate micro and macro cracks. These small load stresses are only damaging if higher load levels, which are able to initiate the crack, precede them. This effect is referred to as an interaction effect. The interaction effect is ignored by the Miner rule.

Ignoring the sequence effect

When a sequence of low cycle amplitude (not necessarily smaller than the fatigue limit) is preceded by a high load cycle, notch root plasticity can occur after this high cycle load. For instance, compressive

residual stresses can occur. These residual stresses have a significant influence on the damage inflicted by the low amplitude load cycles. The effect of the residual compressive stresses is beneficial for the fatigue resistance against the damage of the following low cycle loads cycles. The other way around, residual tensile stresses have a significant negative effect on the fatigue resistance properties. These so-called sequence effects are not accounted by the Miner rule.

Crack size at failure

A cumulative rule requires a definition of fatigue damage. The fatigue damage should include the length of the crack, reminding the initiation and crack growth period, discussed in 2.2 and 2.3. In case of a cyclic high amplitude load the crack at failure will be smaller than the crack at failure due to cyclic low amplitude load. Hence, the crack length at failure depends on the S_{max} of the last load cycle. According to the Miner rule if $\sum n_i/N_i=1$ the damage is 100%. From there, the SN-curve would be a 100% damage line, a line of constant damage. Physically, this is incorrect. The crack at high amplitude last load cycle is smaller than the cracks at low amplitude last load cycle.

In case of a more or less random load, as in service will occur, the sequence effect can be neglected, as the positive and negative effects of the sequence effect are counterbalanced. The sequence effect is not considered in the codes.

Also, the crack size failure is not considered any further in the codes. For example in the Dutch code (NEN 2063) the interaction effect is accounted for the cyclic stresses with amplitude between $\Delta\sigma_f$ and $0.55\Delta\sigma_f$ are included in the SN curves. The SN curve is extended with an extra 'curve', a straight line on the double logarithmic scale, starting from $\Delta\sigma_f$ at $N=10^7$ and ending at $0.55\Delta\sigma_f$ at $N=2*10^8$, as

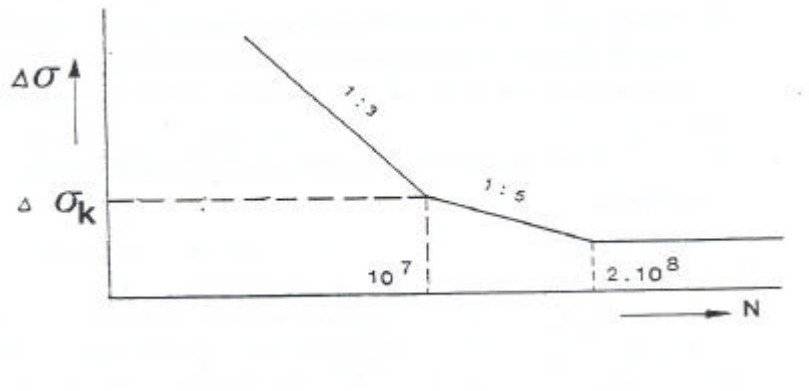

Figure 16: modified SN-curve

given in figure 16. At the right side of $0.55\Delta\sigma_f$, the curve is an asymptote again.

The 'extended part of the SN curve is less steep than the 'regular' part. The slope of the regular part is about 1:3 (the damage caused by this part of the SN-curve is called D_3), the extended part has a slope of 1:5 (the damage caused by this part of the SN-curve is called D_5),. The degree in which the damage of this low amplitude loads is accounted depends on the damage caused by the higher amplitude loads. In order to avoid that after some small D_3, D_5 would be fully accounted, a reduction factor ϕ is introduced. The value of ϕ depends on D_3. The modified Miner rule is

$$D = \sum \frac{n_{i;3}}{N_{i;3}} + j \sum \frac{n_{i;5}}{N_{i;5}} \leq 1.0$$

In case of multiple loading directions, the damage can be summed for the multiple directions. In that case, failure occurs not if D=1 but when D=1.1

$$D = \sum \frac{n_{i;3}}{N_{i;3}} + j \sum \frac{n_{i;5}}{N_{i;5}} \leq 1.1$$

6 Fracture mechanics

6.1 Properties of fatigue crack initiation

In chapter 2 the fatigue life of a specimen is divided in two periods, the crack initiation period and the crack growth period. It was stated then that the fatigue crack initiation is mostly a material surface phenomenon. In section 2.2.2 all aspects influencing crack initiation are summed up. In this chapter crack initiation is considered from a more quantitative and mechanical point of view 6.4.1.

6.2 Properties of fatigue crack growth

6.2.1 Crack growth described by test results

The crack growth period starts when the micro crack has crossed the subsurface area and grows into the material, away from the surface. The growth of the crack depends then on the bulk properties of the material. The crack growth is considered qualitative in section 2.3. In this chapter, the crack growth behaviour will be considered more fundamentally and quantitative.

To describe the crack propagation, a simple test can be pictured. Two simple sheet specimens with a central hole are tested under cyclic tensile load. The sheets have a centric circular hole with saw cuts at the two sides perpendicular to the load direction of a size at each side, as notch starters. The amplitudes of the loads differ, but the stress ratio is the same. The crack growth is recorded by periodically observation at the crack tip. The result can be seen in figure 17a. The results can also be converted into figure 17b, which represents the dN/da-a curves of the specimens. In this figure, the crack growth rate per cycle at a certain crack size a can be found. Both curves start at the same starting point, a_0. To compare the specimen without considering the load levels, the diagram can be translated

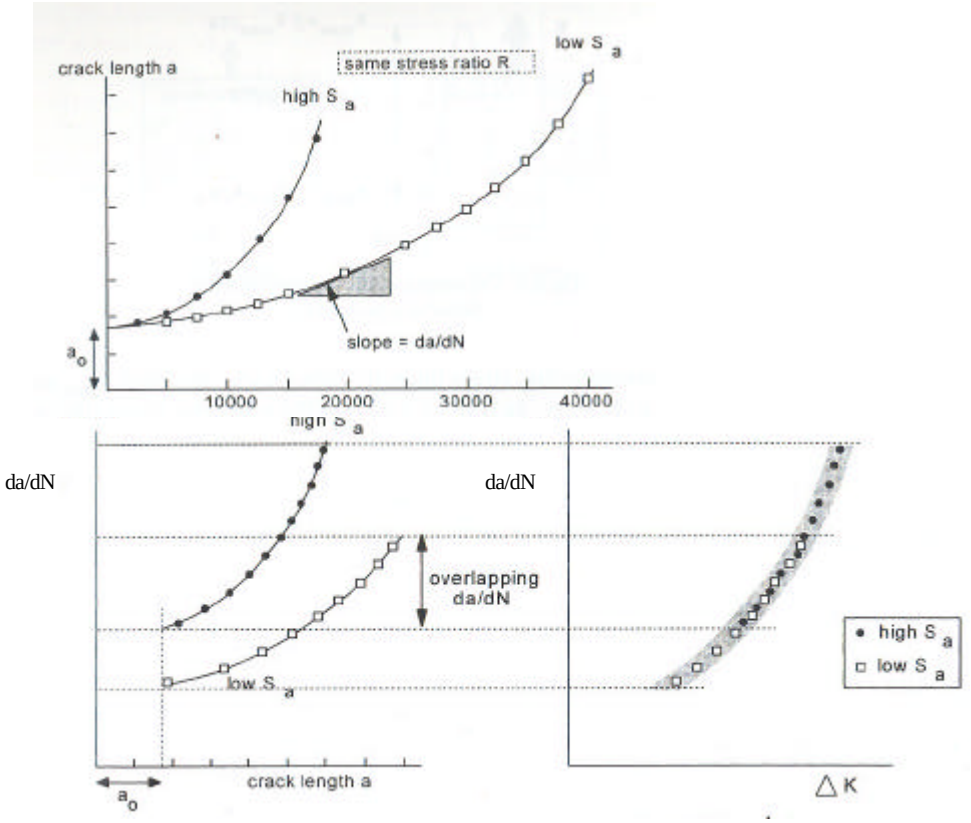

Figure 17: (a) a-N diagram, (b) da/dN-a diagram, (c) da/dN-DK diagram

to a da/dN-ΔK diagram, figure 17c, as K gives a relation between a and σ ($K=\beta\sigma\sqrt{\pi a}$). The two curves now partly overlap. This overlapping part is subject of section 6.2.2.

6.2.2 Stress intensity factor and the similarity concept

As discussed in 2.5, K is a parameter for the severity of stress near the crack tip. If a cyclic load has a nominal range from S_{min} to S_{max}, with an amplitude $S_a=S_{max}-S_{min}$ and a mean stress, then the severe stresses at the crack tip will vary corresponding the ratio between the nominal mean stress and the severe stresses. Hence, K will vary corresponding to this factor. This principle is referred to as the similarity principle and can be expressed by the following formula:

$$R = \frac{S_{\min}}{S_{\max}} = \frac{K_{\min}}{K_{\max}}$$

To describe the similarity principle further another example is given. If two specimens are tested, one with a large crack and one with small crack, and other specimen with the large crack is loaded with a small load and the small crack specimen with a large load, in such a way that the K_{min} and K_{max} values for both specimen correspond per cycle, it is found that the crack extension for each load cycle is in the same scatter band. The crack growth rate depends on the maximum load, minimum load the ratio between loads and the crack in the specimen. The crack growth rate is a function like

$$\frac{da}{dN} = f\left(K_{\max}, K_{\min}\right)$$

or can be rewritten like

$$\frac{da}{dN} = f\left(\Delta K, R\right)$$

as $\Delta K=K_{max}-K_{min}$

da/dN is a function of ΔK, but ΔK depends on the stress ratio R. Also material and geometry aspects need to be accounted in this function. The geometry of the specimen is mainly accounted in K, by the factor β. The factor β is influenced again by the crack size a. Empirical results need to be obtained to find the function of da/dN. It should be noted that the similarity principle does not say anything about the fatigue mechanism nor gives it the size of an extension. It only says that if there are two loading cycles with a similar ΔK, the same Δa should occur. The amount of extension has to be gained by experiment. The $da/dN=f_R(\Delta K)$ can be a measure of crack growth resistance of a specific material.

If fatigue crack growth experiments are performed, the results can be plotted in a da/dN-ΔK diagram on double logarithmic scale. The characteristic diagrams of fatigue crack growth experiments look like figure 17. They have two vertical asymptotes and can be divided into three regions. The left asymptote indicates that there is a threshold for ΔK. If ΔK is below this value, no crack growth will occur. The local stresses near the crack tip will be too low to propagate the crack. The right asymptote gives a critical value for ΔK. For this critical value of ΔK, the critical value K_c is reached for the upper limit of K, $K_{max}=K_c$. If ΔK reaches this critical value complete failure will occur within a few cycles. The da/dN-ΔK diagram can be divided into three regions, closely related to the asymptotes. These regions, indicated by I, II and III are: I the threshold region, II the Paris region, III the stable tearing crack growth region. The regions start where the slope of the da/dN-ΔK diagram on double logarithmic scale is no longer constant. The three crack growth regions of the fatigue crack growth diagram are the topic of 6.3.

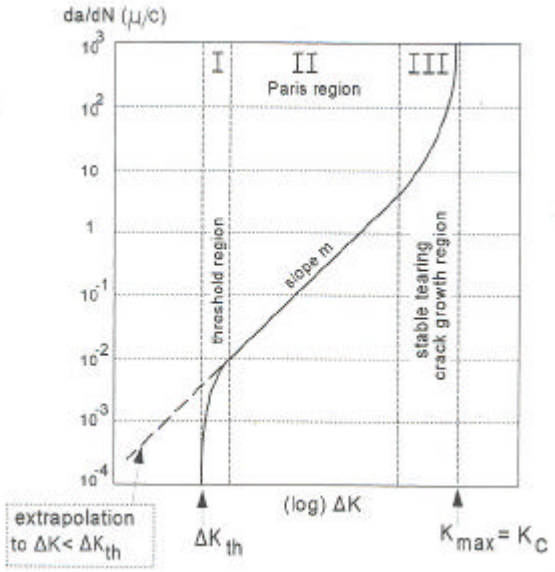

Figure 17: da/dN-DK diagram with the three characteristic regions

6.3 Fatigue crack growth regions

6.3.1 Threshold region

The threshold region is associated with the crack growth mechanism of macro cracks. These cracks were once initiated and developed to a macro scale by a $\Delta K > \Delta K_{th}$, but if the ΔK then is decreased to a level below the ΔK_{th} the crack growth in the specimen is stagnated. If the value for ΔK_{th} is required, this can be gained experimentally. A crack growth experiment can be executed and ΔK can be decreased by (*i*) decreasing $\Delta\sigma_{max}$, (*ii*) increasing $\Delta\sigma_{min}$ or (*iii*) by decreasing both the $\Delta\sigma_{max}$ and $\Delta\sigma_{min}$. In case (*i*), ΔK_{max} the plastic area is decreased, which may retard the crack growth. This does not happen in case (*ii*), but the R will not be constant. As said, the function of da/dN is also related to R. In case (*iii*), R can be held constant, but the size of the plastic area and ΔK_{max} does vary. Experimental research has proved that ΔK_{th} depends on R.
It should be noted that the significance of ΔK_{th} is limited from a practical engineering point of view. If a crack occurs in a structure under a certain load spectrum, it could be assumed that the crack will not be propagated, if $\Delta K < \Delta K_{th}$, but that is not necessarily a safe argument.

6.3.2 Paris region

Paris described the relation between the da/dN and ΔK by a power function:

$$\frac{da}{dN} = C\Delta K^{m}$$

in which C and m both are material constants. If this equation is plotted on double logarithmic paper, this equation gives a linear relation between da/dN and ΔK. This equation does not account for the threshold and the stable crack tearing region, nor the R effect on the crack growth rate.

6.3.3 Stable tearing crack growth region

In the stable tearing crack growth region, the crack growth rate is high. Striations by successive at the crack surface are still visible with an electron microscope. Between the striation patches local ductile tearing can be observed. As the ductile tearing is only local, the failure mechanism is still stable. More cyclic loading is required for failure, but the local ductile tearing implies that final failure is near. The stable tearing period is rather short, so the importance from an engineering point of view is insignificant.
Predictions concerning the final failure appear to be simple, because when by definition failure occurs when $K_{max} = K_c$. However, final failure requires plastic yielding over the entire section. K_c gives an

indication about the stresses according to elastic material behaviour and is as a stress intensity factor useless. K is a fundamentally elastic concept, final failure a fundamentally plastic phenomenon.

6.4 Predictions on fatigue cracks

6.4.1 Crack initiation prediction

In this section the relation between stress, strain and crack initiation is considered. The cyclic stress strain relation and Neubers rule will be applied to make a model for crack initiation.

The fatigue behaviour with strain control of smooth specimen can be expressed as

$$\frac{\Delta e}{2} = \frac{s_f - s_m}{E}\left(2N_f\right)^b + e_f\left(2N_f\right)^c$$

in which
ε is the sum of the plastic and elastic strain
b is the fatigue strength exponent
ε_f is the ductility coefficient
c is the fatigue ductility exponent
A similar formula to calculate the strain in low cycle fatigue has been stated in 2.7.

A cyclic strain controlled test of a smooth specimen gives after a some cycles a stable hysteresis loop, figure 18a. The cyclic stress-strain curve defined as the locus of tips of the stable hysteresis loops from several tests at different completely-reversed, constant strain amplitudes, figure 18b. It was observed that the cyclic stress-strain curve, when magnified by two, approximately describes the stable hysteresis loop shape.

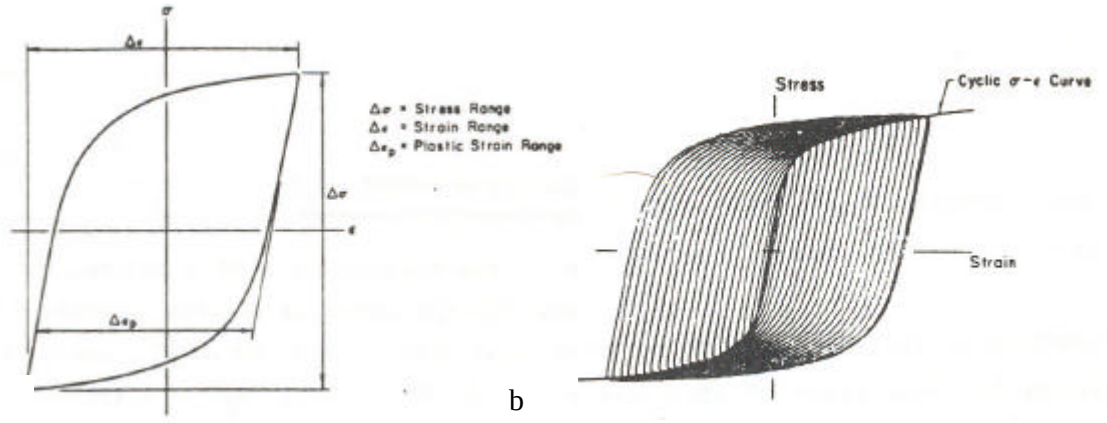

a b

Figure 18(a) Stable stress-strain hysteresis loop (b) cyclic stress-strain curve drawn through stable loop tips

The cyclic stress-strain relation of smooth specimen can be given with:

$$\frac{\Delta e}{2} = \frac{\Delta s/2}{E} + \left(\frac{\Delta s/2}{K}\right)^{1/n}$$

with
K'as the cyclic strength coefficient and
n'as the strain hardening coefficient
both the stress and strain changes are true ranges.

6.4.2 Crack growth prediction

Crack growth under an CA loading

The prediction of a fatigue crack growth under a CA loading can be calculated by applying the Paris relation:

$$\frac{da}{dN} = C\Delta K^{m}$$

for a certain material the constants C and m are required. Values for these constants can be found from previous experimental data. Safe assumptions for these constants are $C=4*10^{-13}$ and m=3.
To calculate the number of load changes under CA loading for a crack extension, the Paris relation can be integrated

$$\Delta N_{a_i \to a_f} = \frac{1}{C}\int_{a_i}^{a_f} \frac{da}{\left(\Delta K^{m}\right)} = \frac{1}{C\left(\Delta S\sqrt{p}\right)^{m}}\int_{a_i}^{a_f} \frac{da}{\left(b\sqrt{a}\right)^{m}}$$

with $\Delta K = \Delta S b\sqrt{ap}$

The integral has to be solved numerically, because often β is also dependent on the crack size. Practical values for β can be found in literature. The factor depends on both the geometry and the load case. The integration should be made over small intervals for a. Hence, the following equation is found for the number of load cycles required for the crack extension crack extension $a_i \to a_f$.

The prediction of crack growth fatigue serves roughly three purposes: (*a*) study of design variables, as a part of a design procedure, (*b*) rough estimate of crack growth in a definite design and (*c*) the crack growth prediction in a specific case, as accurate as possible. The required input to obtain a reliable prediction for the purpose differs strongly for the three purposes, i.e. (*c*) needs a higher accuracy than (*a*). In case of (*a*) some simplifications can be applied and crack growth resistance data can be obtained from literature. These simplifications cannot be applied for (*b*) unless they lead to a conservative approach. For (*c*) FE models should be applied to gather values for K and crack growth experiments should be applied to gain information on the crack growth resistance.

The assumption of the initial crack size a_0 plays an important role in the crack growth prediction. If the initial value would lead to an underestimation of the initial K, a calculation could lead to $\Delta K<\Delta K_{th}$ which would imply that no crack growth would occur. Also, a_0 has a big influence on the initial (macro) crack growth and on the length of the fatigue life. The initial crack growth rate under a CA loading will be the lowest of the fatigue life. As the crack growth rate depends on the initial crack growth, decreasing the initial crack size can largely extend the fatigue life. Thus, the initial assumption of the crack size largely affects the calculated fatigue life.

When a cyclic load is applied to a crack, the crack will open when ΔK increases and close when ΔK decreases. When the crack closes, it has been observed that the crack is closed before ΔK reached its minimum. The part of ΔK that is during the closure is ineffective. This closure is caused by residual compressive stresses near the crack tip. Hence, ΔK will not result in the crack extension that it would have been able to in case none of the loading should have been used to neutralise the plastic compressive stresses at the crack tip area. The ΔK that is used to extend the crack is referred to as ΔK_{eff}. The stress ratio R has an important effect on ΔK_{eff}. Under a high R ΔK_{eff} will approach K, as crack closure is less likely to occur when the crack load is constant loaded with high tensile forces.

Crack growth under a VA loading

When VA loading is applied to a specimen, two types of VA loading can be applied: simple VA loading histories and complex VA loading histories.

Crack growth under simple VA loading

Simple VA loading does, in general, not match the service loading of a structure. However, when fatigue failure is studied, simple loading can contribute to understanding of the mechanism and the interaction between the different stress levels on a specimen.

Significant interaction effects can occur under VA loading. The crack growth rate is dependent on the loading history. In case of the simple VA loading, changing from a high amplitude load block to a low amplitude load block can cause retardation of the crack growth occurs, see figure 19. A similar effect can occur if a single large positive amplitude load cycle (overload, OL) is added in a constant loading cycle. If a single large negative load cycle (underload, UL) is used, a slight increase of the crack growth rate can be expected, though not as strong as the retardation effect. If, instead of a single OL cycle, multiple OL cycles are applied to the specimen, the retardation effect will be increased significantly. This retardation effect occurs in a rather small increment of the crack size. However, after the retardation delay of the OL cycle, the crack growth curve returns to its old da/dN ΔK propagation curve. The retardation effect can mainly be addressed to the crack closure effect. The crack closure effect is caused by compressive stress near the crack tip. These compressive stresses are the residue of the large plastic stresses near the crack tip. Plastic induced crack closure represents a significant part of the interaction effect. The crack propagation behaviour and retardation will be different from plane stress to plane strain. Both cases have different plastic zones. The plastic zones in plane stress situations are bigger. The delay for a given ΔK is larger for a thinner material, as it approaches a plane stress situation more. Also, the delay increases when higher OL is applied to the

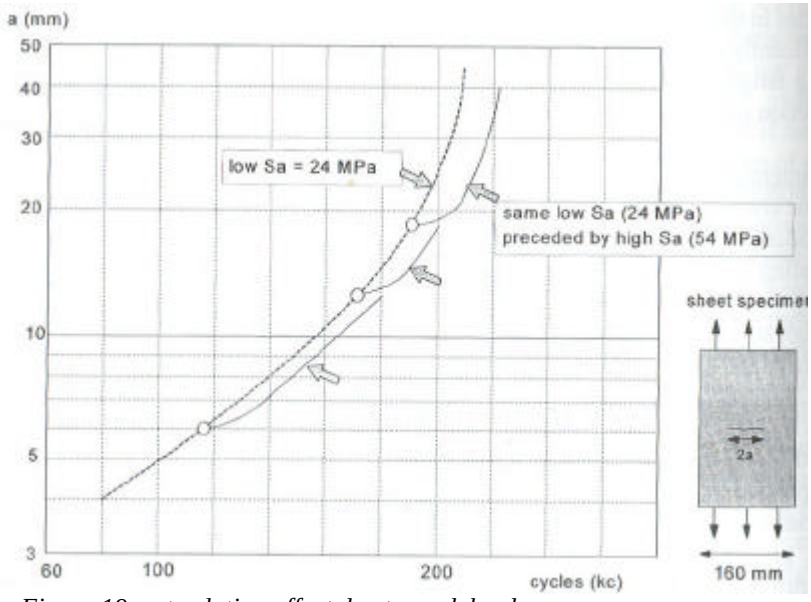

Figure 19: retardation effect due to peak loads

specimen, for both the plane stress and the plane strain situation. The stress situation, plane stress or plane strain, depends on the thickness of the material. Near the surface of the material, plane stress situation will occur more often, as a 3D stress distribution is not possible. Hence, crack closure and crack growth retardation is more likely to occur near the surface.

Crack growth under complex VA loading

Crack growth prediction under VA loading

Most crack growth prediction models predict the crack growth cycle by cycle. This methodology can be described as summing cycle by cycle the extension of the crack:

$$a_n = a_0 + \sum_{i=1}^{i=n} \Delta a_i$$

Two kinds of models can be distinguished: non-interaction models and interaction models. The non-interaction models are the simplest. These models do not consider the load history of the specimen.

The results obtained by these models can be unrealistic and conservative, as the interaction effect under VA loading might be significant. Acceleration and retardation of the crack growth is ignored, while especially the retardation effects are significant. Results of the non-interactive models will be conservative. Crack growth data to include the crack growth resistance should be available, for a number of R values. Crack growth data from CA loading tests can be applied. One remark for the use of CA data: in CA loading crack growth under ΔK_{th} can be assumed to be zero. However, as is pointed out before, the physical meaning of ΔK_{th} is limited. Under VA loading, the crack growth rate in the threshold region should be extrapolated from the data from the Paris region to avoid underestimation of crack growth in the threshold region. The extrapolation has no physical background, but is applied for safety reasons. For the non-interaction models, the Paris relation can be applied

$$\frac{da}{dN} = C\Delta K^m$$

which can be rewritten as

$$\Delta a_i = \sum_{i=1}^{i=n} C\Delta K^m = C\sum_{i=1}^{i=n} \left(\Delta s_i b_i \sqrt{pa}\right)^m$$

It should be noted that β is related to the crack size.

Regarding the interaction models, two kinds of models can be distinguished: interaction models based on crack tip plasticity and interaction models based on crack closure.

Interaction models based on crack tip plasticity calculate the retardation of the crack growth caused by plastic deformation by peak loads near the crack tip. A peak load results in a plastic deformed area with residual compressive stresses at the crack tip. These areas have been discussed in 2.5.4 and formulae for the radii of the crack tips were given. The plastic area after a peak load is much larger than the plastic area after a 'regular' load. The retardation lasts until the plastic area of the peak load has been crossed by the crack.. The retardation effect depends on the radii of the plastic area of the peak load and the 'regular' load i and the propagation of the crack in the plastic area of the peak load after the crack extension of the peak load.

Interaction models based on crack closure are far more complicated than the non-interaction models and the interaction models based on crack tip plasticity. Basically, there are three types of interaction models: yield zone models, crack closure models and strip yield models. The basic steps these models make, are:

- Determine ΔK_{eff} for cycle i
- Calculate $\Delta a_i=(da/dN)_{CA}=f((\Delta K_{eff})_i)$, using CA loading crack growth data
- Calculate $a_{i+1}= a_i+\Delta a_i$
- Repeat these three steps for each load cycle

The differences between these models are related to the ability of the model to use the crack closure phenomenon in the calculation and the way the crack closure is determined (empirical or calculated). Of these models the yield strip model is the most advanced model, using the crack closure and calculating the crack tip plasticity closure itself. All the models calculate the retardation of the crack growth due to an OL. Any prediction of a VA loading interaction model should be validated experimentally under service simulating load cycles.

7 Fatigue strength of welded structures

7.1 Introduction

Welded connections have a characteristic fatigue failure; the failure loads of a welded specimen compared to an unwelded or even a specimen with bolt holes show large differences. In this chapter, fatigue failure in welded structures in general are considered. Welded connections are available in a great variety of shapes, like transverse and longitudinal butt welds, both loaded or unloaded, loading-carrying and non-load-carrying fillet welds, both longitudinal and transverse, cover plates, spot welds et cetera. To gain some basic understanding of fatigue failure in welds, some of the most basic weld details will be considered in 7.3,7.4 and 7.5, namely butt welds and fillet welds.

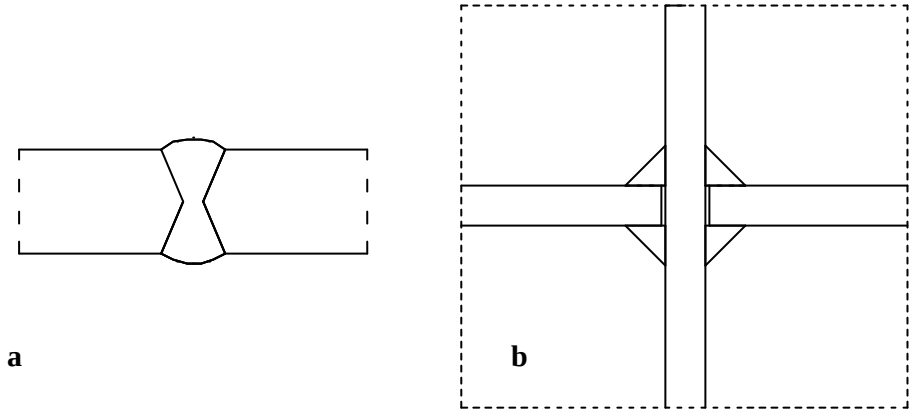

Figure 20: (a) butt weld, (b) cruciform fillet weld

7.2 General aspects fatigue of welded joints

When a connection is welded, a number of fatigue failure effects can be expected. Some of these effects are characteristic for welded structure, some are defects, which are specific welding flaws. In welded connections, there will be always stress concentrations, caused by discontinuities in the welded material shape. A weld will almost always have a sudden change of section in the material, see figure 20 and 21. This change of section will result in an inhomogeneous stress distribution in the material. Two important features of a weld with respect to fatigue failure are the weld toe conditions and the weld root conditions.

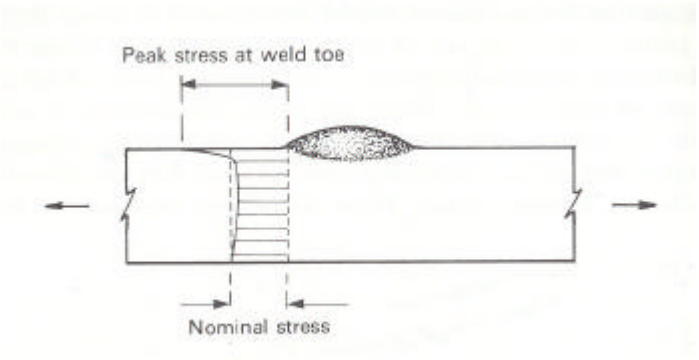

Figure 21: stress concentration near a discontinuity

At the weld toe, the stresses are transmitted from a structural member into the weld. The way the stress is transmitted depends on the profile of the weld. In case there is undercutting or a convex profile, large stress concentrations occur at the weld toe. The welding profile largely determines the stress concentration in the welded section. Undercutting and a convex profile are both flaws, which should be avoided, because they cause even higher stress concentrations. However, another aspect causing stress concentrations are tiny crack like weld discontinuities, called intrusions. These intrusions are the product of the welding process. Undercutting, convex profile and the depth of intrusions vary along the length of the weld. The intrusions result in a fatigue life that is drastically reduced from the fatigue life that could be estimated from the perfect weld shape connection i.e. a connection without any intrusions. In case these small crack-like intrusions at the weld toe are present, the crack initiation period of the connection is nearly omitted.

For some weld shapes another location that initiates severe stresses under transverse loads, namely the weld root. The stress concentrations can be even higher than at the weld toe.

Another source of stress peaks are residual stresses. The welding process initiates residual stresses. Two systems of residual stress are produced. First, there are stresses caused by the assembly, also referred to as reaction stresses. These stresses affect the structure as a whole. Second, there are residual stresses caused by the welding process it self. The heating and the cooling of the connection cause these stresses. During the welding, the material is heated and the material will expand. When the material cools down, the material will shrink. The surrounding material resists this shrinkage and hence introduces stress in the weld.

Specific welding flaws that may occur in a weld: undercut, porosity, slag inclusions, lack of penetration, lack of fusion and cold cracks. All of these welding flaws cause discontinuities in the weld and can lead to stresses concentrations in the weld. Some of these weld flaws are allowed by the codes unto some degree, some flaws are strictly rejected.

Other factors that affect the fatigue of welded joints are the

- Stress relief
- Material properties
- Weld quality
- Size effects

The presence of high tensile residual stresses in welded joints is undesirable. These residual stresses can be relieved by thermal treatment. However, relief of the residual stresses is only important if the loading cycle partly or wholly consists of compressive stresses. For fully tensile loads, the results for relieved and non-relieved connections are almost the same.

A strange contrast between welded and unwelded material occurs, when the material strength is regarded. For unwelded materials, the fatigue strength increases when the material strength is raised. It does not increase proportionally, but it does increase. However, for welded materials, the fatigue strength does not increase when the material strength is increased. This effect is consistent with the fact that the crack growth rate does not vary proportionally or significantly with the material strength. Hence can be concluded that the reduction of the fatigue strength is related to the crack initiation. The crack growth is not sensitive to the complex microstructure of the welded area except for exceptional circumstances.

Beside the production flaws that can occur during the welding process, other imperfections can occur in welds, namely misalignment. Misalignment includes axial misalignment and angular misalignment. Axial misalignment is the eccentricity between two plate materials, angular misalignment is unintended angle between two connected plates. Both cases of misalignment introduce secondary bending stresses in the connection. The bending stresses will introduce a local increment of stress and have a negative effect on the fatigue life of the connection.

The size effect for welded structure is mainly a matter of stress concentration. The thicker the connected parts are, the higher the stress concentration in the transmission zone of the joint is.

7.3 Transverse butt welds

A transverse butt weld is a connection between two plates with a linear weld between them, welded from one side or two sides. The plates are loaded perpendicular to the weld. In transverse butt welds, crack initiation will start most of the time at the weld toe, as the discontinuity of the material starts there and because the surface stresses at the weld toe are the highest in the joint. The severe stresses and thus the fatigue strength are dependent on the weld profile. Applying smooth surfaces and machining the joint can lower the stress concentrations. Gentile stress transition through the members has a positive effect on the fatigue life. Overfill of the welds should be avoided at all time. During the production of the weld, the conditions of the production of the weld influence the features of the weld. Correct preparation, flat weld positioning, easy access and good fit up decrease the chance of weld flaws. Welds made in a workshop are less sensitive for weld flaws than welds on site. Transverse butt welds are sensitive for misalignment. The severe stresses under the same load are bigger when the misalignment is bigger. However, the maximum allowable stresses in the connection, including the secondary bending effect, are in the same scatter band. Misalignment is difficult to avoid, especially for welded panels. 'Real' structures also suffer from misalignment, but less than welded panels, as structures are mostly more restrained.

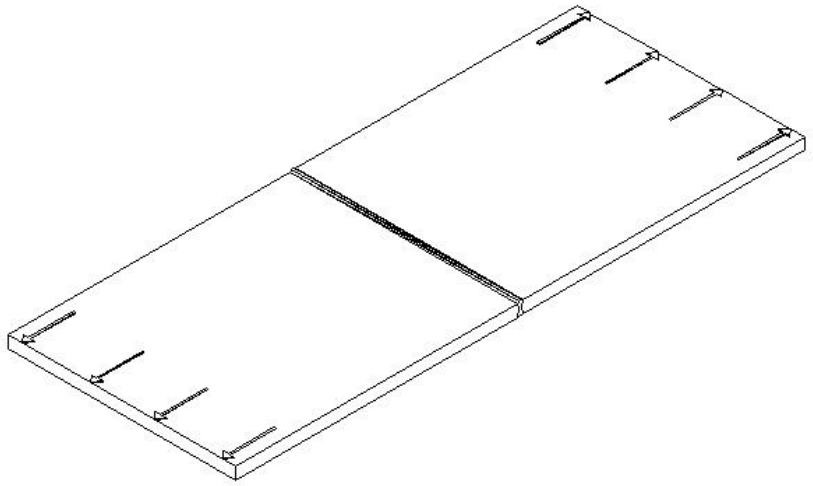

Figure 22: Transverse butt weld

Butt welds can made both from one and two sides. One-sided welds with a good bead and a smooth profile have similar fatigue strength as double-sided welds. The problem is that it can be rather hard or impossible to control. Misalignment, excessive root penetration and root crevice can easily occur, which reduces the fatigue strength significantly. These problems can be overcome by using the TIG welding techniques or certain other welding procedures, using ceramic backing strips. Another option is to apply the electron beam process. The fatigue strength is highly dependent on weld root quality. To ensure the quality of the weld root, permanent backing strips can be applied. However, stress concentrations will still occur at the connection between the backing strip and the weld.

In the previous section it has been mentioned that internal welding flaws cause discontinuities and hence severe stresses. The question, however, rises if the stress concentrations are related to the severe stresses due to the geometry. The importance of a welding flaw is related to the chance it will cause a severe stress in an area which could lead to a macro crack and if it would be possible if the stress severity caused by the welding flaw could interact with stress severity caused by the geometry of the weld.

If a transverse butt weld is at a free plate edge, the stress concentration introduced by the weld is intensified. Also, the weld shape near a free edge is more likely to have a poor shape. Therefore, the fatigue strength of the joint is likely to be reduced.

7.4 Longitudinal butt welds

A longitudinal butt weld is a connection between two plates with a linear weld between them, one sided or two sided. The plates are loaded parallel to the weld. In longitudinal butt welds, the profile does not introduce any severe stress in the section. Severe stresses are introduced by discontinuities in the length of the weld, for example the start/stop of the weld, where the electrode is changed during the welding process. The severe stresses in longitudinal butt welds are less high than the severe stresses in transverse butt welds. Therefore, longitudinal butt welds tend to have higher fatigue strength.

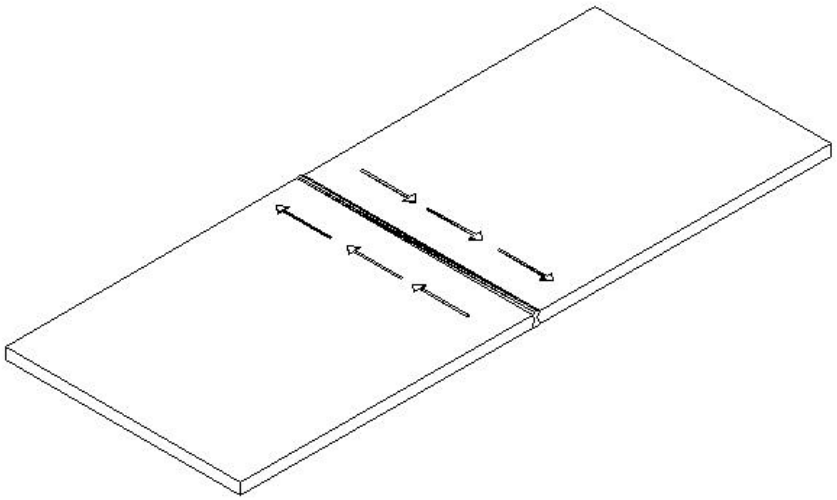

Figure 23: Longitudinal butt weld

There are some differences between the automatic and manual longitudinal butt welds. The automatic welds do not have the start/stop positions and they have hardly any ripples. Therefore, automatic produced longitudinal butt welds tend to have superior fatigue strength. Incomplete penetration, one sided or two sided, does hardly affect the fatigue strength of the welding, as long as it is more or less continuous over the length of the weld. In case of one-sided butt welds, a rough root bead will occur if the penetration is not continuous over the length. These weld ripples at the root bead are more important for the weld, as they can reduce the fatigue strength. In case of one-sided butt welds, they can be avoided by using continuous backing strip. If the strip is not continuous, transverse cracking from the root bead will occur in the boundary area between the two strips. The fatigue strength will drop dramatically if discontinuous backing strips are applied.

Longitudinal butt welds, as it is mentioned before, result in more favourable fatigue strength, if the weld is produced continuously and if the end effect can be avoided. The end effect occurs at the end of one plate on the edge of another plate that is loaded. At this junction there is a large difference in stiffness between the single plate and the double plate. If the end effect occurs, the fatigue strength of the butt welds changes drastically. If the shape of the end weld is poor, the fatigue strength will drop even more. There should be a smooth stress transmission between the two plates, by applying a large radius between the two plates.

7.5 Fillet welded connections

7.5.1 Non-load-carrying fillet welds

A non-load-carrying fillet weld is a welded connection between a continuous, loaded plate and two perpendicular plates, which are not meant to transmit a certain load, figure 24. Fillet welds cause larger changes in the connection geometry than a fillet butt weld. Hence, the severe stresses due to these welds are higher and are the joints more sensitive for fatigue failure.

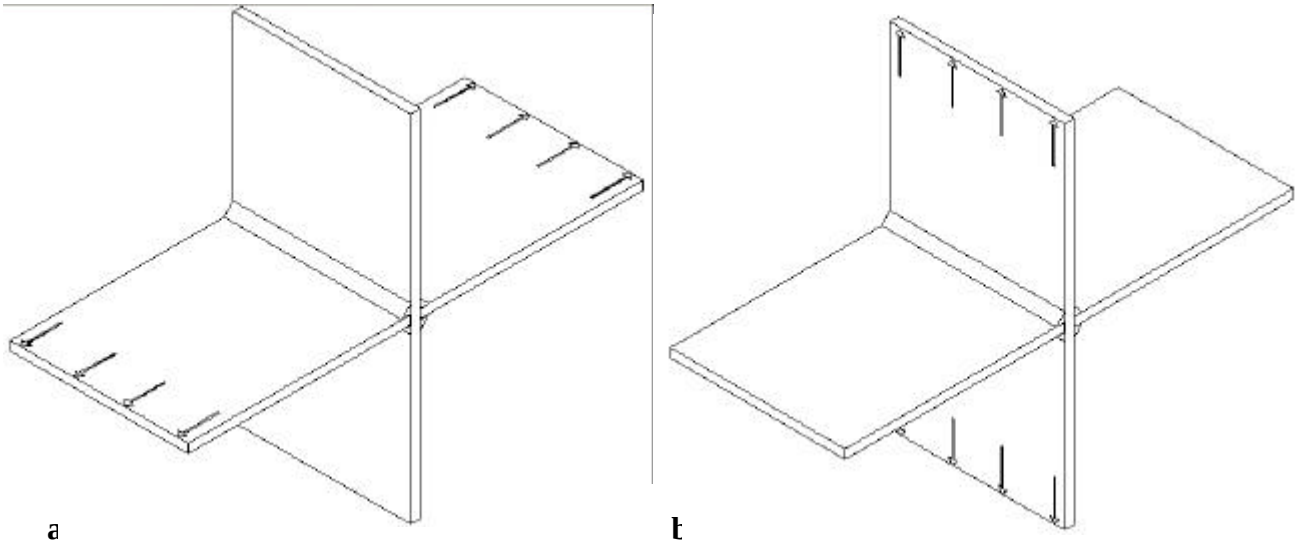

Figure 24: (a) non-load-carrying fillet welded joint, (b) load-carrying fillet welded joint

Non-load-carrying fillet welds are used to categorise a weld. It can happen that a single fillet weld is non-load-carrying for one type of stress in the connection and load carrying for the other stress. Non-load-carrying fillet welds are mainly used for a kind of attachment. Although they are not load carrying, non-load-carrying fillet welds do cause stress concentrations. For fillet welds, size effects are really important. Sizes that do affect the fatigue strength are the connection length and the plate thickness. In case of a double fillet welded transverse attachment, the highest stress concentration will occur at the weld toe. A crack will be initiated at the weld toe and grow through the plate. The actual fatigue strength depends on the fillet shape, the extent of any undercut and the plate thickness.
In some connections a single fillet weld is applied. In such joints, high stress concentrations also arise near the weld root. Fatigue cracking can initiate at the toe or the root. If the crack starts at the root it will not be able to detect this crack.

For non-load-carrying fillet welds, there is no advantage in making the attachment parallel to the direction of the stress, as cracking will initiate at the ends of the fillet weld at nearly the same load levels. At the end of the weld, a small transverse weld can be made. This hardly increases the fatigue strength, but protects the weld ends against corrosion.

7.5.2 Load-carrying fillet welds

A load-carrying fillet weld is a welded connection between two loaded plates in the same plane through a continuous plate. In load-carrying fillet welds, it is useful to differentiate the stresses in the weld and in the parent plate, in contrary to the butt welds, where the nominal stresses in the plates an welds are equal and the non-load-carrying fillet welds, where the main stress are transmitted through the main member. For load-carrying fillet welds, the nominal stresses in the member and in the welds

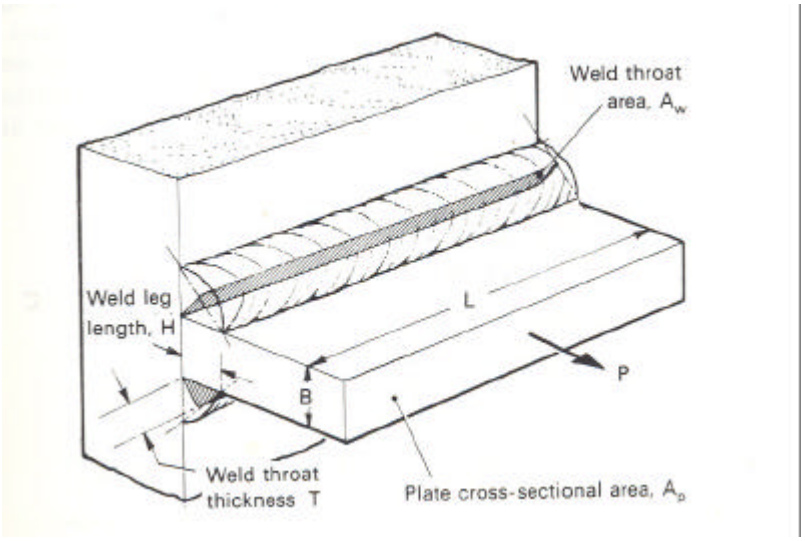

Figure 25: model of a load-carrying fillet welded joint

can be different. In a load-carrying fillet weld, the load P is carried by two weld throat areas, $2A_w$, where the throat area is equal to the weld length L multiplied by the throat thickness T (figure 25). The weld can be dimensioned by comparing the calculated stresses $\sigma_d=P/2A_w$ with the maximal allowable stresses. The ratio plate /weld stress, $2A_w/A_p$, is referred to as the design ratio. This way the stresses for static load should be able to examined. However, to examine a cyclic loaded joint is more complicated. In a cruciform joint there are two locations of stress concentration. Locations where cracks may initiate, are the weld root and the weld toe at the two discontinuous plates. The place where the stress is the most severe depends on the ratio leg length/plate thickness, in which the leg length is the height of the weld. The stress flow in a load carrying fillet weld is given in figure 26.

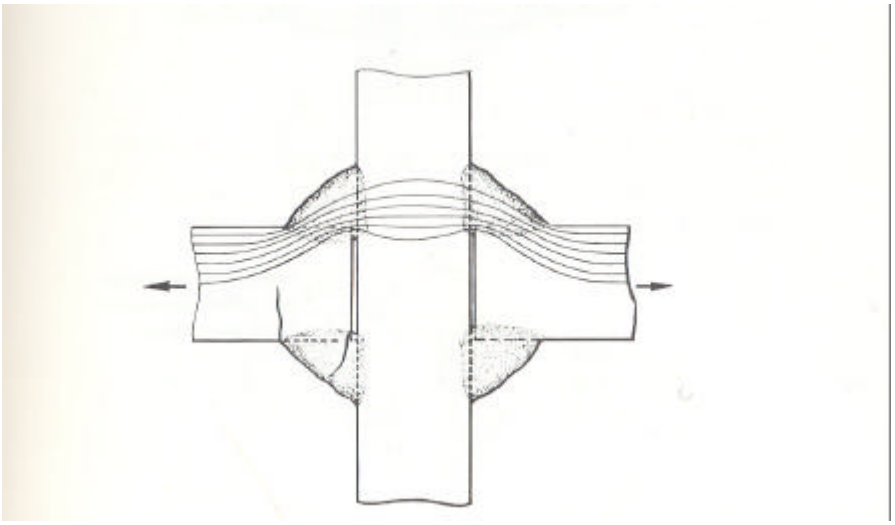

Figure 26: stress flow through a load carrying fillet weld

To improve the fatigue strength of the connection without increasing the amount of material required, partial penetration can be used (figure 27). The stress concentration at the weld is reduced and also the concentration at the toe tends to be decreased. If the partial penetration is extended through the plate, little advantage can be made. The result of the full penetration is a transverse butt welded joint.

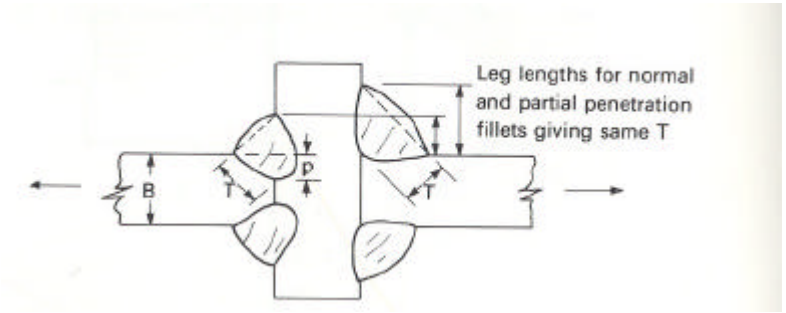

Figure 27: partial penetration of a fillet weld

In case a welded T joint is made and the transverse member is loaded by bending, an extra failure mechanism occur, namely crack growth in the transverse member at the weld toe. The magnitude of the bending stresses has to be accounted.

Longitudinal load-carrying fillet welds are, like longitudinal butt welds, less sensitive for fatigue failure than transverse load carrying fillet welds. Longitudinal fillet welds are also less sensitive to size effects, as the changes of section at the weld toe and root become parallel to the load direction and do not act as a point of stress concentration. The weld ends and start/stop positions along the weld length can cause stress concentrations and do influence the fatigue life.

So far all fillet welds have tacitly been assumed to be double sided. Single sided fillet welds can be produced as well, but from a fatigue point of view, they are not very desirable. The fatigue strength of a single sided fillet weld is very poor. The weld will be exposed to secondary bending and cracks can initiate at both weld toes and the weld root.

8 Fatigue strength of bolted connections

8.1 Fatigue of bolted connections in general

8.1.1 Bolted strap joints

When a simple strap joint is loaded, as in figure 28, the loads will be transferred from the bolt onto the side of the hole. The load transmission will be concentrated on a small area, the bolts will be loaded on shear and the plate on block tearing. The stress flow along side the bolt hole is concentrated very close to the edges of the hole.

In a simple strap joint connection the load can be transferred from the plate to the strap by a single row of joints, or by multiple rows. In case of two rows, the two rows carry both the same loads. The pressure in the hole and the shear in the bolts are equal for both the rows. This is true if the strap thickness is equal to half the plate thickness. From a fatigue point of view, this can be unsatisfactory, because the row near the end of the plate carries a single load P and the one behind that row the double load 2P. The stress at the hole further away from the end can be written as

$$S_{peak} = \tfrac{1}{2}(K_t)_{pinloadedhole} + \tfrac{1}{2}(K_t)_{unloadedhole}$$

if S is the nominal stress in the plate. For the straps it will be the reverse, the highest stress will occur next to the other row of bolts. Fatigue cracks can occur at these locations of maximum stress. The cracks in the plate are invisible, as the straps cover them.
The fatigue failure mechanism will occur in the net section adjacent to the bolt holes.

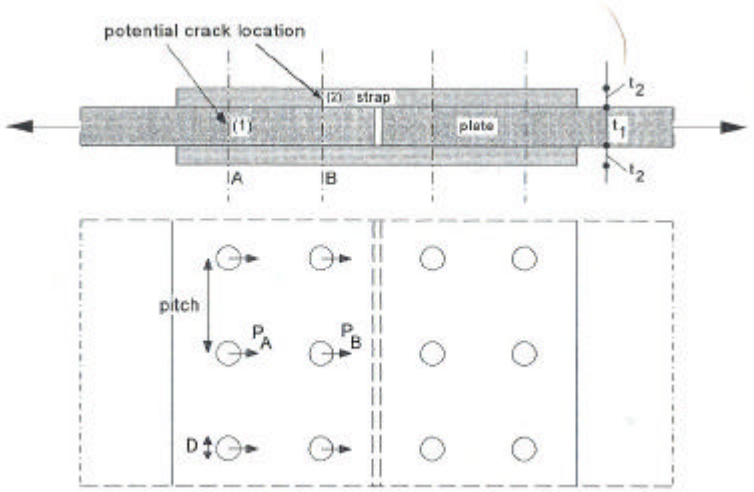

Figure 28: strap joint

8.1.2 Pre-tensioned bolted strap joints

Considering the load transmission in bolted connections, there is an obvious difference between the stress flow in regular bolted connections and pre-tensioned bolted connections. In case of a regular bolted connection the load will be transferred by block tearing in the plate and shear in the bolt. The load transmission in pre-tensioned bolted connections will occur through friction forces between the strap and the plate in contact surface. The transmission is no longer concentrated in the contact area of the bolt and the whole, but spread in a larger area around the bolts, see figure 29. The stresses at the edges of the holes are even lower than in the rest of the section. Because the stresses are spread over a larger area, the connection is less vulnerable for fatigue failure. The fatigue failure also has different features. The fatigue cracks will be initiated on other locations, rather far from the holes.

Tiny cracks in the plate and the strap surface will be initiated as the consequence of the difference in strain between the strap and the plate. The cracks will occur behind the holes, instead of next to the hole. Hence, fretting will start at the surface and the cracks will propagate. From a fatigue point of view, the pre-tensioned connections are more favourable to the regular connections, as the stress concentrations at the material surface are much smaller and not concentrated at the edge of a hole.

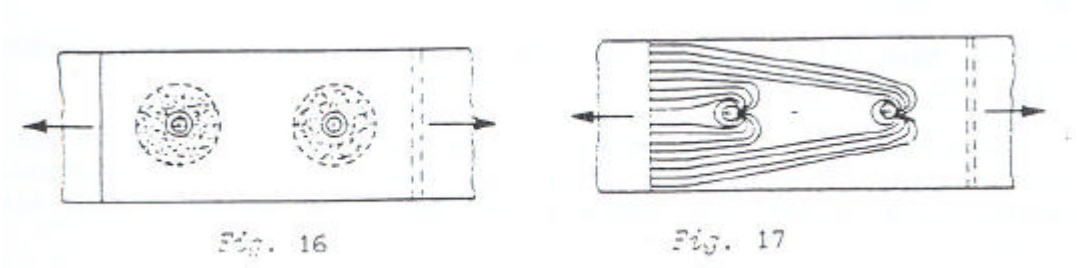

Figure 29: the load transmission areas in bolted joints, left: pre-tensioned joints, right: unpre-tensioned joints

8.2 Bolted joints loaded in tension

Bolts in tension are often used in structures. From a statically design point of view, bolt connections are fine connections considering easy assembly. From a fatigue point of view, bolts are rather poor, because of the notches and abrupt changes of shape. Stress concentration can occur at three places in the bolt:

- In the transition zone between the bolt head and bolt shank
- In the screw thread
- In the groove between the shank and the thread (not always present)

The bolt is loaded on the bolt head, close to the root of the notch. The radius of the notch cannot be made too big, otherwise the bolt will not fit the hole, and hence rather high values for K_t are obtained. The bottom plate of the bolt head should be fixed parallel to the plate beneath, otherwise bending will occur and the stress will be increased further.

The radius of the groove between the shank and the thread is larger than the radius of the screw thread itself, and hence it will not be critical. The radii of screw threads are standardised at low values, leading to high stress concentrations. The load transmission of the bolt to the nut is inhomogeneous, the largest contribution is being given by the first thread, so the stress concentration near this thread is high. Most fatigue failure occurs at this location.

Changing the geometry of the bolts could reduce the severe stresses due to tensile forces in bolted connections. However, the fatigue failure is usually avoided by applying pre-tensioning and high quality bolts.

Screw threads in bolts can be produced by two methods, cutting and rolling. For cyclic loaded bolts, rolled threads are recommended, because of the superior surface quality and the residual compressive surface stress.

8.3 Fatigue of pre-tensioned bolted connections

8.3.1 Pre-tensioned bolted strap joints

If the bolts in a strap joint are pre-tensioned, a different load transmission will occur. The load transmission will not any longer occur by block tearing and shear, but through friction forces between the strap and the plate in contact surface. The transmission is no longer concentrated in the contact area of the bolt and the whole, but spread in a larger area around the bolts, see figure 24. The stresses at the edges of the holes are even lower than in the rest of the section. Because the stresses are spread over a larger area, the connection is less vulnerable for fatigue failure. The fatigue failure also has different features. The fatigue cracks will be initiated on other locations, rather far from the holes.

Tiny cracks in the plate and the strap surface will be initiated as the consequence of the difference in strain between the strap and the plate. The cracks will occur behind the holes, instead of next to the hole. Hence, fretting will start at the surface and the cracks will propagate. From a fatigue point of view, the pre-tensioned connections are more favourable to the unpre-tensioned connections, as the stress concentrations at the material surface are much smaller and not concentrated at the edge of a hole.

8.3.2 Pre-tensioned bolted joints loaded in tension

To overcome the poor fatigue behaviour of bolts, pre-tensioning the bolts can be a solution. Pre-tensioning influences the stress amplitude in a bolt under cyclic load. When bolted connections are assembled, it is usual to apply a prescribed torque moment, introducing an axial load in the bolt. This axial load, the pre-tensioning, increases the mean load, but decreases the stress amplitudes under a cyclic load. Hence the resistance against fatigue failure can be significantly increased. An important condition for this increment is that the contact area between the two connected parts coincidences with the load path of the applied load. The cyclic load on the structure should result in a reduction of the load transmission of the contact area. In the unloaded situation, there is a pre-tension force in the bolts, F_B, which makes equilibrium with reaction force in the contact surface area, F_{CS}. This can be described the following formula

$$P_{bolt} = P_C$$

If a tensile force would be applied on the connection, this should lead to a reduction of P_C and a small increase of P_{bolt}, at least until the external tensile force P reaches the level of the pre-tension force. This can be expressed as:

$$P_{bolt} = P_C + P$$

However, if P reaches a value beyond P_{bolt}, then the bolts will have to take all the extra force. In this model, the stress range in bolts is strongly reduced, as can be seen in figure 30 below, as long as P does not exceed P_{bolt}. This behaviour is very desirable from a fatigue point of view, because for a certain loading domain, there would be only a small load change in the bolts.

The ratio $?P_{bolt}/?P_C$ is determined by the stiffness ratio of the bolts and the contact surface. The fact that the pre-tension force deforms the bolts does not affect the fatigue behaviour of the bolts in a negative way.

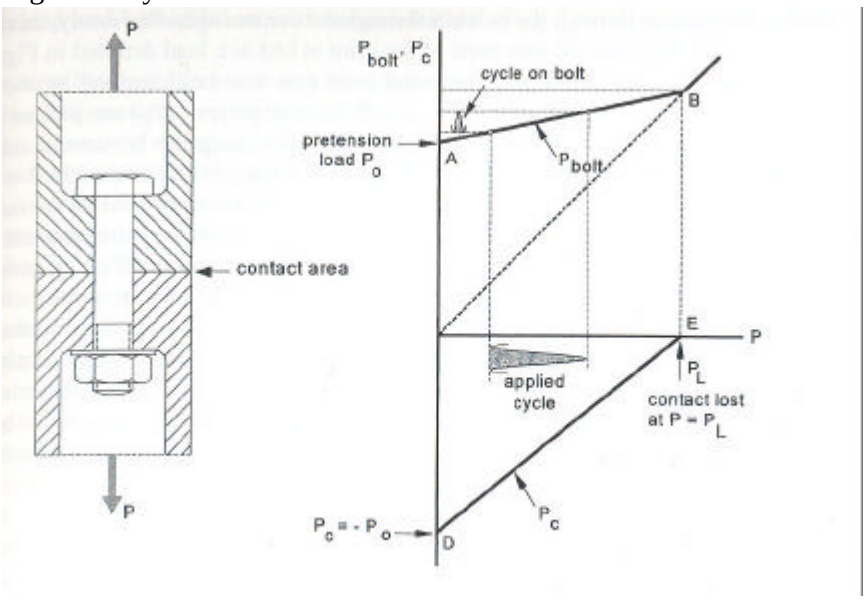

Figure 30: effect of pre-tensioning on the stress amplitude in a bolted joint

9 Fatigue strength of adhesive joints

Adhesive bonding of metal can be achieved under closely controlled conditions. Adhesive bonding of metal-to-metal joints is common to the aircraft industry, but is used in industrial products such as busses as well. Tensile loads on metal-to-metal bond line have the risk of peeling, but strength and fatigue resistance under shear loading show appropriate test results.

Adhesive bonding and riveted joints are both used in lap joints of thin sheet materials. Adhesive bonding joints have the advantage of the absence severe stress concentrations, in contrary to riveted joints, in which the sheets are connected at a discreet number of points. In adhesive joints the plates are continuously connected in the lapping area of the plates, therefore severe stress concentrations do not occur. Another advantage is that there is no metallic contact between the mating materials, so fretting does not occur.

In adhesive joints, two failure mechanics occur, bond line failure and metal failure, figure 31. Bond line failure is cohesion or adhesion failure, respectively failure of the adhesive and the failure between the adhesive and the sheet. Bond line fatigue failure can occur under high amplitudes and short laps. Due to the improvement of adhesive techniques and preparation of the lap surfaces and the avoiding of short laps, bond line failure hardly happens. For a thin substrates sheet metal failure is the dominant fatigue failure. The sheet metal failure is the result of the stress concentration near the end of the lap and the secondary bending stress on the same location. The stress concentration because of the abrupt thickness difference is the lower than expected, because of the difference between the elastic moduli of the sheet and the adhesive. The stress concentration because the secondary bending can be reduced by increasing the lap length.

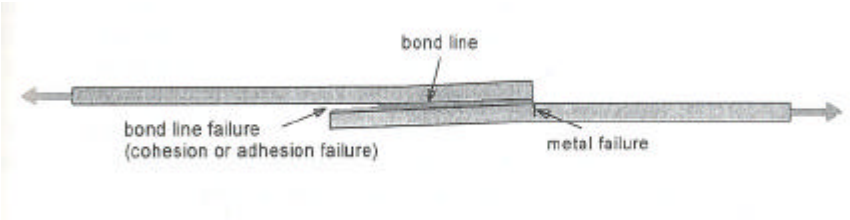

Figure 31: crack initiation is adhesive joints

10 Design of aluminium structures susceptible to fatigue

10.1 Introduction

In this chapter, some of the specific design characteristics for aluminium structures are considered, according to Eurocode 9, part 1-3. Eurocode 9, part 1-3 concerns a number of topics:

- Design methodology
- Loading
- Stress analysis
- Fatigue strength

However, some subjects have been considered already in this report, both from a metallic perspective and a design perspective, some are not a point of interest regarding the scope of this report. Thus, only the specific aluminium issues will be regarded in this chapter.

10.2 Methods of fatigue design

In the code, three different ways of fatigue design are distinguished:

- Safe life design
- Damage tolerant design
- Design by testing

Safe life design

This method is based on calculations using upper bound values for the loads and lower bound fatigue endurance data. This will provide a rather conservative estimate of the fatigue life. Threatening damage will not occur and inspection is not essential to assure safety. To predict the fatigue life, the Miner rule can be applied.

Damage tolerant design

This method is based on allowing crack growth to some extent. Periodical inspection is required to assure safety. When cracks in the structure would occur at a pre-determined size, the part with the crack should be changed or repaired. Because the chance that the structure needs maintenance at some moment is high, the structure will be out of service some period. Crack initiation locations have to be determined on forehand.

Design by testing

Design by testing should be applied in case response data, fatigue strength data, load data and crack growth data are not available.

10.3 Fatigue strength

10.3.1 Detail categories

Like the steel details, the aluminium details are divided into a number of categories, each with their own SN-curve. The fatigue strength of a detail takes into account the following aspects:

- The direction of the fluctuating stress
- Location of crack initiation
- Geometrical arrangement and relative proportion of the detail

It may also depend on:

- The product form
- The material (unless welded)
- The method of fabrication
- The degree of inspection of fabrication

- The quality level (in case of welds and castings)

The details are divided into seven basic groups
- Non-welded materials in wrought and cast alloys
- Members with welded attachments, transverse weld toe
- Members with welded attachments, longitudinal weld toe
- Welded joints between members
- Crossing welds/built-up beams
- Mechanically fastened joints
- Adhesively bonded joints

10.3.2 Fatigue strength data

The general relation between the number of load changes, load levels end SN-curves has been referred to in chapter 4. In case of fatigue strength in aluminium structures the basic fatigue relationship in the range of 10^5 to $5*10^6$ cycles is defined by the equation:

$$N_i = 2*10^6 * \left(\frac{\Delta s_c}{\Delta s_i} \frac{1}{g_{Ff} g_{Mf}} \right)^{m1}$$

with
N_i is the predicted number of cycles to failure under stress range $\Delta\sigma_i$
$\Delta\sigma_c$ is the reference value of fatigue strength at $2*10^6$ cycles, depending on the category of detail
$\Delta\sigma_c$ is the principal stress range at the detail and is constant for all cycles
m_i is the inverse slope of the SN-curve, depending on the detail category
γ_{Ff} is the partial safety factor allowing for all uncertainties in loading spectrum and analysis of response
γ_{Ff} is the partial safety factor allowing for all uncertainties in materials and execution

This equation does not basically differ from the relationship in chapter 4, other than the application of safety factors.

In case of fatigue strength in aluminium structures the basic fatigue relationship in the range of $5*10^6$ to 10^8 cycles is defined by the equation:

$$N_i = 5*10^6 * \left(\frac{\Delta s_c}{\Delta s_v} \frac{1}{g_{Ff} g_{Mf}} \right)^{m_2} \left(\frac{2}{5} \right)^{m_2 / m_1}$$

with $m_2 = m_1 + 2$

The CA loading fatigue limit σ_f, assumed at $5*10^6$ cycles, is the lower boundary for damaging loads under constant amplitude. However, in case of the VA loading, the loading cycles will contribute to propagation of the cracks. To account for the damage of these cycles, the inverse logarithmic slope of the SN-curve should be changed from m_1 to m_2. The cut-off limit $\Delta\sigma_L$, assumed at 10^8 cycles is the absolute lower boundary for damaging loads. Any loads below the cut-off level should be assumed to be non-damaging. The specific SN-curve for a detail can be characterised by $\Delta\sigma_c$ and m_1. Each category in the Eurocode has its own $\Delta\sigma_c$, while the values for m_1 to m_2 remain unchanged. This does not apply to adhesively bonded joints. The detail categories are safe for all values of mean stress, but cannot only be applied for other environments than ambient. Application of m_1 to m_2 can result in a conservative approach for some spectra and result in uneconomical details. In these cases, experimental testing or a fracture mechanic approach could be considered. Details that are not covered by Eurocode should be assessed by reference to published data or alternatively, be tested according to the guidelines for testing for fatigue design, included in Appendix C of the Eurocode.

When the SN curve from steel, as seen in figure 9, is compared to the SN curve of aluminium, the following differences can be seen:

- The slope of the SN curve between 10^4 and $2*10^6$ loading cycles. In the general expression for the the SN curve

$$N_i = 2*10^6 * \left(\frac{\Delta s_c}{\Delta s_i} \frac{1}{g_{Ff} g_{Mf}} \right)^{m1}$$

  m_1 is characteristic inverse value the slope of the curve. In general, the value of this value will be higher for aluminium than for steel. .
- The value of the fatigue strength at $2*10^6$ loading cycles will differ, for details in the same category in aluminium and steel, the fatigue strength for aluminium will be significantly lower than the fatigue strength of steel.

Points of interest in adhesively bonded joints
- Reduction of peel loading to a minimum
- Minimisation of stress concentrations
- Strains in the parent material should be kept below yield level
- Chemical conversion or anodising of the surfaces generally improves the fatigue life compared to degreasing or mechanical abrasion
- Aggressive environments usually reduce fatigue life

The reference fatigue strength of the adhesive joint regarding failure in the bond line is defined as

$$\Delta s_c = k_{c,adh} * f_{v,adh}$$

where
$k_{c,adh}$ is the adhesive joint fatigue strength factor k_{adh} at $N=2*10^6$ cycles
$f_{v,adh}$ is the characteristic static shear strength of the adhesive obtained from a standard static lap shear test

Testing under representative conditions of geometry, environment and environment is recommended for critical applications. If these tests are not executed, high security factors have to be applied.

Mean stress effect
In the Eurocode, the load ranges used to categorise the several details have been obtained under relatively high mean stress conditions. In case the mean stress in a certain detail is compressive or lowly tensile, the fatigue life of this detail may be enhanced. The recommended method to calculate the mean stress for simple loading cycles is the Reservoir counting method, and for longer and more complex loading histories the Rainflow counting method. The conditions under which this enhancement is allowed are:
- Plain material and mechanically fastened joints:
  - In case the absence of residual stresses and fit stresses can be assured.
- Welded joints
  - In case fatigue tests have been performed that simulate the true final state of stress, which account for final residual or fit stresses, and result in consistent higher fatigue strength.
  - In case fatigue strength improvement techniques, that have been proven to result in compressive residual stresses, are being applied, but only in case that yielding in service will not reduce the compressive residual stresses.
- Adhesively bonded joints
  - No allowance for effect for mean stress
- Low endurance range
  - For the loading periods of 10^3 to 10^5 cycles a check should be made to ensure that the tensile stresses will not exceed the ultimate state limit design resistance values for the detail.

Not destructive techniques of investigation on fatigue cracks in an aluminium bridge deck

Jaap Strik
S448826

June 2004

Preliminary report B1
A 2005-13
O 2005-09

Introduction

When a structure is exposed to cyclic loading, fatigue cracks can cause significant damage and fatigue failure can be a critical failure mechanism. To avoid fatigue failure in service, basically two design strategies can be applied: safe life design or damage tolerant design. In case of safe life design, the structure is designed to avoid fatigue cracking during the predetermined. In case of failure tolerant design, damage due to the fatigue mechanism is allowed to a certain extent. Needless to say, the damage tolerant design philosophy will most often result in lighter structures than the safe life philosophy. However, in case fatigue damage is allowed to a certain level, one should be able to assess the damage that occurs in the structure and a measurement plan should be provided. In this report, the possibilities to detect and quantify the fatigue damage in an aluminium bridge are investigated.

Recently, an aluminium bridge is developed by the department of Building Structures of TNO Bouw. The design of the bridge consists of two basic elements: a box girder and the roadway of the bridge. The main point of interest of this bridge is the aluminium roadway, consisting from extruded zigzag profiles that span between the box girders. The box girder and the zigzag profile are parallel to the driving direction of the traffic on the bridge, shown in figure 1.

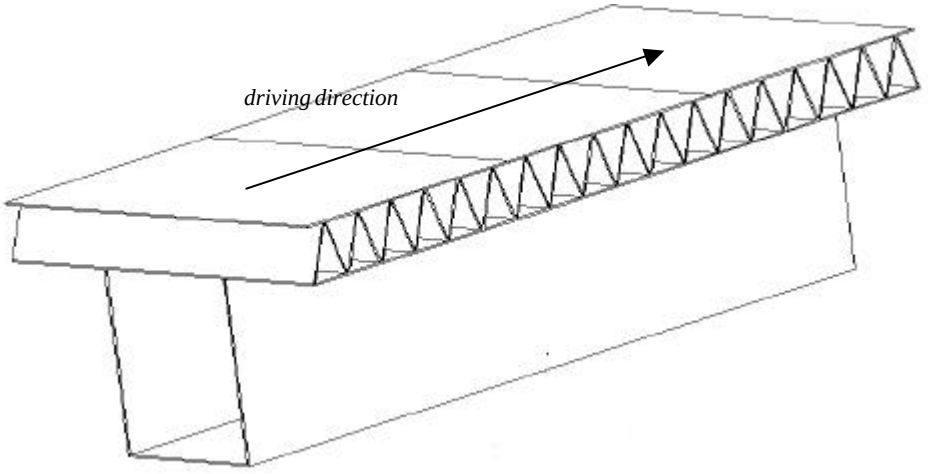

Figure 1: Isometric view of the box girder and zigzag roadway

The extruded zigzag profiles are connected by welds in the top plate and bottom plate. The upper connection in the roadway is the point of interest in this research. The connection and the possible locations of the cracks are given in figure 2. Cracks are the first sign of fatigue failure

When the roadway is used in service by cars and trucks, there will occur a cyclic load at the welded joint. This cyclic load can result in fatigue failure after a number of cycles. To simulate the fatigue behaviour of the structure under these loads, both the welded roadway panels and two partially scaled model of the bridge have been tested on fatigue failure experimentally. In case of the roadway, two groups, each with their own plate thickness, have been tested under three kinds of load levels, until fatigue failure occurs after a number of loads. The roadway sample with the plate thickness equal to the actual thickness of the real bridge has been selected for an investigation on the fatigue cracks near the weld. In figure 3 and 4 an example of a road way sample and a fatigue are given. Possible information that could be gathered about fatigue cracks : location (detection), initial angle of the defect, depth of the crack. To be able to investigate a bridge in service, non destructive techniques (NDT) have primarily been selected for the investigation. From the broad range of NDT techniques, ultrasonics is the first choice for these specimen and eddy current is the second option. The selection of the technique has been advised by dr. ir. M.C.M. Bakker and ing. S.C.H. Van Meer, both from the faculty of Aerospace Engineering of Delft University of Technology.

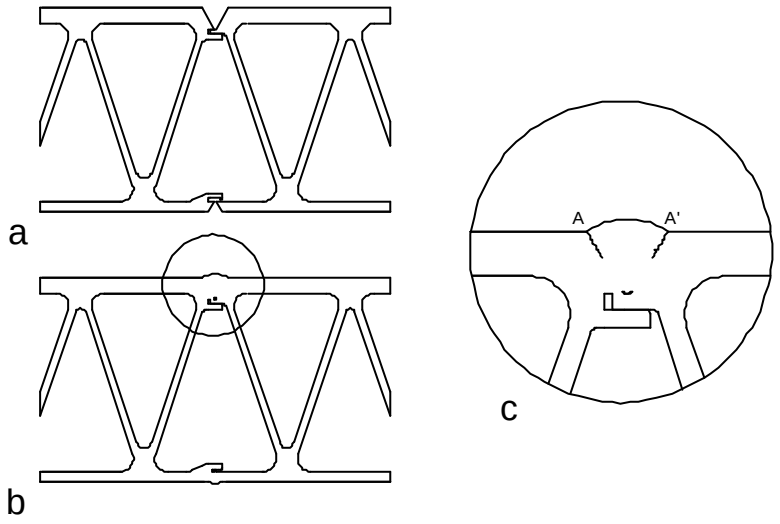

Figure 2: (a) the unwelded two extrusion profiles; (b) the welded connection; (c) the most likely location for cracks to initiate

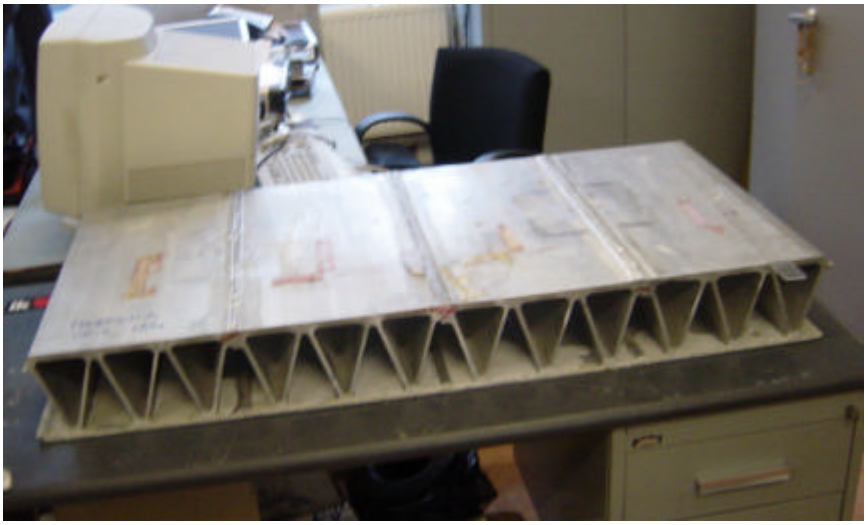

Figure 3: test specimen of the roadway

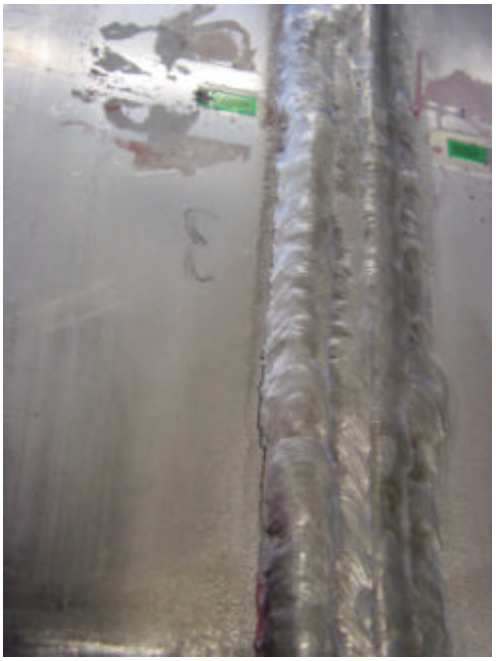

Figure 4: close up of the cracked welded joint

NDT Techniques

From all the available techniques, ultrasonics and eddy current have been selected to use for gathering information about the fatigue cracks. In this chapter, both techniques will be briefly described and the basic principles and the main points of interest will be pointed out.

Ultrasonic measurement

Ultrasonic measurement can be used for investigations of materials that are good wave conductors, such as metals. The main principle of ultrasonic measurement is that an ultrasonic signal is put into the material where it is reflected by discontinuities such as material edges, inclusions and defects. Hence the signal is captured again and by the amplitude of the signal and the time of transmission, information about the specimen can be derived. In ultrasonic measurement, three methods of measuring can be distinguished:

- Pulse echo
- Transmission
- Dual pulse echo

The differences between the methods are the number of sources and receivers required and the distance between the source and receiver. For pulse echo, the source and receiver are one and the same transducer. For transmission separate source and receivers are used and the measurement is applied over a significant distance between the source and receiver. In case of the dual pulse echo, a separate source and receiver are used, but the source and receiver are combined in a single measuring device, well separated by an acoustic isolator. The dual pulse echo method is used when the periods of sending and receiving overlap.

For this investigation, the pulse echo method has been used. Transmission measurements have been applied as well, but the geometry of the joint appeared to be too complex for transmission measurement and pulse echo proved more precise.

For ultrasonic investigation, different frequencies can be used to scan the material. For our research, three different frequencies have been used, 1.0 MHz, 2.25 MHz and 3.5 MHz. The pulse causes a wave field, as in figure 5. The wave field of the transducer can be divided in the primary beam and the secondary and tertiary high intensity beams. The primary beam is straight forward and it is the most intense beam, the secondary and tertiary bean are much weaker. For investigation, the primary beam is used; the smaller and weaker secondary beams can cause side effects like false reflections. Lower frequencies have a primary beam with a bigger radius than the higher frequencies. Hence for two transducers with equal capacity the intensity of the beam of the low frequency transducer is lower than the intensity of the high frequency pulse. Because the radius of the lower frequency has a bigger radius, there is more chance that a low frequency pulse of a transducer meets a discontinuity than a high frequency transducer. In general, the received pulse from a high frequency transducer will have a higher amplitude and will appear clearer on the interface of the measuring system. For the analysis of a material, a

combination of lower and higher frequencies can be applied, lower frequencies for global investigation, higher frequencies for more local investigation.

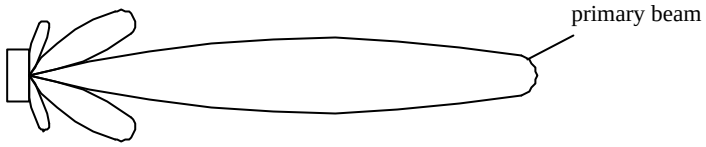

Figure 5: Ultrasonic wave field with primary, secondary and tertiary intensity beams

After the definite selection of the ultrasonic method for this welded joint, a number of scans have been made on varying locations, both cracked and uncracked, in order to recognise the phenomena that can occur in the measurements. Phenomena that can occur in the measurement are not only the fatigue cracks, but include the heat affected zone and the material surface as well. Collecting a number of scans of the connection, similarities can be recognised in the scans. Next, the differences can be analysed.

The scanning procedure goes as follows: at first the transducer is covered with a thin film of gel. The gel is applied to improve the transmission of the ultrasonic waves; the gel is a much better wave conductor than air. Hence the transducer is placed on the wedge. The bottom surface of the wedge, which will be placed on the material surface is also covered with a thin film of gel. The wedge is placed on the surface with one side first to let the out the air between the surface of wedge and the material surface as much as possible. The wedge is placed directly next to the weld toe on a reference position. The

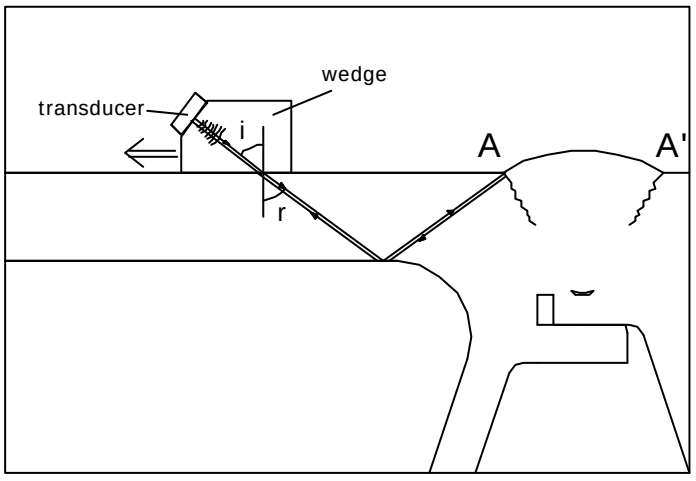

Figure 6: Method of detection using the echo pulse method with a single skip

distance between the focus point of the wedge (the point where the ultrasonic pulse is focused on when it is put into the material) and the weld toe is 10 mm for the constant angle wedges and 30 mm for the variable angle wedge. Subsequently, the wedge is moved away from the weld in steps of 5mm, as shown in figure 6. This scanning method has been performed under various angles and with various frequencies. A characteristic group of scans has been included, which will be discussed in the Results section. The scans can be divided in two groups, A-C and D-G. Scans have been made with a circular .5 inch radius transducer, connected regular perspex wedge, figure 8. Scan D-G have been made with a rectangular .5*1.0 inch inch transducer with a variable angle perspex wedge, shown in figure 7.

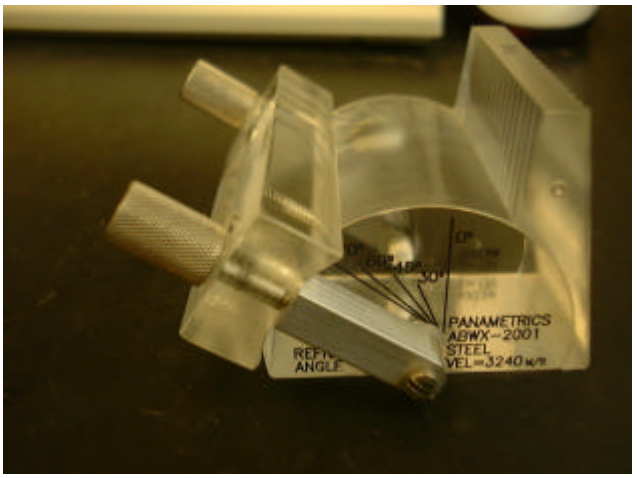

Figure 7: Wedge with variable angle

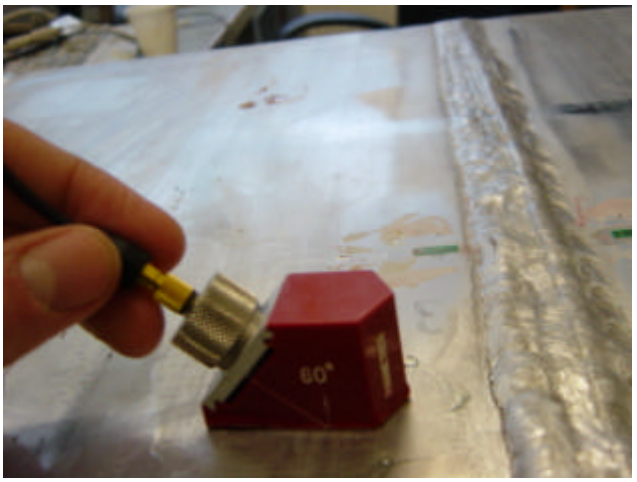

Figure 8: transducer on a regular wedge

Eddy Current

Eddy current technique uses the differences in electro-magnetical properties of metal and air. Eddy current is based on the following principle: a coil with a high frequency current is held close to the material surface. The high frequency current results in an electro-magnetical field, shown in figure 9. The electro-magnetical field causes an electric current at the surface of the metal. In case there is a discontinuity in conductivity near the surface, such as a crack (air is a very bad electrical conductor), the electro-magnetical field will be influenced and hence a crack can be detected.

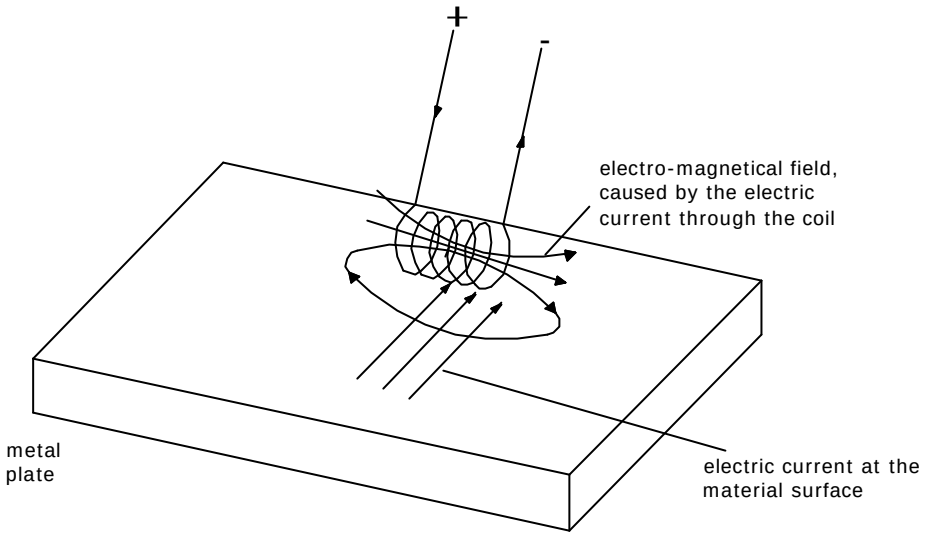

Figure 9: principle of eddy current: an electronic current is sent through a coil, causing an electro-magnetic field that causes an electronic current at the material surface.

Eddy current has been used in this investigation to detect cracks near the surface, which worked quite well. However, eddy current is suitable mainly for detection and cannot provide any further quantitative information about the crack, likethe angle of initiation or the crack depth.

Results

Graphical output

During the measuring a signal is received between 0 to 120 µs after the pulse has been sent for a constant wedge measurement and between 20 to 140 µs for a variable wedge measurement. The measurements are taken on different locations. All positions of a measurement series are on a straight line. The distance between two successive measuring spots is 5mm. In the graphical output of the measurements, the distance between the focus point and the weld toe has been placed along the horizontal axis. The time between sending and receiving the signal has been placed along the vertical axis. The intensity of the received signal is being expressed by the colour in the chart. Red represents a high intensity, blue a low intensity. The intensity presented in the graphical are *relative* intensity. In the first period after the transmission of the signal, no reception from the material should be expected, the signal would not be able to leave and re-enter the wedge in the intermediate time. Then, after some time, a reaction *could* be expected, but not necessarily. The maximum time is for our specimen defined at 120 µs.

The graphical results of the scans are divided in two groups: scans A-C and scans D-G. Scans A-C are made with a regular constant angle wedge, scans D-G with a variable angle wedge. All locations and assumptions about the way the plate the joint was cracked are shown in figure 10 and 11.

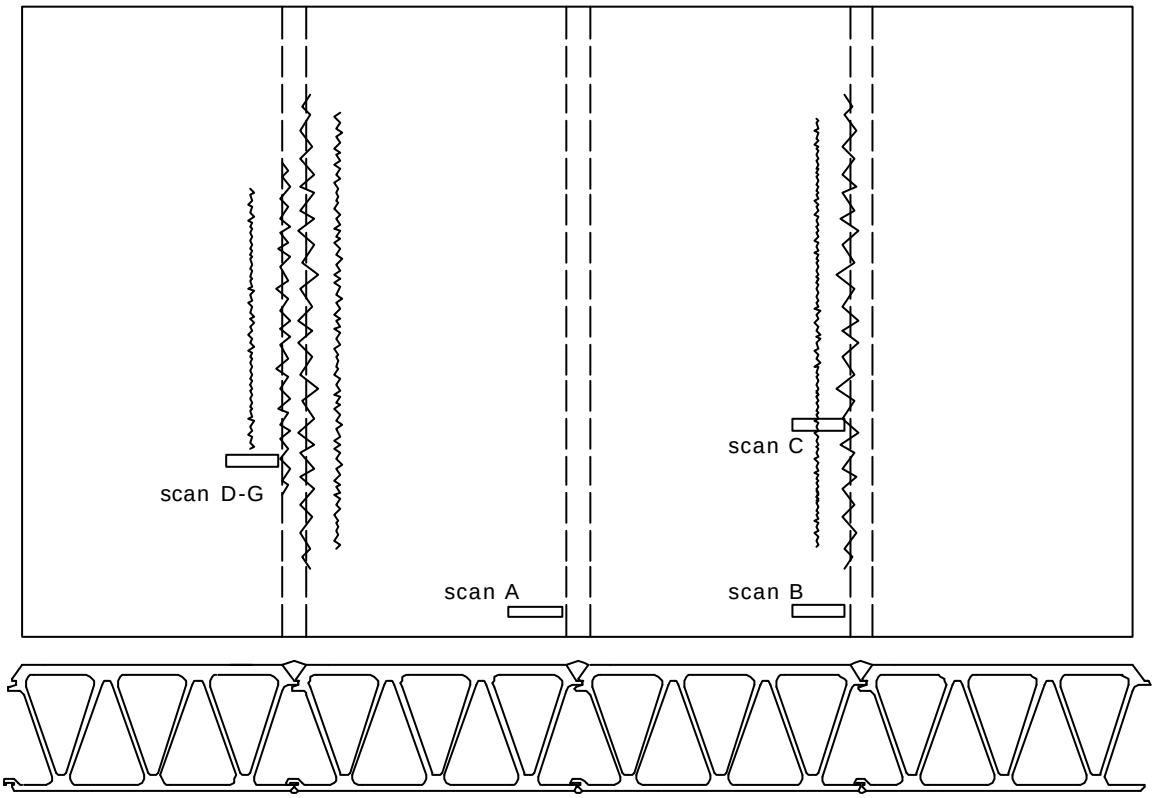

Figure 10: top view (upper drawing) and front view of the road way specimen, with the four scanning areas. In the to p views, two kinds of cracks can be distuinguished, namely the cracks at the weld toe (the rough crack line) and the crack in the middle of the 'triangle'(the fine crack line)

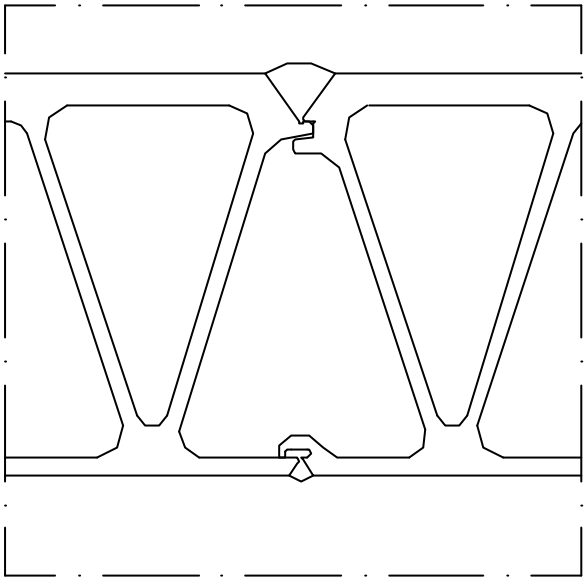

scan A-B

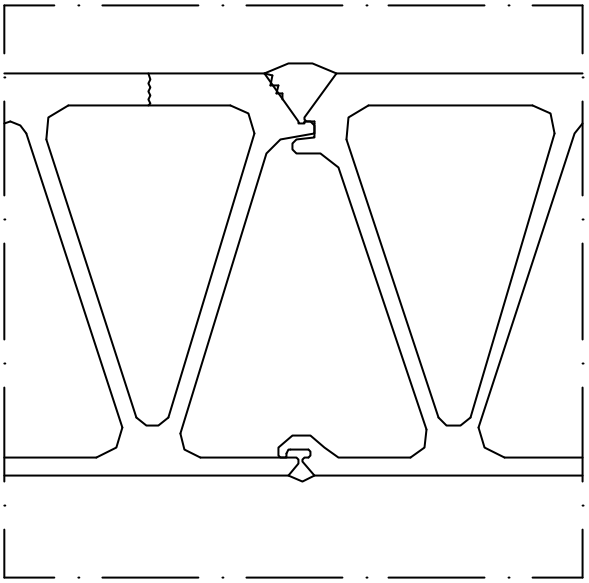

scan C

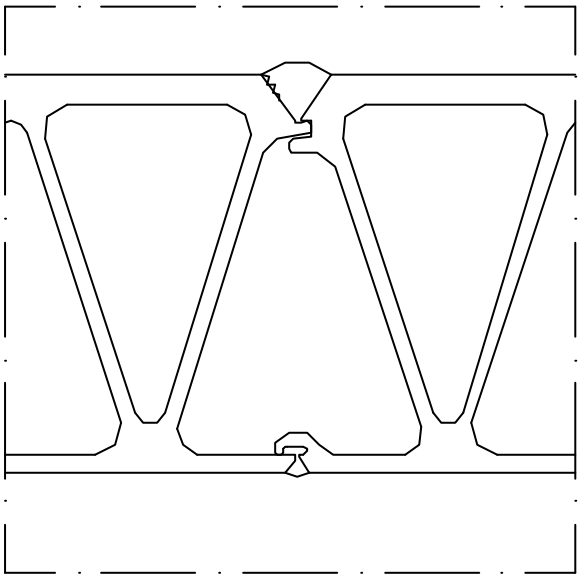

scan D-G

scan	angle	frequency [MHz]	defects
A	55	3.5	0
B	55	3.5	0
C	55	3.5	2
D	62	3.5	1
E	70	3.5	1
F	75	3.5	1
G	80	3.5	1

Figure 11: sections of different scanned areas. In scan A-B there are none defects, in scan C two defecst, one at weld toe and one at the mid of the span and in scan D-G there is one defect at thetoe of the weld. In the table the used angles and frequenciesare given

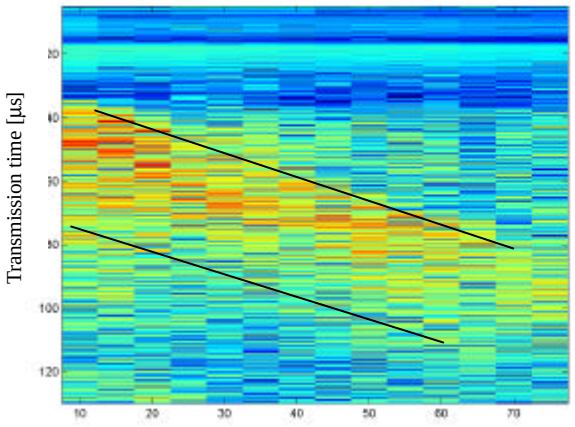

Scan A: 55 degrees angle, 3.5 MHz, no defect

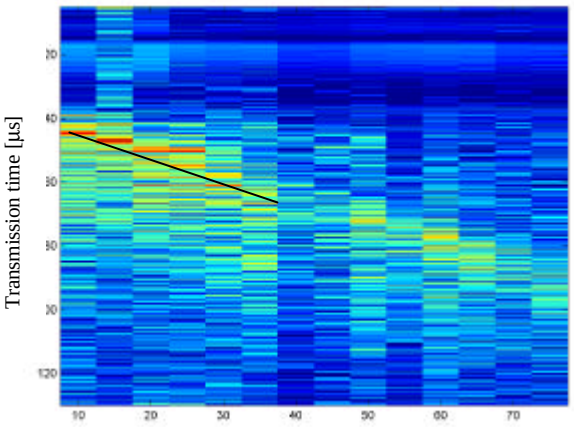

Scan B: 55 degrees angle, 3.5 MHz, no defect

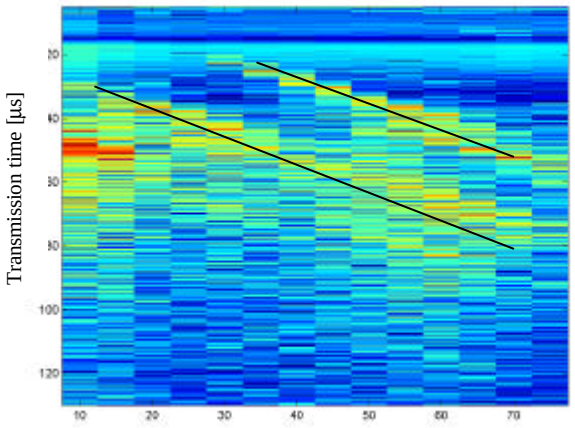

Scan C: 55 degrees angle, 3.5 MHz, 2 defects

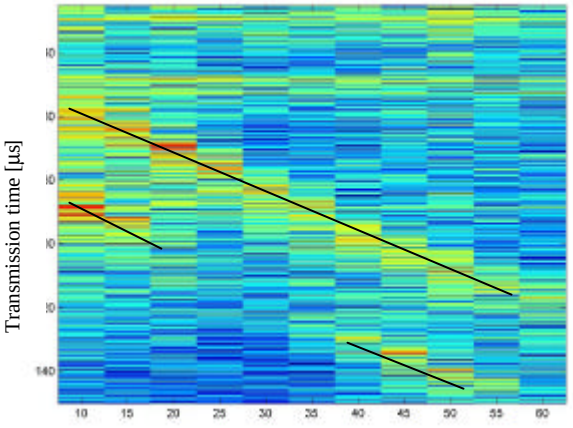

Scan D: 62 degrees angle, 3.5 MHz, 1 defect

Figure 1 : Graphical output of scan A-D

Detection

When the results of the scans of cracked and uncracked are compared, there can be differences between the scans. The graphical output of scans A-D is given in figure 12. The two uncracked scans have been performed on different welds. The heat affected zone in scan A gives a bit of a blurry response with a high intensity zone, while in scan B the details in picture are sharper. Both scans are of uncracked joints. When scan C and scan D are compared (notice that the wedges are different!) some tendencies can be distinguished, which are marked with black lines. When all scans, scan A-G (graphical output of scans E-G are shown in figure 13), are compared, the tendencies of the cracks become more clear and the typical crack gradient can be discerned. Scan C and scan D

have one main corresponding tendency, in scan C the lower line in scan D the upper line. The signals on that line have an equal transmission time in the aluminium, notice that two different wedges are used. The wedge of scan D is bigger than the wedge of scan C, the length of the transmission through the wedge is longer, therefore the delay of the signal. In scan C, another tendency can be spotted. When the surface is studied closely, a very crack be seen, see figures 10 and 11 for the location of the crack. The crack in the mid of the span must be very fine, because the crack at the weld toe is still visible even when the signal is passing the fine crack twice. The parallel cracks are larger at the bottom of the plate than at the top of the plate. A number of small cracks are visible. The small cracks are linked, but it can be seen that some of them have their own location of initiation.

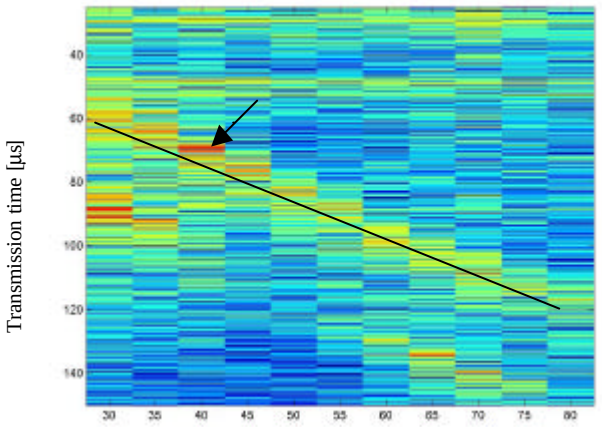

Scan D: 62 degrees angle, 3.5 MHz, 1 defect

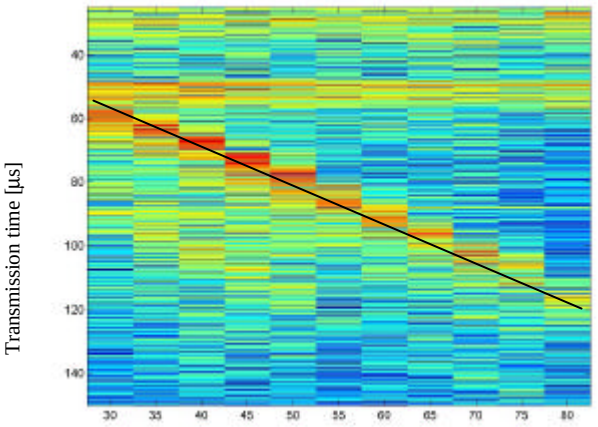

Scan E:70 degrees angle, 3.5 MHz, 1 defect

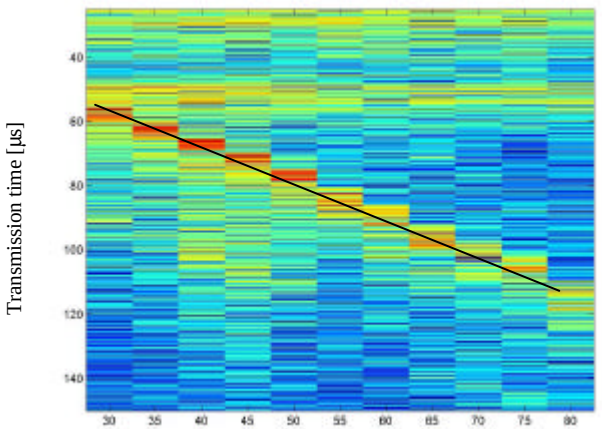

Scan F: 75 degrees angle, 3.5 MHz, 1 defect

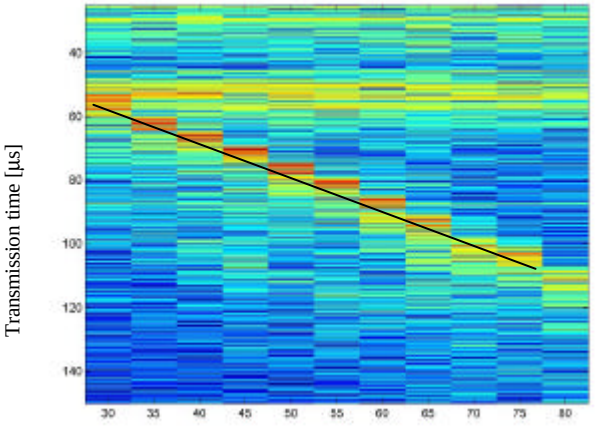

Scan G: 80 degrees angle, 3.5 MHz, 1 defect

Figure 13: Graphical output of scan D-G

Quantitative information

On a location where the parallel cracks were not present (figure 10), the scans D-G, using four different angles, have been made. The angle of the wedge has been va ried in order to find the complement of the angle of initiation of the crack. When the complement of the angle is used, the intensity of the received signal will be significantly higher than the other reflections. Hence in one of the scans, one clear red spot should occur, as the returned signal of the complementary angle at the weld toe should be much stronger than the other returned signals. One should be conscious that the initial angle not necessarily is found in the chart with 'reddest' line, in contrary! Mind that the intensities in the charts are all relative intensities.

The signal that comes out the most clear is the signal in scan D, the 62 degree scan. At about 40 mm and 65 µs the received signal appears to be the strongest; this spot is marked by the arrow. In scan E-G the response around this time is also quite strong, but the difference is not so obviously clear. The angle and the skipping model, shown in figure 6, could be compared with a model of the used scanning configuration, used in this particular scan. The assumed ultrasonic model is a model in which the wave field skips once at the bottom of the plate, next it is reflected by the crack tip and skips again at he bottom of the plate and arrives at the transducer. The incoming and outgoing angle between the signal and a flat plate are equal.

Checking the angle r (figure 14), if the signal would be reflected precisely at the crack tip and the skip would perfectly symmetric:

$$\tan(r) = \frac{\frac{1}{2}u}{t}$$

where:
u is the distance between the focus point and the weld toe
t is the thickness of the plate
u=40 mm; t=11.8mm

r=60°

Considering the discontinuous measuring, a deviation of 2° is a reasonable deviation. If the complementary angle r is 62°, then the initial angle of the crack s would be

s=90°-r=28°

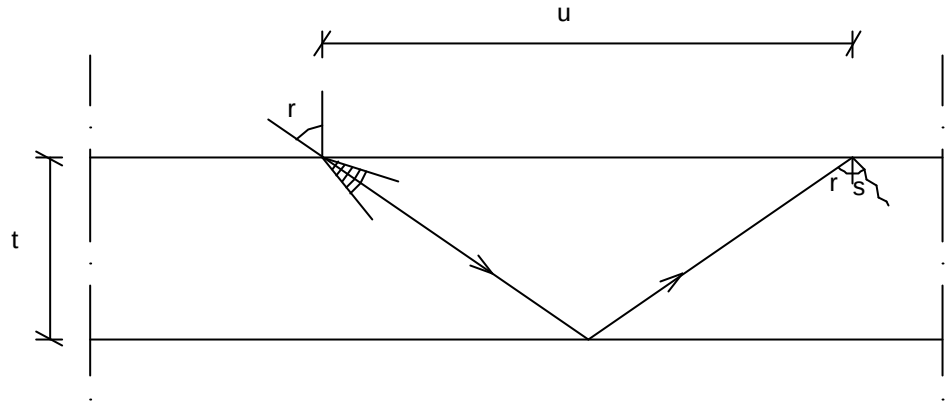

Figure 14: checking the initial angle

Quantitative predictions about the crack depth could not be made using the pulse echo technique on this specimen.

Conclusions

- The ultrasonic detection technique for fatigue cracks in the welded connections in this part of the aluminium bridge is suitable.
- A rough estimate of the initial angle of the fatigue crack at the weld toe can be made using ultrasonic detection.
- The fine cracks in the middle of the plate (shown in the drawing of Scan C, figure 10), parallel to the weld toe have apparently been initiated at the bottom of the plate, since the crack is much longer there. During the experiments a variable amplitude pressure will be applied on the surface on top of the specimen. This load causes a bending moment, which is taken by the plate and the weld. When the crack at the weld toe has been initiated and the crack grows into the material, the capacity of the weld toe to handle the bending moment in the plate will decrease. Hence, the bending moment in the mid of the span will increase. Stresses will increase as well, and the crack can be initiated.
- Parallel cracks, as they have appeared in this specimen, do influence the precision of the scanning of the cracks at the weld toe. Thus, making a precise scan of the whole welded connection with this method will be complex, as there is a lack of space between the weld toe and the parallel cracks.
- Quantitative estimations of the crack depth cannot be made with the presented method of investigation.
- Considering the fact that at every given scan in this report there was a kind of graphical output, it can be stated that for an appropriate application of ultrasonic detection, sufficient experience is required. For the scanning of a single joint, multiple scans are required in order to gain any unambiguous information about the crack.

Discussion and recommendations

Considering the results of this investigation, the pulse echo technique is an appropriate technique for detection of cracks in this part of the aluminium bridge. However, the presence of fatigue cracks does not imply that the structure will fail immediately. In contrary, it could remain in service for much more loads cycles before it requires maintenance. To be able to state whether or not it is safe to use the use the structure, one has to know how deep the crack is. The ultrasonic technique considered in this report is not suitable to give quantitative information about the depth of the crack in this particular structural element. The application of lamb waves (low frequency waves with a wave length bigger than the plate thickness, making the whole plate vibrate) using dual pulse echo technique is thought to be a possible alternative in this case. By measuring the amplitude of the waves in this plate, the crack depth could be estimated. Because the sending and receiving period will overlap, a dual pulse echo transducer should be applied.

Modelling crack growth and fatigue life predictions in adhesively-bonded joints

Jaap Strik
S448826

July 2004

Preliminary report B2
A 2005-13
O 2005-09

Nomenclature

a	crack length
a_f	crack length at final failure
b	width
c	half of the bonded overlap length
D	linear coefficient
D_f	flexural rigidity of substrate
D_{fc}	flexural rigidity of the bonded lap region
E_a	Young's modulus of adhesive
E_s	Young's modulus of substrate
G	strain energy release rate
G_c	adhesive fracture energy
G_{inf}	strain energy release rate for an infinitely long joint
G_{max}	maximum strain energy release rate applied in a fatigue cycle
G_{th}	threshold strain energy release rate
h	substrate thickness
k	bending moment factor
K	stress intensity factor
N	number of cycles
N_f	number of cycles to failure
n	linear curve fitting constant (Region II)
n_1	threshold curve fitting constant
n_2	fast fracture curve fitting constant
T	load per unit width
T_{max}	maximum load per unit width in a fatigue cycle
t	adhesive layer thickness
μ	shear modulus of the adhesive
s_{max}	maximum peel stress
t_{max}	maximum shear stress
?	Poisson's ratio

1 Introduction

When an adhesively-bonded joint is applied in service, it can be exposed to a variable loading resulting in fatigue failure. To be able to predict the influence of the fatigue effects on the life span of the joint, research should be performed. To be able to predict the fatigue behaviour in a structure in service, three approaches are available:

- Analytical research
- Numerical research
- Experimental research

The selection depends on the kind of information that is desired. In this report the crack growth, and more particular the influence of the crack depth on the energy release rate in a single lap joint are scrutinised. The investigation is split into two parts, namely modelling of the lap joint and comparison with analytical models. The investigation will be performed by a numerical finite element method (FEM) research. Next, the results of the FEM analysis will be compared with three analytical prediction methods, found in literature.

The main purpose of the investigation is to explore the possibilities to predict the crack growth using FEM analysis and to study the difficulties of this method. The investigation will focus primarily on a simple adhesively-bonded joint, a single overlap joint. The applied mechanical analysis in this case is linear elastic fracture mechanics, performed with the finite element programme DIANA 8.2.

2 Predicting fatigue life

To predict crack growth in joints different crack growth characteristics can be applied, such as the stress intensity factor or the energy release rate. The stress intensity factor is most common used characteristic used for fracture mechanics. However, concerning adhesively-bonded joints the relation between the energy release rate *G* and the crack length *a* is used in literature to predict the fatigue life of the joint as it describes the phenomenon the most accurate. The relation between the crack growth per cycle and the maximum applied strain energy release rate G_{max} per cycle can be described by the modified Paris' law. The modified Paris Law accounts for the threshold behaviour and the final failure, whereas the normal Paris Law only covers the crack growth in the linear range of the da/dN-? G diagram, region II in figure 1.

$$\frac{da}{dN} = DG_{\max}{}^{n}\left(\frac{1-\left(\frac{G_{th}}{G_{\max}}\right)^{n_1}}{1-\left(\frac{G_{\max}}{G_c}\right)^{n_2}}\right)$$

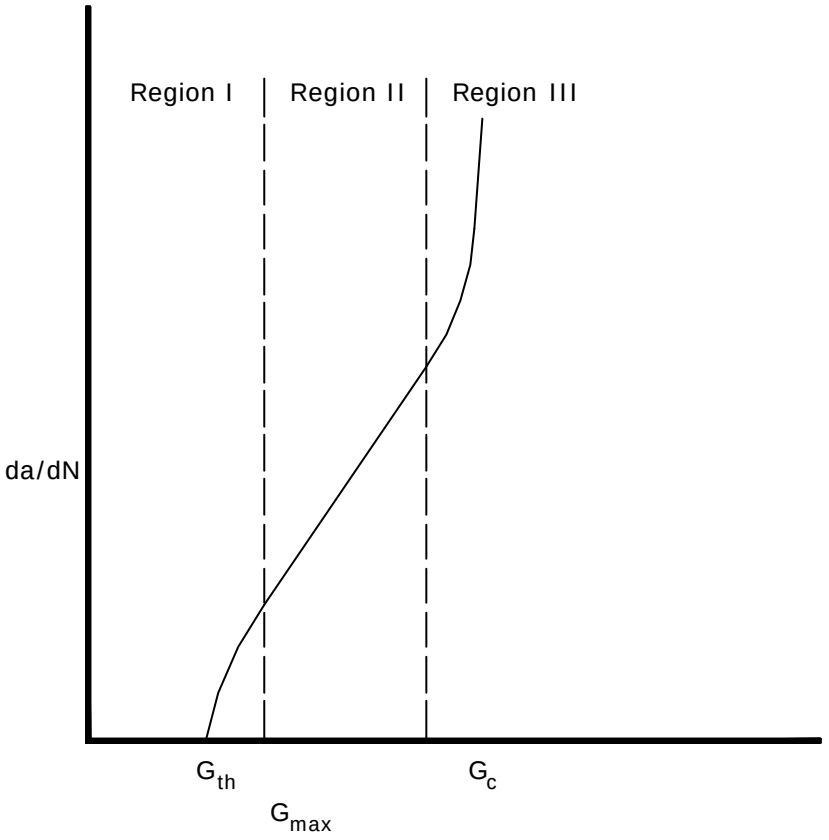

Figure 1: da/dN-G_{max} diagram

Paris' law can be rewritten and integrated in order to derive the number of loading cycles until fatigue failure (N_f):

$$N_f = \int_{a_o}^{a_f} \frac{1}{D G_{\max}^{\ n}} * \left(\frac{1 - \left(\frac{G_{\max}}{G_c} \right)^{n_2}}{1 - \left(\frac{G_{th}}{G_{\max}} \right)^{n_2}} \right) da$$

In this formula, crack depth a and energy release rate G_{max}, increase during the fatigue life of the joint. The crack depth a and G_{max} are related. G_{th} and G_c are respectively threshold strain energy release rate and the adhesive fracture energy. They are respectively the lower and upper boundary for G_{max} for crack growth in the joint. Every combination of materials, environment and pre-treatments has its own G_{th} and G_c. The values of these crack growth constants can be determined experimentally. The three curve fitting constants n, n_1 and n_2 can be derived from the da/dN-G_{max} diagram. The da/dN-G_{max} diagram can be determined experimentally.

The relation between a and G is dominated by the mode of the loading of the crack. Also, the position and the number of cracks may be of influence. Basically, a crack can be loaded by three different modes (figure 2):

- Tension (I)
- Shear (II)
- Tearing (III)

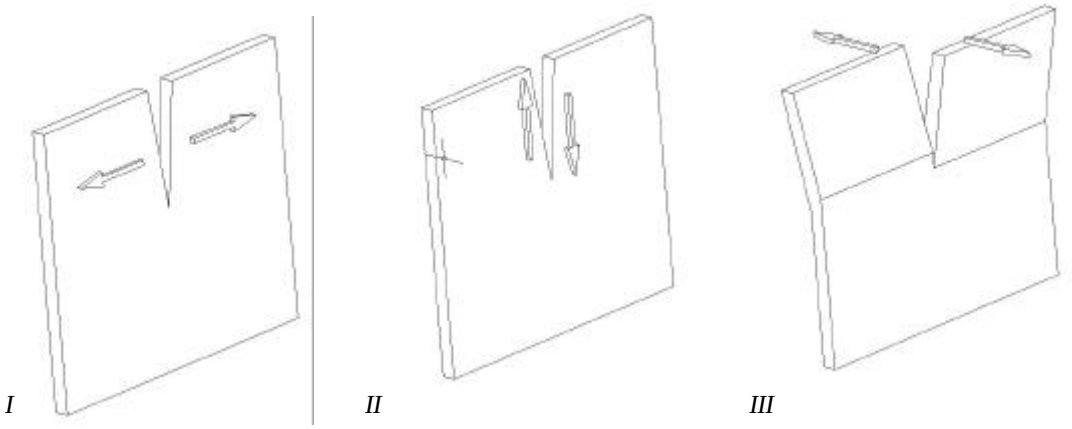

Figure 2: the three crack loading modes: 1 Tension, 2 Shear and 3 Tearing

For pure mode *j* $G=G_j$, for a mixed mode, G is the sum of G_I, G_{II} and G_{III}

.

For the single lap joint in this investigation, only the first two modes are of interest. The main point of interest is to find a suitable method to describe the relation between a and G_{max}. This relation can found both analytical and numerical. In literature, three different methods to relate a and G_{max} for a single lap joint with a crack at both ends have been found in 'The prediction of crack growth in bonded joints under cyclic fatigue loading, part II' by H. Hadavinia et al (International Journal of Adhesion and adhesives, 2003 463-471). These methods will be regarded later on in this report, in chapter 4. First, the numerical method will be focused on.

Resuming: in order to predict the fatigue life of an adhesively-bonded joint, described by the number of loading cycles under constant amplitude N_f, the relation between a and G_{max} should be described as accurate as possible. This relation between a and G is scrutinised using FEM calculations.

3 Modelling cracks in adhesively-bonded joints

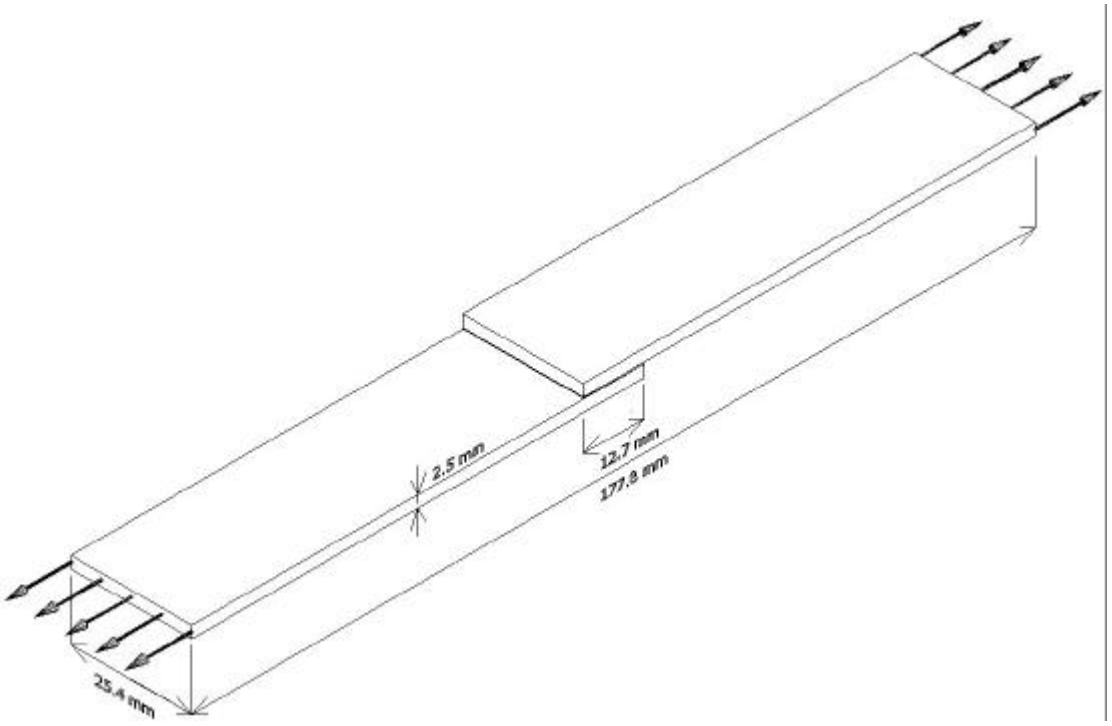

Figure 3: the single lap joint studied in this investigation

3.1 General modelling

The adhesively joint studied in this report is a single lap adhesively-bonded joint, shown in figure 3. The same joint has been used in 'The prediction of crack growth in bonded joints under cyclic fatigue loading, part I' by H. Hadavinia et al (International Journal of Adhesion and adhesives, 2003 449-469). All information used in this report with respect to material related crack growth properties and geometry has been obtained from this article. The joint can be modelled two dimensionally, as shown in figure 4. The joint has been modelled like it would be tested on fatigue in a laboratory. That means that both ends of the specimen would be clamped. Notice that at the right side of the model where the load acts, the horizontal displacement should be constant over the height. Therefore a constraint should be applied at the that surface. Not applying the constraint will cause serious inaccuracy. Both the substrate, aluminium, and the adhesive, (hot-curing toughened-epoxy-adhesive EA9628), have been modelled using 8 node plane strain elements. Severe stresses and strains are expected around the crack tip, therefore the mesh is the most dense there. The crack tip, where the most severe stresses will occur, has been modelled with a crack tip element. The crack tip element moves the mid nodes of the 8 node element around the crack tip to quarter-point position (a quarter of the length of one side away from the crack tip). The rearrangement of the mid nodes is required to be able to handle the stress and strain peaks near the crack tip. The crack tip element gives K and G as output.

In this investigation it is assumed that the crack will grow at the centre of the adhesive layer. Two cases have been studied, a single crack and a double crack.

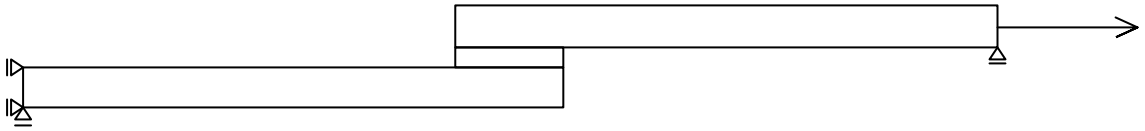

Figure 4: mechanical model of the single lap joint

The substrate and the adhesive, aluminium and epoxy both have their characteristic material properties. In this model, both materials have been assumed isotropic and elastic. However, in order to gain knowledge about how to make a FEM model of an adhesively-bonded joint, the E-modulus of both materials has been varied. The density of the mesh has been varied as well, in order to find the optimal number of elements to model the crack tip. Using a very dense mesh can give a very high accuracy, but it requires more computing capacity of the system. A good mesh is the result of an assessment of accuracy of the result and the required capacity of the computer system.

The layout of the model and the meshes of the two crack models is shown in figures 5, 6 and 7.

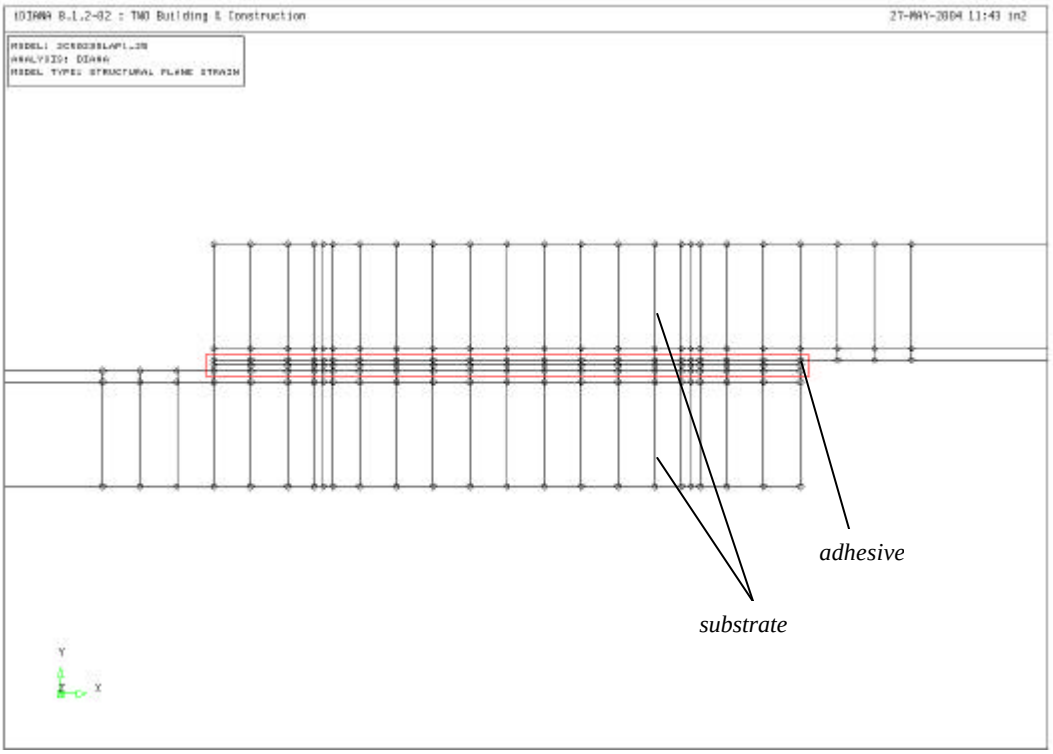

Figure 5: lap joint, divided into surfaces

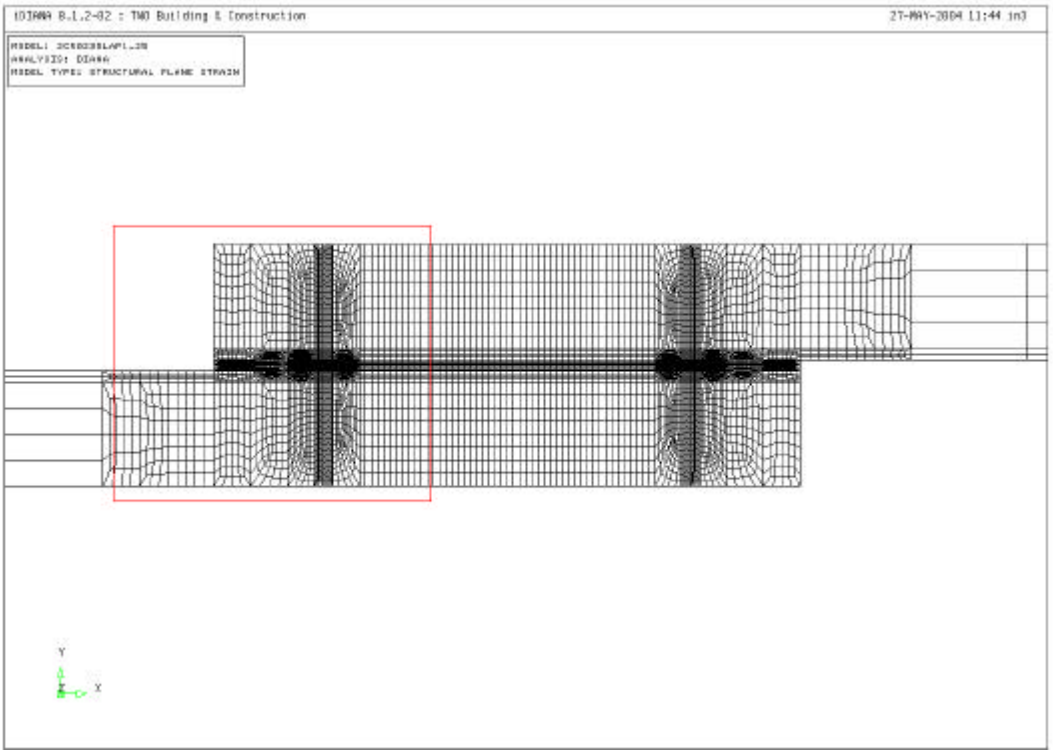

Figure 6: mesh of the lap joint

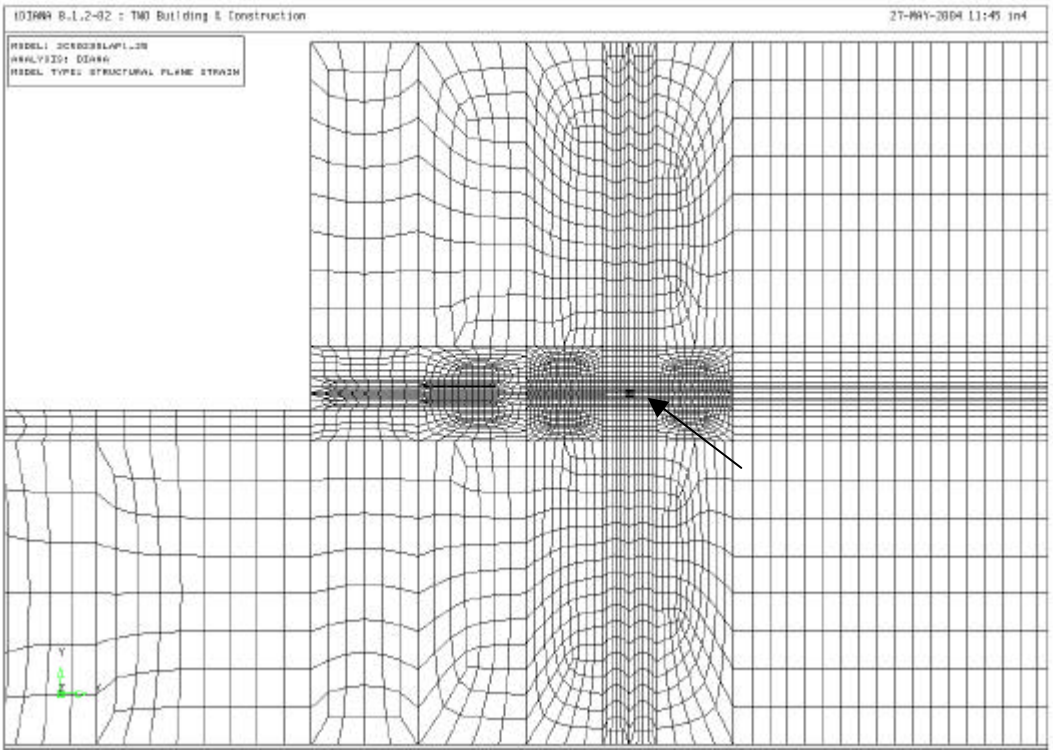

Figure 7: detail of the mesh of the lap joint., the crack tip element is shown at the point of the arrow.

3.2 Results of single sided and double sided cracked joint models

In figure 8, the result of a single and a double crack FEM calculation are plotted. These results have been obtained using the original material properties of the materials. The material properties of the adhesive have been obtained from 'Structural adhesives directory and databook' Bob Hussy and Jo Wilson, 1996. Note that the maximum crack depth of one of the 'double' cracks is only half the lap length and therefore half the maximum crack depth of the single cracked joint. It can be seen that until a crack depth of about 4mm, the computed values of G are nearly equal for both models. Hence it can be concluded that for the accuracy of the result for the first 30% of maximum possible crack depth it hardly matters whether or not there is a smaller defect present at the other of the crack. If the crack grows beyond that depth, the energy release rate increases dramatically for the cracks in the double crack lap joints. For both the single and the double crack joint, this severe increment of the energy release rate starts at about 60% of the maximum possible crack depth.

As can be seen in figure 9, the computed fatigue life for the single crack joint is always bigger than the double cracked lap joint. Calculations have proved that the fatigue life of the single crack lap is about 68% longer than the double crack lap joint. The difference is becoming smaller when the load approaches the fatigue limit.

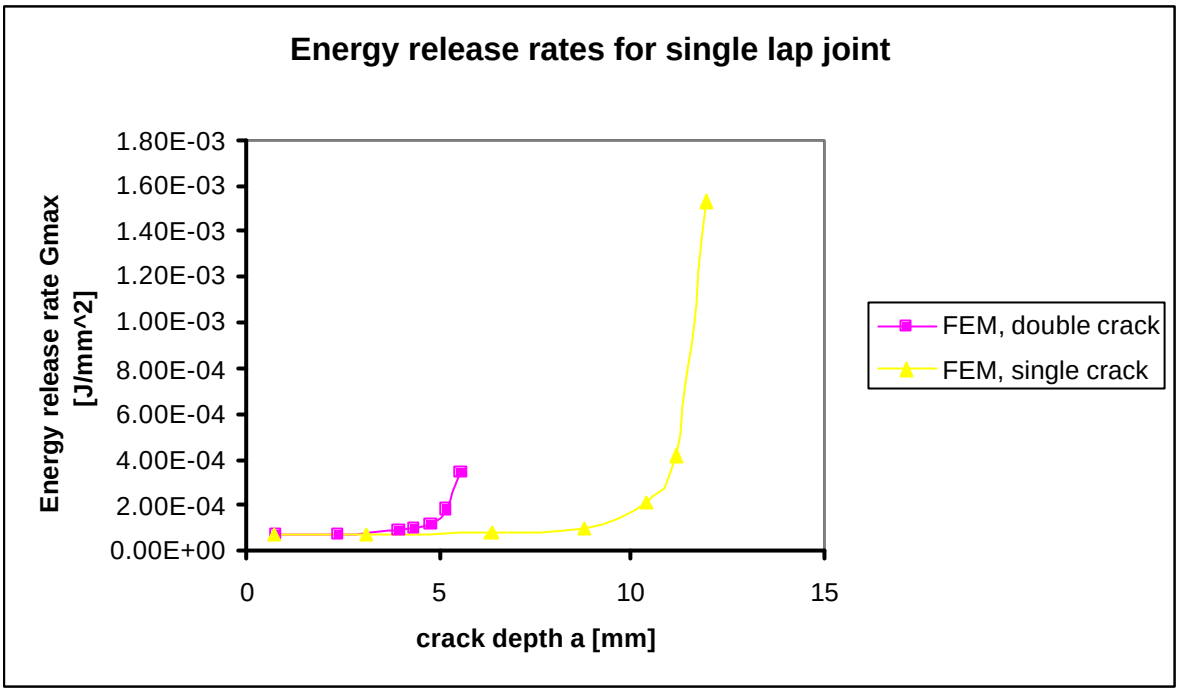

Figure 8: Energy release rates for a single and a double crack joint. The results have been obtained under a unit load of 1.0 N/mm over the height of the substrate.

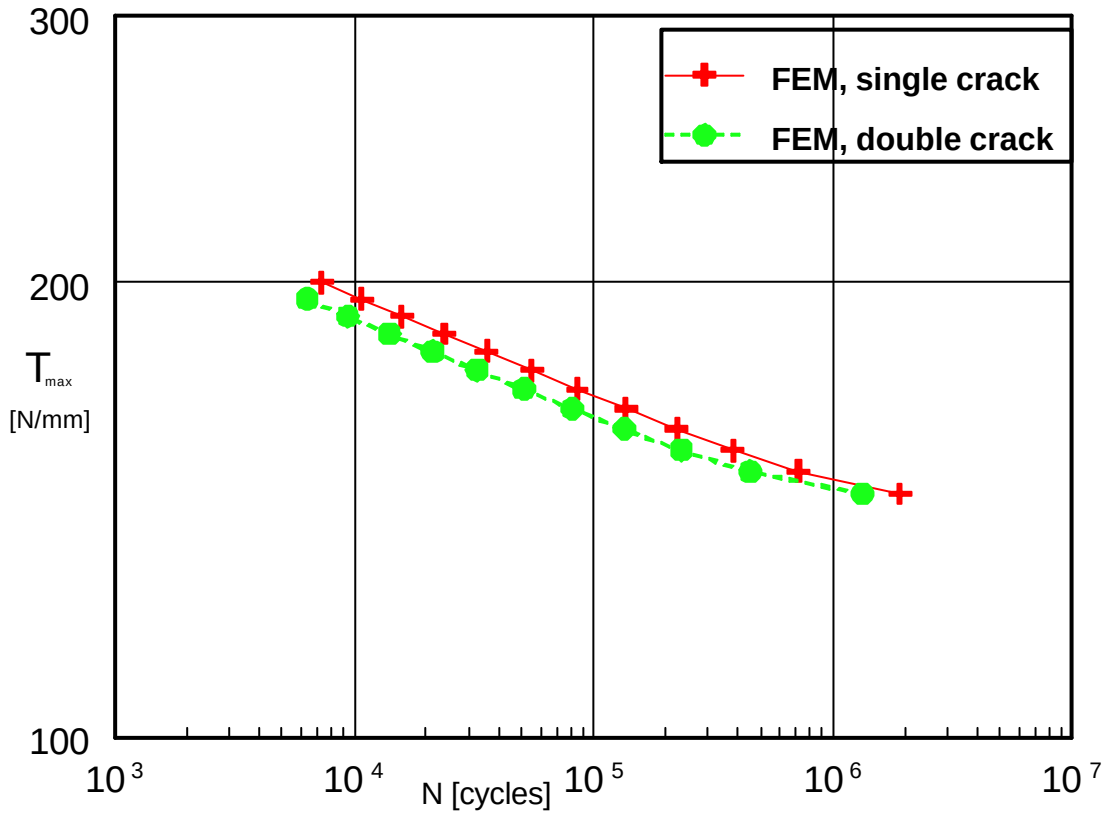

Figure 9: T-N diagram for a single crack and a double crack lap joint

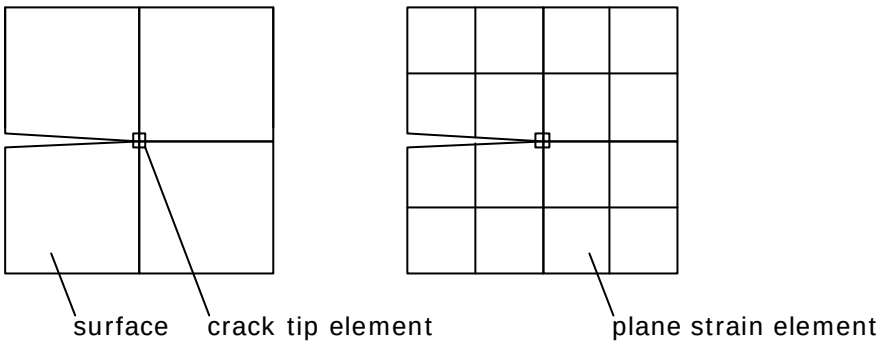

*Figure 10: (left) the applied FEM layout of the surfaces in the adhesive around the crack tip and the crack tip element. Two surfaces have been used.over the height of the adhesive layer. (right) Mesh of the surfaces around the crack tip. The division of the surfaces in this mesh is 2*2.*

3.3 Varying the density of the mesh

3.3.1 Parameters

As said in section 3.1, the density of the mesh influences the accuracy of the results and the required time and computing capacity to perform the calculation of the model. In this investigation, the density of the mesh of the surfaces around the crack tip (shown in figure 10) has been varied. Three densities have been used to calculate the energy release rate of the cracks, namely 2*2, 6*6 and 24*24. The first density is the lowest density possible over half of the height of the adhesive layer, the latter is an extremely fine mesh to check the accuracy of the first two mesh densities. All calculations concerning the variation of the crack depth have been made for a lap joint with a single crack. Three different crack depths have been used to characterise the crack growth, namely 0.75 mm, 6.35 mm and 11.95 mm. The calculations have been made for all the variations of the E modulus for both adhesive and substrate. The variations of the E modulus will be regarded later in this chapter. The results of the two variation studies are shown in the figures as points, as the numbers of results are insufficient to draw the *G-a* curves. However, to get the feeling of the influence the results of the variation calculations given here, combined with the *a-G* curves in figure 8 should be sufficient.

3.3.2 Results

The results of the calculations are included in figures 12 and 13 and in Appendix I. When the results are compared it appears that the differences are marginal. The biggest differences appear at the deepest cracks. Even then, the differences are 1% for the 2*2 mesh and 0.5% for the 6*6 mesh. For designing purposes, a deviation of 1% is acceptable. If the 2*2 mesh is used, the mesh shown in figure 10 can become less dense in general, as the mesh of the complete joint had to be applicable for 24*24. The adjustment to 2*2 simplifies the model and the time required to compute the model decreases significantly.

3.4 Varying the E modulus of substrate and adhesive

3.4.1 Parameters

The material properties of the applied materials, both the adhesive and the substrate, influence the energy release rate. In figure 11 two examples are given for two extreme ratios between the E modulus of the substrate and the adhesive. In case (*a*), the stiffness of the substrate is infinite. Therefore, the substrate will not deform at all. The main operative loading mode is mode II, shear. In case (*b*), the stiffness of the bond zone is infinite. The bond zone does not deform, the only displacement is rotation. The operative mode in this case is a combination of mode I and II, tension and shear. In this investigation the influence of the elasticity of the materials has been studied. The E modulus of both materials has been varied. The actual values of the E modulus of the adhesive and the substrate are 2380 N/mm^2 and 70000 N/mm^2 respectively. When one material is varied, the other one remains constant at its actual value. In case of the adhesive the E modulus was varied to 1000 N/mm^2, 11900 N/mm^2 and 70000 N/mm^2. In case of the substrate the E modulus was varied to 2380 N/mm^2 and 14000 N/mm^2.

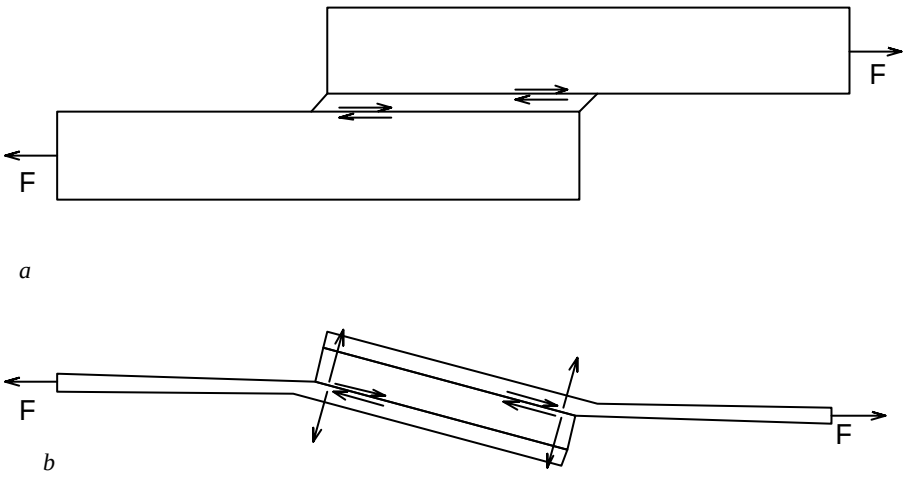

Figure 11: Influence of the substrate on the deformation of the specimen and the loading mode of the crack. (a) the E modulus of the substrate is infinite. In (b) the E modulus of the lap zone is infinite.

3.4.2 Results of varying the E modulus of the adhesive

In table 1 and figure 12 , the FEM results for three cracks are shown for four different adhesives. For all the curves in figure 12, the E modulus of the substrate remains constant on 70000 N/mm^2. All results have been obtained with the fine 24*24 mesh. In table 2 and figure 13, the FEM results for three cracks are shown for three different substrates. For all the curves in figure 13, the E modulus of the substrate remains constant on 2380 N/mm^2. All results have been obtained with the fine 24*24 mesh.

The main differences occur at the big crack size when the adhesive is varied. In the initial phase of the crack growth life and at half the lap, the maximum difference between the two lowest E moduli of the adhesives is about 60% and 100% respectively. The difference between the different adhesives can hardly be seen. At final failure, the difference is about 2100%. The crack depth is dominant in this case.

When the substrate is varied, the influence of the crack depth is less dramatic. The difference between the different substrates in the chart is obvious. The influence of the E modulus is rather constant for the smallest two cracks, the ratios between the values of G of the different substrates is fairly constant. Considering the biggest crack, G increases stronger for the low E modulus.

Thus, considering these results it becomes clear that for small cracks (<half lap length), the influence of the E modulus of the adhesive is relatively small. The level of G is dominated by the stiffness of the substrate. When the crack approaches the maximum crack depth, the influence of the E modulus of the adhesive on the results of the calculations increases strongly. The influence of the substrate is still significant as well, but not as strong as the adhesive's. One should note that the influence of the adhesive is great when the crack is past at least half of the joint, but that the main part of the cycles occurs in the initiation phase and at the start of the crack growth.

*Table 1: Values of G for three crack depths a, with a variable E modulus of the adhesive. All results have been obtained with a mesh density of 24*24.*

E		a		
substrate	adhesive	0.75	6.35	11.95
70000	1000	7.16E-05	1.01E-04	3.44E-03
70000	2380	6.26E-05	7.67E-05	1.54E-03
70000	11900	5.67E-05	6.40E-05	4.27E-04
70000	70000	4.54E-05	5.31E-05	1.56E-04

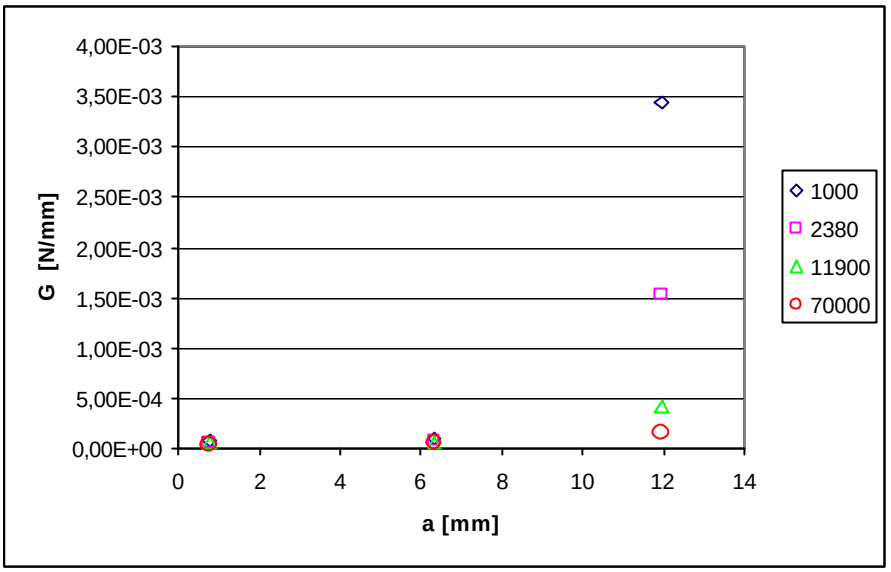

*Figure 12: G for three crack depths a, with a variable E modulus of the adhesive. All results have been obtained with a mesh density of 24*24.*

*Table 2: Values of G for three crack depths a, with a variable E modulus of the substrate. All results have been obtained with a mesh density of 24*24.*

E		a		
adhesive	substrate	0.75	6.35	11.95
2380	2380	1.34E-03	1.56E-03	4.60E-03
2380	11900	2.83E-04	3.20E-04	2.13E-03
2380	70000	6.26E-05	7.67E-05	1.54E-03

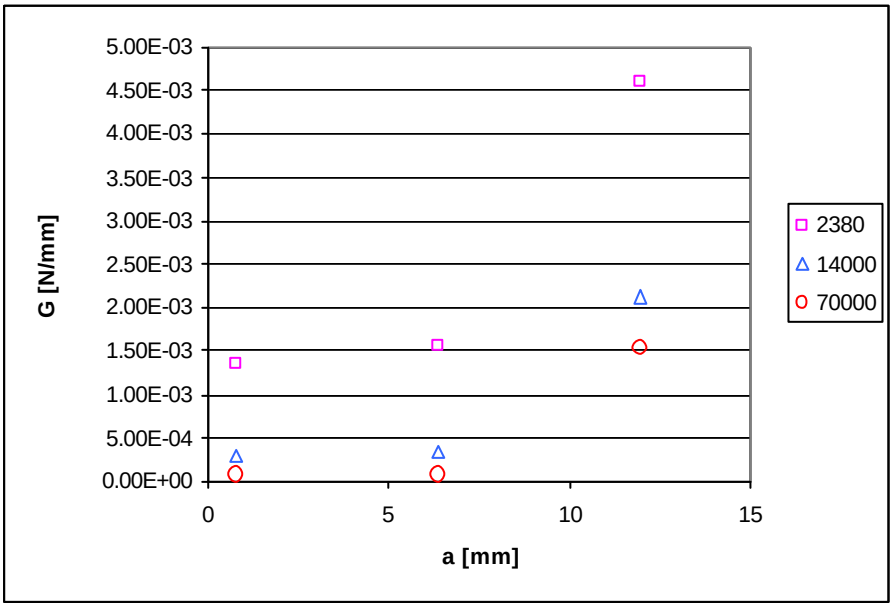

*Figure 13: G for three crack depths a, with a variable E modulus of the substrate. All results have been obtained with a mesh density of 24*24.*

4 Comparison Analytical solutions and FEM

4.1 Analytical models

In 'The prediction of crack growth in bonded joints under cyclic fatigue loading, part II' by H. Hadavinia et al (International Journal of Adhesion and adhesives, 2003 463-471), three analytical models have been found for the calculation of G_{max} for a single lap joint with two cracks. In these models, different kinds of loading modes are described. The characteristics of these three models will be described shortly. Next, the results of the models will compared with the FEM calculations. The formulae of each model are included in the appendix.II All models are compared in this section for the single lap joint with cracks growing at both ends of the joint, including the FEM model.

The three analytical models are:

- the Kinloch-Osiyemi (KO) model
- The Fernlund, Papini, McCammond and Spelt (FPMS) model
- The Krenk and Hu (KH) model

Kinloch-Osiyemi model

The KO model considers the transverse tensile stresses, or peel stresses, which act at the end of the single lap joint. The KO model has as basic assumption that mode I (tension, figure 2) is the operative failure mode.

Fernlund, Papini, McCammond and Spelt model

The FPMS is based on the J-integral method for large deformations, together with large-deformation beam theory. The energy release rate calculation is based on the axial strain and from the induced bending moment, caused by the rotation of the substrates.

Krenk and Hu model

In the KH model, the maximum applied strain energy release rate is computed considering the maximum peel stresses and the maximum shear stresses in the single lap joint for the maximum load. The KH model considers the mode I (tension) and mode II (shear) (figure 2) contribution. The KH model takes into account the reduction of the bending moment due rotation of the substrates.

The different models and the FEM calculation have been compared for crack depths between 0 and 5.575 mm using a reference load of 1.0 N/mm over the height of the substrate. Next, the results have been extrapolated. The result can be seen in figure 14. The results of the FEM calculations are used to predict the number of cycles to failure. To be able to make this calculation, several material specific properties are required. The crack growth properties have been obtained from 'The prediction of crack growth in bonded joints under cyclic fatigue loading, part I' by H. Hadavinia et al (International Journal of Adhesion and adhesives, 2003 449-461). The calculation has been elaborated for the specimen shown in figure 2, with aluminium as substrate and a hot-curing toughened-epoxy adhesive. The constants for the calculation are related to the preparation method of the specimens as well. For this calculation, a chromic acid etch preparation has been used. It has been found that this preparation test results in a crack in the adhesive layer. The T_{max}-N curves derived with the four methods are shown in figure 15.

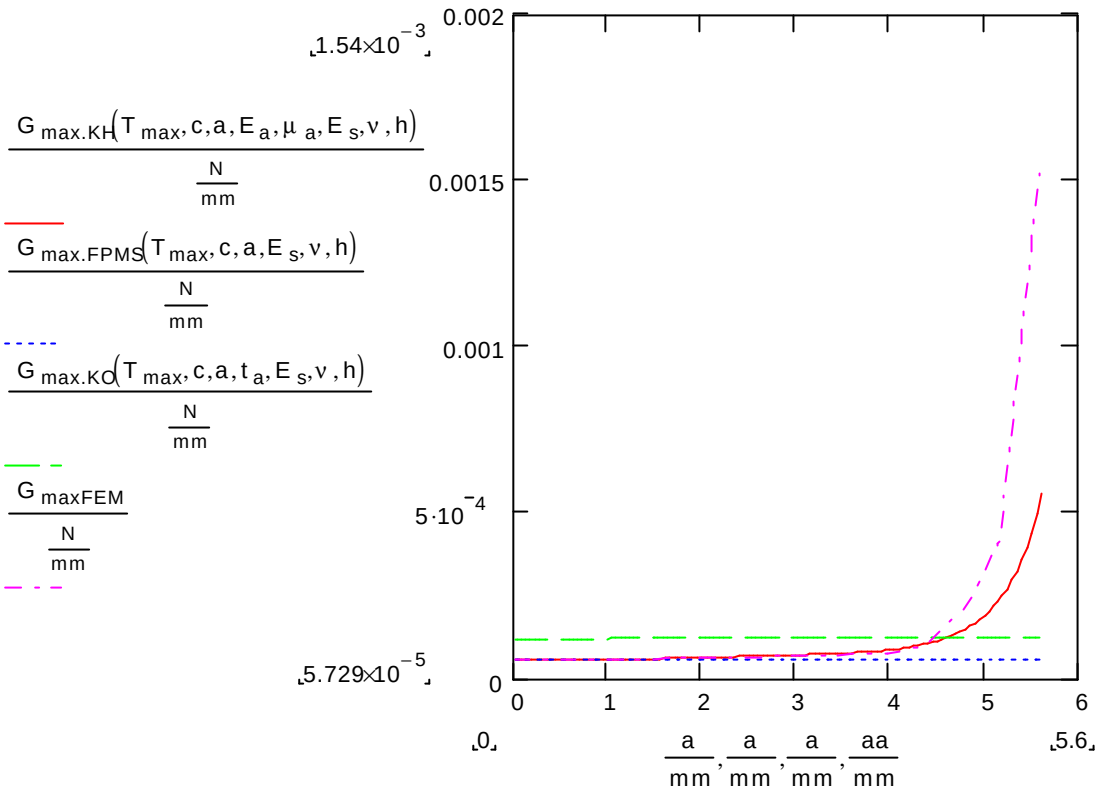

Figure 14: G-a curves for the three theoretical models, KO, FPMS, KO and the finite element results FEM

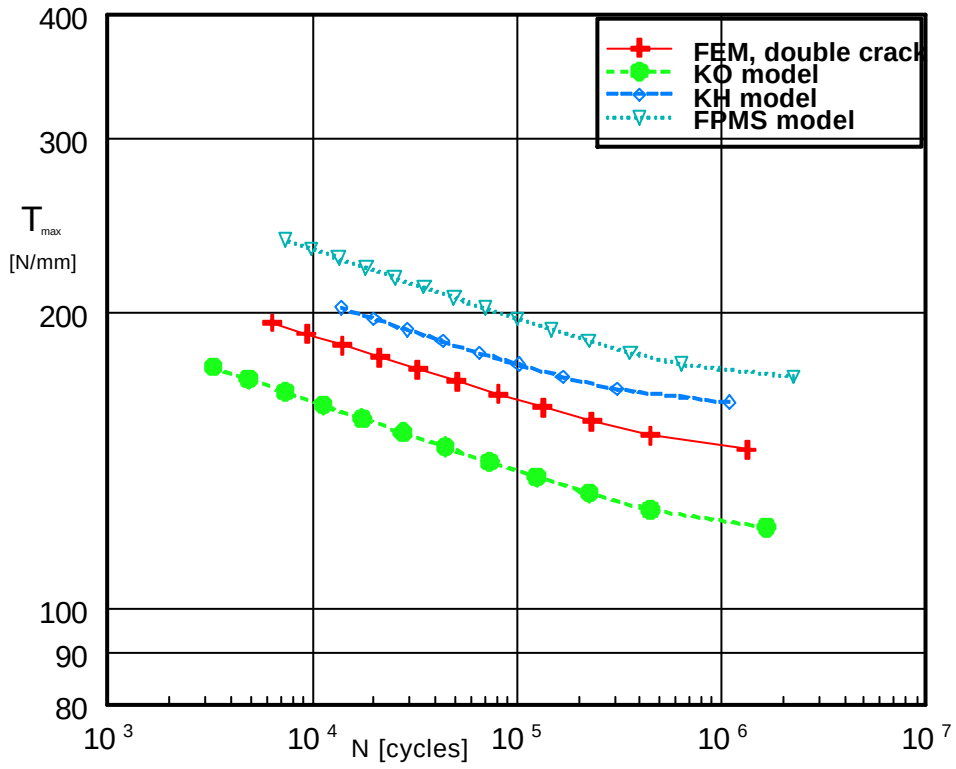

Figure 15: T-N curves for the three theoretical models, KO, FPMS, KO and the finite element results FEM

4.2 Results

Considering the four charts in figure 15, KO can be seen as the lower boundary and FPMS as the upper boundary for predictions of N_f. FEM, KH and FPMS all describe the the mixed mode of shear and axial loading, where as the KO model only describes mode I. In figure 14, it can be seen that the models that describe the mixed mode all concur the first three millimeter. Hence, the FPMS maintains linear until failure. FEM and KH concur until 75% of the maximum crack depth. Then, both models increase exponentially until final failure.Especially the FEM and KH model seem to be in good agreement.

Comparing the T-N curves of the models, as can be seen in figures 14, there are differences and similarities between the models. First regarding the shapes of the curves, two pairs can be seen. FPMS and KO look similar, as do FEM and KH. KO and FPMS both neglect the fast crack growth in region III of the da/dN-G_{max} diagram. For the prediction of the fatigue life the influence of region is small, most of the fatigue life the cracks will be in region II and the da/dN-G_{max} curve will be straight. The KO model accounts for mode I only. It gives significantly higher results for G_{max} than KH and FPMS and lower classification in the T_{max}-N diagram. For this connection KO appears rather conservative.

5 Conclusions

The prediction of the fatigue life using the results of a FEM calculation has been proven to be possible. The results of the calculations that have been made in this research are in rather good agreement with the given analytical results. Therefore, if the crack growth constants are known, an estimate can be made for this kind of adhesively-bonded joint under the given conditions. However, to verify the results of the calculations, experiments should be performed.

With respect to the modelling of an adhesively-bonded lap joint, an optimum mesh using square elements for the area around the crack tip has been found, for both deviations of 0.5 % and 1.0 %. For design purposes, a deviation of 1.0 % is thought to be reasonable.

With respect to the modulus of elasticity of the adhesive and the substrate, an indication has been given about the influence of the modulus of elasticity on the energy release rate related to the crack depth. The indication can play a role in the first estimate of fatigue behaviour when another substrate or adhesive is chosen. It can be seen that the influence of the adhesive becomes small if the E modulus is increased. Only in case the E modulus of the adhesive is strongly decreased, the effect will be significant, especially regarding designing purposes.

6 Recommendations

For this research, only cracks in one position, ie. at the middle of the adhesive layer, are studied. For the given materials, this assumption should be right in practice. However, to be able to make predictions in general, the other possibility, cracks along the interface or combinations of cracks in the adhesive and the interface, should be scrutinised as well.
Furthermore, this investigation was only focused on one type of adhesive. An interesting next step could be the comparison of several adhesives, since the range of mechanical properties of adhesives is broad. By using other adhesive layers, it could be possible that the range of the layer thickness and the E-modulus is completely different or even the complete mechanical behaviour is different. In that case, the modelling recommendations given might have to be reviewed.
Another interesting parameter to adjust is the geometry. Especially for practical applications in civil applications, more knowledge should be available about the possibilities in other geometries.

Appendix I

Table A: Values of G for varying mesh densities and varying E moduli of the substrate for three crack depths a, calculated with FEM

a=0.75 mm

E		mesh division of the surfaces around the crack tip		
substrate	adhesive	2*2	6*6	24*24
70000	1000	7.17E-05	7.17E-05	7.16E-05
70000	2380	6.25E-05	6.25E-05	6.26E-05
70000	11900	5.66E-05	5.66E-05	5.67E-05
70000	70000	4.54E-05	4.54E-05	4.54E-05

a=6.35 mm

E		mesh division of the surfaces around the crack tip		
substrate	adhesive	2*2	6*6	24*24
70000	1000	1.01E-04	1.01E-04	1.01E-04
70000	2380	7.69E-05	7.67E-05	7.67E-05
70000	11900	6.40E-05	6.40E-05	6.40E-05
70000	70000	5.31E-05	5.31E-05	5.31E-05

a=11.95 mm

E		mesh division of the surfaces around the crack tip		
substrate	adhesive	2*2	6*6	24*24
70000	1000	3.49E-03	3.45E-03	3.44E-03
70000	2380	1.56E-03	1.54E-03	1.54E-03
70000	11900	4.31E-04	4.28E-04	4.27E-04
70000	70000	1.56E-04	1.56E-04	1.56E-04

*Table **B**: Values of G for varying mesh densities and varying E moduli of the adhesive for three crack depths a, calculated with FEM*

a=0.75 mm

E		mesh division of the surfaces around the crack tip		
substrate	adhesive	2*2	6*6	24*24
2380	2380	1.34E-03	1.34E-03	1.34E-03
14000	2380	2.83E-04	2.83E-04	2.83E-04
70000	2380	6.25E-05	6.25E-05	6.26E-05

a=6.35 mm

E		mesh division of the surfaces around the crack tip		
substrate	adhesive	2*2	6*6	24*24
2380	2380	1.56E-03	1.56E-03	1.56E-03
14000	2380	3.20E-04	3.20E-04	3.20E-04
70000	2380	7.69E-05	7.67E-05	7.67E-05

a=11.95 mm

E		mesh division of the surfaces around the crack tip		
substrate	adhesive	2*2	6*6	24*24
2380	2380	4.59E-03	4.60E-03	4.60E-03
14000	2380	2.15E-03	2.14E-03	2.13E-03
70000	2380	1.56E-03	1.54E-03	1.54E-03

Appendix II

The Kinloch-Osiyemi (KO) model

$$G_{\max} = \frac{12}{E_s h^3}\left(\frac{T_{\max(}(h+t_a)}{2}\right)^2\left(\frac{1}{(1+l(c-a))^2}\right)$$

$$l = \sqrt{T_{\max}/D_f}$$

$$D_f = \frac{E_s h^3}{12(1-n^2)}$$

The Fernlund, Paipini, McCammond and Spelt (FPMS) model

$$G_{\max} = G_{\inf}\left(1+\frac{3}{4}\frac{1-\tanh^2(l_l c-a)}{\left(1/\sqrt{8}+\tanh(l_l c-a)\right)^2}\right)$$

$$G_{\inf} = \frac{T_{\max}{}^2}{4E_s h}$$

$$l_l = \sqrt{T_{\max}/D_{fc}}$$

$$D_{fc} = \frac{E_s(2h)^3}{12(1-n^2)}$$

The Krenk and Hu (KH) model

$$G_{\max} = \frac{t_a}{2}\left(\frac{s_{\max}{}^2}{E_a}+\frac{t_{\max}{}^2}{m_a}\right)$$

$$s_{\max} = l_s{}^2 M_0\frac{\sinh(2l_s(c-a))-\sin(2l_s(c-a))}{\sinh(2l_s(c-a))+\sin(2l_s(c-a))}+l_s{}^2 V_0\frac{\cosh(2l_s(c-a))-\cos(2l_s(c-a))}{\sinh(2l_s(c-a))+\sin(2l_s(c-a))}$$

$$t_{\max} = -\frac{1}{8}l_t\left(T_{\max}+\frac{6}{h}M_0\right)\coth(l_t(c-a))-\frac{3}{8(c-a)}\left(T_{\max}-\frac{2M_0}{h}\right)$$

$$l_s{}^4 = \frac{E_a}{2t_a D_f}$$

$$l_t{}^2 = \frac{8}{ht_a}\frac{m_a(1-n^2)}{E_s}$$

$$M_0 = \frac{1}{2}kT_{\max}h$$

$$V_0 = kT_{\max}\sqrt{3\frac{T_{\max}}{hE_s}}$$

$$k = \left[1 + l\,(c - a)\right]^{-1}$$

$$l = \sqrt{\frac{T_{\max}}{D_f}}$$

Fatigue in adhesively bonded aluminium joints

Experimental and numerical research on adhesively bonded aluminium lap and tubular joints

Jaap Strik
S448826

March 2005

Department of Structural Design,
Faculty of Architecture, Building and Planning,
Eindhoven University of Technology

A 2005-13
0 2005-09

Preface

This report is the final product of my graduation project. I have been working on it with lots of pleasure from the end of 2003 until the start of 2005 at both the department of Building Structures at TNO Bouw, Delft and the department of Structural Design at the faculty of Architecture, Building and Planning at the Eindhoven University of Technology (TUE).
At the start of the project, the scope was very broad and gradually, the goal of the project became more specific. The process can roughly be subdivided into three phases: the literature survey, three minor researches and a final major research. These phases can respectively be seen as the introduction, practical experiencing and a fundamental research. The introduction was a fundamental, material and joining technique independent investigation for fatigue. In the follow-up, the three minor researches, three different fields of applied knowledge on fatigue have been investigated for a month and a half each. The topics investigated are the following: non destructive crack detection in aluminium structures, fatigue life predictions on simple adhesively bonded joints in aluminium and classification of welded aluminium joints for fast aluminium ships. The topic of the major investigation is evolved out of the last two researches. I wanted to combine experimental research and FEM research in a challenging field of engineering. Fatigue in adhesive joints is still a rather new topic, so lots of interesting, fundamental work is ahead and therefore I have selected this subject.

I would like to thank first of all my committee, prof ir Frans Soetens (TNO Building and Construction Research, TUE) dr ir IJsbrand van Straalen (TNO Building and Construction Research) and Dianne van Hove (TNO Building and Construction Research, TUE) for their great support and guidance. Also, I would like to thank the department of Building Structures at TNO Building and Construction Research for offering me the opportunity for working in such a pleasant environment. From TNO Building and Construction Research I thank Erik Botter especially for his great support on application of FEM and adhesive technology. I also have to give some props to the Pieter van Musschenbroek laboratory at the faculty of Architecture, Building and Planning at TUE, and especially to Theo van de Loo and Martien Ceelen for their critics, being helpful and having a laugh. I owe the faculty of Aerospace Engineering at the Delft University of Technology for letting me use their facilities.
Of course, I would like to thank my friends and family for their support and interest and especially my girlfriend Theone for all the love and patience.

I hope you enjoy reading!

List of symbols

a	crack depth
D	linear coefficient
E_{adh}	modulus of elasticity of the adhesive
E_{sub}	modulus of elasticity of the substrate
FEM	Finite element method
G	energy release rate
G_c	critical energy release rate, if the energy release rate approaches G_c rapid failure will occur
G_{max}	maximum energy release rate in a load cycle
G_{min}	minimum energy release rate in a load cycle
G_{th}	threshold value of the energy release rate; if the energy release rate of a cracking mechanism reaches this value, no further crack extension will occur
h	height of a specimen
l_o	lap length
K	stress intensity factor
LEFM	Linear elastic fracture mechanics
N	number of cycles
N_f	number of cycles until failure
P	force
P_{max}	maximum applied force in a load cycle
P_{min}	minimum applied force in a load cycle
R	ratio between the minimum and the maximum load in a load cycle
w	width of a specimen
DG	range between the maximum and minimum energy release rate in a load cyde
DK	range between the maximum and minimum stress intensity factor in a load cycle
DP	range between the maximum and minimum applied force in a load cycle
n_{adh}	Poisson ratio of the adhesive
n_{sub}	Poisson ratio of the substrate

1 Introduction

As far as the state of the art engineering is concerned, adhesively bonded joints are a rather new and very interesting kind of joining technique. Application of adhesively bonded joints requires a fundamentally different perspective on joining techniques, geometrical configuration and stress transmission. To be able to apply adhesive joints in a responsible way, the main application fields have to be explored. The characteristics of the joints have to be stated qualitatively and quantitatively.
One of the fields of interest for adhesively bonded joints is the application in building and civil engineering in joints that are exposed to variable loads and fatigue failure. In this investigation, the following purpose is aimed for:

A method that links finite element modelling with material characteristics obtained with an experimental programme in order to establish a model to predict the fatigue life of an adhesive joint that is loaded by a constant amplitude cyclic load.

Considering fatigue behaviour in adhesively bonded aluminium joints, the following subjects will be discussed:

- Experimental research on crack growth in adhesives
- Finite Element Method (FEM) research on crack growth characteristics, applying Linear Elastic Fracture Mechanics (LEFM)
- Experimental research on adhesively bonded tubular joints and double lap joints
- FEM research on adhesively bonded tubular joints and double lap joints
- Life time predictions on adhesively bonded tubular joints and double lap joints

For those who are not familiar with fatigue in general, I would like to refer to my literature study on fatigue [1]. This literature study briefly comprehends the most important issues about fatigue. It is partly based on a selection of study material from the faculty of aerospace engineering and civil engineering at Delft University of Technology.

This study focuses on fundamental research of fatigue in adhesive joints. It tries to combine material characteristic research with LEFM research. Figure 1 shows a schematic representation of the research. The whole study consists of the prediction method and the validation of this method. The investigation can be subdivided in four steps, the first three concern the actual prediction method.

A. Material related research (experimental / LEFM FEM)
B. Geometry related research (LEFM FEM)
C. Fatigue life calculation (numerical)
D. Experimental validation

In chapter 2 an introduction is given to respectively adhesive joints and fatigue. Briefly, adhesive technology is explained. In chapter 3, linear elastic fracture mechanics and its application are presented. In chapter 4, the method to gather the material related data is described and the required specimen and experimental set-up is considered. The next experimental part and the validation experiments on adhesive joints, are described in chapter 5. All experimental crack growth results are given in 6. In chapter 6, the numerical research is described and the results of the research are given. The results of the fatigue life prediction model and the output of the fatigue experiments on the double lap and tubular joints are given as well. In 9, 10 and 11, respectively all results will be discussed, the conclusions are drawn and recommendations are given.

The eight blocks given in the flowchart are described in the various chapters of the report. Block 1 is discussed in 4, block 2 in 6.2, block 3 in chapter 6, block 4 in 6.3 and 6.4, block 5 in 3 and 6.1, block 6 in 8, block 7 in 5 and 8.

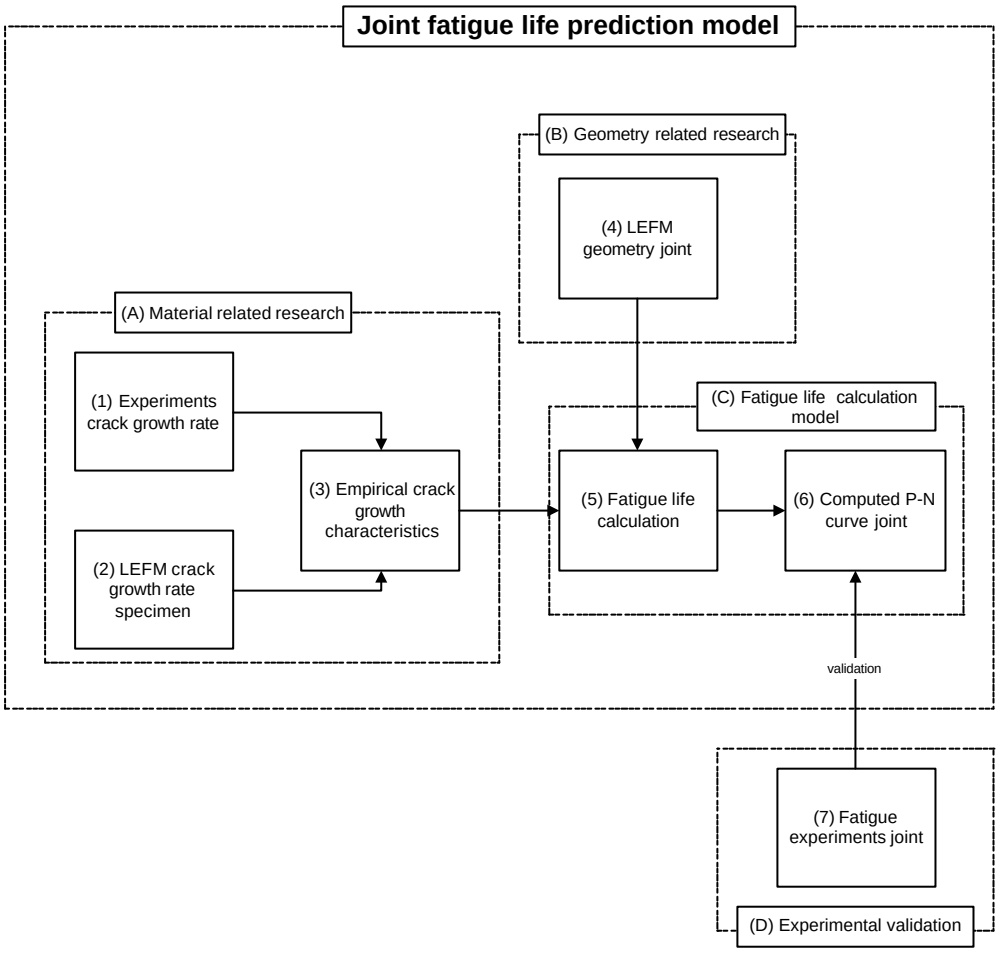

Figure 1: overview of the joint fatigue life prediction model

2 Adhesively bonded joints and fatigue

This chapter is a general introduction to adhesive technology and structural application. It is meant to give some background information to give a little bit of feeling with bonding technology. Points of interest are the load transfer mechanisms in adhesive joints and the failure mechanisms. Also the different sorts of adhesives are listed and shortly described. [2] has been used as a source for the general information on adhesively bonded joints. None of the information which has been extracted from this work is exclusively published by this writer and is generally available.

2.1 Adhesively bonded joints

Adhesive bonds are a large group of various adhesives with a very large variety of properties and applications. Adhesives have been used since the ancient cultures around the Mediterranean Sea like the Romans, the Greeks and the Egyptians. The first adhesives were based on organic sources, like animal bones or bees' wax. To really improve the features of these adhesives, they needed to be modified synthetically. The real break through came around the Second World War. At that time, fully synthetic adhesives have been produced. Since then, adhesives have been modified until now. Over the last sixty years, there has been a great development in synthetic materials.

An adhesive joint is fabricated by putting an adhesive, a paste or a liquid, between two solid components that need to be joined. The solid components are often referred to as adherend or substrate. In this report, the latter will be used. The rigid connection is established during the curing period of the adhesive. The environmental conditions can play an important role in the period required for the curing and for the properties of the final joint. The rigid joint is the result of a chemical process. In this chemical process, the adhesive will be affected, contrarily to the substrate, which will hardly react. If the established connection is rigid enough to transfer load from one component to the other, the connection is called a structural adhesively bonded joint.

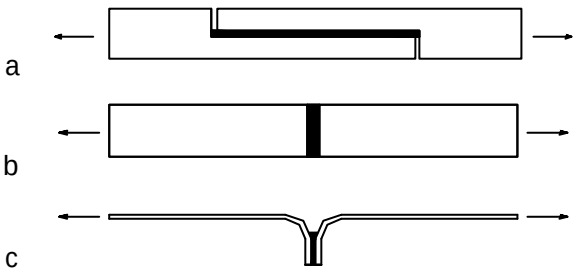

Figure 2: Three loading modes of adhesive joints: a) shear, b) tension, c) peel

When an adhesively bonded joint is used in a structure, it can transfer load in globally three manners: shear, tension and peel, see Figure 2. The first is preferred, the latter two should be avoided. The loads tension and peel cause high tensile stress peaks close to the bond line, which are difficult to sustain. In case of shear, these tension peaks are significantly lower. In the design process the nature of the load should be well considered. The following loads can be distinguished:

- Short term static
- Long term static
- Impact load
- Low cycle fatigue

- High cycle fatigue

An important factor in the designing process is creep. Other important factors are temperature, humidity and the exposure to ultraviolet radiation.

Regarding the failure mechanisms of adhesively bonded joints, three failure mechanisms can be distinguished (Figure 3):

- Failure in the bond line. This type of failure can initiate in regions where the most severe stress peaks occur. This type of failure is referred to as cohesive failure.
- Failure in the interface between the adhesive and the substrate. This type of failure can occur at an interlayer, for instance an oxide layer. This type is also known as adhesion failure.
- Failure in the substrate. One of the substrate components fails.

Besides these ´pure´ failure mechanisms, mixed mode mechanisms can occur as well. The type of failure is affected by the type of loading and by the manufacturing process of the joint.

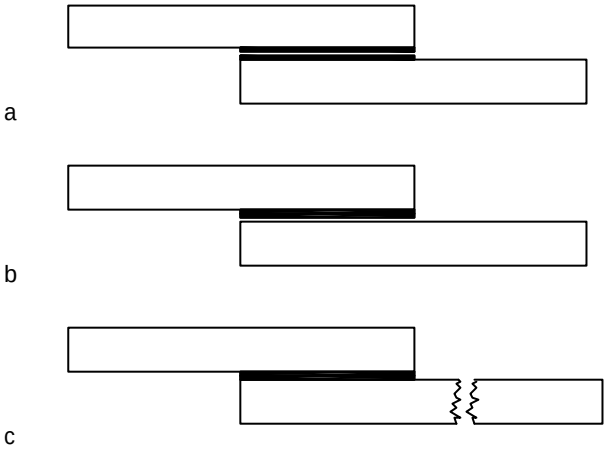

Figure 3: three failure modes of adhesive joints: a) cohesive failure; b) adhesive failure; c) failure in the substrate

Introduction in cohesive mechanisms and adhesive characteristics

When an adhesive joint fails cohesively, the fracture is initiated in the bond line of the joint. To explain this failure mechanism, understanding of adhesive systems is needed. The cohesive behaviour of adhesives can be explained with knowledge from polymer technology. Polymers are macromolecules, large atom chains that are built from smaller molecules, monomers. In polymer technology, four different molecular structures are known: linear, branched, crosslinked and network. For linear polymers, long flexible chains of molecules are weakly bonded by physical connections. For branched polymers, side chains are connected to the linear structure. These side chains are physically bonded to this linear structure. The crosslinked polymers have side chains as well, but these chains are chemically bonded to the linear structure. These chemical bonds are stronger than the physical. Network polymers are the strongest of polymers, the polymers consist of molecules with more chemical bonds, forming a network of monomers. Most structural adhesives are crosslinked and network polymers.

Another method to categorise polymers is the distinction in elastomers, thermosets and thermoplastics. An elastomer is based on a polymer with a low degree of crosslinking. It can be stretched to a high extension and recover without permanent plastic deformation. A thermoset is based on a high degree of crosslinking, forming a complete network polymer. The mechanical behaviour of the thermoset is more rigid than that of the elastomer. Both types degrade rather than melt above a certain temperature. A thermoplastic can be melted without disintegrating. Thermoplastics are based on linear or branched polymers.

The mechanical properties of polymers are fairly complex. Under relatively low stresses, the mechanical material behaviour is linear elastic. When the polymer is stretched, the energy stored is reversible. The relation between stress and strain can be described by the modulus of elasticity E. The lateral strain in the polymer can be described by the Poisson's ratio n. Under higher loads, the stress strain relation is no longer linear elastic. In that case, a part of the energy is stored in a viscous manner. When high strains occur in the adhesive, the bonds in the polymer fail and fracture occurs.
Under long term loads the polymer shows a kind of visco-elastic behaviour. It can be described as a mixture of elastic behaviour of a solid and the deformation behaviour of a viscous liquid, where the strain rate depends of the level of loading. The behaviour of the material is determined by the temperature and the rate and period of loading. Beside the 'classical' stress strain description, the material behaviour at failure can be described by fracture mechanics. Fracture mechanics are often used in case of fatigue. The application of linear elastic fracture mechanics will be regarded in chapter 3.

Another important aspect about the mechanical behaviour of polymers is the degradation of the mechanical properties during the life span of the polymer. During the ageing of the polymer, the degree of polymerisation decreases, i.e. the macromolecules falls apart in smaller molecules. This process occurs under influence of water, temperature, chemicals and presence of ultraviolet radiation. The mechanism of degradation and the influences of the different factors are very complex and are still subject of study.

Introduction in adhesive mechanisms

When an adhesive joint fails adhesively, the location of failure is the interface between the bond line and the substrate. Engineers mostly avoid adhesive failure, but after ageing of the joint adhesive failure can become dominant. To describe the failure mechanism accurately, the interaction along the interface should be well understood. Two different bonds act in the interface between the substrate and adhesive, namely physical and chemical bonds. The weaker physical bonds are based on Van der Waals forces, diplo forces and hydrogen bonds. These bonds are formed by electrostatic attraction between chemical neutral molecules. The stronger chemical bonds are based on ionic, covalent and metallic bonds. Chemical bonds require reactive chemical groups that bond on the surface of the substrate material.

Bonding systems

The conventional, most widely used groups of adhesives in structural applications are epoxy, polyurethane and acrylic adhesives. They offer strength, toughness and resistance against degradation, which make them applicable in structures. Epoxies are available in various formulations and can be applied to join a large range of materials. Epoxies have good strength properties, but tend to be rather brittle. The toughened variations are more favourable for structural applications. One component epoxies are cured at high temperatures, while two component epoxies cure at room temperature due to an additional hardener. An important aspect for a good performance of epoxy is an appropriate condition of the surface. Some epoxies require an intensive pre-treatment for an optimum bonding during their life span. Epoxies can be

developed for a wide range of applications. Their resistance against heat and chemicals is very good, if the right version is applied. Polyurethanes are also available in one and two component versions with a wide range of different formulations, like epoxy. The strength of the one component version is rather low, the strength of the two component mediocre. Beside these strength properties, most polyurethane adhesives have an excellent toughness and durability with little effort for pre-treatment of the surface. The single component polyurethane cures due to moisture, the two component version has an additional hardener. Acrylics (modified acrylics) are available in different formulations. Most often they come as two component adhesives. One component is put on one surface, the other component on the second surface and then the two surfaces can be joined, without mixing of the components. The strength properties of acrylics are rather good, while a moderate effort should be made to secure the durability of the joint.

In this research, two adhesives have been applied: an epoxy and an MS polymer. The epoxy is a two component epoxy. The MS polymer is relatively young adhesive. From the three 'conventional' adhesives it is most similar to polyurethane, being very tough and flexible. MS Polymer - Silane-modified adhesives and sealants based on MS polymers (Modified Silane Polyether) are designed as one-component systems. Due to their chemical structure MS polymers exhibit good weathering and aging resistance without need of complex pre-treatment. The MS polymer applied here, combines the favourable properties of sealants and adhesives. The curing of the MS polymer is based on the availability of moisture in the surrounding air. In appendix I the product information for the adhesives is included. Due to pledge of secrecy towards the manufacturer of the MS polymer, this information has been excluded in this version of the report. The mechanical properties are given nonetheless. The mechanical properties of the adhesives are: E modulus: 2380 N/mm^2 and 3.5 N/mm^2 and Poison ratio 0.35 and 0.45 for respectively the epoxy and MS polymer. The material properties have been found in respectively [7] and [10].

2.2 Adhesively bonded joints and fatigue

Adhesively bonded joints are different from other kinds of structural joints, such as bolted or welded joints. Especially the mode in which the connection can be loaded differs. Adhesively bonded joints are loaded preferably with shear loads, like stated in the previous paragraph. This preference for shear loading has important implications for the geometrical configurations the connection can be applied for.

Tensile forces in the bond line should be avoided to sustain the adhesive layer. With respect to fatigue design, the same point can be made. Fatigue cracks will always grow perpendicular to the first principle stress direction. So, for both adhesively bonded joints and dynamically loaded structures severe tensile stresses are undesirable.

One of the main differences between adhesively bonded joints on one hand and bolted and welded joints on the other hand is the difference in required area to transmit loads. In bolted and welded connections loads are transmitted by strictly metallic types of materials. In adhesively bonded joints another type of material, a polymer, is used to transmit loads. The material properties of polymers and metals differ fundamentally. The strength properties of most polymers will be significantly lower than those of the metals that are applied in load bearing structures. Therefore, most often adhesive joints need more area to transfer the load. This 'large' required area, together with manufacturing related factors, results into joints with relatively small geometrical discontinuities compared to metallic joints, like bolted or welded connections. The reduction of geometrical discontinuities results in a smooth load transfer at critical positions in and near the joint, like the ends of the joint. The relatively low stress peaks are very favourable in terms of fatigue behaviour.

Adhesive technology can be used for instance for a single lap joint and a tubular joint, shown in Figure 4. The single lap joint has been the subject of a preliminary study,[3]. In both connections, the adhesive layer will be mainly loaded with shear. However, due to eccentricities, the connection will be loaded with a bending moment as well. The bending moment results in pressure and tensile zones in the adhesive layer. The mode of loading will be discussed in 3.4. In this study, two types of adhesive joint geometries will be considered: the double lap joint and the tubular joint.
Both connections are assumed to have good fatigue properties, as the main load on the bond line is shear. In both joints the stresses are transmitted gradually and the geometrical discontinuities are favourable, especially compared with welded equivalents.

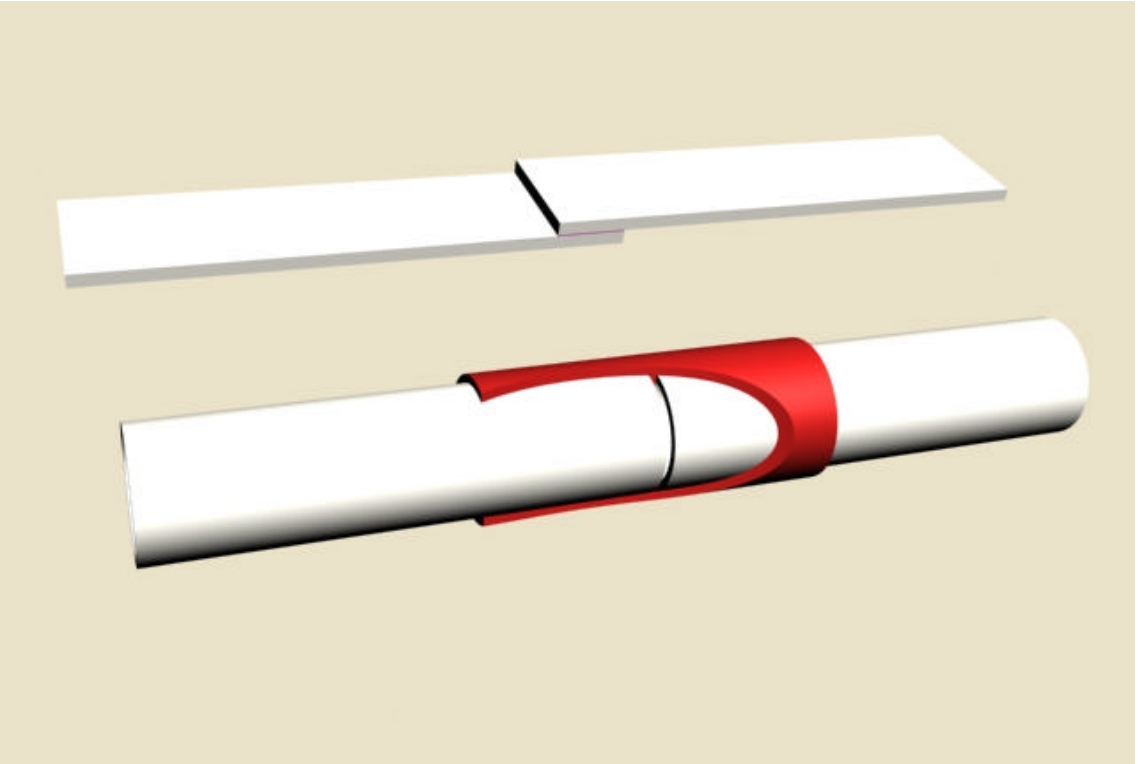

Figure 4: (top) single lap joint (bottom) tubular joint

3 Predicting the fatigue life of an adhesively bonded joint

In this chapter, fatigue failure is introduced. At first, fatigue failure and adhesive joints are regarded. Subsequently, an important characteristic for crack growth and fatigue failure in adhesives, the energy release rate, is described. The energy release rate is initially introduced using a simple example. Next, the application of the energy release rate in fatigue life prediction models is considered. The fatigue life prediction model is one of the main points of interest in this report. In this chapter, the general description of the prediction model is regarded. In other chapters, the particular input for the model for the joints studied in this research is going to be dealt with. The relation between the prediction model to the other subjects can be seen in Figure 5. Finally, the loading mode of cracked joints is investigated. Two main sources of literature have been used for this chapter, which have been quoted freely, namely [11] and [12]. The information that has been used here is not solely been published by these writers and is generally accessible. The publications offer a decent introduction in this field of work.

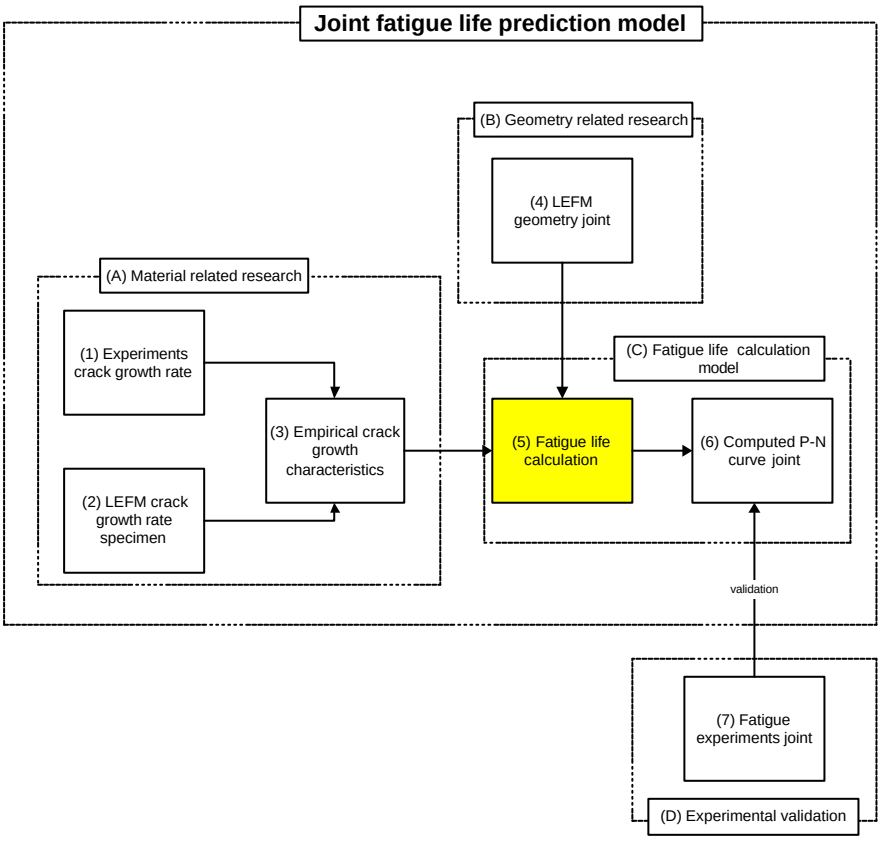

Figure 5: joint fatigue life prediction model flowchart

3.1 Fatigue failure and adhesive joints

When an adhesively bonded joint is subjected to cyclic loading, fatigue failure can occur. Whether or not fatigue failure occurs depends on the loads and the number of stress cycles. When the joint is loaded to a load level that approximates the static strength of the joint, only a relatively small number of stress cycles can cause fatigue failure of the joint. Such fatigue failure is referred to as low cycle fatigue. Fatigue failure is called low cycle fatigue when the amount of

stress cycles until failure does not exceed the boundary of about 10^4 load cycles. Low cycle fatigue occurs if the load level has a certain level that can initiate micro cracks in the first couple of load cycles. This number of cycles is mainly an indication, it is not a clearly defined border. When the connection is subjected to a load range that is significantly lower than the static strength, the number of cycles until failure is higher than in case of low cycle fatigue. It is referred to as high cycle fatigue. When the amplitude of the stresses is decreased, the number of stress cycles until failure will increase. At a particular load level, fatigue failure will not occur. This stress level is referred to as the fatigue limit. In most cases the fatigue limit starts somewhere between $5*10^6$ and $1*10^8$ cycles.
The difference of the stresses between the static strength and the fatigue limit are substantial. The relation between the stress range due to the cyclic stresses under a constant amplitude and the number of stress cycles until failure can be represented in a diagram, the S-N curve, shown in Figure 6.

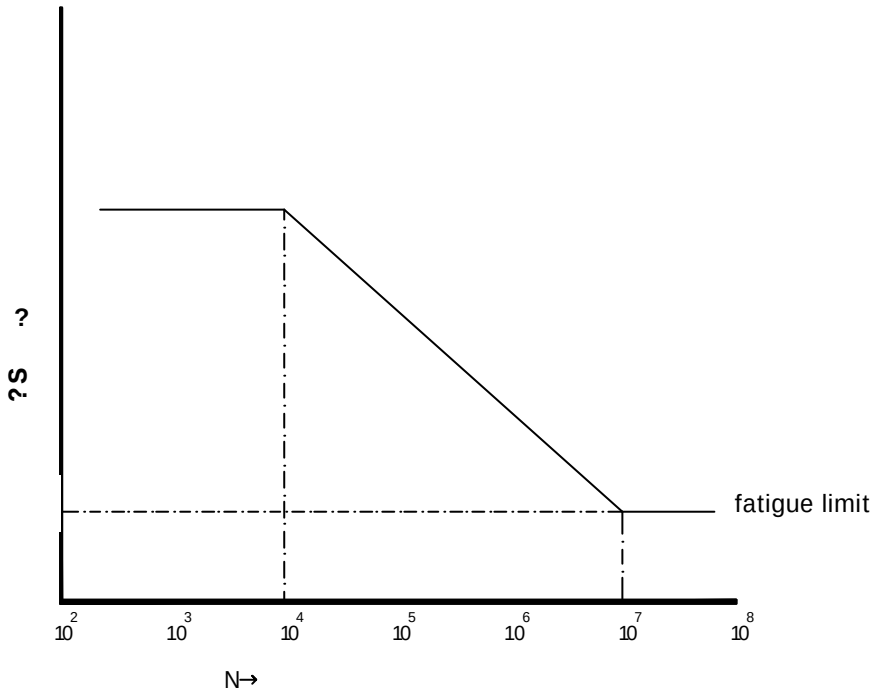

Figure 6: S-N curve

In the *S-N* diagram the relation between the number of cycles with a constant amplitude, *N*, and the nominal stress range, *DS*, is modelled linear on double logarithmic scale between the low cycle fatigue limit and the fatigue limit. On the left and right side of the linear relation, two asymptotes are drawn. The left asymptote represents the low cycle fatigue, the right asymptote the fatigue limit. The relation between the load level and the number of cycles is an empirical relation. The *S-N* curve is a frequently applied design tool in the designing of connections subjected to fatigue. For instance, in the European standards for building structures in aluminium, EC 9 part 1-3, a number of S-N curves for various joints have been included.

To be able to predict the number of load cycles until failure fracture mechanics can be applied. In the engineering of adhesively bonded joints, the number of load cycles under constant amplitude load is predicted using the energy release rate, *G*. There is an empirical relation between the crack extension per load cycle, *da/dN*, and the energy release rate. In paragraph 3.2 the energy release rate will be considered. In paragraph 3.3 the application of the energy release rate in prediction models will be regarded.

3.2 Energy release rate

When a strip is loaded with a tensile load *P*, causing a homogeneous stress *S*, it becomes longer, see *Figure 7a*. The total displacements of both ends is *u.* To stretch the material, work has to be done and potential energy is added to the material of the strip, as shown in the graph of Figure 7d. When one side of the strip is released, the potential energy will also be released. This only occurs if the strip is deformed elastically. The equation for the elastic potential energy is

$$U = \frac{1}{2}Pu = \frac{1}{2}SWt\,\frac{S}{E}H = \frac{1}{2}\frac{S^2}{E}HWt \qquad \textit{Equation 1}$$

with

H	the height of the specimen
W	the width of the specimen
t	the thickness of the specimen

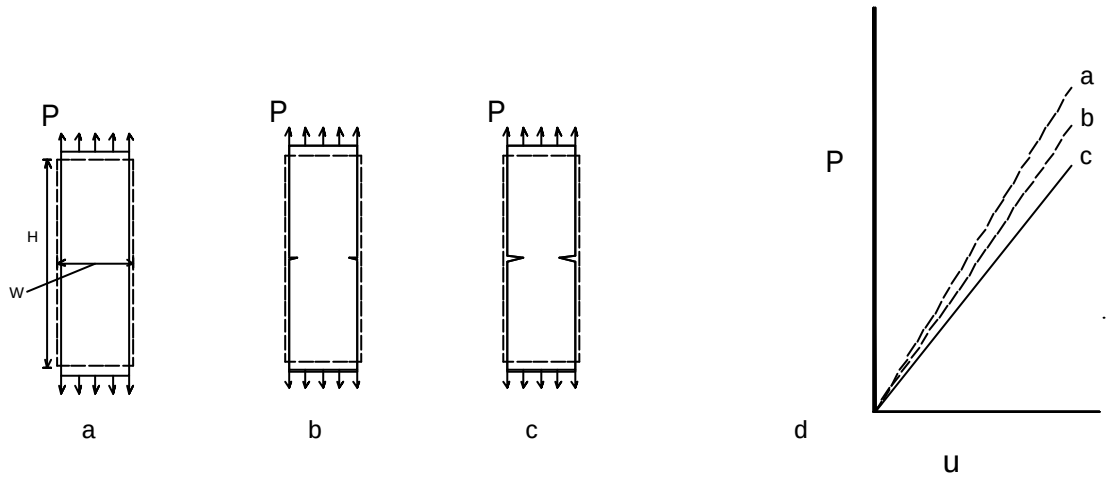

Figure 7: the release of potential strain energy in a cracked strip

In case the strip has a crack and is exposed to the same elongation, like Figure 7b, less load is required. Thus, for the same elongation, the strip will absorb less strain energy. When the crack length increases, as in Figure 7c, relaxation occurs in the cracked strip. For the same deformation, a lower load level is required and therefore the average stress level in the strip is decreased.. If the crack would be extended from the length in Figure 7b to the length of Figure 7c, the release of energy is equal to difference of the area under the *P-u* diagram, the area between the line b and line c of Figure 7d. The energy release rate is defined as the amount of strain energy that is released per infinitesimal crack extension:

$$G = \frac{\partial U}{\partial a}$$ *Equation 2*

When a cracked specimen is loaded, the applied load will try to extend the crack to minimise the strain energy. The energy release rate is also referred to as the crack driving force.

The *da/dN-G* diagram, shown in Figure 8, represents the energy release rate in relation to the fatigue life. The diagram consists of three regions. In region II, there is a linear relation between *da/dN* and *G*. Region II is also often referred to as the Paris' region. In Region I G_{th} is the lower boundary of *G*. G_{th} is the threshold value for *G*, if *G* is smaller than G_{th} no crack extension will occur. In region III, G_c is the upper limit of *G*. If *G* approaches G_c, closely, rapidly tearing of the material lead to failure within a small number of cycles will occur. In this report, the determination of these characteristics are subjected in chapter 7.

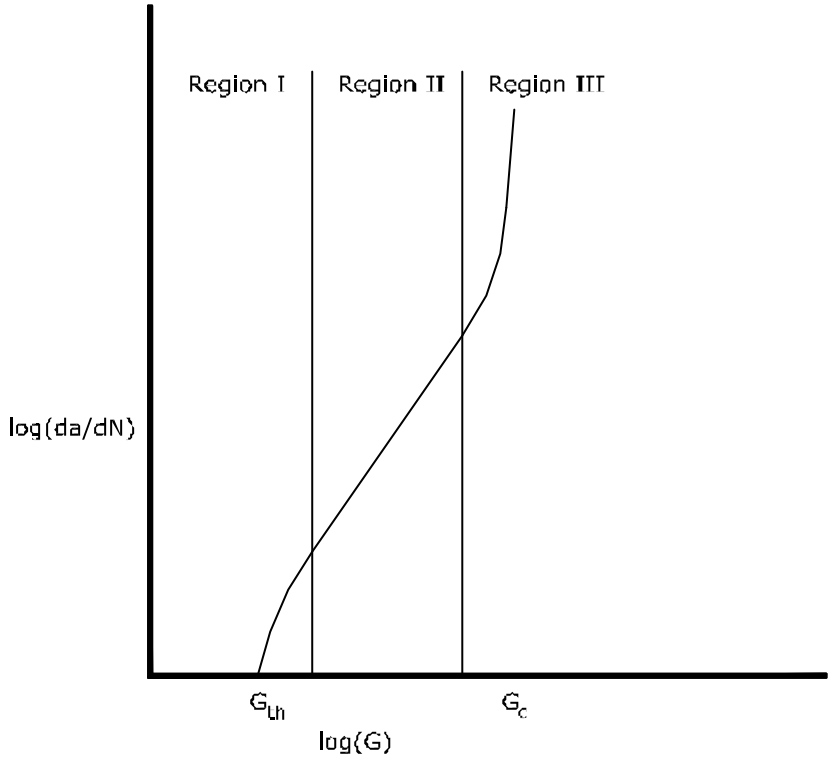

Figure 8: da/dN-G diagram

3.3 Prediction models

To be able to predict the fatigue life of an adhesively bonded connection, the empirical relation between *da/dN* and *G,* shown in Figure 8 is used [12]. The relation between the crack growth per cycle and the m energy release rate in a single load cycle, *G,* can be described by the modified Paris' law. The particular *G* that is substituted can be G_{max}, the maximum energy release rate in a single load cycle or *DG,* the range between the maximum and minimum energy release rates. Both G_{max} and *DG* are considered in this report. The modified Paris Law accounts for the threshold behaviour and the final failure, whereas the normal Paris Law only covers the crack growth in the linear range of the *da/dN-G* diagram, region II:

$$\frac{da}{dN} = DG^n \left(\frac{1-\left(\frac{G_{th}}{G}\right)^{n_1}}{1-\left(\frac{G}{G_c}\right)^{n_2}} \right)$$ *Equation 3*

where

a	crack depth [mm]
N	number of cycles [c]
da/dN	crack growth rate [mm/c]
D	Linear coefficient
G	energy release rate [N/mm]
n	slope of the *da/dN-G* diagram
G_{th}	threshold value for the energy release rate. If *G* is lower than G_{th}, no crack growth will occur. G_{th} is the lower limit for the energy release rate. [N/mm]
n_1	curve fitting coefficient at the G_{th} asymptote. [-]
G_c	critical value of the energy release rate, when *G* reaches G_c, rapid tearing of the joint and failure occur. G_c is the upper limit for the energy release rate. [N/mm]
n_2	curve fitting coefficient at the G_c asymptote. [-]

Paris' law can be rewritten and integrated in order to derive the number of loading cycles until fatigue failure (N_f):

$$N_f = \int_{a_o}^{a_f} \frac{1}{DG^n} \left(\frac{1-\left(\frac{G}{G_c}\right)^{n_2}}{1-\left(\frac{G_{th}}{G}\right)^{n_2}} \right) da$$ *Equation 4*

with

N	number of load cycles until failure [c]
a_0	initial flaw [mm]
a_f	final crack depth [mm]

In this formula, crack depth *a* and energy release rate *G*, increase during the fatigue life of the joint under a constant amplitude load. The crack depth *a* and *G* are related. In equation 4, *D,* G_{th}*,* G_c*, n,* n_1 and n_2 are material (both substrate and adhesive) and loading mode (paragraph 3.4) related and can be found by experimental crack growth rate research, as it is going to be shown in chapters 4 and 6. These characteristics can be applied for fatigue life predictions on cyclic loaded joints bonded with a similar adhesive, surface treatment and loading mode. The surface conditions of the substrate have a large influence on these constants. Concerning the energy release rate of a particular connection, *G* is related to *a* and to the joint geometry and magnitude, position and sort of load. The relation between *G* and *a* is the topic of chapter 6.

3.4 The loading of the crack

The relation between *a* and *G* is influenced by the mode of the loading of the crack. Also, the position and the number of cracks may be of influence. Basically, a crack can be loaded by three different modes (Figure 9):

- Tension (I)
- Shear (II)
- Tearing (III)

For pure mode *j*, $G=G_j$, for a mixed mode, *G* is the sum of G_I, G_{II} and G_{III}. The mode of loading is based on both the geometry and the load case of the structural member. The different modes can have their own *da/dN-G* diagram. In general it is believed that mode I is the most severe case for an adhesively bonded joint. However, this is not always the case. For instance in [4], where the mixed mode was the most severe case.

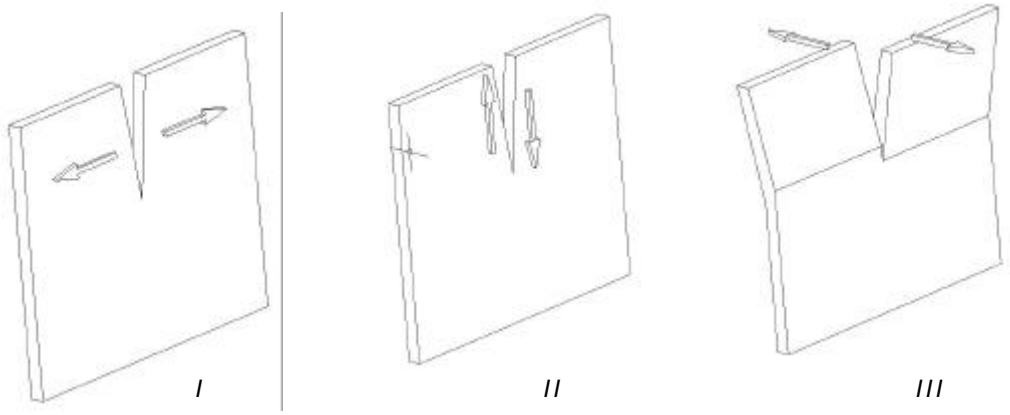

Figure 9: the three crack loading modes: I Tension, II Shear and III Tearing

4 Crack growth characteristics

This chapter deals with the practical part of the finding of the crack growth characteristics. Which specimen can be used, which experimental set-up can be applied, what needs to be measured and what kind of calculations is linked to the experiments. There is also a theoretical / numerical part related to the crack growth characteristic investigation, which is described in 6.2.

To make accurate predictions on the fatigue life of adhesively bonded joints, crack growth characteristics are required. The crack growth characteristics depend on the type of materials i.e. substrate and adhesive, the preparation of the substrate, environmental conditions and the mode of the loading. The characteristics can be determined experimentally for one set of loading mode, pre-treatment and environment. A particular type of specimen has to be selected and manufactured. In literature, a broad selection of specimens is found. The main difference between these specimens is the applied mode of loading of the crack tip. In 4.1, a number of specimens is regarded. From this group of specimens, one specimen is selected to apply for the determination of the crack growth characteristics of the used adhesives. In 4.2, the selected specimen and its properties are regarded. All details about manufacturing and testing features will be described. In 4.4 the experimental set-up is described. The relation between the experimental to the rest of the prediction model can be seen in Figure 10.

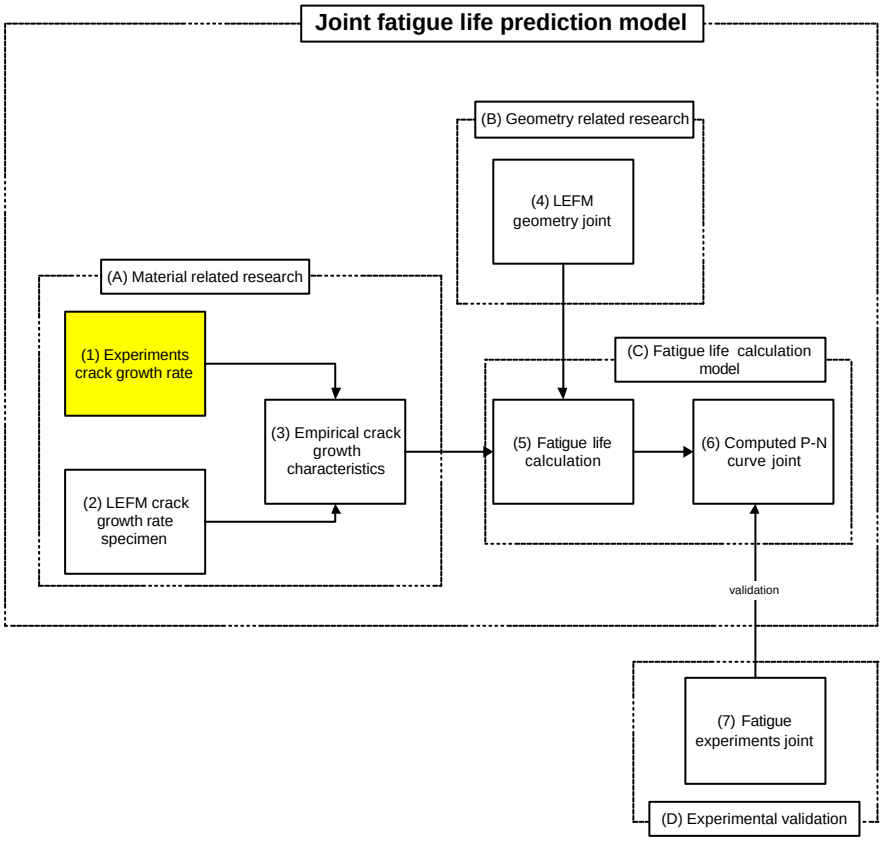

Figure 10: joint fatigue life prediction model flowchart

4.1 Specimen for determination of the crack growth characteristics

In literature [4], [5], [6], [8], [9], [11], a broad selection of specimen that can be used for obtaining crack growth characteristics has been found. An overview of all specimens is given in figure 11. To compare the specimens the four main properties are stated in Table 1, which results in a ranking. The ranking has been used as a guideline for the selection of the specimen.

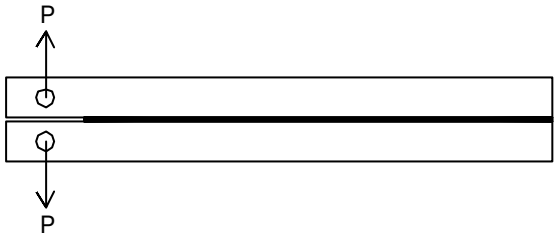

a

- Double Canticlever Beam
- Straight forward ASTM specimen;
- Mode I;
- Variable *G* during crack extension.
- [8] and [9]

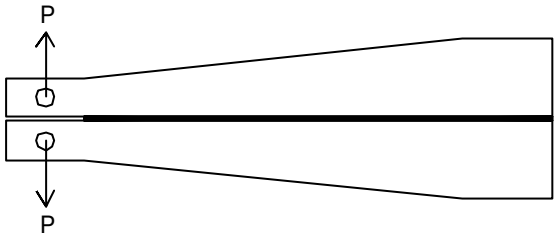

b

- Tapered double Canticlever Beam
- Alternative for a;
- Mode I;
- Constant *G* during crack extension.
- [8], [9] and [11]

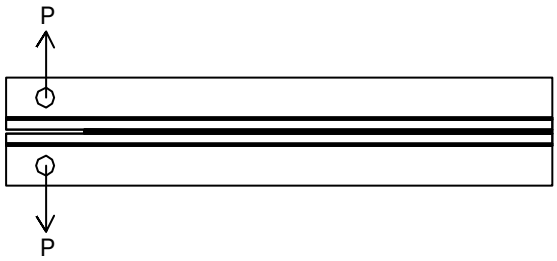

c

- Reinforced double cantilclever beam
- Alternative for a;
- Mode I;
- Variable *G* during crack extension.
- Mainly apllied when thin substrates are subjected
- [4]

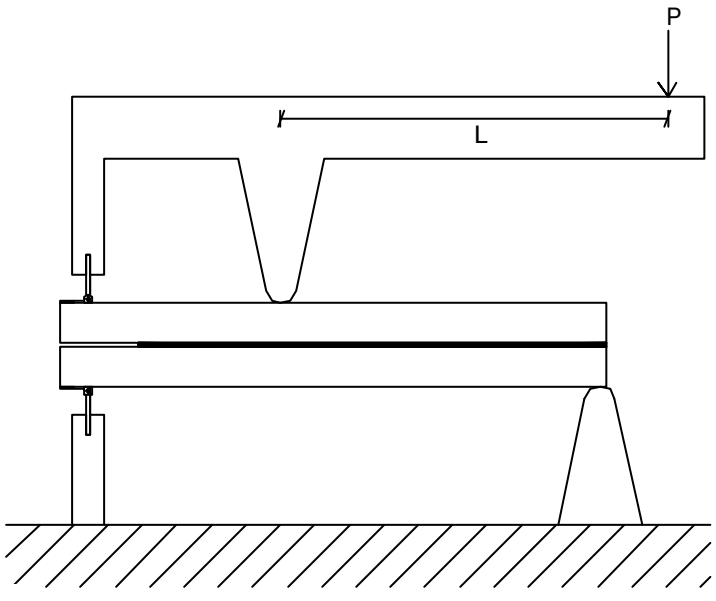

d

- Mixed mode bending specimen
- Mixed mode (I+II) specimen
- Variable *G* during crack extension.
- By varying *L*, the ratio between mode I and II can be adjusted
- Advanced experimental set-up required
- [5]

figure 11: variants of the crack growth characteristics specimen

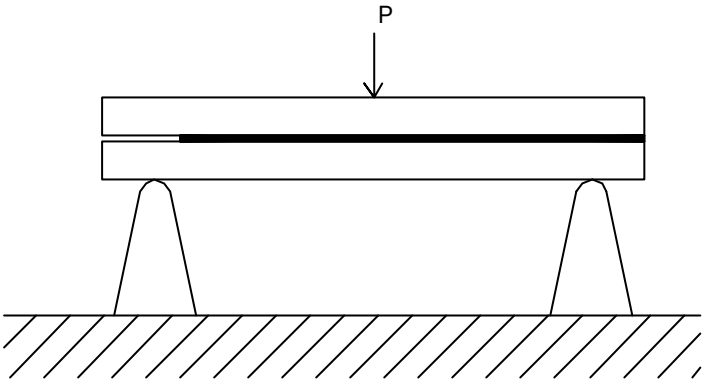

e

- End notch flexure specimen
- Mixed mode (I+II) specimen
- Variable *G* during crack extension.
- The crack is forced to close when loaded
- [9]

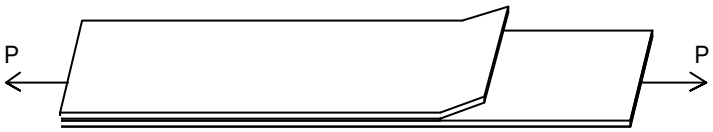

f

- Cracked lap specimen
- Mixed mode (I+II) specimen
- Variable *G* during crack extension.
- By varying the lengths of the lap (top substrate) and the length of the strap (bottom substrate), the ratio between mode I and II can be adjusted. This ratio can also be adjusted by tapering the lap by machining
- [9]

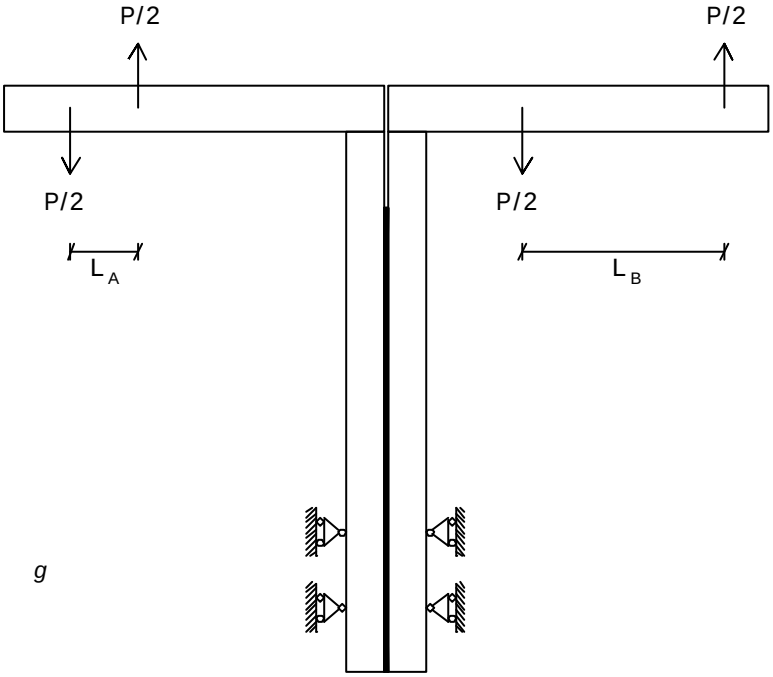

g

- Uneven bending moments specimen
- Mode I, II and mixed mode specimen
- Constant *G* during crack extension.
- Two bending moments are applied. Depending on the direction and the ratio L_A / L_B a mode I, II or mixed mode test can be executed.
- Advanced experimental set-up required
- [6]

Figure 12: variants of the crack growth characteristics specimen

	Mode	Manufacturing	Set-up	Forced crack closure	Ranking
a) Double Cantilever Beam	I	+	+	+	1
b) Tapered Double Cantilever Beam	I	0	+	+	3/4
c) Reinforced Double Cantilever Beam	I	0	+	+	3/4
d) Mixed Mode Bending Specimen	I+II	+	-	+	5/6
e) End Notch Flexure Specimen	II	+	+	-	5/6
f) Cracked Lap Shear Specimen	I+II	+	+	+	2
g) Uneven Bending Moments Specimen	I/II/I+II	-	-	+	7

Table 1: Comparison of the crack growth characteristic specimens, + refers to a positive influence, -to a negative

Concerning the load mode: in the double lap and tubular joint the main mode at the crack tip is mode II. However, the specimens found for testing on mode II crack growth are fairly advanced. The set-up has to be developed for this particular specimen, therefore the application of these set-ups are out of the scope of this research. A basic set-up should be used to fully comply with the experiment without complicating the experimental process. Also, mode II is expected to be the major mode, but some mixed mode could occur as well. The rate between mode I and mode II is not known at the start of the experiments. Therefore, it is decided to pick a specimen and set-up that is basic and results in a lower boundary approximation of the fatigue life of the specimen. As can be seen the double cantilever beam (DCB) specimen scores well in the ranking. The manufacturing of the specimen is relatively easy and the testing set-up is simple. With the results of this test, a lower boundary estimate could be determined. Hence, the results of this estimation are going to be compared with the experimental results. A modification of the numerical solution to indicate the influence of the conservative approach will be investigated after the results have been gathered.

4.2 Double Cantilever Beam Specimen

4.2.1 Description of the specimen

The DCB specimen is a standardised specimen in ASTM D3433, shown in figure 13 [8], [9].

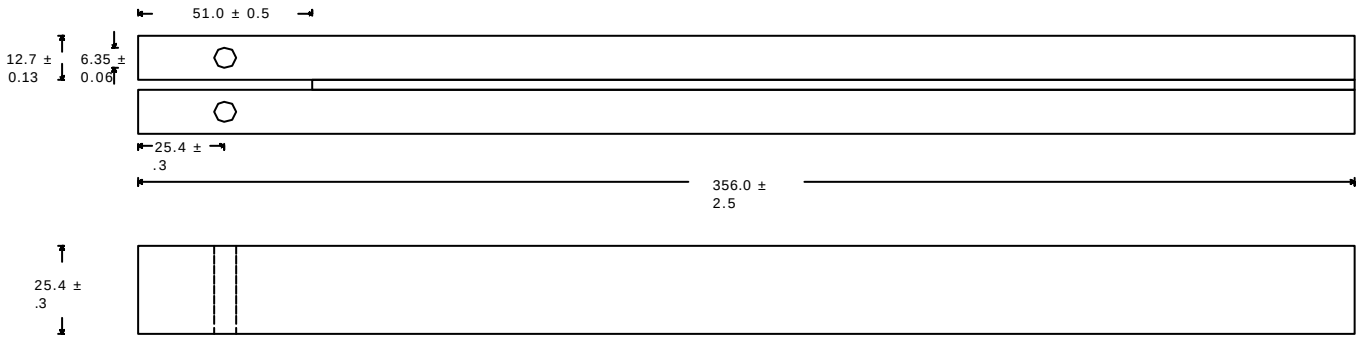

figure 13: DCB specimen, all dimensions in millimetres

The ASTM specimen has been modified for this research. All dimensions of the standardised specimen are according to the Empirical systems. Due to the availability of substrate material in standardised (S.I. units) and the effort, resulting in extra risks such as the bending of the strips after milling, to modify standard dimensions to Empirical dimensions, the standardised dimensions have been chosen requiring less work. This implies that some of the results of these experiments have to be scaled if the results are compared to other experiments. The final specimen geometry and manufacturing method will be given in 4.2.2.

The principle of the DCB is as follows. Two aluminium strips are connected by an adhesive layer. The crack is made to extend by applying two tensile forces at the two eyes of the specimen, perpendicular to the adhesive layer. Between the load line and the adhesive layer is an initial distance of 25.4 mm. An initial defect can be made using a thin foil. The specimens are manufactured and the manufacturing process is checked according to [8]. If the applied method differs from the protocol it will be noted. Please note that the protocol is primarily meant to determine the toughness of an adhesive, not to determine the fatigue characteristics. Anyway, the protocol gives some guidance regarding production techniques and other useful tips.

4.2.2 Manufacturing the specimen

The specimens are manufactured from extruded aluminium strips, 12*25 mm^2, the strip material is AA6082 - T6 51. The manufacturing of the specimen consists of three steps:

1. Manufacturing of the strips
2. Adhesively bonding of the strips
3. Finishing the specimen

In the first step the material is sawed to the right length and holes are drilled at the two ends of the strip, as shown in figure 14. To create good bonding conditions the strip is going to be degreased and grit-blasted with silicium grains. The epoxy DCB specimens are going to be anodised. The pre-treatment for anodising consists of the following steps: degreasing, (deep) etching (bath: 175 g/l NaOH, 55°C), cleaning the etched surface (bath: HNO_3 water = 1:1 room temperature) and anodising (bath: 100g/l PO_4, 20°C). The adhesive has to be applied within the same day. The extra preparation is required to ensure cohesive failure in the bond line. During the whole experimental part of the research, a preliminary series of epoxy DCB specimen have been manufactured and tested with an alternative pre-treatment. This pre-treatment consisted of degreasing, etching (bath: 150-275 g/l H_2SO_4 and 30-55 g/l H_2CrO_4 35°C) and anodising (same bath). However, the specimens in this preliminary series failed because of lack of bonding. Therefore, the current pre-treatment has been selected.
In the second step, two bolts are put through the drilled holes and a spacer is positioned at the end of the strip. The thickness of the spacer depends on the adhesive. In case of the epoxy, a spacer of 0.3 mm is used, in case of the MS Polymer three spacers of 1 mm each are used per end. To create an initial crack, first a bit of adhesive is put on the strip, then two thin sheets of HDPE (a plastic available for domestic use), 7.5 µm each, are positioned on top of the strip. Subsequently, the rest of the adhesive layer is applied, including a bit of adhesive covering the top of the thin sheets. The HDPE have been tested on forehand on adhesion with the adhesives. The second strip is slowly placed over the two bolts onto the spacers. The assembled specimen is shown in Figure 15. During the manufacturing process, the distance between the crack tip and the loading point is variable. On top of the second strip a weight in placed in order to push the adhesive out of the specimen, until the upper strip rests on the spacers. The complete width of the specimen has to be filled with the adhesive. When the complete width of the specimen is filled with adhesive, there s some excessive material. The adhesives require time to cure, the epoxy needs a week, the MS polymer requires four weeks. In step three, the sheets of HDPE are pulled out, once the adhesive has cured. The bolts can be taken out as well. To remove this excessive adhesive and all discontinuities on the side of the substrate, the specimen was milled

at both sides. Per side 0.5 mm of substrate material was removed. It occurred to the MS polymer specimen that the sides of the substrates were milled perfectly flat but that the adhesive had a small convex into the adhesive layer (Figure 16). The chisels of the mill have torn the tough adhesive fibers out of the bond line. Finally the two holes on the side were drilled. These holes are used to apply the load on the specimen.

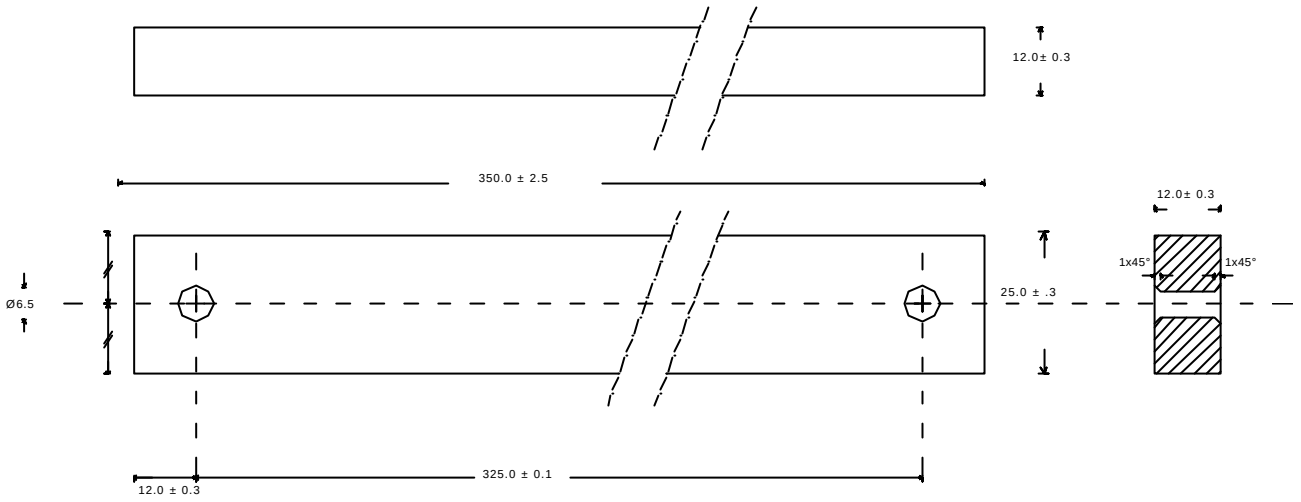

figure 14: technical drawing of a single strip

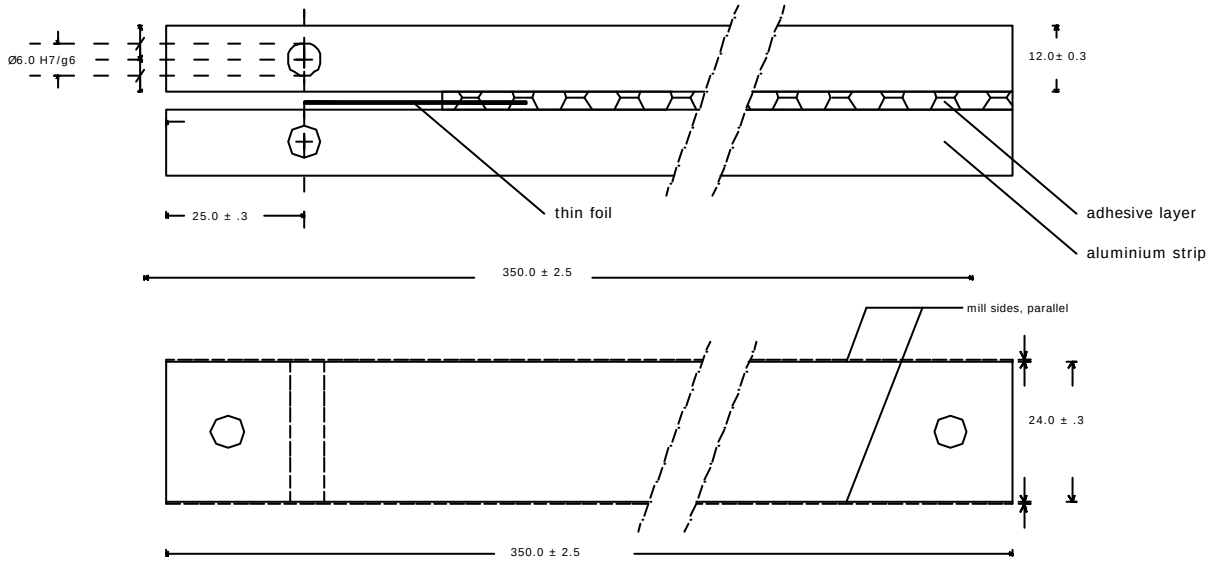

Figure 15: technical drawing of the assembled specimen

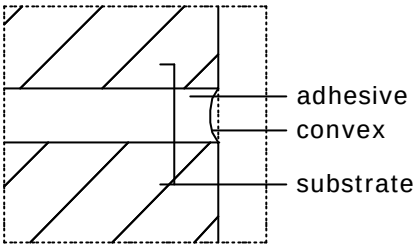

Figure 16: detail of the cross section of the MS polymer

4.3 Calculating G

The purpose of the DCB specimen is to find a relation between *G* (or a related quantity like ΔG or G_{max}) and *da/dN*. Both *G* and *a* have to be computed, they can be derived from the displacements at the end of the specimen. In this paragraph, the alternatives to calculate *G* are reviewed.

Basically, there are two methods to calculate *G* in the DCB specimen:

- FEM calculations
- analytical solutions

Concerning the analytical solutions, in [8] and [9], three solutions have been found:

- Simple beam theory
- Corrected beam theory
- Experimental compliance method

From the analytical solutions, the simple beam theory is the easiest to apply and compare with the results from FEM. The simple beam theory can be used as a rough validation for the FEM results. The FEM approach will be described and compared with the results of the simple beam method in 6.2.

The FEM calculations are used to derive a relation between the displacements and the crack depth and a relation between the crack depth. For both the displacement / crack depth relation and the crack depth / energy release rate relation a mathematical relation is derived for both adhesives. This relation is used as the primary determination method for the calculation of crack depth and energy release rate based on the displacements of the end of the specimens. A scheme of the processing model from DCB output to *da/dN-G* diagram is shown in Figure 17.

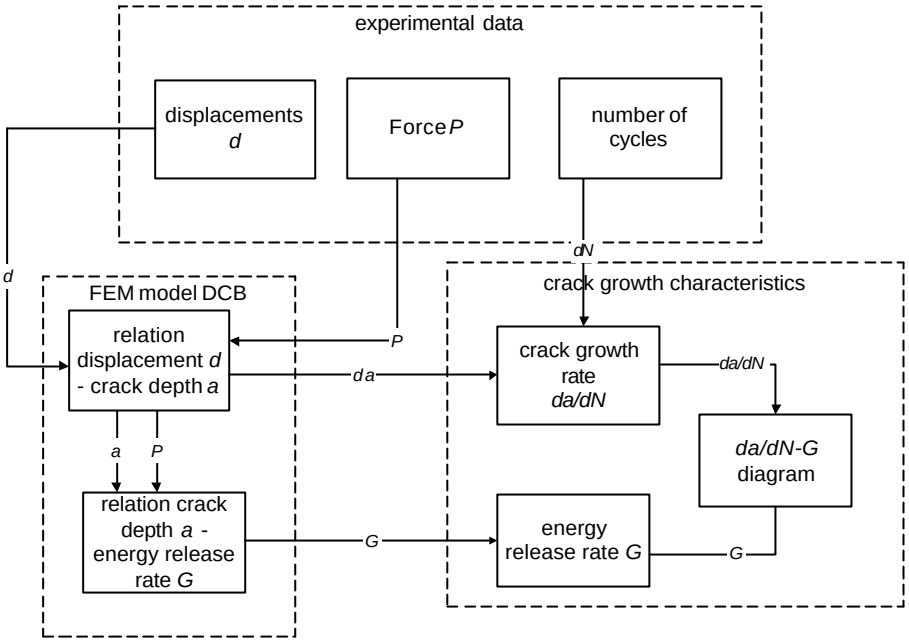

Figure 17: scheme of the model that has been used to process the measurements from the DCB specimen to the da/dN-G diagram

Simple beam theory

The simple beam theory describes the DCB specimen with the classical beam theory. The displacements of the load points of the specimen are described as if the strips are beams with a length from the end to the crack tip. The beams are assumed to be connected rigidly in the adhesive zone and the small deflection theory is valid.

The compliance C [mm^2/N] is a measure of the deformation of the specimen under a unit load. The compliance can be can be described by

$$C = \frac{8(a^3 + a h_s^{\,2})}{E_s h_s^{\,3}}$$ *Equation 5*

h_s thickness of the strip
E_s elastic modulus of the substrate

The simple bean theory links the displacements of the ends directly to the energy release rate. According to the small deflection beam theory, the mode I energy release rate of the DCB can be described by

$$G_I = \frac{P^2}{2w} * \frac{\partial C}{\partial a}$$ *Equation 6*

with
P the applied force
w width of the strip

If equation 5 is substituted in equation 6, it results in

$$G_I = \frac{4P^2}{w^2 E_s}\left(\frac{3a^2}{h_s^{\,3}} + \frac{1}{h_s}\right)$$ *Equation 7*

The simple beam theory does not include the deformation of the adhesive zone or the deformation of the substrate in the uncracked zone.

4.4 Experiments

The experiments have been performed at the Pieter van Musschenbroek laboratory at the Faculty of Architecture, Building and Planning at Eindhoven University of Technology. The experiments have been done in a hydraulic dynamic machine, using a force-controlling device of 10 kN. The specimens have always been loaded in tension. The loading pattern in the time is a sine wave, Figure 18. The experiments have been performed under frequencies between 1 and 30 Hz, depending on the load and the required displacement of the machine. All the frequencies and loads are included in the measuring report. Per adhesive, two series of tests have been executed each with their own load case. The difference between the load cases was the ratio between the minimum and the maximum load. This ratio can be described with the dynamic load ratio R, $R=P_{min}/P_{max}$. The experiments have been performed with $R=0.1$ and $R=0.5$. The fatigue behaviour of adhesive joints is influenced by R. The influence can be explained by the behaviour of the molecules in the adhesive. The molecules in the adhesive are long macromolecules whether or not linked or side branched. When the adhesive is applied, the stresses in the adhesives are negligible. When the specimen is loaded with a cyclic load with $R=0.1$, the macromolecules are loaded and unloaded, until they disintegrate. A R value of 0.1 is preferable to 0 or even a negative value, as the change from a negative loading to a positive load introduces mechanical difficulties in the experimental set-up. In the case of $R=0.5$, the molecules are pre-stressed, loaded to with maximum load and unloaded to the pre-stress level.

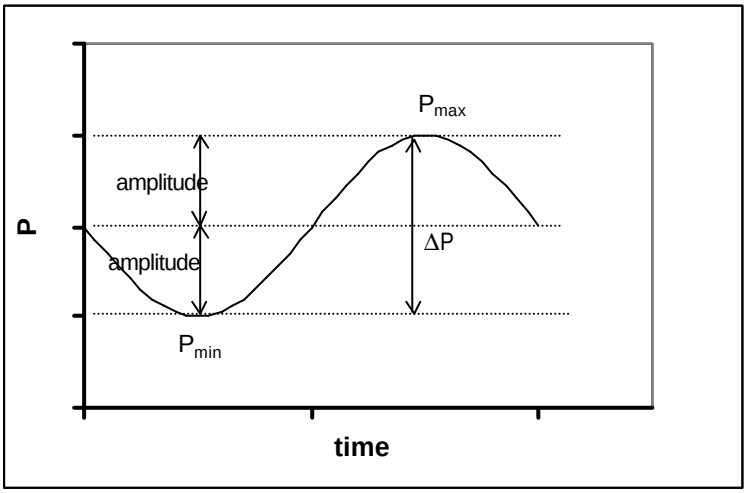

Figure 18: load pattern

In Figure 19, Figure 20 and Figure 201 the experimental set-up is shown. The specimen is connected with two rods to an aluminium fork. The rods fit exactly with the specimen and the fork, but allow rotation, they act as hinges. The forks are attached with thread rods to the dynamic loading machine. At one end, (the right end in Figure 19 and Figure 20) the specimen is attached with a string to a rigid point to carry the dead weight of the specimen. The choice to use a string over a more rigid constraint has been made to avoid 'dancing' of the specimen on the constraint or introduction of unfavourable reaction forces or moments. At the other end a linear variable differential transducer (lvdt) system is attached to the specimen. The lvdt is shown in close-up in

Figure 201. The lvdt is a displacement measuring device that is able to measure small displacements without friction at a distance of 25 mm from the centre of the end of the specimen. The displacements at the end of the specimen are an indication of the stiffness of the specimen. The stiffness of the specimen is related with the crack depth in the adhesive layer. The relation between the crack length and the displacements at the ends of the specimen under a unit load has been studied using linear elastic FEM models, which will be regarded in 6.2. For several crack depths between 25 and 65 mm for the epoxy specimen and between 55 and 105 mm the displacement at the end of the specimen has been calculated for a unit load. The smaller crack depths for the epoxy specimen have been selected in conjunction with the brittle behaviour of the adhesive in the preliminary series. In the preliminary series the artificial cracks in the epoxy were between 50 and 60 mm deep. The initial crack in the epoxy DCB specimen are between 20 and 40 mm deep, the initial cracks in the MS polymer are between 50 and 60 mm. The cracks in the epoxy specimen extend until a depth of a maximum of 65 mm, the cracks in the MS polymer until a depth of 125 mm. Hence, a curve has been fitted through the results of these calculations with a maximum deviation of 2%. So, for every displacement a (virtual) crack depth can be calculated. Initially, the crack has been followed visually on the side of the specimen, but this method has been proven inaccurate.

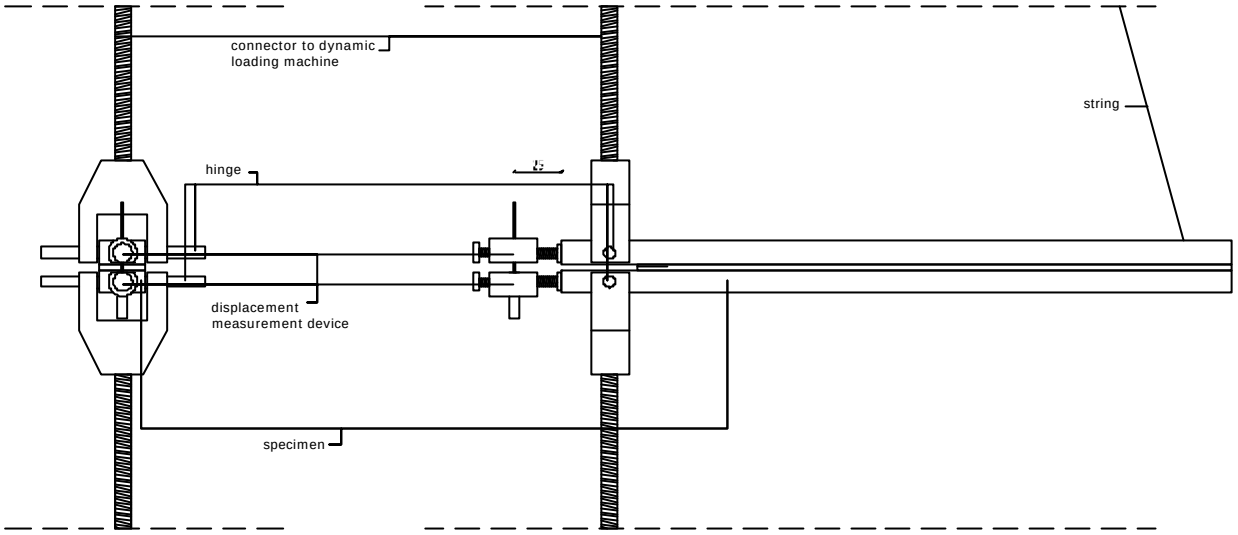

Figure 19: displacement measuring device and the connection between the dynamic machine and the DCB specimen

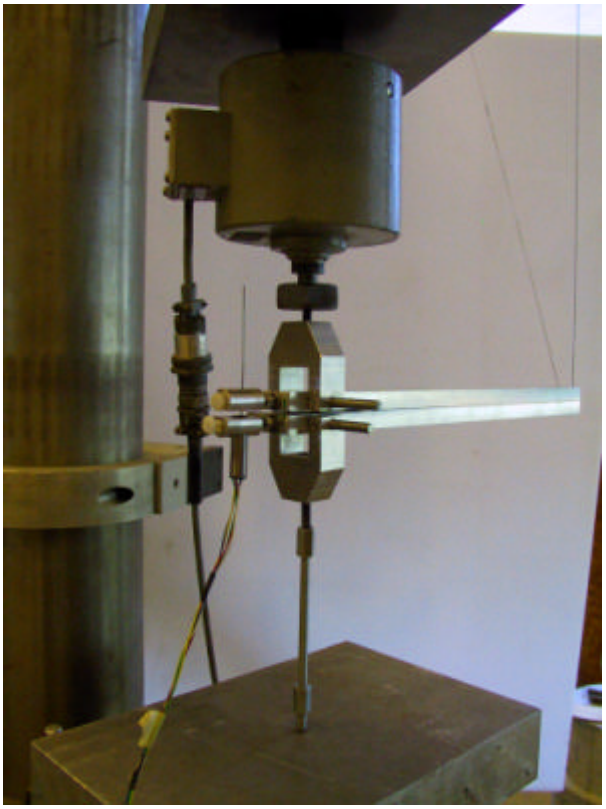

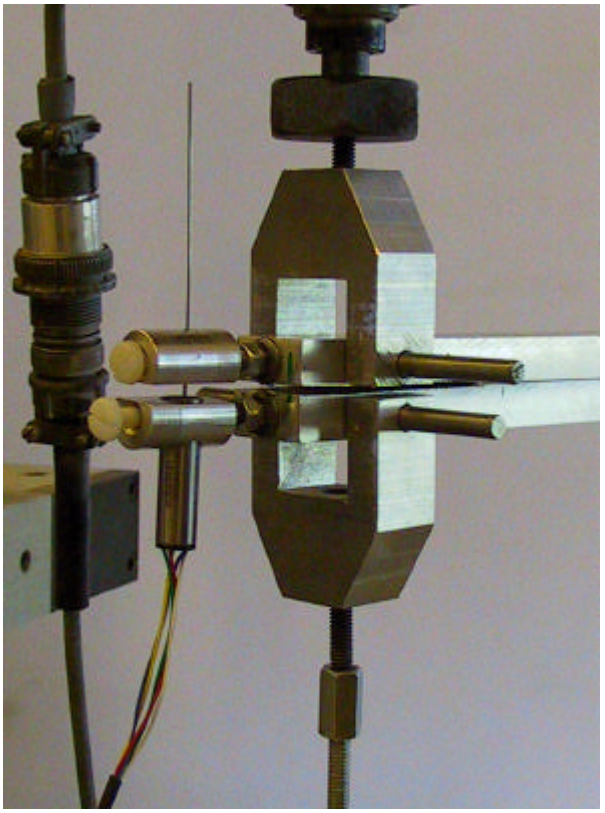

Figure 20 and Figure 21: Experimental set-up, global and detail.

5 Fatigue experiments

In this chapter, the specimens that are the object of the prediction model and that have been used for the validation of the various predictions are described. The geometries as they are given here are also the input for the FEM models of chapter 6. Two sorts of geometries are used: a double lap joint and a tubular joint. In case of the tubular joint, two adhesives have been used, the MS polymer and the epoxy. For the tubular joint only the epoxy is applied. The place of this chapter within the rest of the investigation is shown in Figure 22.

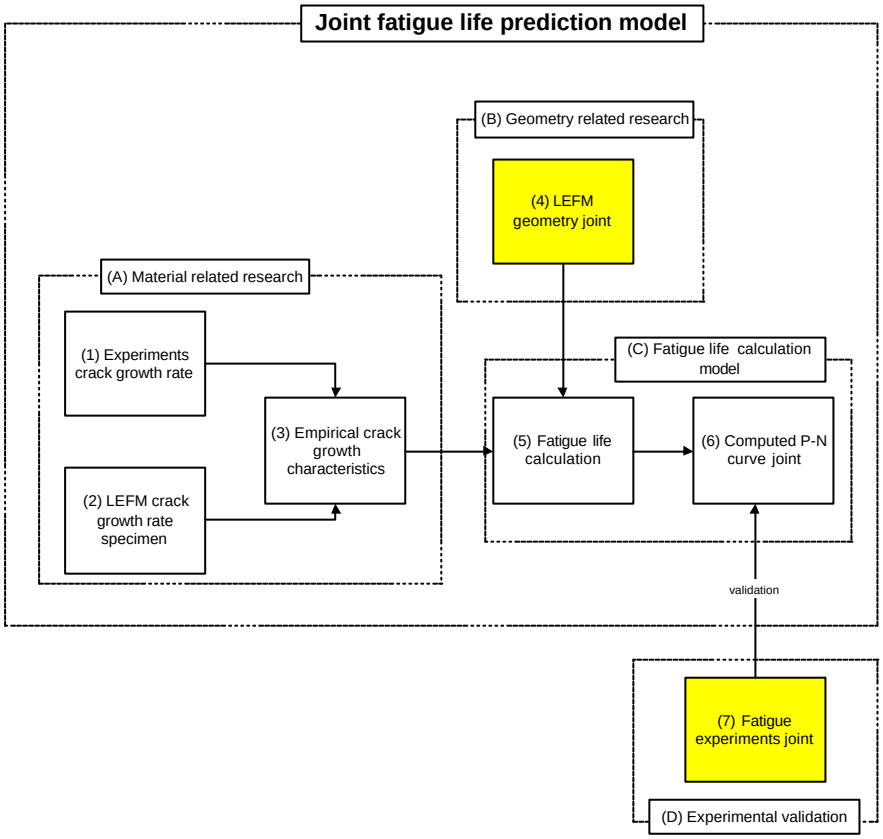

Figure 22: joint fatigue life prediction model flowchart

5.1 Double lap joint

The experimental data from the DCB specimen have been obtained from a TNO research on the properties of adhesively bonded joints [10].

5.1.1 Epoxy specimen

The double lap joint with the epoxy adhesive is a joint that consists of two aluminium strips, 200 mm* 27.0 mm*6.0 mm, joined by two smaller strips of 41 mm*27.0 mm*6.0 mm. The long and the short strip are joined by an epoxy bond line of 0.25 mm. The epoxy double lap joint is shown in Figure 23. Both the short and long aluminium strip are made of 6082 T6 51. The strips are first milled, degreased, etched (bath:150-275 g/l H_2SO_4 and 30-55 g/l H_2CrO_4 35°C) and anodised (bath: 100g/l PO_4, 20°C) before they were joined.

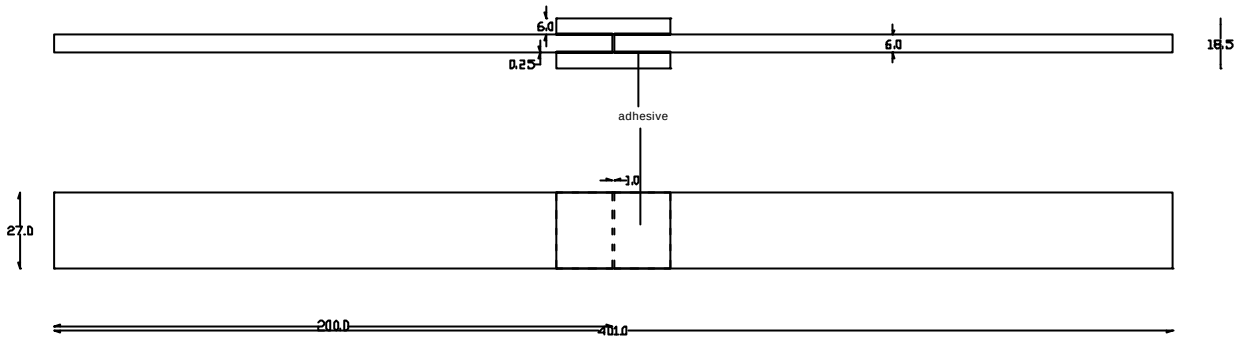

Figure 23: double lap epoxy specimen, dimensions in millimetres

5.1.2 MS polymer specimen

The double lap joint with the MS polymer adhesive is a joint that consists of two aluminium strips, 200 mm* 37.0 mm*6.0 mm, joined by two smaller strips of 41 mm*37.0 mm*3.0 mm. The long and the short strip are joined by an MS polymer bond line of 3.0 mm. The MS polymer bond line has a width of 27 mm, so on both edges there is an off-set of 5 mm. The MS polymer double lap joint is shown in Figure 24. Both the short and long aluminium strip are made of 6082 T6 51. The strips are first milled, degreased, and grit blasted before they were joined.

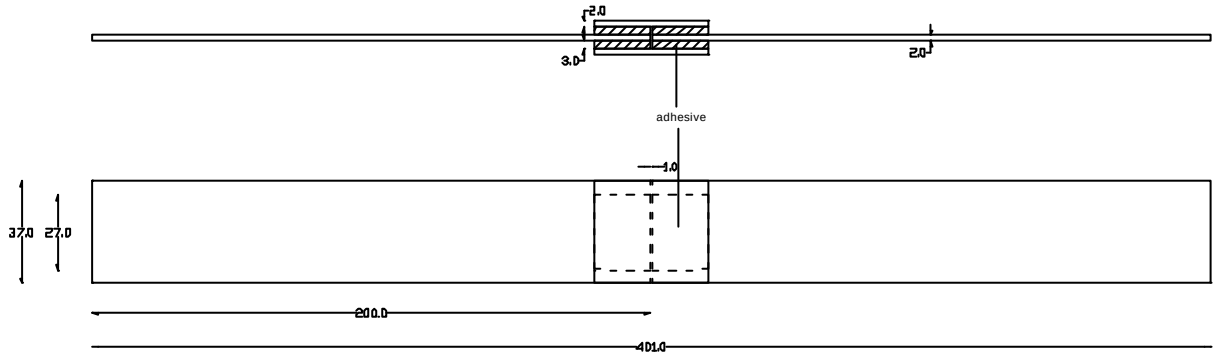

Figure 24: double lap MS polymer joint, dimensions in millimetres

5.1.3 Experimental set-up

All the experiments on the double lap joints have been executed in the CMC laboratory, TNO Building and Construction Research, Delft. The experimental set-up is shown in Figure 25. The specimen is clamped on both ends. The clamps are rigidly connected to the cylinder.

The epoxy specimens are loaded with a cyclic load with maximum of 21.6, 16.2 or 10.8 kN under a frequency of 2.5Hz. The MS polymer specimens are loaded with a cyclic load with a maximum of 600, 900 and 1200 N. The 900 N load was applied under a frequency of 5Hz, the other loads were applied under a frequency of 2.5Hz. For both adhesives all loads have been applied for R=0.1 and R=0.5.

Figure 25: experimental set-up for the double lap joint

5.2 Tubular connection

5.2.1 Tubular specimen

The tubular joint has been assembled from three components, namely two smaller tubes and one greater tube, shown in respectively a and c. All dimensions are allowed to have a standard deviation of ±0.05 mm, unless it is specified otherwise in the drawings. The greater tube has two edges with a length of 5 mm each which have an inner diameter of 57.0 mm, while the rest of that tube has a inner diameter of 57.6 mm. These edge are meant to centre the two smaller tube and leave a space between the greater and smaller of 0.3 mm for the bond line.
Both the smaller and the greater tube have been made from AA 6082 T6 51. Both tubes had a preparation of the surface. The pre-treatment for anodising consists of the following steps: degreasing, (deep) etching (bath: 175 g/l NaOH, 55°C), cleaning the etched surface (bath: HNO_3 water = 1:1 room temperature) and anodising (bath: 100g/l PO_4, 20°C).

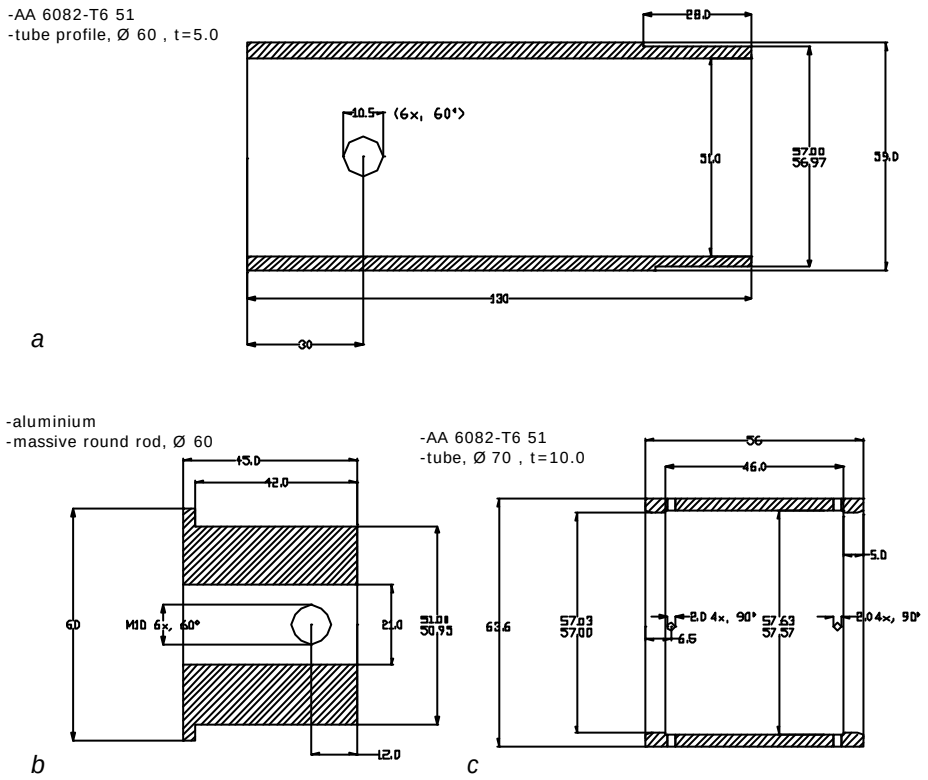

Figure 26: parts of the tubular joint, a) the smaller tube, b) connector to the dynamic bench, c) the greater tube

The greater tube has been put epoxy on the inside between the edges. The epoxy is also put on the smaller tube (57 mm) as well. Subsequently, a core is placed in one of the two smaller tubes. Next, the greater tube is slowly shoved over the smaller tube. Finally, the second smaller tube is shoved into the greater tube. Due to the core inside the smaller tubes and the small tolerance between the smaller tube and greater tube and the smaller tube and the core, the adhesive has only one possibility to leave the space between the tube and that is through the holes in the greater tube. To push the adhesive out through the holes, the assembler has to apply pressure on the tubes. Due to the pressure on the adhesive, the air included between the tubes is pushed out as well.

After the adhesive was cured, the edge of 5 mm and the section with the leaking holes has been removed, leaving a lap length of two times 20 mm. The section adjacent to the edges has been tapered, to avoid a major discontinuity at the border between the wall thickness of 3 and 4 mm. Next the connector are inserted. M20 bolts are placed through the connectors in longitudinal direction. The connectors are connected with six M10 to the smaller tube.

The assembled and finished specimen is shown in Figure 27 and Figure 28.

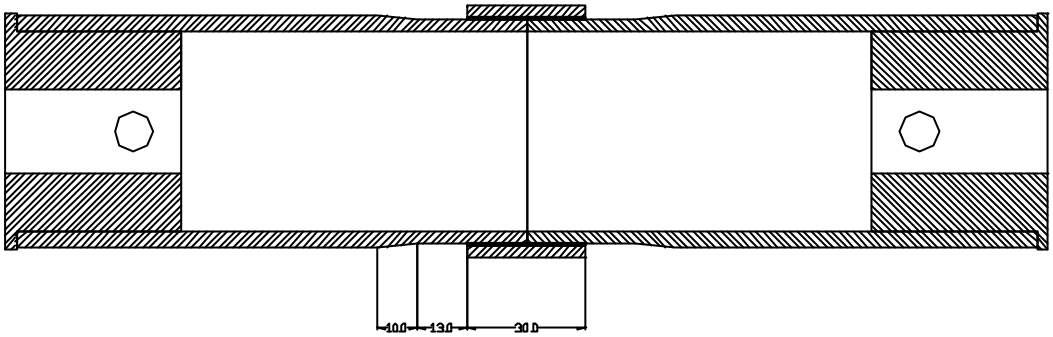

Figure 27: assembled and finished tube joint

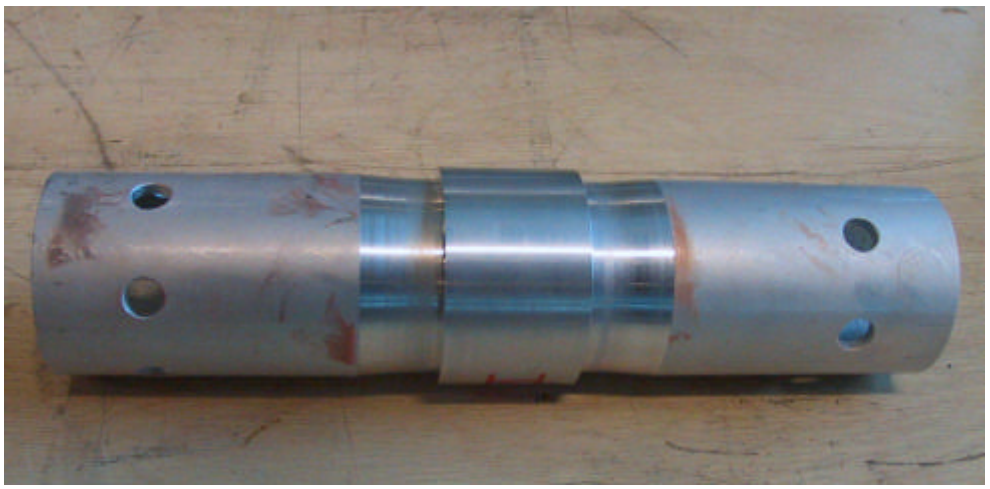

Figure 28: assembled tube joint

5.2.2 Experimental set-up

The tubular joint specimen has been connected to the dynamic load machine using connectors (Figure 26b). As has been stated in the former paragraph, the connectors are joined with bolts with the specimen. The experimental set-up is shown in Figure 29.

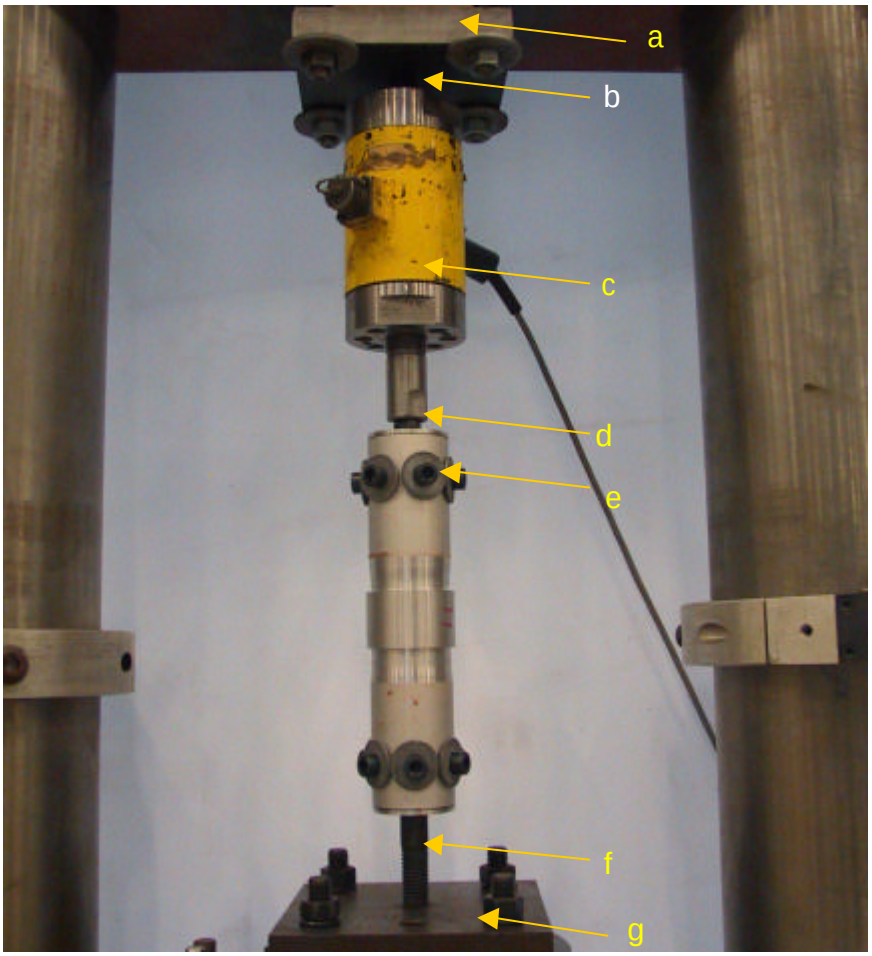

Figure 29: experimental set-up

Beside the specimen itself, the set-up consists out of seven components:

a) Solid steel plate
b) Bolt (M20)
c) Load cell (max 100 kN)
d) Bolt (M20)
e) Bolted connection connector specimen
f) Bolt (M20)
g) Solid steel plate

The upper steel plate is connect to a rigid bench, the lower steel plate is connected to the piston. In the chain of the experimental set-up, a single bolt has been applied three times. A single bolt can transfer (mainly) tension, so when the specimen is loaded, the chain is going to find the position in which can transfer only tension.

6 FEM research

This chapter concerns the numerical part of crack growth due to fatigue in the adhesive joints. In chapter 4 and 5, the geometries of all specimens used within this investigation have been described. The structural behaviour of these geometries can be simulated using FEM analysis. The main purpose of this chapter is to find the relation between the crack depth *a* and the energy release rate *G* for the tubular and the double lap joint, using the results of the FEM calculations. The FEM results are going to be analysed in order to find a formula using a curve fitting application

As a start, the method that is used to apply the FEM results is described in 6.1. The three geometries, DCB, double lap joint and the tubular will be described per type in 6.2, 6.3 and 6.4. First the modelling will be regarded: type of analysis, applied constraints type of elements etc. A point of interest related to the geometries is the influence of the lap length on the energy release rate. Per geometry the results will be shown. In Figure 30, the relation of the FEM research with the rest of the study is shown.

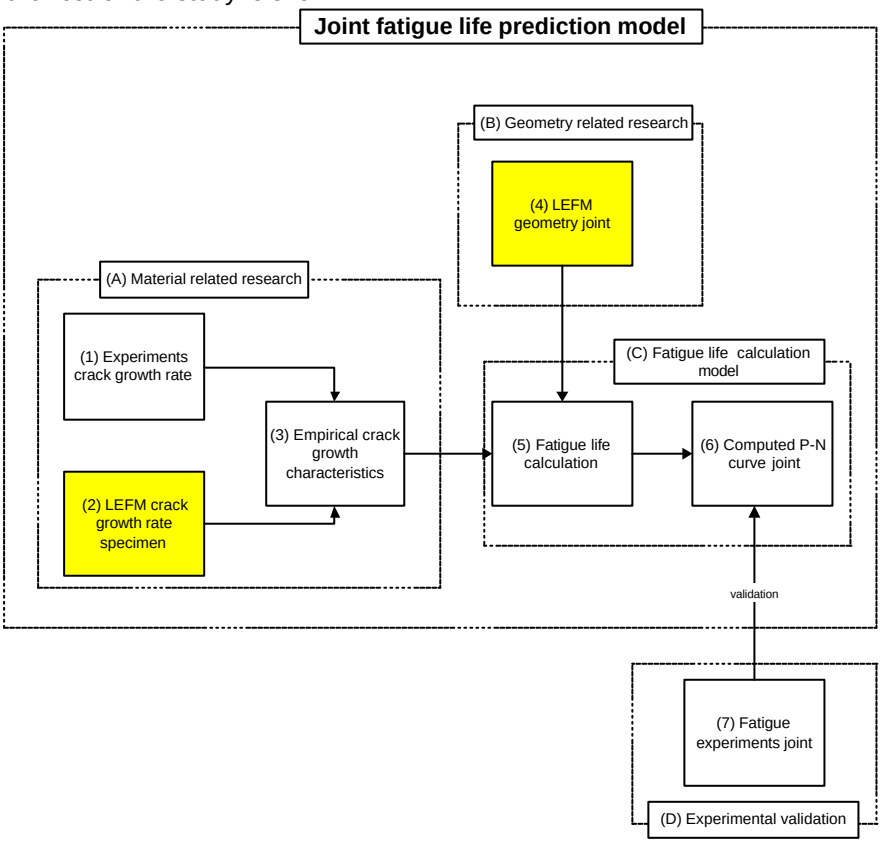

Figure 30: joint fatigue life prediction model flowchart

6.1 Application of FEM output

In 3.3 it has been stated that to predict the fatigue life of an adhesively bonded joint, the energy release rate for a number of cracks has to be computed and the modified Paris' law can be applied. All the FEM models that have been solved to obtain crack growth characteristics in this chapter are linear elastic. Geometrical or physical non-linear models cannot be solved with the available fracture mechanics application. During the modelling and regarding the results, it has

become clear that for good results for the fracture mechanic calculation the linear elastic models are sufficient. In the FEM models in this chapter, the models are subjected to a unit load. In the output of these calculations the energy release rate *G* is assumed to be a quadratic function of the applied force *P*:

$$G = f(h, E_{adh}, E_{sub}, b, a, l, n_{ash}, n_{sub}) * P^2 \qquad \textit{Equation 8}$$

This approach is consistent with the simple beam theory in 4.3.

After the models are solved and the results are generated, the output is analysed in order to find accurate mathematical descriptions to describe the mechanical behaviour of the geometries of the joints. The description gives a relation between the crack depth *a* and the energy release rate *G*. These mathematical descriptions are determined by curve fitting of the results. All the curve fitting data are included in Appendix II. *G* can be calculated for a unit load and the results can be scaled to the favourable load. By scaling the loads gradually, the range between G_{th} and G_c can be found. If the value of *G* at the initial crack is below G_{th}, no cracking will occur. If *G* is larger than G_t, the fatigue life will only last a few cycles
Once the relation between *G* and *a* is obtained, it can be substituted in the modified Paris' Law integral (equation 4) to come to fatigue life predictions under various constant amplitude loads. Multiple fatigue life predictions can be translated to a P-N curve for a joint geometry. The P-N curves will be considered in paragraph 8.

6.2 DCB

In 4.3 the calculation method to arrive at a *da/dN-G* diagram has been explained. In Figure 17, a scheme for the method has been given. This scheme includes a block of FEM calculation for the DCB specimen, which is going to be outlined in this paragraph.

6.2.1 Model

The model that has been used to calculate *G* for the DCB specimen is a 2D model, a plane strain model. In a plane strain model, all strains perpendicular to the plane of the model are assumed to be zero over the whole plane. The FEM models have been calculated, built and solved in DIANA 8.1. The elements used are 8 node plane strain elements (CQ16E) and a crack tip element (PT1CR). The DCB specimen has been modelled only half, as it is symmetric. The crack is assumed to grow through the middle of the adhesive layer. To be sure that this assumption was correct, a validation model has been made. The results of this validation will be discussed later on in the results section.
The global layout for the DCB is shown Figure 31, the mesh around the crack tip is shown in Figure 32. In both figures the arrows points to the crack tip element in the adhesive layer. The crack tip element is a special point element, it transfers the mid-nodes of the adjacent elements to quarter point position (Figure 33) to calculate the crack growth characteristics *G* and *K*, respectively the energy release rate and the stress intensity factor. The characteristics are calculated using a method that is based on the *J* integral. The calculation is linear elastic. The background theory about the calculation is out of the scope of this report.

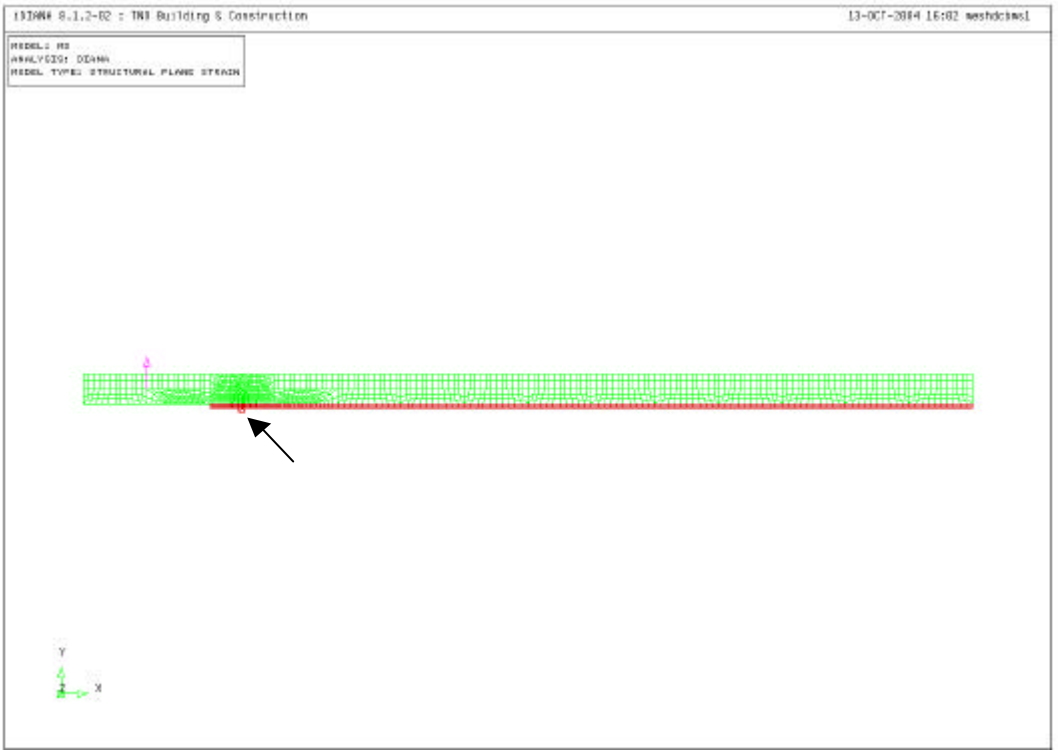

Figure 31: mesh of the DCB specimen

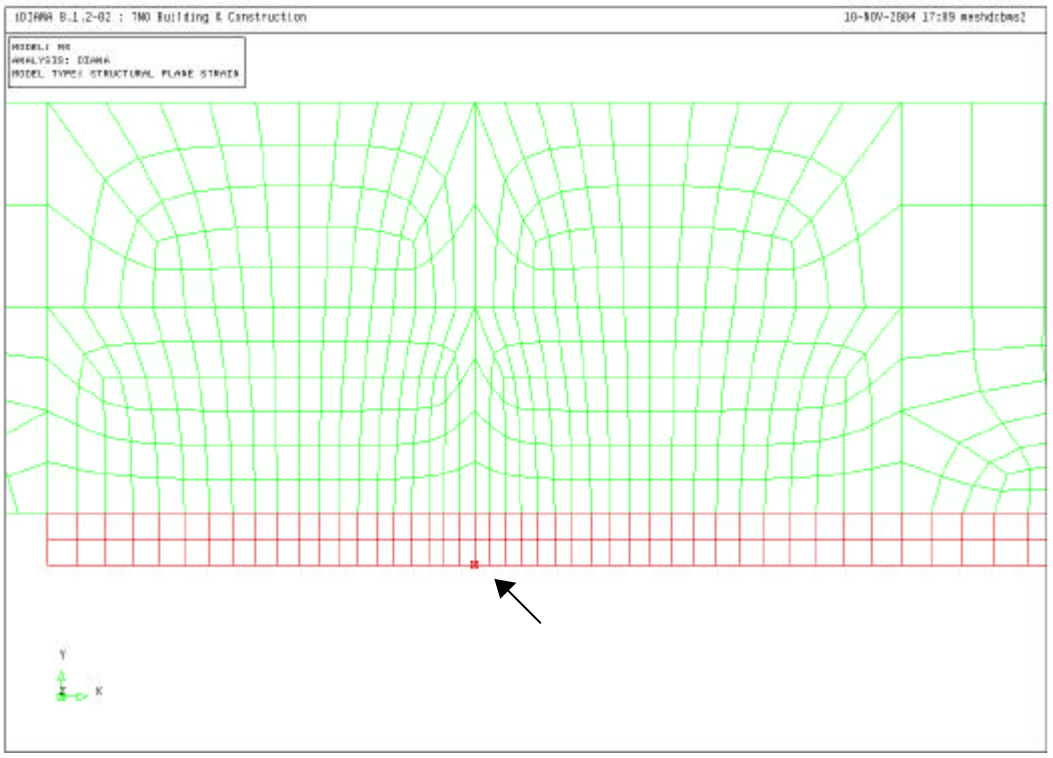

Figure 32: mesh around the crack tip

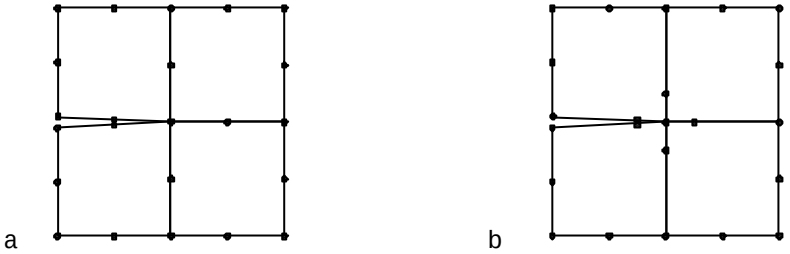

Figure 33:a) standard mesh of four 8 node elements around a crack tip; b) modified mesh around the crack tip, all the mid-nodes adjacent to the crack tip have been transferred to quarter point position

At the right side of this crack tip element, the nodes at the bottom edge in the adhesive layer are constrained in vertical direction. The constraints along this edge act as a symmetry axis. At the left side of the crack tip, the nodes at the lower edge are released in both directions. At the point where the specimen is loaded with a unit force (at the lower end of the pink arrow, Figure 31), the model has a horizontal constraint.
There are three differences between the epoxy and the MS polymer model. At first, the material properties are different. Second, the thickness of the epoxy bond line is 0.3 mm, the MS polymer bond line is 3.0 mm. Third and last difference is the density of the applied mesh. Because the adhesive layer of the epoxy model was very thin compared to the height of the substrate, a very fine mesh is used, in order to avoid heavily deformed elements, which could affect the accuracy of the model's results. In the case of the MS polymer, such a fine mesh would have been a waste of modelling and processing time, therefore the number of elements in the model was kept as small as possible.

6.2.2 Results

The results of the comparison are shown in table 2 and Figure 34 for a FEM calculation and an analytical solution, the simple beam theory, given in 4.3. The curves are the derived curves, which are used in the prediction models. The transformation from data points to curves is included in appendix II. The deviation between the curves and data points never exceeds ±3%. The crack depths have been chosen with the DCB experiments in mind. The analytical results are included in the table and figure to check whether the analytical method and FEM match. The simple beam theory does not include the properties of the adhesive layer or the thickness of the bond line in its description, whereas the FEM model does include the E modulus, Poisson ratio and the layer thickness. The simple beam theory assumes a rigid inclination at the crack tip. Considering the mechanical properties, this assumption of a rigid inclination is a point where the two adhesives differ. The epoxy specimens have such a thin bond line with a relatively high E modulus that a rigid inclination is an acceptable concept for modelling. In contrary to the MS polymer specimen, which is connected by a thick and flexible bond line. Bending of the substrate solely causes the deformations in the simple beam theory, while in the FEM model shear of the substrate and deformation of the adhesive are accounted as well.
Regarding the results it is clear that FEM approach for both adhesives and the simple beam theory have results in the same order of magnitude. When the results of the MS polymer and epoxy are compared in Figure 34, the difference is obvious. The MS curve is on a higher level than the epoxy curve. Both charts seem to have a similar form and curvature. Comparing the FEM curves with the analytical curve, the expectations that have been stated before are confirmed. The curve of the stiff epoxy specimen matches the analytical curve nearly perfectly.

The line of the MS polymer shows a significant difference with the analytical solution. Apparently, the flexibility of the MS polymer has impact on the deformation behaviour of the joint, considering the difference with the analytical that does include the behaviour of the adhesive.

Concerning the asymmetric crack, the crack along the interface, in [11], two different crack positions have been compared, namely through the centre and along the interface between the adhesive layer and the substrate. It came out that the results hardly differed. Still, a validation calculation was desirable. Unfortunately, the software is not able to calculate *G* on the exact interface of the two materials. Therefore, a check has been performed for a slightly different problem. Instead of modelling a crack along the interface, a very thin layer of adhesive on the substrate has been modelled for the epoxy model. Basically, the crack has been moved down very close to the interface, without reaching it. The thin layer approach has been done twice, for two different thicknesses, one of a sixth and one of a tenth of the adhesive layer thickness. The symmetric crack results are slightly higher than the interface crack results. The difference came out to be marginal and on the safe side compared to the symmetric crack.

table 2: results of calculations for G, modelled with a FEM for epoxy and MS polymer, and described with an analytical material independent model

	G [N/mm]		
	FEM		analytical
a	epoxy	MS polymer	
20	6.81E-05		4.44E-05
25	8.69E-05		6.68E-05
30	1.14E-04		9.40E-05
35	1.45E-04		1.26E-04
40	1.80E-04		1.63E-04
45	2.18E-04		2.06E-04
50	2.60E-04		2.53E-04
55	3.05E-04	9.80E-04	3.05E-04
60	3.55E-04		3.62E-04
65	4.13E-04	1.10E-03	4.24E-04
75	5.39E-04	1.25E-03	5.63E-04
85	6.74E-04	1.46E-03	7.22E-04
95	8.25E-04	1.69E-03	9.00E-04
105		1.94E-03	1.10E-03
115		2.20E-03	1.32E-03
125		2.48E-03	1.55E-03

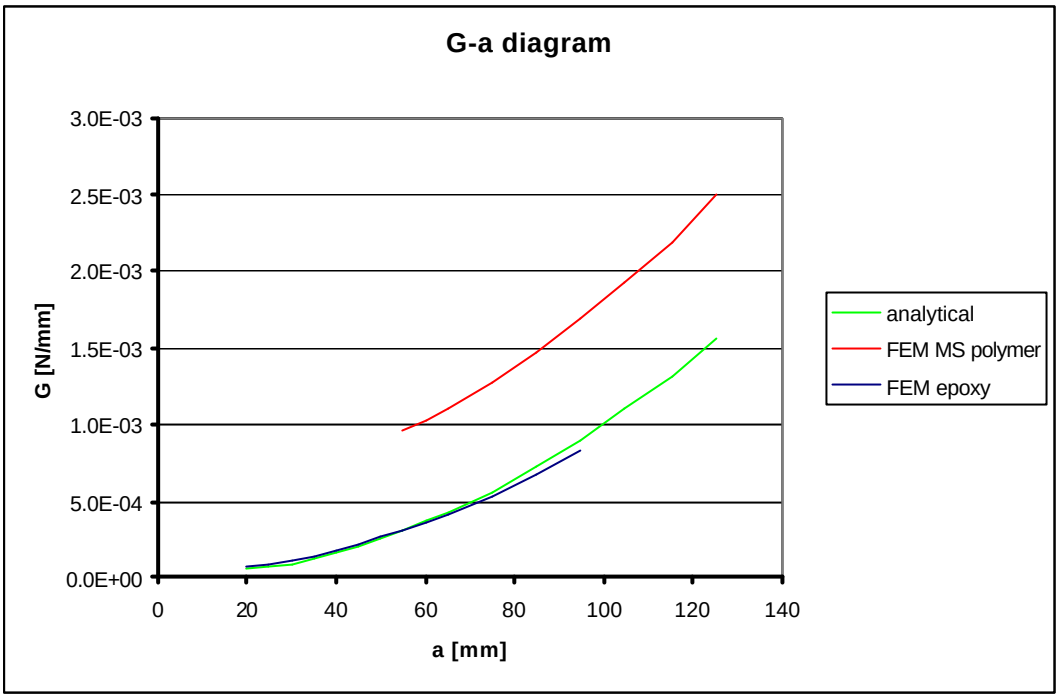

Figure 34: G-a diagram DCB, calculated with a FEM model for epoxy and MS polymer and calculated with an analytical material independent model for a unit load and unit width

6.3 Double lap joint

6.3.1 Model

The double lap joint is tested for two different adhesives, an epoxy and an MS polymer, shown in Figure 23 and Figure 24. The experiments on the double lap joints are a part of [10]. The geometry of the epoxy joint and the MS polymer joint are respectively shown in Figure 23 and Figure 24. The adhesives are the same as the adhesives of the tests with the DCB specimen. There is a small difference: in the double lap joint the adhesive layer has a thickness of 0.25 mm, in the DCB specimen and in the tubular connection the adhesive layer have a thickness of 0.30 mm.
The bonding and mechanical properties of the two adhesives differ significantly; therefore the dimensions of the specimens for the two adhesives differ. The adhesives have each an optimum thickness. The epoxy specimen has thicker substrate material, 6 mm compared to the MS polymer specimen, 3 mm.

The modelling scheme is shown in Figure 35. The specimen has two symmetry axes, therefore only one quarter of the whole joint has been modelled, this part is shown in Figure 37. Mind that the strip has a thickness of only a half of the thickness of the real strip, as the symmetry axis lies along the centre line of the strip. Along this centre line the displacements in vertical directions are precluded. Essentially, the calculation method of the double lap joints is the same as the DCB specimen. Both the connections have been modelled assuming a plane strain situation. The models have been made using 8 node plane strain elements (CQ16E) and a crack tip element (PT1CR). The crack is assumed to grow through the centre of the adhesive layer. In the FEM model it is supposed that per adhesive layer two cracks will occur during the fatigue life. The

cracks grow at a similar speed. In the results the cracks will be referred to as left and right, as in Figure 36. The FEM model with the two cracks can be seen in Figure 38. This assumption will be evaluated in 6.3.2. In Figure 38, the mesh near the crack tip is shown for the MS polymer model.

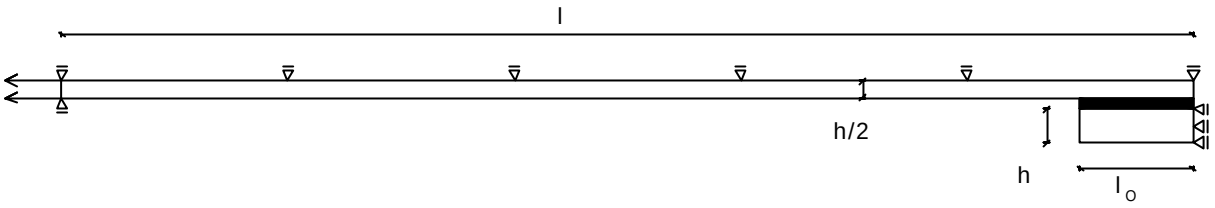

Figure 35: modelling scheme of the double lap joint

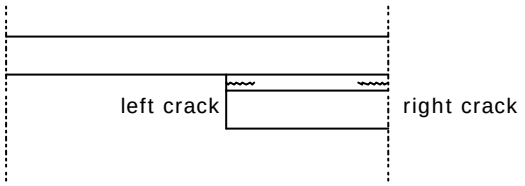

Figure 36: lay out crack zone

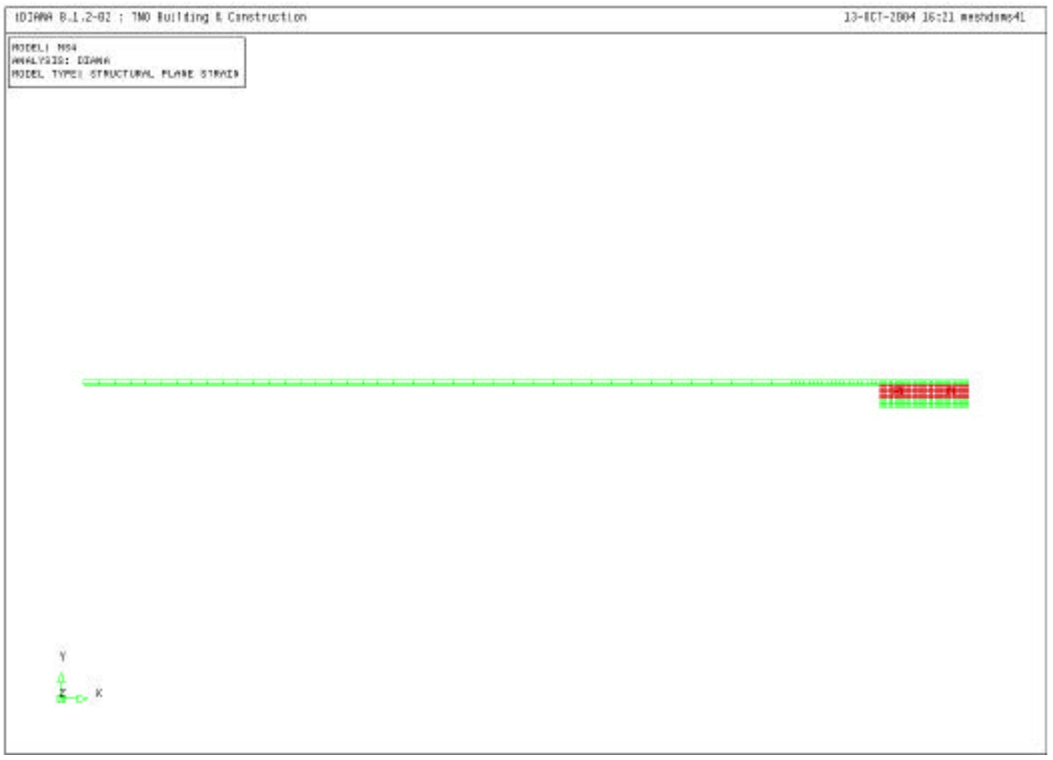

Figure 37: mesh of the double lap (MS polymer): in green the substrate, in red the adhesive

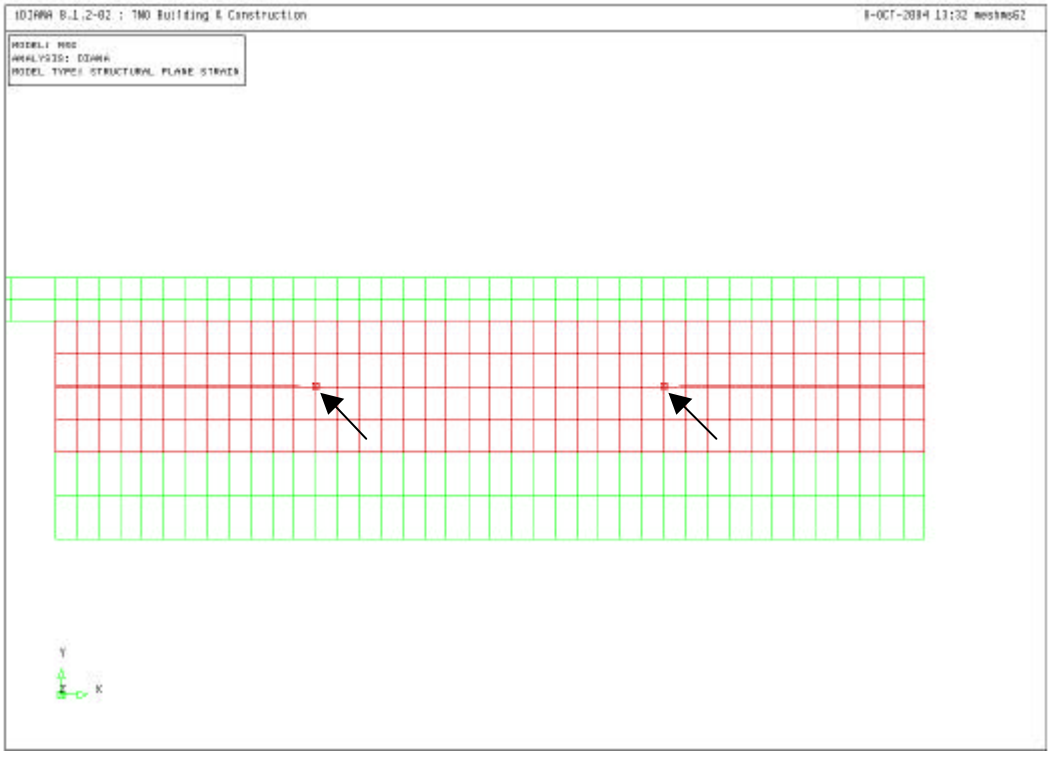

Figure 38: mesh in the adhesive layer around the crack tip (MS polymer)

When the model is loaded, the connection will deform. An example of the deformation is shown in Figure 39. In this joint geometry the model will lap itself near the crack tip, at the point of the arrow in Figure 39. Naturally, lapping in a FEM model is not according to the behaviour of the real physical connection. In reality, in the physical connection, the lower part of the substrate will press against the upper part of the substrate. To investigate the influence of the pressure, contact elements can be used. The contact elements avoid lapping in the FEM model. However, with the introduction of these contact elements a new difficulty has been introduced. The contact elements require a geometrical non-linear calculation, whereas the crack tip elements require a linear elastic calculation. To make a first estimate about the influence of the influence of the lapping, the result of a linear elastic calculation and a geometrical non-linear calculation have been compared, mainly focussing on the stress distribution around the cracked area. In figure 41 a and b, the stresses in the x-direction are shown for respectively the model without and with the contact elements. The global stress distribution is hardly affected by the presence of the contact elements. The main difference in the results is the calculated stress level near the crack tip. This difference is logical, as the crack tip elements moves the mid-nodes around the crack tip. However, the difference in the stress levels between the two models is marginal.

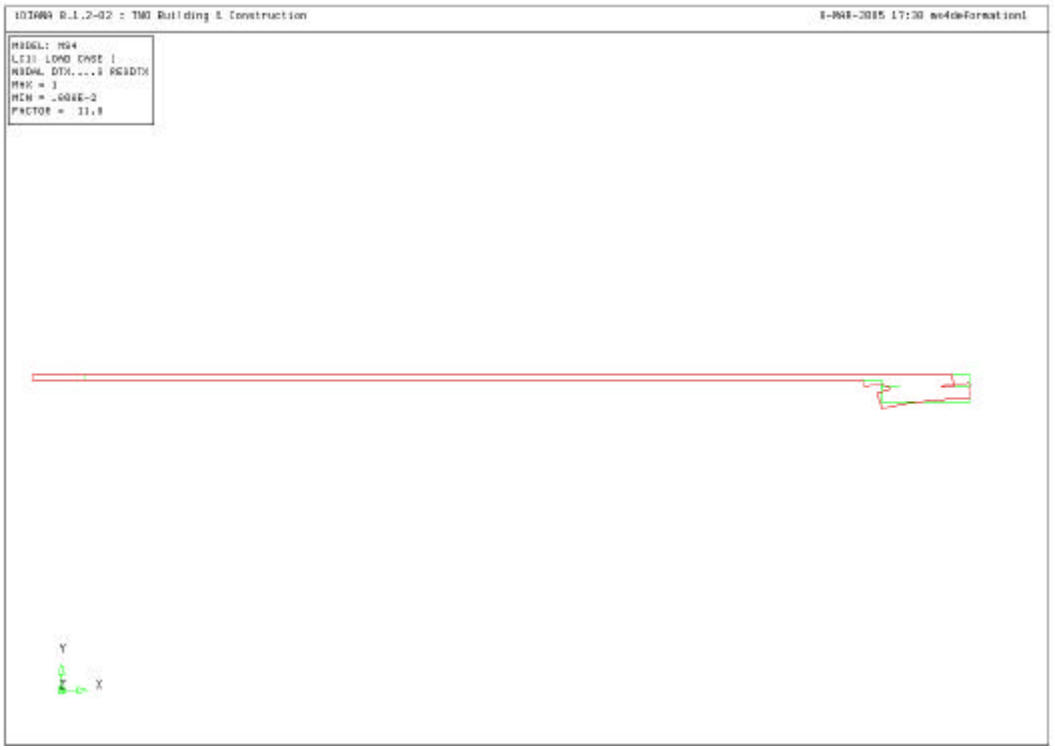

Figure 39: lap joint; in green the edges of the original edges, in red the deformed edges in the double lap connection

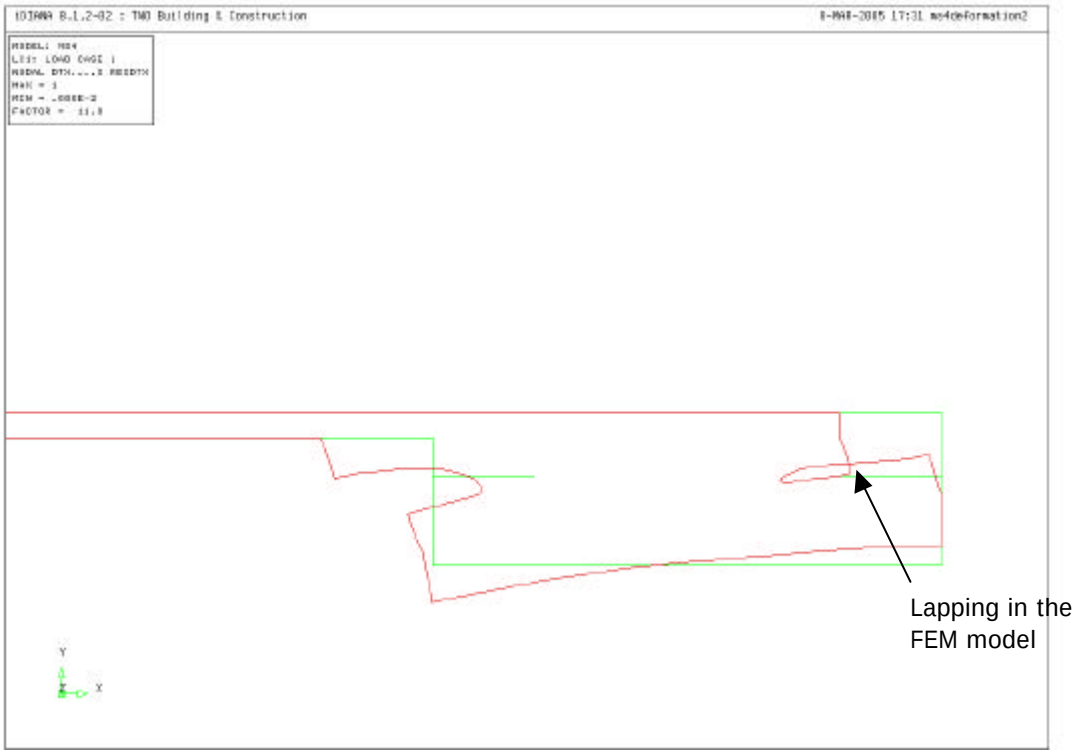

Figure 40: lap joint, close-up; in green the edges of the original edges, in red the deformed edges

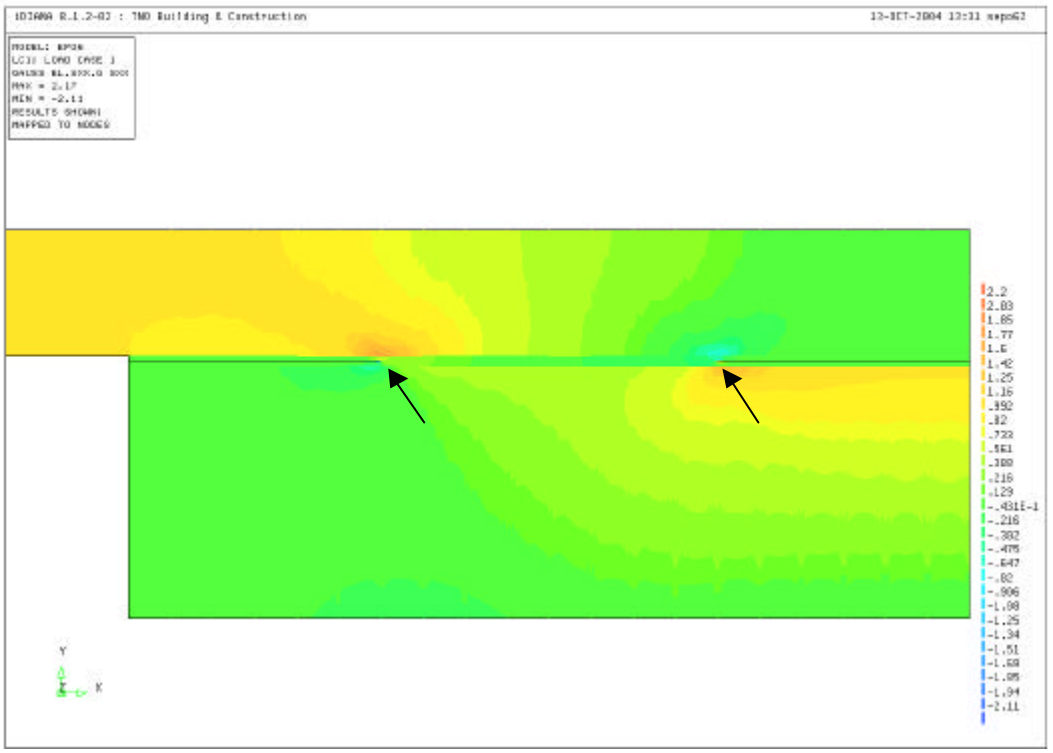

a

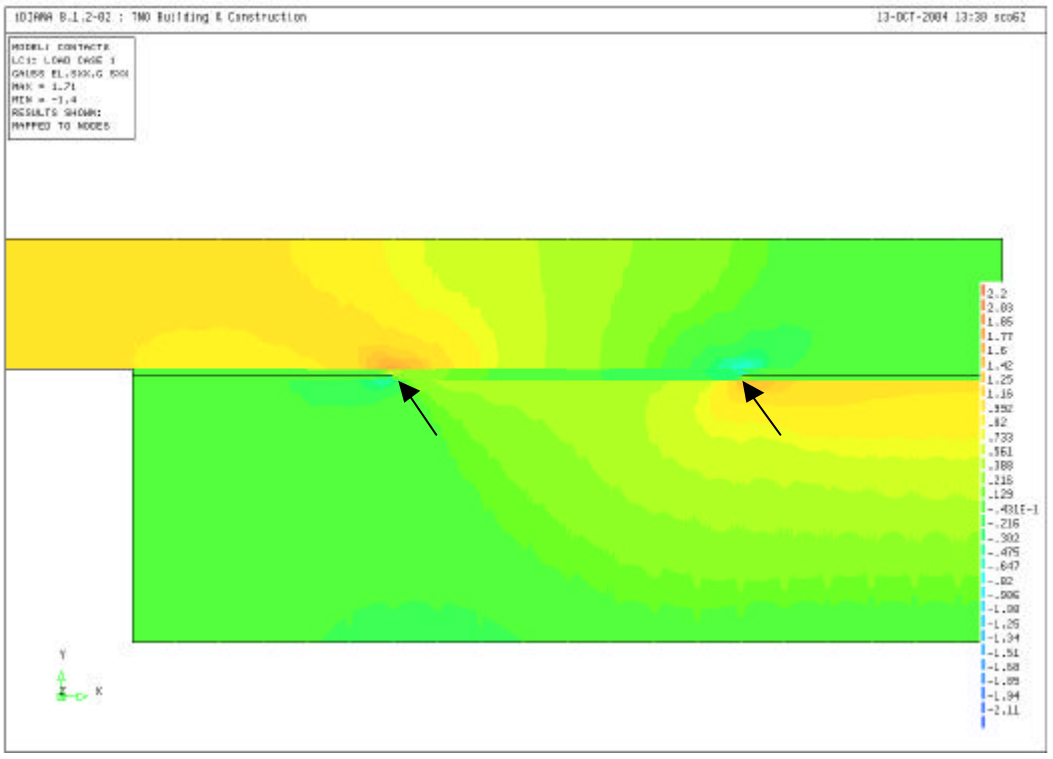

b

figure 41: (a) stress gradient in the double lap connection (epoxy) calculated with the linear elastic model (b) stress gradient calculated with the geometrical non linear model, including contact elements

6.3.2 Results

In Figure 42 and Figure 43, the results for respectively the epoxy and the MS polymer are given. The curves are the derived curves, which are used in the prediction models. The transformation from data points to curves is included in appendix II. The deviation between the curves and data points never exceeds ±5% for at least the first 70% of the lap length in case of the epoxy. In case of the MS polymer, the maximum deviation between the curve and the FEM results does not exceed 9% for at least the first 70% of the lap length. The results are all for a half specimen. When the results are regarded, the following points should be noted:

- Concerning the level of the results, when the epoxy results and the MS polymer results are compared, it can be noted that the results of the MS polymer are about three orders of magnitude greater than the epoxy results, both the joints with 20 and 40 mm lap length.
- For the MS polymer, the left and the right curve nearly perfectly concur. In the case of the epoxy joint, the right curve follows the left curve on a distance until at least 60% of the lap length before the left and right are approaching each other. The fact that the MS polymer left and right curves nearly coincide in contrary to the epoxy could be explained by the flexibility of the MS polymer joint. Apparently, the bond line of the MS polymer is so flexible that the difference between left and right is nearly totally levelled up.
- The left and right curves per joint are within the same order of magnitude. When both ends of the adhesive layer have a similar surface and crack initiation occurs at both sides, it is likely that the crack will progress with at the same time as the energy release rate at both cracks is in the same order of magnitude. In case of the MS polymer the energy release rate left and right is even equal. However, in case of the epoxy, the right crack will grow slower than the left crack. The assumption that the cracks is going to grow from two sides like in Figure 38 seems to be probable on the condition that the chance that crack initiates at both ends of the adhesive layers is equal.
- For epoxy the positive influence of the lap length is obvious. By doubling the lap length, the energy release rate is decreased significantly, with a reduction of at least 50%. Especially reduction of the energy release rate at the initiation of the crack has a strong influence on the fatigue life. The application of a longer lap, resulting in a reduction of G, would lead to a substantial increment in fatigue life of the joint under an equal load. In the case of the MS polymer, the energy release rate at the initiation of the crack is about equal for both lap lengths. Once the crack starts to grow, the energy release rate grows significantly faster for the short lap than for the long lap. The effect of doubling the lap length will be stronger for the epoxy joint, because the reduction of G at initiation is stronger for the epoxy than for the MS polymer.

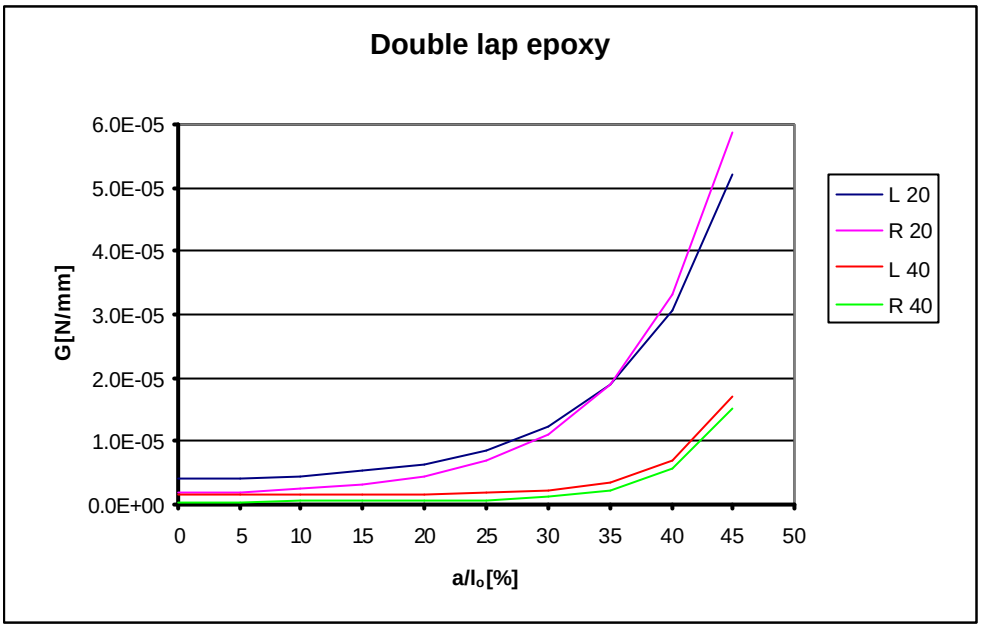

Figure 42: G-a/l_o diagram epoxy for the double lap connection, unit width 1 mm and a load of 1 N

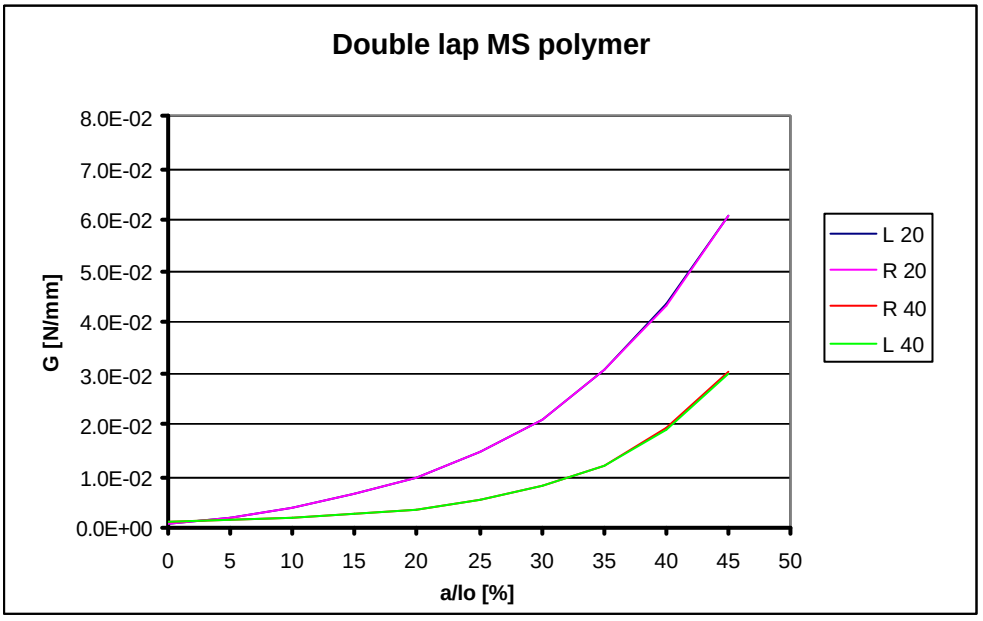

Figure 43 G- a/l_o diagram MS polymer for the double lap connection, width 1 mm and a load of 1 N

6.4 Tubular connection

6.4.1 Model

Note that the tubular connection is only modelled for epoxy. As it is too complex and impractical for this project to produce tube joints for MS polymer, the analysis is skipped. When the FEM

model cannot be validated by experiments, the use of the FEM results is dubious, except for strictly theoretical purposes.
The tubular connection can be modelled with a 3D model or with an axisymmetric 2D model. The 2D axisymmetric model has the advantage that the amount of elements that is required to obtain accurate results is much smaller than the 3D model. The time required to build the model and to solve the model is far less for the axisymmetric model. An axisymmetric model is built as a plane 2D model. This plane is rotated around a central axis. The distance between the plane and the axis determines the diameter of the model.
The modelling scheme of the tubular joint can be seen in figure 44. The scheme seems to have a lot of similarities with the double lap joint, but do mind that the plane shown in figure 44 needs to be rotated around the central axis. The most important difference between the double lap and the tube model are the constraints and the analysis type. The strip material of the double lap connection in the double lap joint model had a thickness of *h/2*, the thickness of the smaller tube is *h*. Even more important are the constraints of the models. The axisymmetric model has a symmetry (rotation-) axis. Axisymmetric models in general can deform free in radial direction, but displacements in tangential direction are impossible. In the used model type, loads can only be applied within the plane. A scheme of the model is given in figure 44, where all constraints can be seen. The lay out of the crack zone is the same as the double lap joint, Figure 36. Vertical displacement of the left end of the inner tube and horizontal displacements of the right end of the outer tube are precluded. Furthermore, the joint is assumed to crack from two sides, like the double lap joint.

Like for the double lap joint, the lap length l_o of axisymmetric models is varied. Models with a lap length of 15, 20 and 40 mm have been solved.

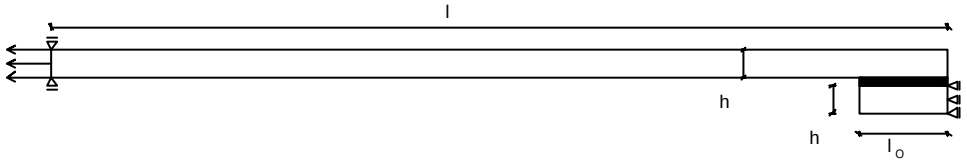

figure 44: Modelling scheme of the tubular joint

6.4.2 Results FEM

In Figure 45, the results of the calculations of the tubular joint for the epoxy joint for lap lengths 15, 20 and 40 mm are given. The curves are the derived curves, which are used in the prediction models. The transformation from data points to curves is included in appendix II. The deviation between the curves and data points never exceeds ±5% for at least the first 70% of the lap length. The results are given for a complete, round tube with an outer diameter of 57 mm, loaded with a unit load of 1 N for the whole surface of one end. The adhesive layer is 0.3 mm thick. The energy release rate has been calculated for a crack that is 57*π=179 mm long.
Regarding the results, the following points of interest can be noted:

- The results for all lap lengths show a difference between the left and the right curve. In all cases, the left curve lies higher than right curve. For all curves, the right curves grow to the same level as the left curve.
- The results for left and right are in the same order of magnitude. It is most likely that under similar conditions of the surface at both sides cracks will nucleate and grow at the same time, probably the left faster than the right.
- For this tube geometry the influence of the lap length is obvious. Increasing the lap length from 15 to 20 mm reduces *G* with 30% for the left crack and even a bit more for the right crack. Increasing the lap length lap from 20 to 40 mm reduces *G* nearly 50% compared to the 20 mm joint and even 64% compared with the 15 mm joint.

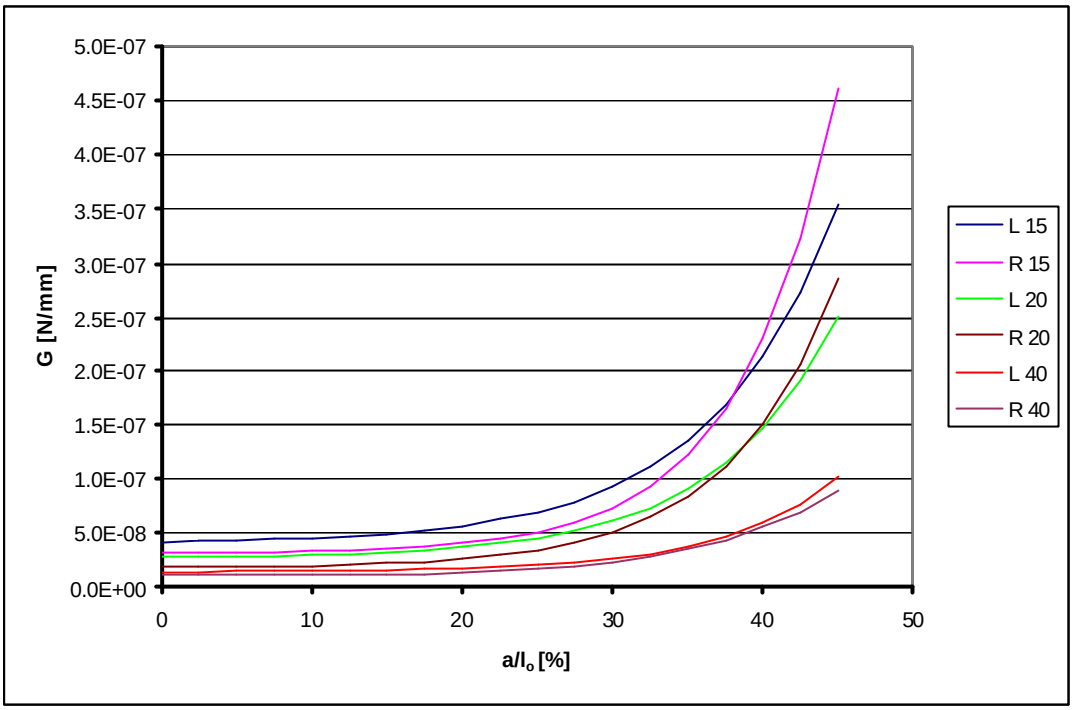

Figure 45: G-a/l$_o$ diagram epoxy for the tubular connection, diameter of the bond line 57 mm and a load of 1 N

7 Experimental results crack growth experiments

In this chapter, the experimental results of the crack growth experiments are going to be presented. At first, the criteria for the determination of the constants are described shortly. Then, the *da/dN-G* diagrams are presented. Finally, all results are discussed. All results given in this chapter have been calculated according to the scheme in Figure 17, using the formulas derived in the former chapter.

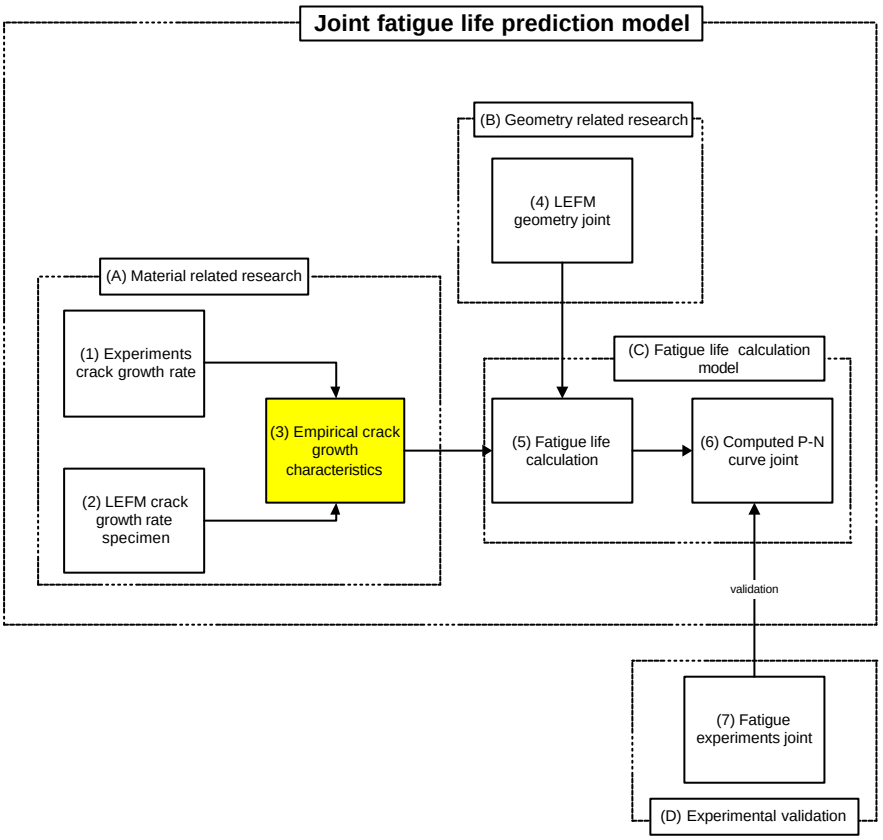

Figure 46: joint fatigue life prediction model flowchart

7.1 Concerning the crack growth constants

Previously in chapter 3, the modified Paris' law (equation 4) has been introduced. In this law G is used as the main crack growth parameter to predict the fatigue life of a joint. For practical application of this formula, both ΔG and G_{max} can be used. G_{max} concerns about the maximum load on the joint and ΔG includes the load range. In practice it is expected that both the load range and the maximum load effect the fatigue life. It is rather arbitrary to select the load range instead of the maximum load or vice versa, as it is likely that both influence the fatigue life in the case of adhesively bonded joints. Therefore the results of the DCB specimen experiments will be given for both G_{max} and ΔG in order to avoid excluding one of both perspectives on this dilemma. A fundamental approach to find a optimum parameter concerning the energy release rate is not going to be made here. A more pragmatic approach is more favourable in this place and time, both results are going to be regarded and discussed.

In the *da/dN-G* diagrams in the following pages, the results have been grouped per specimen. All results from a single specimen have one colour. After all experimental results have been gathered, an exponential regression analysis has been applied to find an average curve through the so-called Paris region. This average is the dotted diagonal in the diagram. For the epoxy two asymptotes have been found, G_{th} and G_c, for the MS polymer only one asymptote was found, G_c. These asymptotes have been added to the *da/dN-G* diagrams. The lower limit, G_{th}, has been found by gradually lowering the loading on the specimen, until no further changes in displacement of the end of the specimens could be detected. The combination of load and displacement can be used to derive the crack depth and energy release rate. The lowest calculated energy release rate where still increment in the displacement takes place, is the threshold value. Preferably, this threshold value is not a single measurement, but a group of measured values. In the case of the MS polymer, this limit has not been found. In the last part of the fatigue life of the specimen (this is not a very clearly defined limit, but about $da/dN > 3.0*10^{-3}$ mm/c), the crack starts to grow very fast, unless the load is being decreased. The bonding is literally torn apart. The upper value is here assumed to be at the point where the crack still grows but has not failed yet. The upper limit was assumed here to that highest energy release rate when the crack is growing at its maximum speed. In some cases, the crack growth at the point of collapse has been added as well. However, these points have not been used as an upper limit, the critical value was assumed to occur as the crack was still growing to assure to have a safe value for the critical value of the energy release rate. Do note that the vertical asymptotes in the *da/dN-G* diagrams are just 'drawn' in the chart on double log scale and the values for both G_{th} and G_c are read from the horizontal axis. To combine the diagonal from the Paris region with the asymptotes, the diagonal from the Paris region has been modified, so it fits well with both the diagonal and the asymptotes. The curve that has been found through this modification (modified Paris curve), is drawn with the continuous line. All coefficients related to the curves and asymptotes can be found in Table 3.

All mathematical descriptions between *d*, *a* and *G* that have been used determining the crack growth characteristics can be found in Appendix II.

Table 3: crack growth coefficients

		R [-]	G_{th} [N/mm]	G_c [N/mm]	D [-]	n [-]	n_1 [-]	n_2 [-]
epoxy	G_{max}	0.1	0.025	0.8	1.02E-01	2.984	10	10
	G	0.1	0.023	0.8	1.05E-01	2.984	10	10
	G_{max}	0.5	0.040	1.5	3.34E-03	2.625	10	10
	G	0.5	0.040	1.2	7.11E-03	2.625	10	10
MS polymer	G_{max}	0.1	-	2.3	1.04E-03	2.228	10	10
	G	0.1	-	2.3	1.06E-03	2.228	10	10
	G_{max}	0.5	-	3.0	1.93E-04	1.354	10	10
	G	0.5	-	2.3	2.85E-04	1.354	10	10

7.1.1 Epoxy

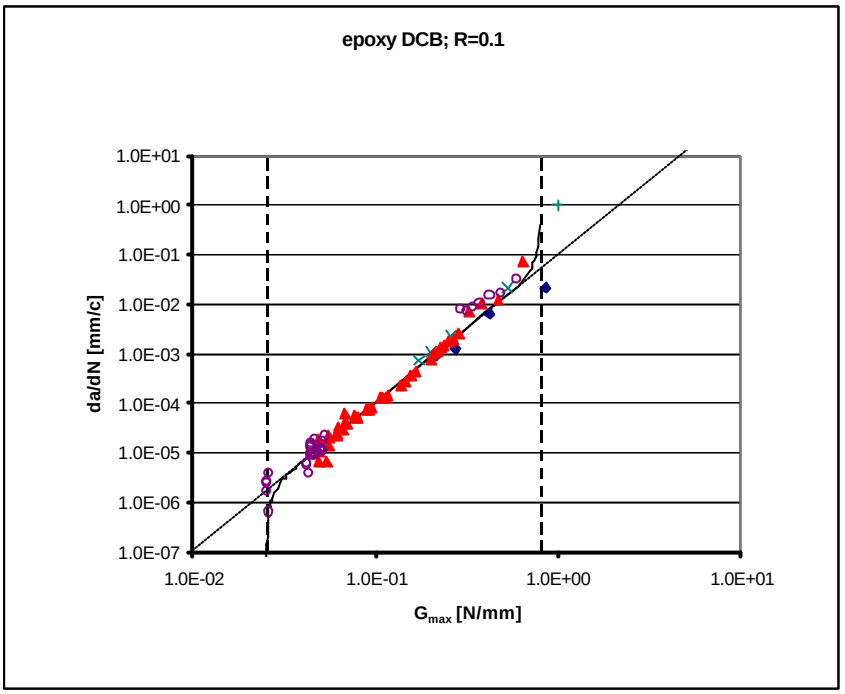

Figure 47: da/dN-G_{max} diagram for the DCB epoxy specimen for R=0.1

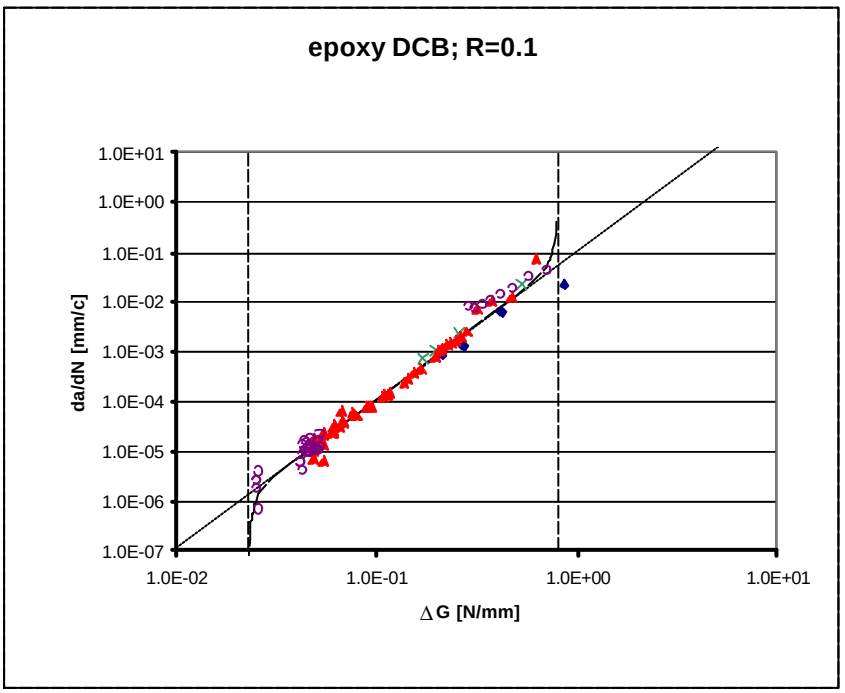

Figure 48: da/dN-DG diagram for the DCB epoxy specimen for R=0.1

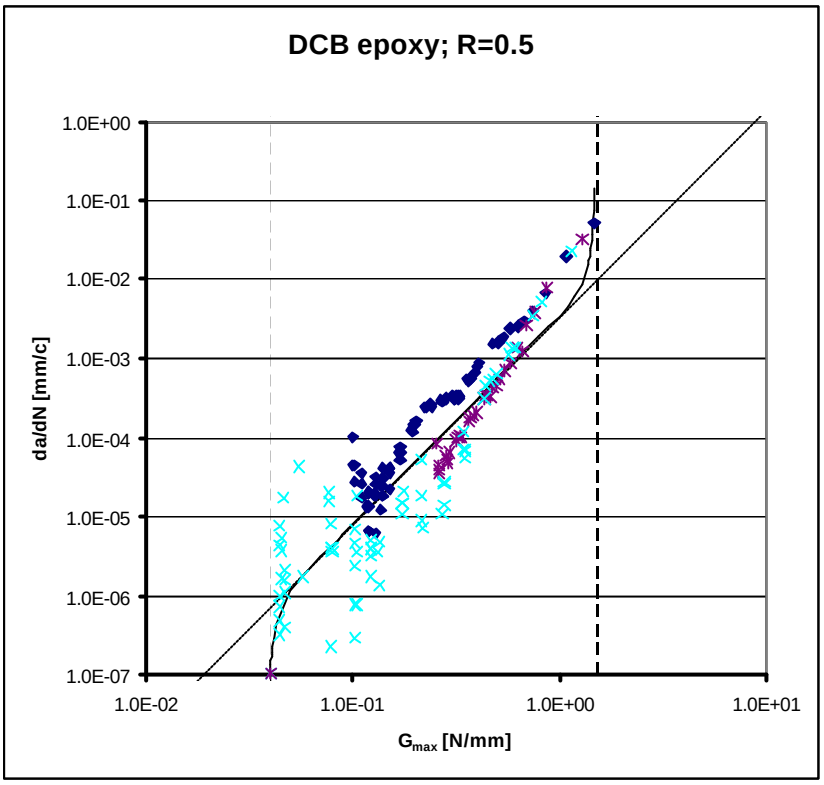

Figure 49: da/dN-G_{max} diagram for the DCB epoxy specimen for R=0.5

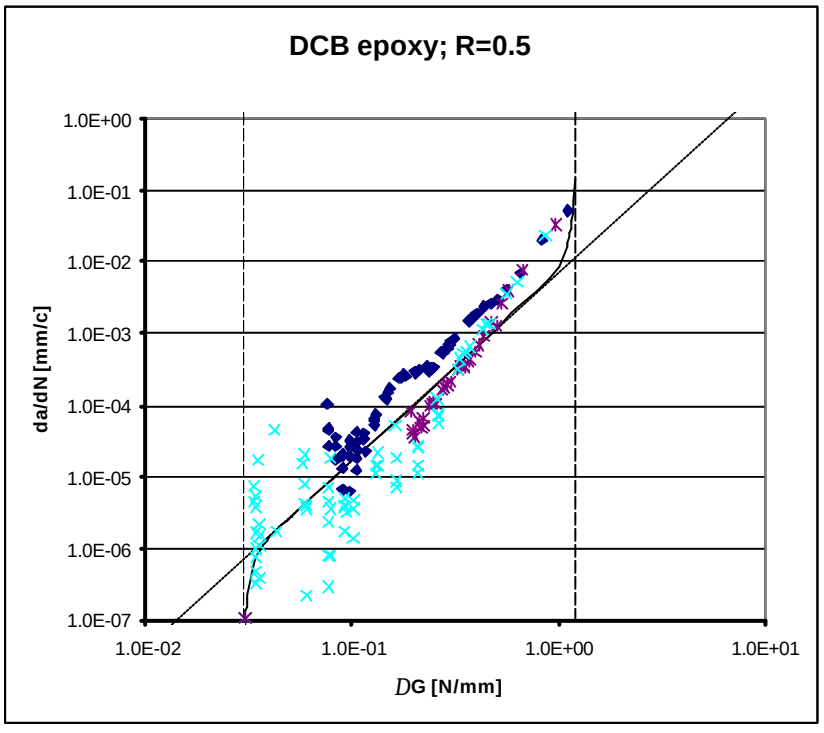

Figure 50: da/dN-DG diagram for the DCB epoxy specimen for R=0.5

7.1.2 MS Polymer

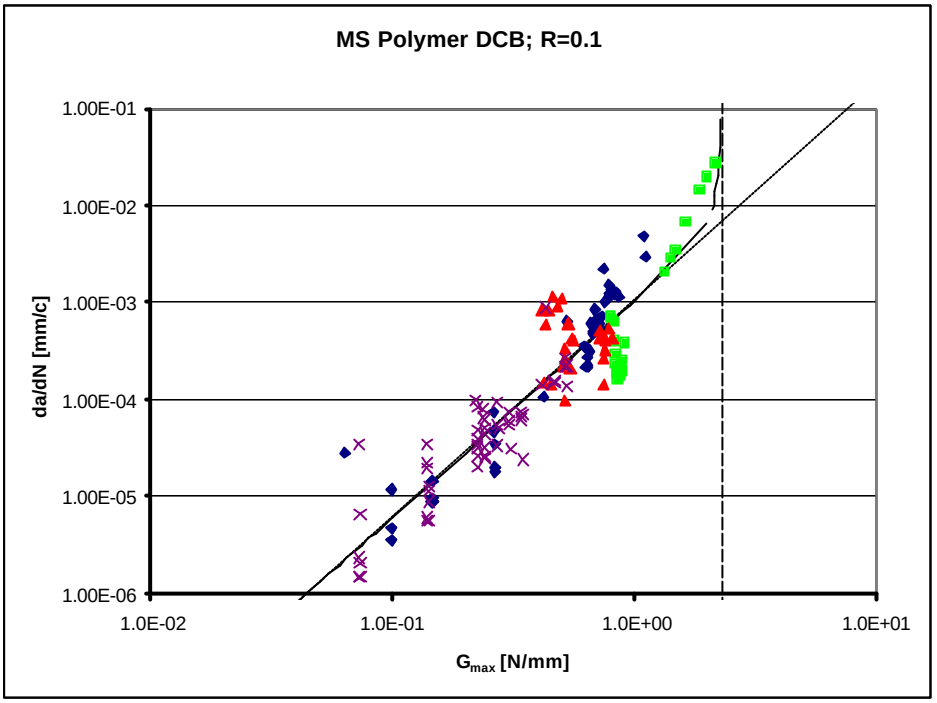

Figure 51: da/dN-G_{max} diagram for the DCB MS polymer specimen for R=0.1

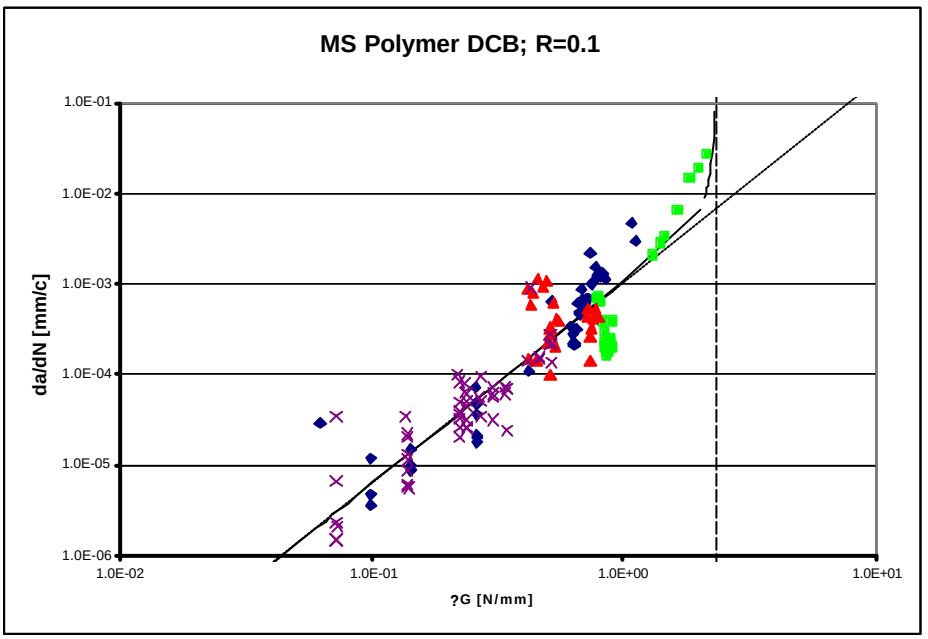

Figure 52: da/dN-DG diagram for the DCB MS polymer specimen for R=0.1

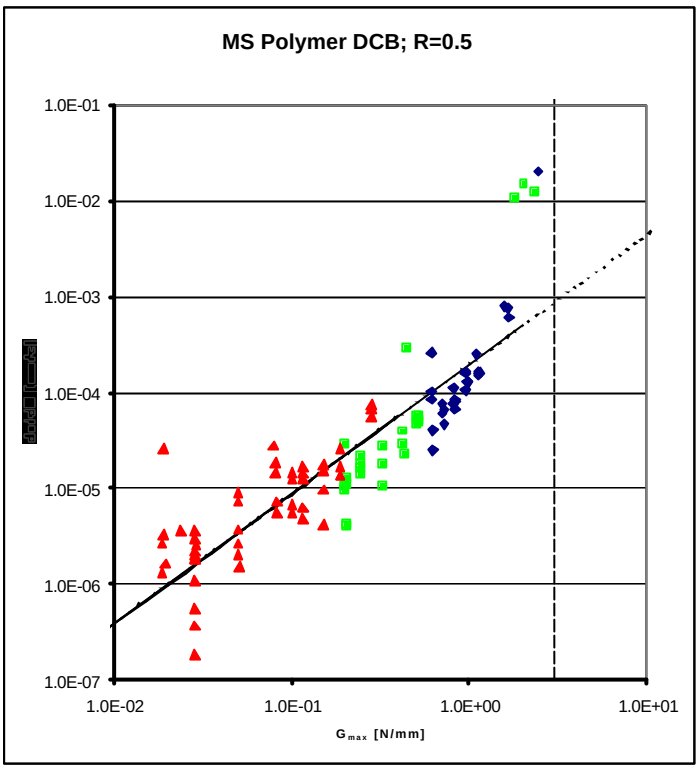

Figure 53: da/dN-G_{max} diagram for the DCB MS polymer specimen for R=0.5

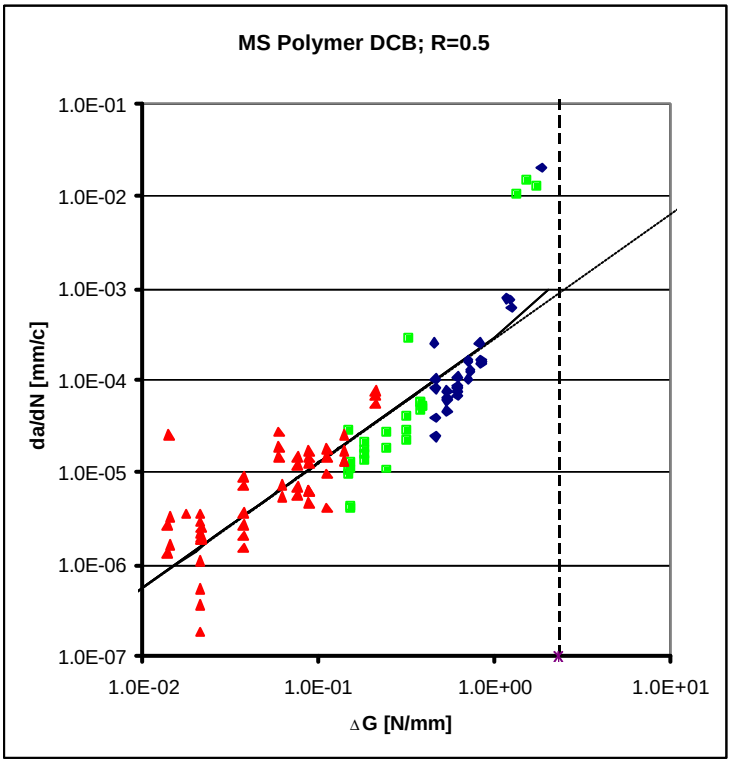

Figure 54: da/dN-DG diagram for the DCB MS polymer specimen for R=0.5

7.1.3 Discussion

a) Epoxy

During the testing of the two adhesives, the cracking behaviour of the adhesives was fundamentally different. In Figure 55, the typical cracking behaviour of the two adhesives is shown. The crack in the epoxy started at the artificial crack tip at the plastic foil. During the fatigue life, the crack grew symmetrically in the adhesive, both left and right grew at a similar speed. No strains were visually detectable in the thin adhesive layer. Once, the crack growth rate has reached a level of about $3*10^{-3}$mm/c, the epoxy tends to behave rather brittle. When the crack had reached a depth of about 100 mm, the specimen suddenly collapsed. The remaining bond line is rapidly torn apart. The difference between the part that failed under fatigue and the part that has been torn apart in the last load cycle can be very easily seen in Figure 56a.

After testing, the state of the bond line can be studied for critical flaws. In case of the epoxy specimens, hardly any discontinuities can be seen in the bond line. During the assembling of the epoxy, the adhesive was very easily processable, which is reflected in the cracked surfaces. Although, in case of the epoxy specimens, a complete preliminary series has been made. This series consisted of specimens that were degreased, etched and anodised before the adhesive was applied on the surface (see for the complete pre-treatment of the preliminary series in 4.2.2). However, the bonding between the epoxy and the aluminium was insufficient and the specimen suffered from very brittle failure due to a lack of adhesion. This shows once more how important it is to have a very accurate pre-treatment.

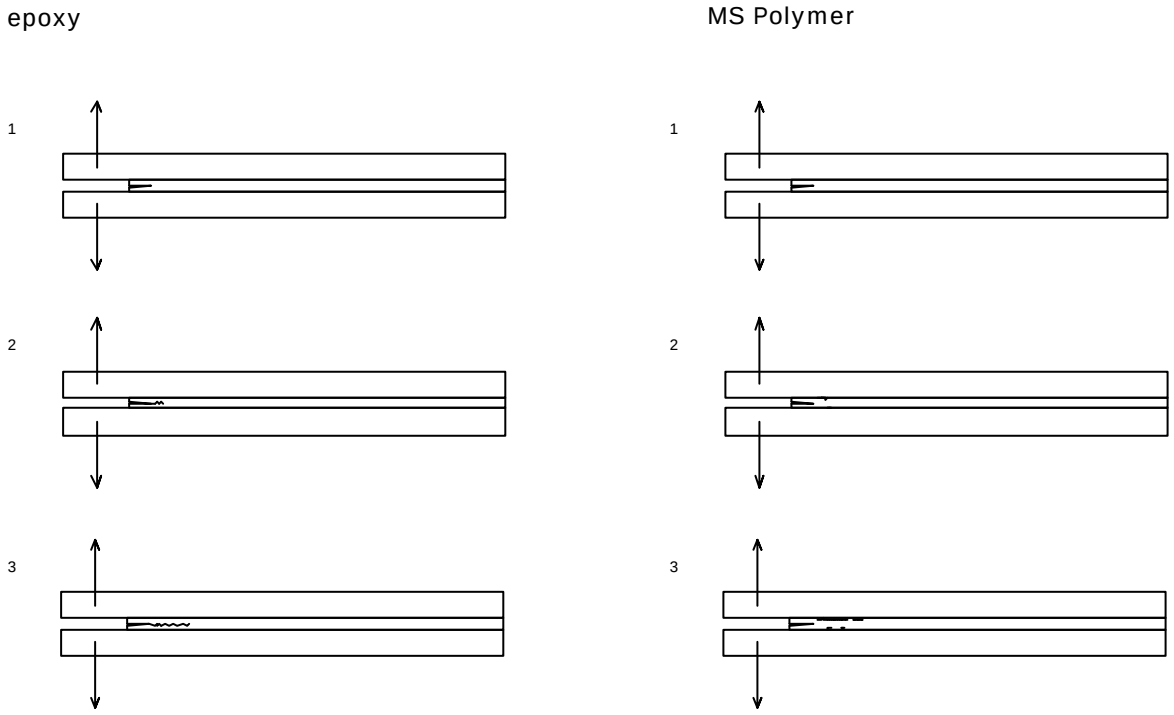

Figure 55: typical cracking behaviour in three steps for epoxy and MS polymer; in step 1 the artificial initiation crack, step 2 initiation of the fatigue crack and step 3, growth of the fatigue crack

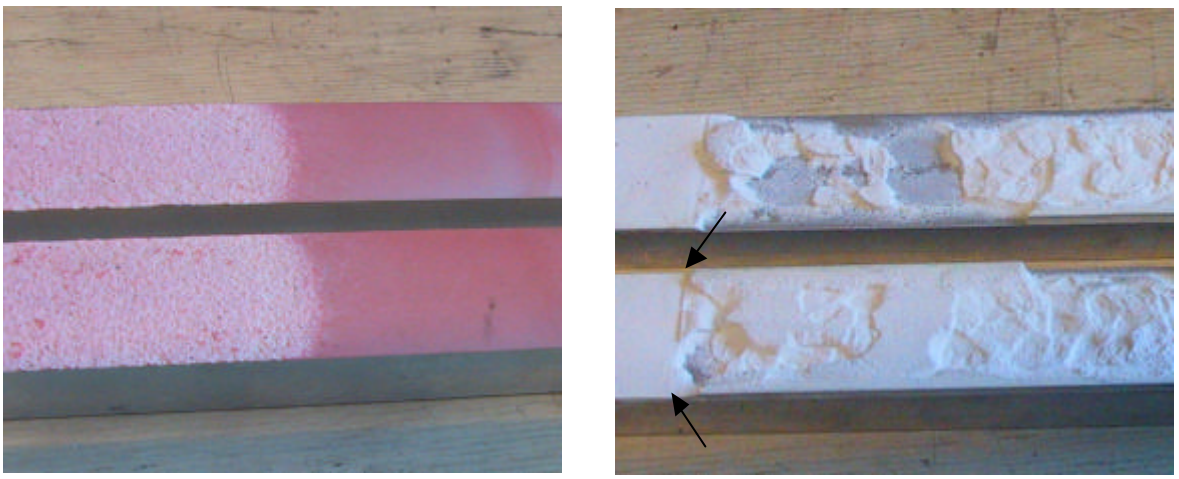

a *b*

Figure 56: a) cracked surface of an epoxy specimen, left the fatigue crack, right the strength crack; b)cracked surface of the MS polymer specimen, the two arrows mark the start boundary between the artificial crack and the fatigue crack

A remark that has to be made is that although the crack grows symmetrically, according to the assumptions that have been made in the FEM model, it was not possible with the present experimental set-up and equipment to make an accurate measurement of the crack depth. Therefore, the crack depths in the epoxy are *virtual* crack depths. Nevertheless, the measurements that have been made are still valuable, as the absolute values measured are not as important as the differences between the displacements in two measurements and the derived crack depths.

In Figure 47-Figure 50, the *da/dN-G* diagrams for the epoxy are shown. Considering these results, two important differences concerning scatter should be noticed. The deviation in scatter is larger for R=0.5 than for R=0.1 and the scatter in the left half of the diagrams is larger than the scatter in the right half. The epoxy data points are mostly on a rather straight line for a single specimen, except for the data near the threshold, where the deviation is significantly bigger. In Figure 49 and Figure 50, a significant deviation between the specimens can be seen. One of the three specimens lays higher than the other two. Possibly the difference is caused by slightly inferior conditions when the adhesive was applied for that ("blue") specimen. The "cyan" specimen in the same figure shows a severe deviation at low crack growth rates close to the threshold. Once the crack growth rate increases, the deviation is significantly reduced.

Concerning the difference in scatter between the left and right halves of the *da/dN-G* charts, it can be stated that if the applied cyclic load is increased, the deviation of the *da/dN-G* results decreases. One should keep in mind that the points with a lower crack growth rate require more cycles for an accurate measurement than the points with a higher crack growth rate. It seems that, under a high load, the crack growth rate is a sound constant. The crack will extend at the same speed, regardless the state of the adhesive layer, no matter if there are discontinuities or not. In the case of a relatively low load, it is more likely that the rate of extension of the crack depends on tiny flaws in the adhesive layer or interface. Such a discontinuity can accelerate the crack growth rate for a small period (for instance a measurement interval), which can be seen in the diagram.

Still, considering the difference between R=0.1 and R=0.5,there is a difference in behaviour between the two groups. In the case of R=0.1, the load on the specimen goes from nearly unloaded to fully loaded to nearly unloaded in a single cycle. When the specimen is loaded with the lower boundary load, $0.1*P_{max}$, the adhesive layer has a low fairly low pre-stress level. Due to

practical reasons, complete unloading of the specimen was not favourable in these test series, therefore R=0.1 has been selected instead of R=0. So, the specimen is unloaded, loaded and again unloaded. In case of R=0.5, the specimen is pre-stressed with 0.5*P_{max}, loaded to P_{max} and again unloaded to the pre-stress level 0.5*P_{max}. Besides the use of a (higher) pre-stress level, the testing conditions are equal, so the level of pre-stress does influence the crack growth behaviour. Testing with R=0.1, the crack will always grow at a similar speed, when it is loaded with the same load and a similar crack depth. Testing with R=0.5, the growth rate is fluctuating. Possibly, the growth rate is then more dependent on the condition of the structure of the adhesive, i.e. the way that the polymers in the adhesive are connected to each other and the presence of flaws, like tiny air inclusions, adhesive particles that have not completely reacted during the curing period or missing links in the network. With R=0.1, every load cycle forces a defect every cycle, while R=0.5 grows faster or slower depending on the state of the adhesive.
It is obvious that in case of R=0.1, the difference between the parameters P_{max} and DP is rather small compared to R=0.5.
Notice that there is a difference between the slopes, n=2.984 and 2.625 for respectively R=0.1 and 0.5, a difference being just over 10%. This difference could partly be caused by the scatter in the R=0.5 diagram.

b) MS polymer

In the case of the MS polymer, the crack did not extend from the artificial crack tip, Figure 55. Instead, the polymer was developing a crack on the surface interface between the aluminium and the adhesive most of the time at a distance of about 3 mm from the crack tip. Apparently, the adhesive is so flexible that it can redivide the severe stresses around the crack tip very efficiently. The crack at the interface extends a bit along the interface before growing into the adhesive layer, shown in Figure 55-2 and Figure 57. Apparently, the resistance of the adhesive against crack growth is superior to the bonding capacity at the interface between the adhesive and the substrate. The adhesive layer is deformed a lot during the loading cycles, both the deformation parallel and perpendicular to the loading direction can be observed clearly.
Considering the deformation behaviour of the adhesive and the substrate it seems logical that the adhesive loses bonding due to the big difference in deformation. Also, the shape of the sides of the MS polymer DCB specimen (Figure 16) introduce stress, which can contribute to the loss of bonding at the interface. The rate between the E modulus of the substrate and adhesive is 70000:3.5, so the substrate is 20000 times as stiff. At the interface, the deforming adhesive and the rigid substrate are connected, which must lead to substantial stresses. Considering the initial flaws in the adhesive, it is likely that the cracks at the interface start at one of the tiny discontinuities in the adhesive.
The MS polymer shows a very tough cracking behaviour. Even when the bond line is cracked more than half, the remaining part does not collapse. It is not able to carry a large load, but it does not fail due to the large deformation capacity of the adhesive layer.

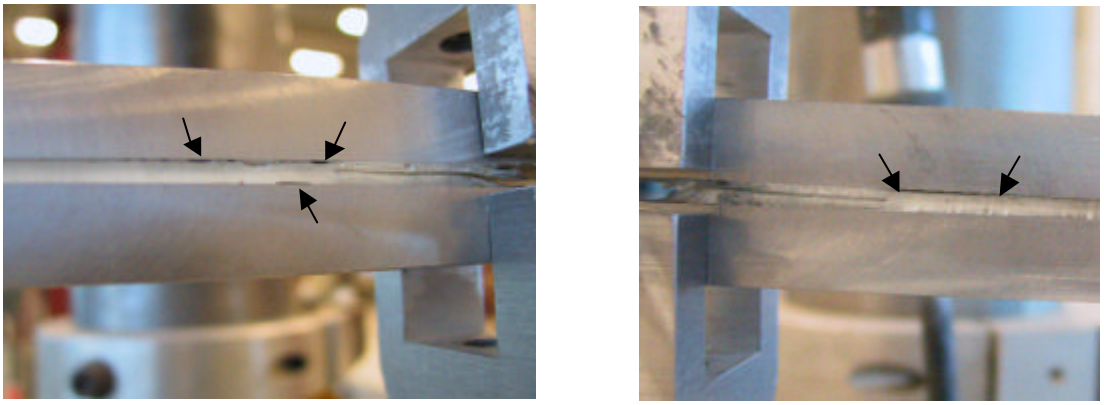

Figure 57 a (left) and b: close up of the DCB specimen. In both figures the artificial crack can be seen through the centre of the bond line. In a) the fatigue cracks grow at the top and bottom of the bond line, in b only at the top.

Once the specimen has collapsed the difference between fatigue and strength failure can hardly be distinguished, Figure 56b. The crack surface through the thick adhesive layer grows between the discontinuities such as small air inclusions and the side ends of the adhesive more or less ad random.

After final failure, the cracked surface has been studied. In case of the MS polymer several tiny air inclusions were discovered. When the MS polymer is applied, the adhesive is very thick. For the air it is rather difficult to escape from the adhesive once it is entrapped. However, besides the air inclusions, no severe initial flaws could be detected within the bond line.

With respect to the cracking mechanism, it should be noticed that the crack like it is assumed in the FEM model in 6.2.1, a crack nucleating at the artificial crack tip, does not occur in the MS polymer specimen, as can be seen in Figure 57. However, with the described measuring method using the displacements at the end of the specimen, it is possible to derive the compliance of the specimen for a *virtual* crack and from there the energy release rate of that virtual crack. This virtual crack is a crack that is related to a specimen with a particular crack depth that allows a particular displacement under a unit load. This displacement can be translated to the virtual crack depth that allows equal displacements under a unit load. The virtual crack has the properties of the crack that is assumed in 6.2.1: growing straight through the centre of the adhesive, perpendicular to the line of the applied force and starting from the artificial crack tip. An important note should be made on the application of the virtual crack method in a specimen that shows an evidently irregular cracking behaviour: the measurements will inevitably contain distortion, more than the measurements of a regularly cracking specimen.

Regarding the results in Figure 51-Figure 54, some notes should be made. First of all, the difference in scatter between the epoxy and the polymer is substantial. The MS polymer data points have a much larger deviation. The difference can be explained by the difference in cracking behaviour. The cracking path of two epoxy specimens is nearly identical, while the cracking pattern of two MS polymer specimens could show significant differences. For instance, when the two cracks in Figure 57 are regarded, one can easily spot the differences between the two sides, let alone the difference between two specimens.
Another difference that catches the eye is the absence of the left asymptote, the threshold energy release rate. In the case of the epoxy the asymptote was rather easily found, at a certain level of loading, no differences in displacement could have been measured for a longer period and when the load level was slightly increased, the displacement were slightly rising again. This

strategy failed for the MS polymer, no univocal limit could have been found, as has been stated before in 7.1. For the R=0.1 it was not possible due to the control mechanism of the dynamic bench, because the lower load limit has been reached. For R=0.5 it has not found either, even for very small load ranges increments in the displacement were found. The accuracy of the measurements becomes dubious under these small loads and displacements. Also the searching for the threshold is very time consuming if the increments become very small. The upper limit, G_c, has been found measuring in the period before the failure of the specimen.

Like in the epoxy series, there is also a difference in the scatter between the left and right half of the *da/dN-G* diagrams and between the results of R=0.1 and R=0.5. Also for the MS polymer, the left halves of the diagrams show significantly more scatter and the results for R=0.1 have a smaller range than the results of R=0.5.
Both the differences could be explained with the same reasons as for the epoxy. The difference between left and right can be subscribed to the dependence on discontinuities: the higher the load level, the less the crack growth is dependent on discontinuities in the bond line. This explanation is even more likely in case of the MS polymer, where a lot of flaws can be found in the bond line. Concerning the influence of R, the larger scatter range can be explained by the dependence on the structure of the adhesive and bonding when R is increased.

8 P-N curves

In this chapter, the crack growth results of chapter 7 and the *G-a* relations of the various cracked joints of chapter 6 are combined in the modified Paris' law from chapter 3 (equation4). This results in a number of *P-N* diagrams. These numerical derived *P-N* curves are going to be validated with experimental results from the specimens described in chapter 5. In a *P-N* diagram the number of loads until failure, *N*, is plotted against the applied force *P* on double logarithmic scale. Per joint geometry, adhesive and load characteristic (P_{max} , the maximum force, or DP, the range between the maximum and minimum load), four curves have been plotted. For both the left and the right side of the joint a curve was drawn, because it is expected cracks will grow from both sides of the joint. This assumption has been verified for the double lap joints in practice, where the crack growth can be observed during the testing of the specimen. Per adhesive and geometry the *P-N* curve is drawn for both P_{max} and DP on the vertical axis. The choice to plot the curves for both has been made to investigate both the influence of the maximum load P_{max} and the load range DP. The experimental results have been plotted together with the most pessimistic prediction curves, for all cases the left crack, to compare the lower boundary estimation with the experimental data.

In the calculations, the joint was considered as 'collapsed' once a crack has reached the depth of 6 mm. This selection of the maximum crack depth has been taken because of the applicability of the mathematical formulas for the relation between *a* and *G*. This relation was for all joints very accurate to describe until at least 65 % of the lap length (appendix II). The effect of using 6.5 mm instead of 10 mm does hardly effect the *P-N* curve, only the low cycle fatigue platform will be slightly lowered. The last part of the lap length has a marginal influence on the fatigue life of the joint, as the energy release rate is increasing fast in the last phase of the fatigue life. For each side two different *R* values have been considered, R=0.1 and R=0.5. All the available experimental data has been added in the *P-N* curves.

The *P-N* curves are going to be discussed in 8.4.
In Figure 58 the relation between chapter 8 and the other chapters can be seen.

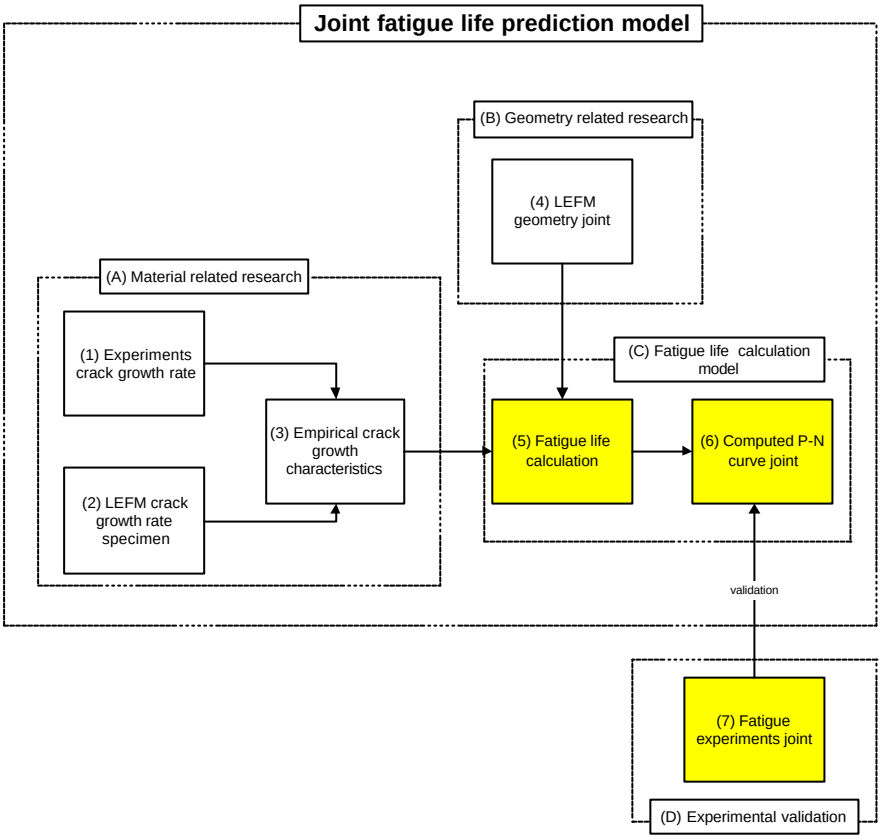

Figure 58: joint fatigue life prediction model flowchart

8.1 Experimental data

Table 4: experimental results of fatigue tests on epoxy double lap joint, lap 20 mm

R	P_{max}	P_{min}	N_f
0.1	16200	1620	447063
	16200	1620	183095
	21600	2160	42238
	21600	2160	86076
0.5	10800	5400	6238106
	21600	10800	1698805
	21600	10800	2153067

Table 5: experimental results of fatigue tests on MS polymer double lap joint, lap 20 mm

R	P_{max}	P_{min}	N_f
0.1	600	60	180375
	600	60	124120
	900	90	2900
	900	90	1410
	1200	120	234
	1200	120	460
0.5	600	300	305211
	600	300	2212113
	900	450	12036
	900	450	19289
	1200	600	2083
	1200	600	816

Table 6: experimental results of fatigue tests on epoxy tube joint, lap 15 mm

R	P_{max}	P_{min}	N_f
0.1	50000	5000	33000
	38000	3800	36400
	30000	3000	420000
	35000	3500	220800
0.5	64000	32000	75000
	72000	36000	27300
	50000	25000	1080000

8.2 Double lap joint

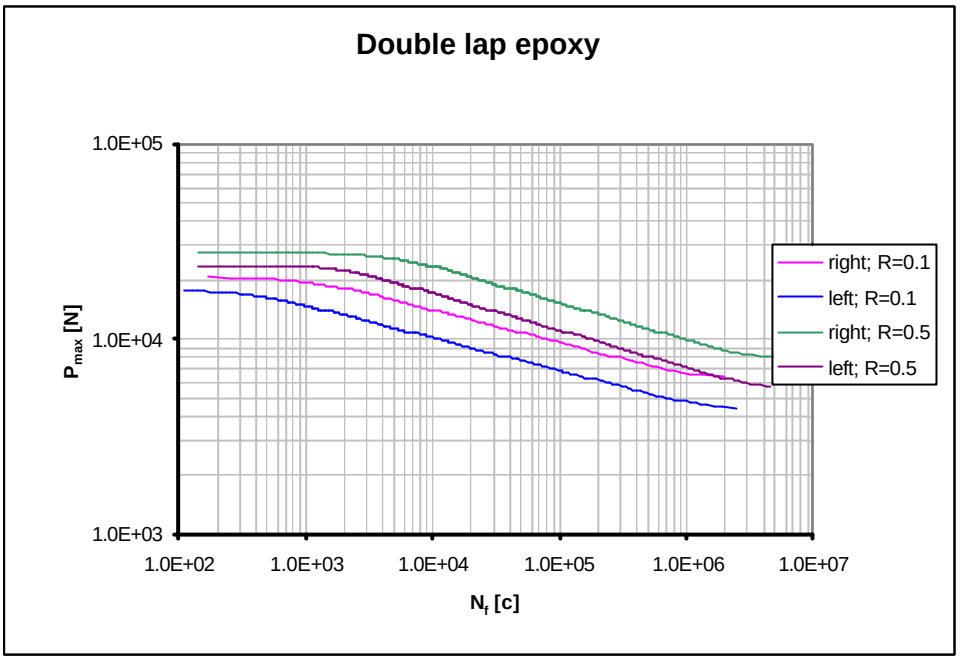

Figure 59: P_{max}-N derived curves for the epoxy double lap joint, lap 20 mm

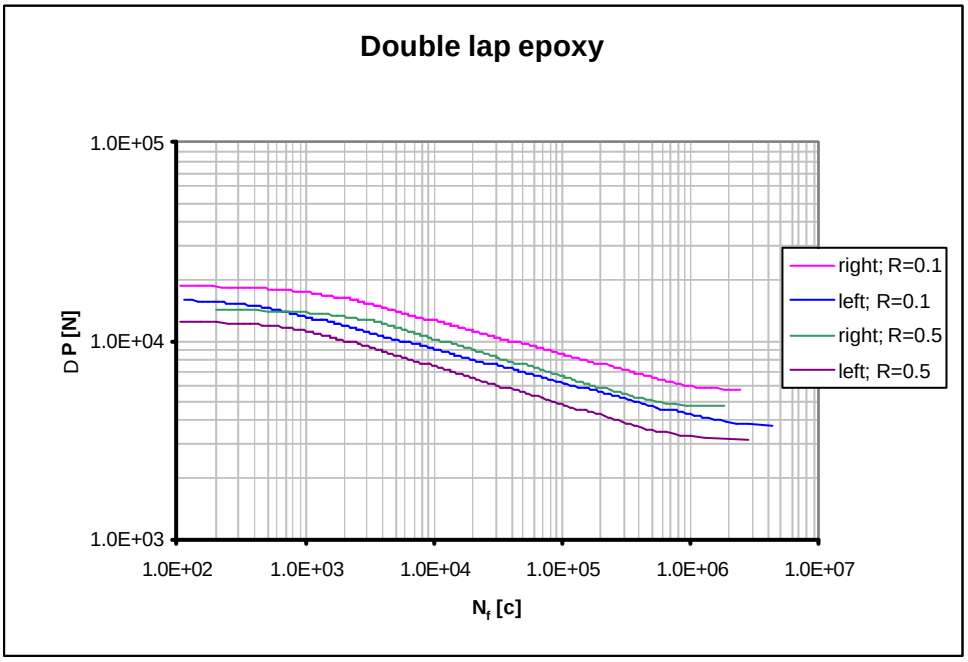

Figure 60: DP-N derived curves epoxy double lap joint, lap 20 mm

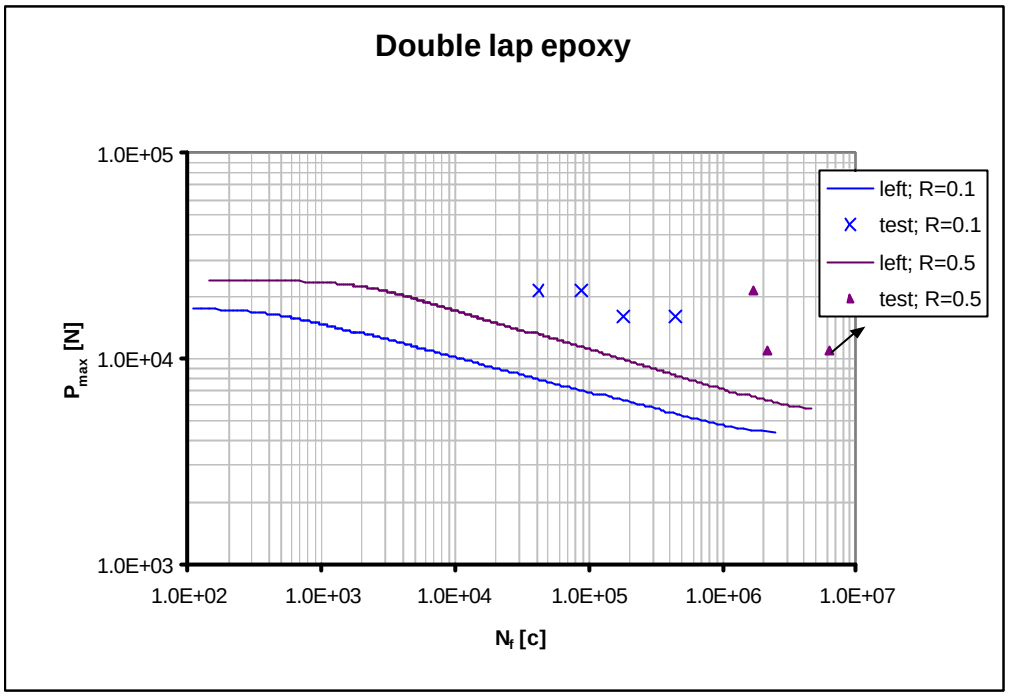

Figure 61: P_{max}-N diagram double lap joint 20 mm; prediction and experimental result

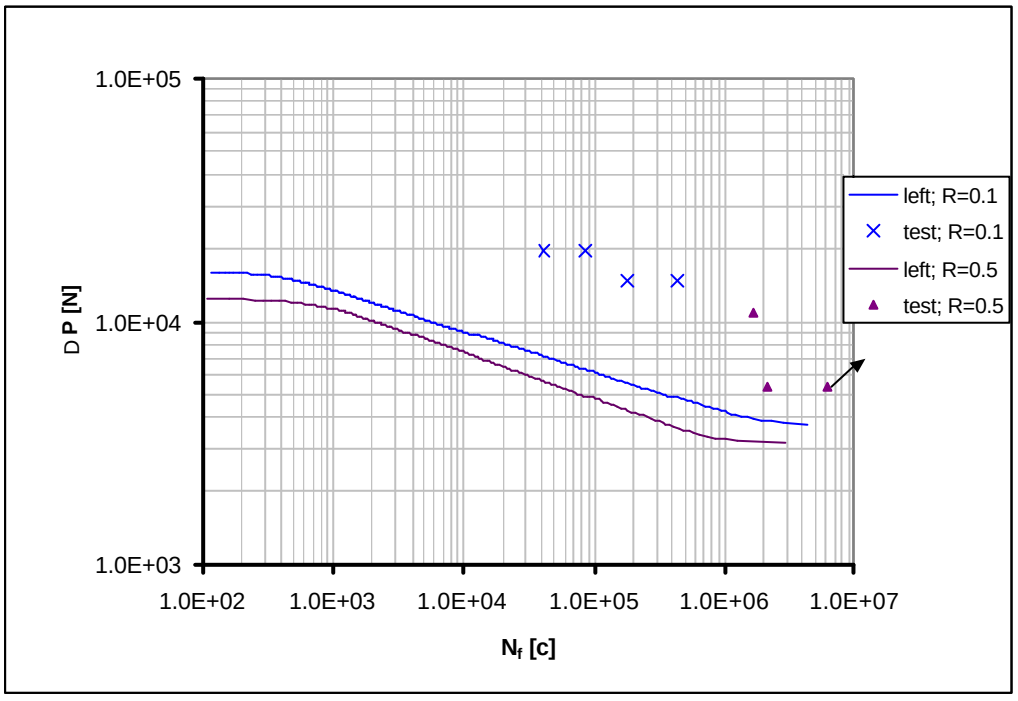

Figure 62: D P-N diagram epoxy double lap joint 20 mm; prediction and experimental result

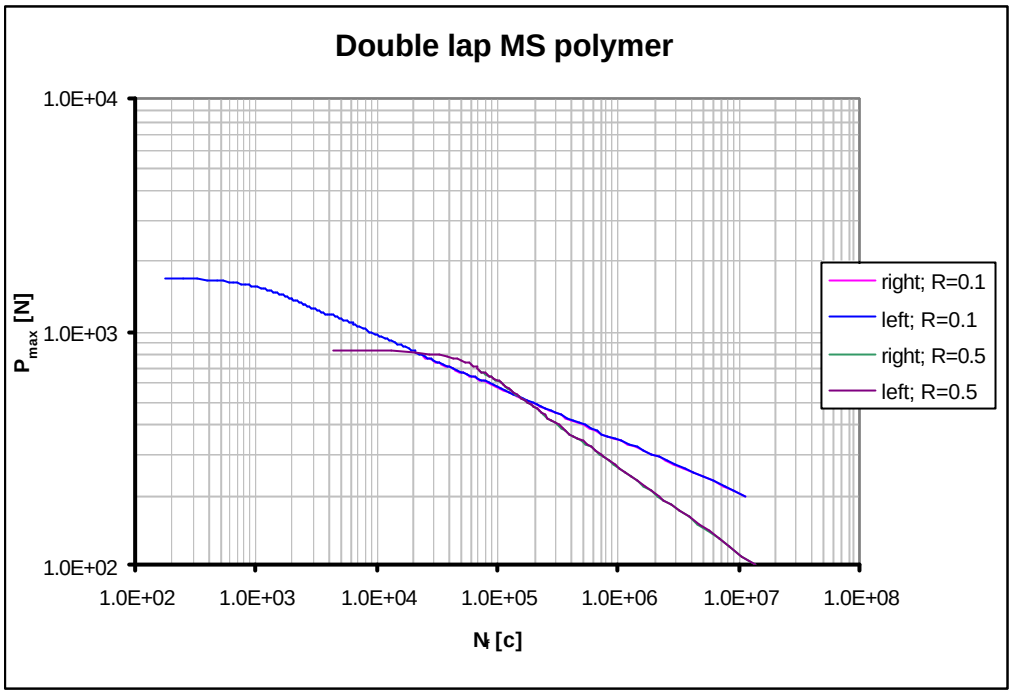

Figure 63: P_{max}-N derived curves MS polymer double lap joint, lap 20 mm

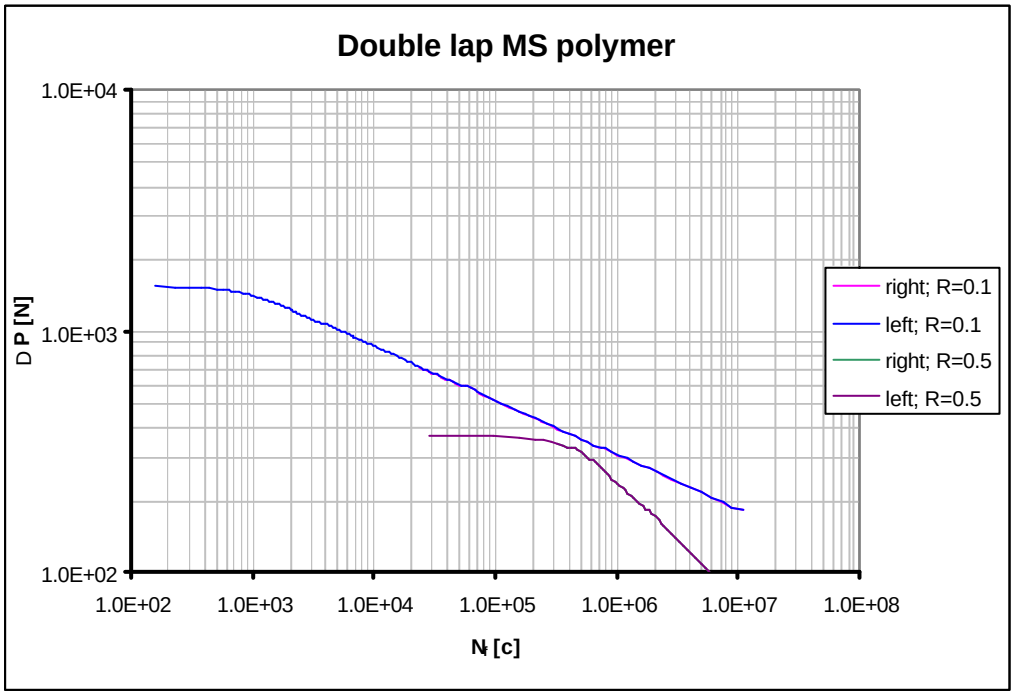

Figure 64: D P-N derived curves MS polymer double lap joint, lap 20 mm

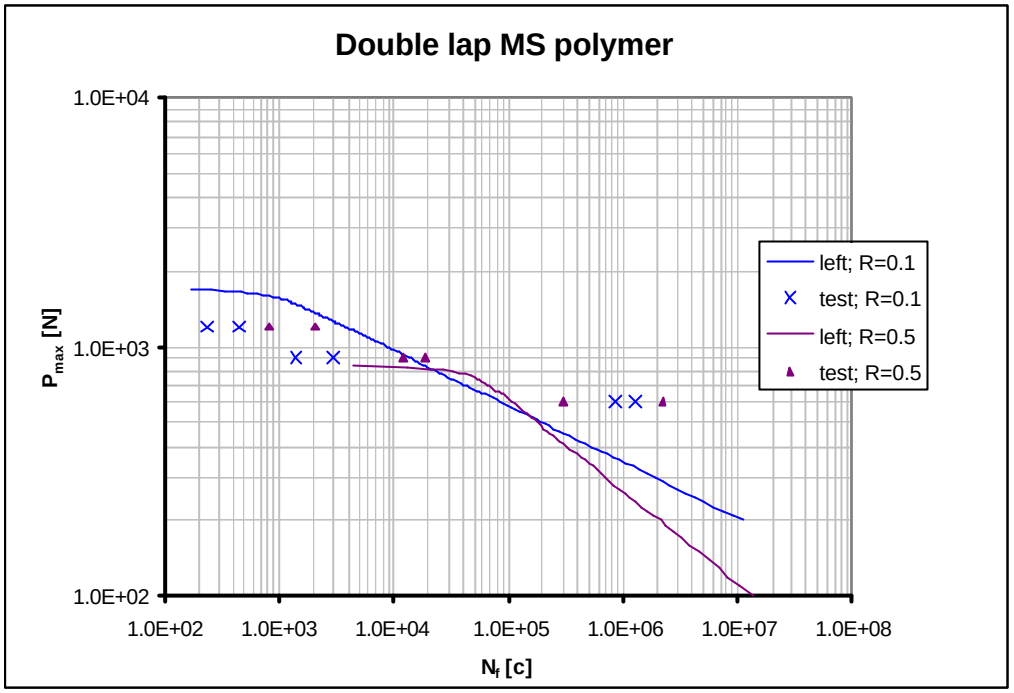

Figure 65: P_{max}-N diagram MS polymer double lap joint 20 mm; prediction and experimental result

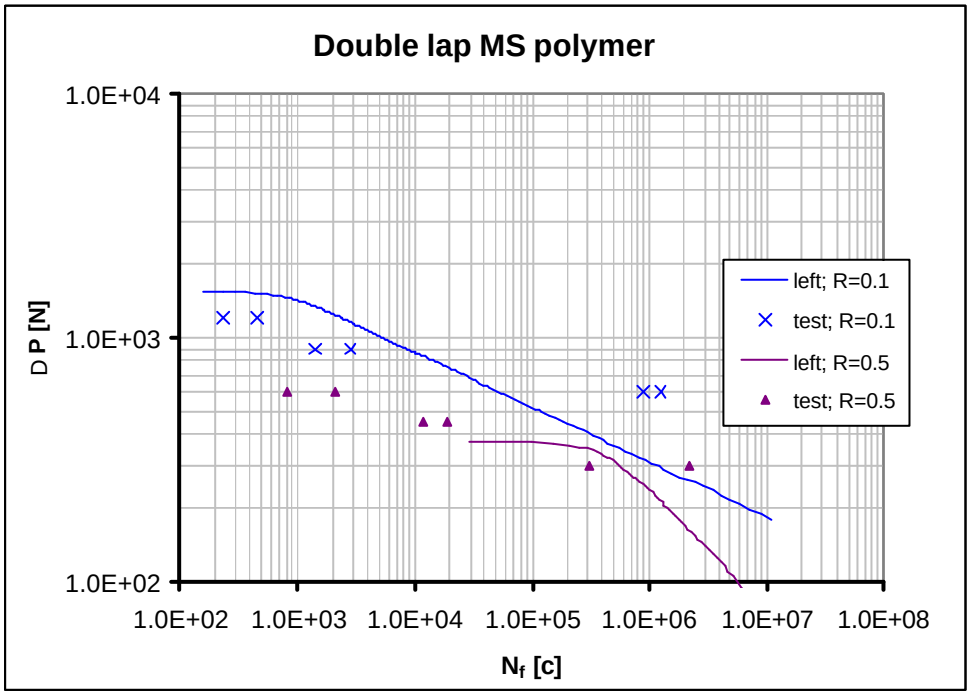

Figure 66: D P-N diagram MS polymer double lap joint 20 mm; prediction and experimental result

8.3 Tubular joint

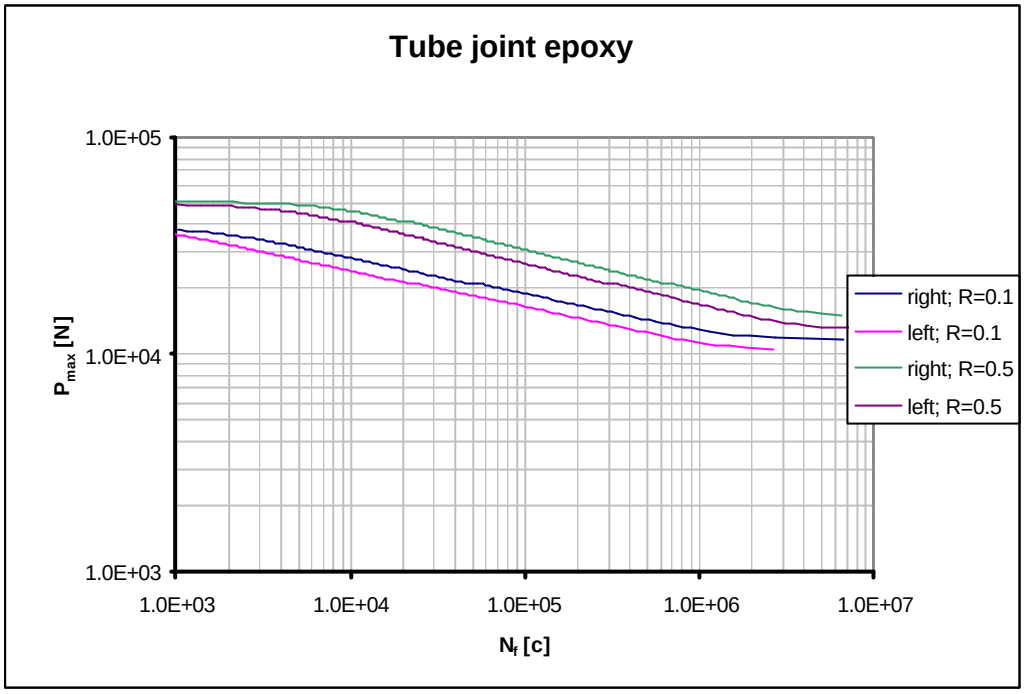

Figure 67: P_{max}-N diagram epoxy tube joint, lap 15 mm

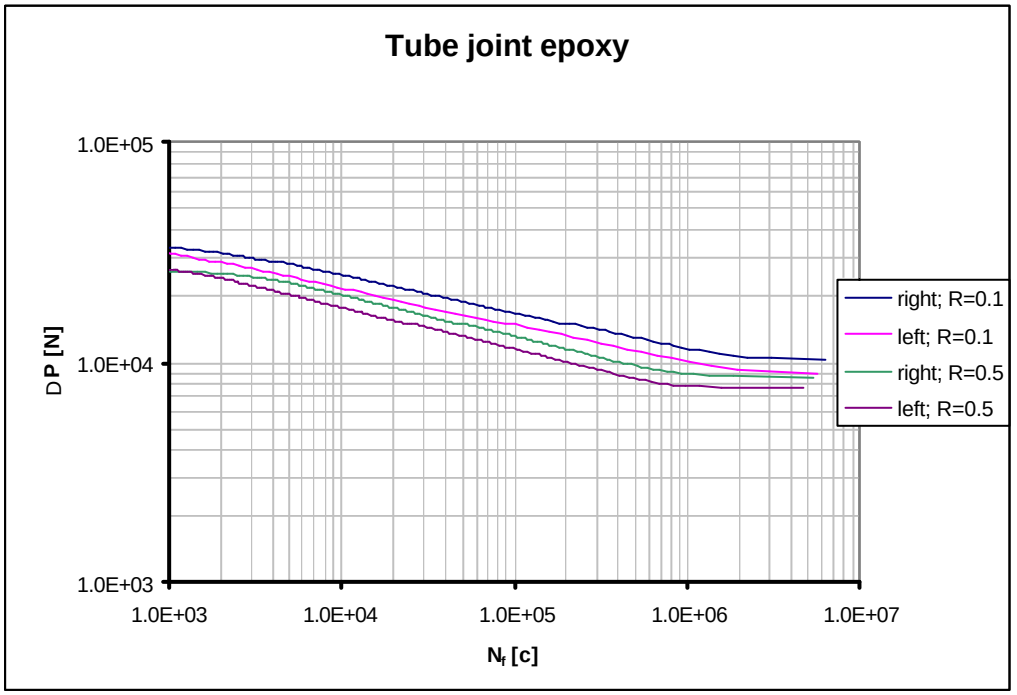

Figure 68: DP-N diagram epoxy tube joint, lap 15 mm

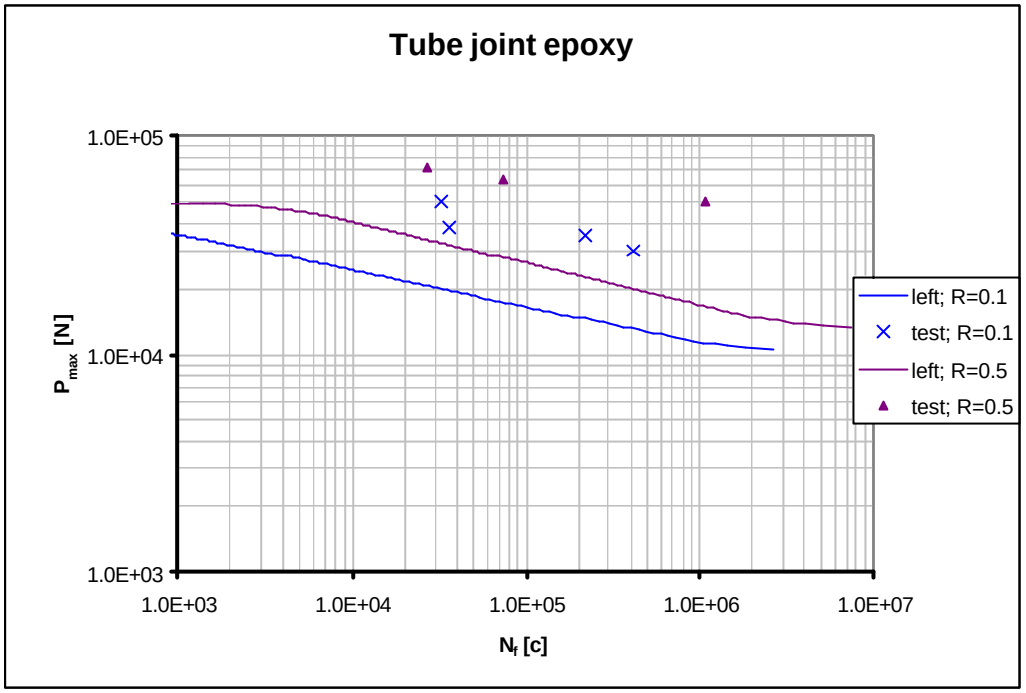

Figure 69: P_{max}-N diagram epoxy tube joint 15 mm; prediction and experimental result

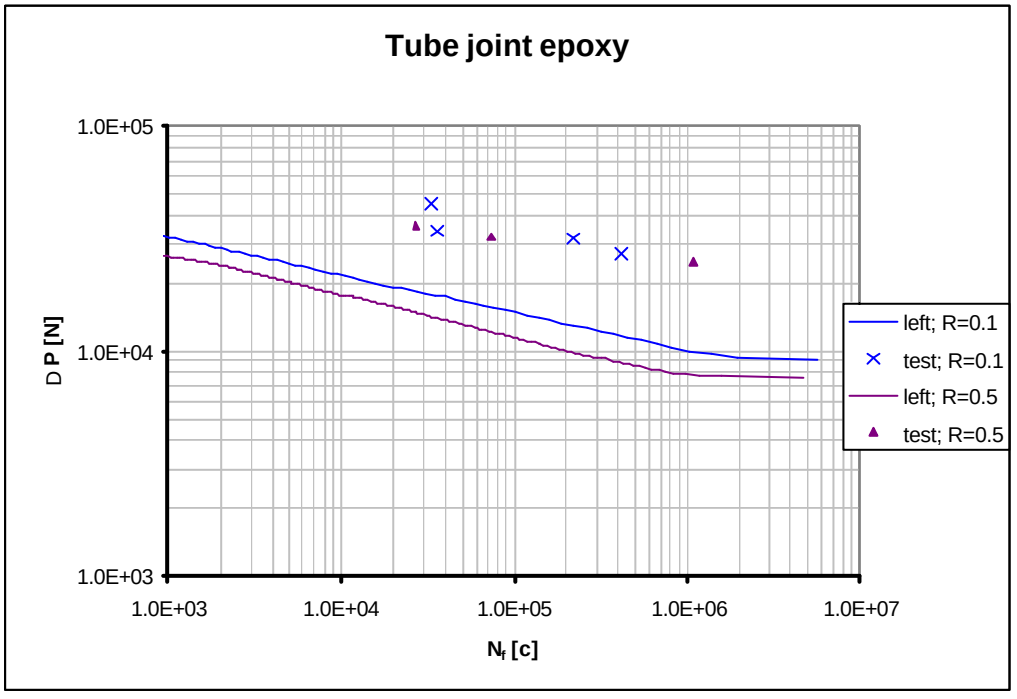

Figure 70: DP-N diagram epoxy tube lap joint 15 mm; prediction and experimental result

8.4 Discussion

Regarding all predictions and experimental results, there are five points of interest to be discussed here:

8.4.1 Computed prediction curves

In Figure 59: P_{max}-N derived curves for the epoxy double lap joint, lap 20 mm

, Figure 63, Figure 67 and Figure 60, Figure 64, Figure 68 respectively all P_{max}-N_f and ΔP-N_f diagrams are shown for the three joint geometries. Considering these figures, it can be stated that the left crack curve always gives the lower boundary. In case of the MS polymer joints the left and right curve perfectly match. The left curve is, as a lower boundary, used to compare the predictions with the experimental data for all joint types. Concerning the *R* values, the fatigue life of adhesive joints seems to be dependent on both the maximum load and the load range rate, because if the fatigue life would only the depend on one of the two, the curves and experimental results would match in the *DP-N* or P_{max}–*N* diagrams.

8.4.2 Epoxy double lap; prediction and experimental results

Regarding the results Figure 61 and Figure 62 it can be stated that the predictions that have been done are all lower boundary predictions, like they were intended. The difference between the prediction curves of the P_{max}-N_f and the ΔP-N_f approach is negligible. Also, the accuracy for both $R=0.1$ and $R=0.5$ is about equal, although one should notice the difference in position of the experimental results of $R=0.1$ and $R=0.5$ in the *P-N* diagrams. The values of 0.1 are in the area where the curves still have a slope. The prediction curve and the experimental results have a similar slope for $R=0.1$. For $R=0.5$, values are rather close to the high cycle fatigue platforms at the (prediction) fatigue strength of the double lap joint. Hence, the comparison between the slope of the curve and the experimental data is useless for $R=0.5$. Anyway, concerning the results in Figure 61 and Figure 62 it can be stated that the prediction method results in a conservative approach of the lower boundary values.

8.4.3 MS polymer double lap; prediction and experimental results

In Figure 65 to Figure 66, the P-N curves and experimental data for the MS polymer are given. In Figure 65 and Figure 66, the difference with the results of the epoxy series is clearly visible. In the case of the MS polymer specimens the calculated curves gives a rather good approach , where a conservative prediction would be expected, which is remarkable, considering the idiosyncratic crack growth behaviour. It is generally believed that mode I, on which the curves are based, is the most severe load case for an adhesive bond line. In the low cycle fatigue region, the prediction model slightly overestimates the fatigue life, while it underestimates the high cycle fatigue life.
Beside the overestimation another aspect catches the eye. When a line would be drawn through the statistical average values of the experimental data points, this line would have a rather different slope than the P-N curves. Note that the six point (in both *R* series) most left in the diagrams have an N_f smaller than 3000 cycles, which means that they lie on the low cycle fatigue platform, which can reach to 10000 or even more cycles. Nevertheless, the slope of the experimental data is less steep than the calculated curve, even when a line would be drawn from the platform. The slope of the derived curve is directly dependent on the slope of the curve from the DCB data, so the results of the DCB experiments appear to be inconsistent with the results of

the double lap joint. This inconsistency could be related with the difference in loading mode or with the distortion in the output of the measurement due to the irregular cracking.
Note that the deviation between the pairs of experimental results have a bigger variation for R=0.5 than for R=0.1, just like the results in the *da/dN-G* diagrams. The difference in accuracy of the predictions for both *R*-series and for $\Delta P/P_{max}$ is marginal, for all four combinations, it is about equal. For the MS polymer, both the experimental results and the prediction curve match better for the P_{max} approach.

8.4.4 Epoxy tube joint; prediction and experimental results

Regarding the results in

Figure 69 and Figure 70, it can be stated that the prediction model as it used here gives lower boundary predictions for the epoxy tube joint. The predictions for the tube seem slightly better, although the validation groups are not large enough to draw hard conclusions concerning the comparison of the predictions for the two geometries. Anyway, the difference between the experimental values and the computed prediction curves are in the same range for both geometries. Also, the slope of the experimental data appears similar for both geometries. The difference between the P_{max} and ΔP predictions and experimental values for the epoxy tubular joint is similar to the epoxy double lap joint. At first sight, no significant difference in accuracy can be found. Notice that for the ΔP approach the experimental results and the prediction curve make a better match. Also for the difference between the two *R* values, no significant difference can be determined. Although the predictions for 0.1 seem slightly better, the validation groups of experiments are not large enough to confirm this observation.
Finally, considering the difference between the prediction curves of the double lap joint and the tube joint, it can be stated that the difference between the level of the curves has the same rate as the difference in area of the bond lines, about a factor of 2.6.

8.4.5 ΔG versus G_{max}

Considering all computed curves and experimental results, it can be concluded that the differences in accuracy between the ΔG and G_{max} approach are marginal in this investigation. There can be seen another difference, namely the differences between the distance of the curves for the two load cases R=0.1 and R=0.5. For the epoxy tube both the experimental results and the prediction curves for both *R* values made a better match for the ΔG method. In the case of the epoxy double lap joints, the experimental data of the two load cases cannot be compared due to the results on the high cycle fatigue platform for R=0.5, but the distance between the two curves is smaller for the ΔG approach. For the MS polymer double lap joints the G_{max} method's results for R=0.1 and R=0.5 are matching better. Considering all results given in this report, no fundamental conclusions can be drawn concerning the ΔG-G_{max} dilemma. None of both is favourable over the other. With respect to the results it can be stated that both the maximum load and the load range rate *R* have an influence on the fatigue life of the adhesive joint. The difference in output of the prediction model under different *R* values is dependent on the choice of the type of *G*, but differs from one adhesive to another.

9 Discussion

Epoxy
Concerning the epoxy adhesive, the DCB specimen appears to work quite well for providing mode I crack growth information. The only problem that arose during the whole series was the sudden collapse in the preliminary series. The specimen cracks as expected, the crack grows gradually through the adhesive from the artificial tip, precisely according to the assumptions made in the crack growth model: the crack grows over the whole width of the specimen with the same speed at both sides of the specimen through the adhesive. Therefore both the crack depth and the energy release rate can be described and computed rather accurately. With respect to the paragraph 7.1.1, it can be stated that per specimen the obtained results lie all in a straight line, at least for *da/dN* being greater than 10^{-5}mm/c. Between the specimens there are deviations, but it is only a matter of increasing the number of specimens to overcome that inaccuracy.

When the output of the DCB specimen series is applied in the fatigue life predictions for the double lap joint and the tube joint, the results of the predictions are conservative, judging on the validation *P-N* series presented in chapter 8. The prediction model gives solid lower boundary values for both joint geometries, for both *R* values and for both G_{max} and *DG* approaches. Although the size of the group of tested joints is only big enough to have a fairly rough indication on the accuracy of the prediction model, but for this purpose, validation, this data set serves quite well.

About the application of this particular adhesive, the following remark should be made: the adhesive is easily processable, it has a favourable viscosity and can be used without complex measures to avoid initial flaws during assembling. However, the main point is to have a very sound preparation of the surface before the application of the adhesives, otherwise the joint could suffer from adhesive failure.

MS polymer
Concerning the MS polymer *da/dN-G* data in paragraph 7.1.2 it can be stated that the deviation within the data of a single specimen is relatively large, especially when it is compared to the epoxy data. The data of the various specimens are all in the same range, the difference in deviation between the different specimens is relatively small.

The predictions for the MS polymer double lap do concur with the experimental data, while an underestimation was expected, regarding the severity of the modes. However, regarding the starbge crack growth behaviour, the whole prediction model is hold up to the light. Two critical points are named out here. With respect to the entire procedure for the MS polymer double lap joint, the following aspects could be critical:
a) Detection/measuring method used for crack growth in the MS polymer DCB
b) The difference in loading mode between the double lap joint and the DCB specimen

Ad a) A possible reason for the difference in slope of the *P-N* curves are the wrong values for the constants in the modified Paris' law. A cause of these wrong values can be the method of measuring used for the DCB specimen. Before the start of the experiments it was assumed that the crack would grow through the centre of the MS polymer bond line. It has been stated before in chapter 6, this assumption came out to be incorrect, the cracks in the adhesive are growing along the interface, Figure 57. Now consider the following example:

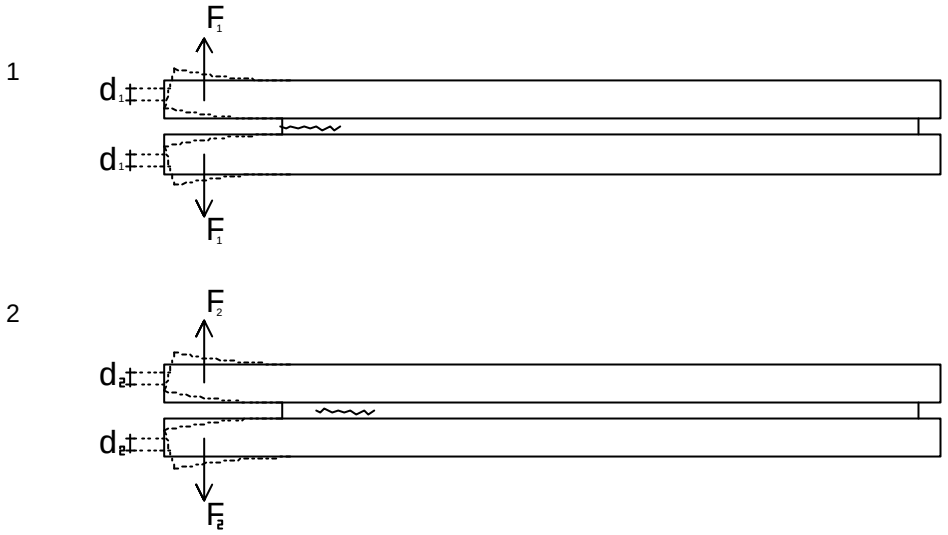

Figure 71: crack positions

Two DCB specimens are given, both with a crack. The cracks have the same lengths, but a different position. If the forces in both models, F_1 and F_2, are equal, the displacement d_1 would be bigger than d_2 due to the position of the crack. Because in the crack calculation model the crack depth *a* is directly derived from the displacements and it does not concern the position of the crack, the computed crack length in case 1 would be bigger than case 2. The energy release rate is directly computed using the crack depth, assuming the crack grows through the centre. With respect to the energy release rate in this example, two factors that affect the accuracy can be distinguished: first, the crack depths that have been computed and used to calculate *G*, may have been underestimated. If the input for the energy release rate is too low, the computed energy release rates are also lower than the actual energy release rate. Second, the cracking mechanism in the DCB specimen is different to the mechanism in the FEM model. This means that the formulas that are derived from the FEM model calculate the energy release for a mechanism that is unlike the actual mechanism in the DCB. With respect to the *da/dN* results, if the crack depths are underestimated, the differences in crack depths will be underestimated as well.
The cracking mechanism in this example is of course a simplification of the real mechanism in the MS polymer, where the cracks initiate at various locations along the interface without growing through the bond line until a late stadium. Regarding the fact that the cracks do not grow across the whole width of the specimen means that the plane strain FEM model that has been applied, is not very exact. Basically, there are two parameters that cause inaccuracies when they are derived: the crack depth and the energy release rate. Both parameters cannot be calculated properly due to the irregular cracking behaviour.

Concerning the application of the DCB, the following can be stated: if the DCB specimen is used in future experiments to characterise the crack growth behaviour, a new method of description is required, or the prediction model as it stands cannot be used accurately. A new way of describing *da/dN* could be thought of, as the method to determine a univocal measure for the crack depth *a* in this adhesive is difficult. Also the model to calculate the energy release rate in the adhesive could require some attention. As it seems impossible to univocally determine the crack depths, the energy release rate might not be directly linked to the crack depth. An alternative is to modify the MS polymer DCB as it is, while the specimen is easy to manufacture. Perhaps an adjustment of the thickness of the bond line could improve the cracking behaviour. When the bond line is thinner, the re-distribution of the stresses near the artificial crack tip becomes more difficult and increases the chance that the crack will extent from the artificial tip.

Ad b): The loading mode in the double lap joint is mainly mode II, whereas the loading mode in the DCB specimen is mode I. The prediction for the double lap has been made using mode I characteristics. Mode I is for most adhesives the most severe loading case, so the characteristics from mode I should lead to a conservative approach, which is clearly not the case. Then again, in literature no crack growth characteristics have been found for an adhesive like the MS polymer, so the conclusion that mode II is equally or more severe than mode I should not be excluded on forehand, although it might not be likely considering other adhesives.

Concerning the application of this adhesive it has to be noted that the MS polymer is applicable with little effort on the preparation of the surface where it is applied. Bonding between adhesive and substrate is easily obtained. However, the processability of the MS polymer suffers from the viscosity of the paste. When it is applied, the adhesive behaves more like a semi-viscous, sticky substance than like a liquid. This poor viscosity results in difficulties during the assembling of the components of the joint. The risk of tiny air inclusions is severe. With respect to fatigue, this porosity of the adhesive layer is a serious problem, as micro-cracks in cyclic loaded joints tend to nucleate from discontinuities in the joint. The presence of pores makes the properties of the adhesive unreliable for fatigue application, which is a pity because of the toughness, flexibility and the ability to distribute severe stresses, all favourable material properties concerning fatigue.

10 Summary and conclusions

The prediction method that is presented in this report is meant to provide lower boundary values for the fatigue life of adhesively bonded joints under a cyclic constant amplitude load. The method consists of three steps:

1) Gathering and processing crack growth data from the adhesives, resulting in a relation between the energy release rate *G* and the crack growth rate *da/dN.*
2) Modelling the joints of interest in a finite element programme using linear elastic fracture mechanics and thereupon obtaining a mathematical description of the energy release rate *G* as a function of the crack depth *a.*
3) Integration of the obtained crack growth characteristics of step 1 and the mathematical relation between *a* and *G* of step 2 resulting in a prediction of the fatigue life of an adhesively bonded connection under a particular cyclic load with a constant amplitude.

In this investigation, the method is used for two types of adhesives, a rigid adhesive and a flexible adhesive, respectively epoxy and MS polymer. Concerning step 1, the following can be stated:

With respect to the application of the DCB specimen to obtain crack growth characteristics for epoxy the following conclusion can be made:

- The method is applicable for this particular adhesive and bond line thickness, while the behaviour of the specimen is accurately to simulate using FEM. The crack growth data obtained using the DCB specimen combined with the FEM based method to compute both crack depth and energy release rate results in a consistent data set with a small deviation per specimen, except when the lower boundary of the crack growth rate is scrutinised.

With respect to the application of the DCB specimen to obtain crack growth characteristics for MS polymer the following conclusion can be made:

- The method, using the current set-up, is not very well applicable for obtaining accurate crack growth data of the MS polymer in this particular thickness. The actual crack growth mechanism is difficult to simulate. The cracking behaviour of this flexible adhesive is difficult to describe using the standard quantities, crack depth *a* and crack growth rate *da/dN.* Hence, the measurements that have been executed are relatively difficult to process accurately. The scatter in the collected data is significant over the whole crack growth rate range.

With respect to the second step of this prediction method it can be stated that the FEM models, using plane strain and axi-symmetric models are relatively easy to model and solve.

Concerning step 3, the following can be stated:

With respect to the prediction model using fracture mechanics and the modified Paris' law for the epoxy double lap joint the following the conclusions can be made:

- The prediction model, using mode I crack growth characteristics obtained with the DCB specimen to predict the fatigue life of a joint loaded with mode II, gives fairly conservative estimates on the fatigue life of the double lap joint.

With respect to the prediction model using fracture mechanics and the modified Paris' law for the MS polymer double lap joint the following the conclusions can be made:

- The prediction model, using mode I crack growth characteristics from the DCB specimen to predict the fatigue life of a joint mainly loaded with mode II, gives a reasonable accurate

prediction for the fatigue life of the double lap joint, despite the unreliable crack growth information which it has been based on.

With respect to the prediction model using fracture mechanics and the modified Paris' law for the epoxy tubular joint the following the conclusions can be made:

- The prediction model, using mode I crack growth characteristics obtained with the DCB specimen to predict the fatigue life of a joint loaded with mode II, gives sound lower boundary predictions when it is applied for the tubular epoxy joint.

Summarising all the conclusions above and considering all results, the following conclusions can be drawn about the whole prediction method, regardless of the type of adhesives or joint geometry:

- The application of the DCB specimen is an appropriate method to gather crack growth data for an adhesive, on the condition that the cracking mechanism can be described accurately using FEM applications.
- The application of FEM plane stain and axisymmetric FEM models for LEFM calculations and curve fitting programmes for processing FEM data can lead to reliable descriptions of the crack growth in a particular geometry.
- Using mode I crack growth characteristics to predict the fatigue life of an adhesively bonded joint loaded with shear or mode II can lead to conservative lower boundary values, on condition that the crack growth behaviour of the particular adhesive can be simulated accurately.
- Both the maximum load and the load range ratio have an influence on the fatigue life of an adhesively bonded joint.

11 Recommendations

Concerning the method to gain the epoxy crack growth characteristics it is recommended to find a method to monitor the crack growth in the DCB specimen closely to obtain more secure crack growth measurements. One suggestion to obtain more accurate data is the application of a camera with a strong lens that moves along the specimen as the crack extends. Accurate measurement would lead to a great improvement of accuracy, as not only *da/dN* but also *G* depends on the crack depth. Also, an actual measurement of the crack is a good manner to monitor the description of the crack by the FEM based model.

Concerning the crack growth data for the MS polymer, a more fundamental approach is required. As such, the physical crack depth *a* is hard to define for the MS polymer. A new measure for the crack depth could be developed, for instance an advanced equivalent crack depth. An alternative is the development of a specimen where the crack does grow symmetrically from the artificial crack tip through the bond line or along the interface. Adjusting the layer thickness of the adhesive would lead to a reduction of the flexibility of the bond line. Reducing the deformation capacity could lead to a more regular cracking behaviour of the adhesive.

Regarding the mode of loading, it is interesting to manufacture an epoxy specimen that would load the crack on mode I and make a prediction using the already obtained crack growth characteristics. The prediction should be validated by experimental research on a group of specimens.

Another point of interest is the influence of the mode of loading on the crack growth characteristics and on the predictions for both adhesives and all three specimens. To obtain these crack growth characteristics for mode II, a new specimen and a new set-up should be applied. An overview of possible specimens found in literature has been given in 4.1. Another interesting follow-up would be the prediction and experimental validation on mixed mode joints for these specimens, once the mode II crack growth characteristics are available.

References

[1] ‘General overview od literature survey on fatigue behaviour’ - J.H.A.Strik, 2004
[2] ‘Development of design rules for structural adhesive bonded joints’ – IJ.J.van Straalen, 2000
[3] ‘Modelling crack growth and fatigue life predictions in adhesively-bonded joints’ - J.H.A.Strik, 2004
[4] ‘Effects of mixed loading on the durability of structural adhesive joints’ by Michael Samulak and Dr John Harris, SAE conference in Bristol, 2004
[5] ‘Refinements to the mixed-mode bending test for delamination toughness’ – James R. Reeder
[6] ‘A general mixed mode fracture mechanics test specimen: the DCB-specimen with uneven bending moments’ Bent F. Sørensen, Kenneth Jørgensen, Torben K. Jacobsen, Rasmus C. Østergaard 2004
[7] ‘Structural adhesives, directory and databook’ – compiled by Bob Hussey and Jo Wilson, 1996
[8] ‘Protocol for the determination of the Mode I adhesive fracture energy, G_{IC} , of structural adhesives using the double tapered cantilever beam (DCB) and tapered double cantilever beam (TDCB) specimens, version 00-08’ B.R.K. Blackman and A.J. Kinloch. 22-06-00]
[9] ‘Experimental methodologies to determine the fracture properties of adhesive joints’ - R. Davidson and R.J. Lee, 1995
[10] ‘Flexible adhesives for structural applications- phase I: Development of prediction models and analysis of adhesive properties’ IJ. Van Straalen, H. Botter, TNO Bouw, 2004
[11] ‘The prediction of crack growth in bonded joints under cyclic-fatigue loading’ H.Hadavina, A.J. Kinloch, M.S.G. Little, A.C. Taylor; International Journal of adhesion and adhesives, 2003
[12] ‘Fatigue of structurs and materials’ – Jaap Schijve, 2001

Appendix I: technical information on adhesives

Epoxy:

3M

Scotch-Weld™

9323 B/A Structural Adhesive

Product Data Sheet

Updated : March 1996
Supersedes : July 1995

Product Description

9323 B/A is a two part room temperature curing adhesive offering the following advantages:

Extremely high strength.

Toughened Epoxy system with good elevated temperature resistance.

High environmental resistance.

Mixed adhesive is thixotropic for ease of application.

Available in 3M premetered applicator.

High impact resistance.

Physical Properties
Not for specification purposes

	BASE	ACCELERATOR
	Toughened Epoxy	Modified Amine
Specific Gravity	1.15	1.10
Mix Ratio By Weight By Volume	100 100	27 29
Consistency	Thixotropic paste	Red paste
Solids Content	100%	100%
Colour	Off White	Orangy Purple
Work Life	50g mixed material 2 hours 30 minutes 127g mixed material 2 hours 158g mixed material 1 hour	
Shelf Life	6 months from date of despatch by 3M when stored in the original carton at 21°C (70°F) & 50 % Relative Humidity	

Performance Characteristics
Not for specification purposes

Service Temperature Range	-55°C to 82°C (-67°F to 180°F)	In low load bearing applications the adhesive bonds in temperatures up to 150°C.
Water Resistance	Good	
Weathering Resistance	Good	
Fuel and Oil Resistance	Excellent	

Performance Characteristics (Cont...)
Not for specification purposes

Overlap Shear Strength

on FPL etched 1.6mm thick 2024 T3 clad aluminium.

Test Conditions	15 Days at RT		24 Hours at RT + 1 hour at 80°C		2 hours at 65°C	
	N/mm²	psi	N/mm²	psi	N/mm²	psi
-55°C	38.1	5525	29.0	4200	23.7	3535
23°C	36.2	5250	40.8	5915	39.6	5740
60°C	29.0	4200	32.0	4640	Not Tested	
82°C	22.1	3200	23.4	3390	25.4	3680
120°C	4.0	580	3.5	505	Not Tested	
150°C	2.6	380	2.5	360	Not Tested	

T-Peel Strength

on FPL etched 0.8mm thick 2024 T3 clad aluminium.

In order to ensure optimum peel properties with this product, it is recommended that joints be assembled within 20 minutes of applying the adhesive to the surfaces. Prior to application the above work lives remain valid.

Test Conditions	24 hours at RT + 1 hour at 80°C		2 hours at 65°C	
	N/cm	piw	N/cm	piw
-55°C	10.3	6	11.6	6.5
+23°C	52.2	30	58.5	33
+82°C	43.3	25	54.3	31

Durability

on etched aluminium.

Values refer to overlap shear strength on 1.6mm thick 2024 T3 clad aluminium.

Test Conditions	15 Days at room temperature		2 hours at room temperature + 60 minutes at 80°C	
	N/mm²	psi	N/mm²	psi
Control 30 Days Immersion	38.2	5540	41.6	6030
Water at RT	34.3	4970	38.9	5640
Gasoline at RT	36.6	5300	38.0	5510
M.15 at RT	30.2	4380	32.0	4640
JP4 at RT	35.8	5190	39.3	5700
Engine Oil at RT (20W40)	36.4	5280	40.9	5885
Hydraulic Oil at RT (Skydroll 500B)	37.3	5410	36.8	5335
5% Salt Spray at 35°C	33.9	4870	35.1	5090
120°C Dry Heat	34.9	5060	33.1	4800
70°C, 95% RH	32.8	4755	35.3	5120
50°C, 95% RH	37.0	5365	36.0	5220

Impact Strength

The following data show typical data obtained with bonds made and tested using an IZOD pendulum impact device according to AFNOR 76-115 test method.

Substrates:
Upper 25mm x 25mm x 8mm.
Lower 35mm x 25mm x 8mm.

2024T3 etched aluminium.

Glue line thickness: 0.125mm

Unit : kJ/m²

	15 Days at RT	1 hour at 80°C	2 hours at 56°C
Impact Value	17.4 ± 4.4	28.7 ± 3.3	32.2 ± 3.2

Suggested Cleaning Procedure for Aluminium:

Vapour Degrease - Hang skins in condensing vapours of perchloroethylene for 5 minutes.

Alkaline Degrease - Immerse in Oakite No. 164 solution (9-11 oz/gallon water) at 82°C to 93°C (180°F to 200°F) for 10 - 20 minutes. Rinse in generous quantities of clear running water.

Acid Etch - Place in either of the following solutions for 10 minutes at 66°C ± 4°C (150°F ± 5°F).

Rinse - Rinse face sheet in clear running water.

Dry - Air dry 15 minutes, force dry 10 minutes with parts at 66°C ± 4°C.

If primer is to be used, priming should be done within 4 hours of surface preparation.

	A (FPL Etch)	B
Distilled Water	30 parts by wt	30 parts by wt
Sulphuric Acid	10 parts by wt	10 parts by wt
Sodium Dichromate	1 part by wt	4 parts by wt

Cure Cycle:

In general the curing of 9323 B/A to a thermoset condition is a time-temperature relationship. The only pressure requirements are that the parts must be held in contact and alignment during the cure cycle.

To effect a useful cure in a reasonable length of time, a minimum temperature of 24°C (75°F) is required. The following cure cycle is suggested to obtain dense glue lines which give the standards reported.

Standard Room Temperature Cure:

Prepare overlap shear bonds in the manner described and allow to cure as follows:

Apply 2 psi bonding pressure uniformly to the bond line using dead weights.

Allow Panels to cure undisturbed at a temperature of 24°C (75°F) for 24 to 48 hours.

In addition to standard room temperature cure, the following times and temperatures will give a minimum of 2,000 psi tensile shear at 24°C (75°F) on acid etched aluminium.

Temperature		Time
5°C	(40°F)	7 days
66°C	(150°F)	120 minutes
121°C	(250°F)	5 minutes
177°C	(350°F)	2 minutes

Additional Product Information

Work Life:
The work life of mixed 9323 B/A is approximately 2 hours 30 minutes in a mass of 50grams at an ambient temperature of 23°C.

The work life of the mixed adhesive will be lengthened by reducing the temperature or amount of adhesive and will be shortened by higher temperature or larger amounts of adhesive.

Caution: Heat is generated during cure.

Directions for Use

Proper adhesive application is as important as proper joint design, surface preparation and adhesive choice to obtain maximum joint properties. Poor adhesive application techniques can result in partial or complete failure of an assembly.

9323 B/A performance data was developed using the following suggested procedures. Variation from these procedures should be fully evaluated by the user to ensure bond properties sufficient to meet the requirements of any particular assembly.

Surface Preparation:
A thoroughly cleaned, dry, grease-free surface is essential for maximum performance. Cleaning methods, which will produce a break free water film on a metal surface are generally satisfactory.

Adhesive Mixing:
Mix only those amounts of adhesive which can be used within the work life of the mixture. To achieve optimum physical properties of the adhesive, mixing of the base and accelerator must be very thorough. Care should be taken not to incorporate excessive air into the adhesive during mixing and application as entrapped air will tend to give a porous and weakened bond. When weighing the components, be sure that containers are free of wax or oil. When thoroughly mixed the adhesive should be a uniform colour. As a final check to ensure that the components are adequately mixed, spread a thin film on white paper and examine closely for streaks of base or accelerator. Temperature of the adhesive should not exceed 27°C (80°F) during mixing.

Equipment Suggestions:
Application can be carried out with a spatula, trowel or flow equipment. Suitable two part metering and mixing equipment is available. Contact your 3M Representative for assistance in selecting application equipment to suit your specific needs.

Bond Line Thickness:
Optimum performance is obtained with a 0.002" to 0.005" (0.05 - 0.125mm) cured bond line. For maximum peel strength allow 0.010" (0.25mm) glue line thickness.
Coverage 4m²/litre (at 0.010" thickness).

Clean Up:
Excess adhesive can be cleaned prior to curing with Scotch-grip Solvent No. 2.
NOTE: Solvent No. 2 is flammable. When using solvents for clean up it is essential that proper safety precautions are observed.

Applications	Bonds metal, glass, ceramics, plastics, composites and rigid rubbers.	Particularly suited to applications requiring resistance to harsh environments. e.g. oil, gasoline, anti-freeze, dry heat.	
Health and Safety Information	**PART A** contains: 2,4,6 - Tris (Dimethylaminomethyl) phenol, polymeric diamine. **PART B** contains: Epoxy Resin. **Precautions:** Irritating to skin. Risk of serious damage to eyes. May cause sensitisation by skin contact. May be harmful if swallowed. Avoid contact with skin and eyes. Wear suitable gloves and eye/face protection.	**First Aid:** **Eye Contact:** Immediately flush eyes with copious amounts of water for at least 15 minutes, holding eyes open. Call a physician. **Skin Contact:** Wash immediately with plenty of soap and water. **Ingestion:** Drink two glasses of water and call a physician immediately. Do not induce vomiting.	For further Health & Safety information, please contact our Toxicology Department on Bracknell (0344) 858000.
Specifications	May be released to AFS 1899 and DTD 900/1622.	Water Research Council Approval.	

Values presented have been determined by standard test methods and are average values not to be used for specification purposes.
Our recommendations on the use of our products are based on tests believed to be reliable but we would ask that you conduct your own tests to determine their suitability for your applications.
This is because 3M cannot accept any responsibility or liability direct or consequential for loss or damage caused as a result of our recommendations.

3M

Specialty Tapes & Adhesives

3M United Kingdom PLC
3M House,
28 Great Jackson Street,
Manchester,
M15 4PA

Customer Service :

Tel 0161 236 8500
Fax 0161 237 1105

3M Ireland
3M House, Adelphi Centre,
Upper Georges Street,
Dun Laoghaire,Co. Dublin,
Ireland

Customer Service :

Tel (01) 280 3555
Fax (01) 280 3509

Appendix II: curve fitting

Introduction

In this appendix, the mathematical descriptions of the relation between the displacements and the crack depth and the relation between the crack depth and the energy release rate are given. The general format of these functions has been assumed for the DCB specimen as:

$a = b * d^c + f$
$G = b * a^c + f$

The optimum format for the description of the *G-a* relation for the double lap joint and tube joint is assumed to be:

$G = b * e^{ac} + f$

The values of *b*, *c* and *f* have been found by a curve fitting application in MathCad. All values and curves can be found in paragraph.

Double cantilever beam

Table 1: G-a curve coefficients for the DCB for epoxy and MS polymer

joint type	adhesive	relation	b	c	f
DCB	epoxy	a(d)	239.73	0.352	-18.2
	MS	a(d)	200.00	0.600	0.0
	epoxy	G(a)	1.32E-07	1.911	2.670E-05
	MS	G(a)	8.77E-08	2.064	6.211E-04

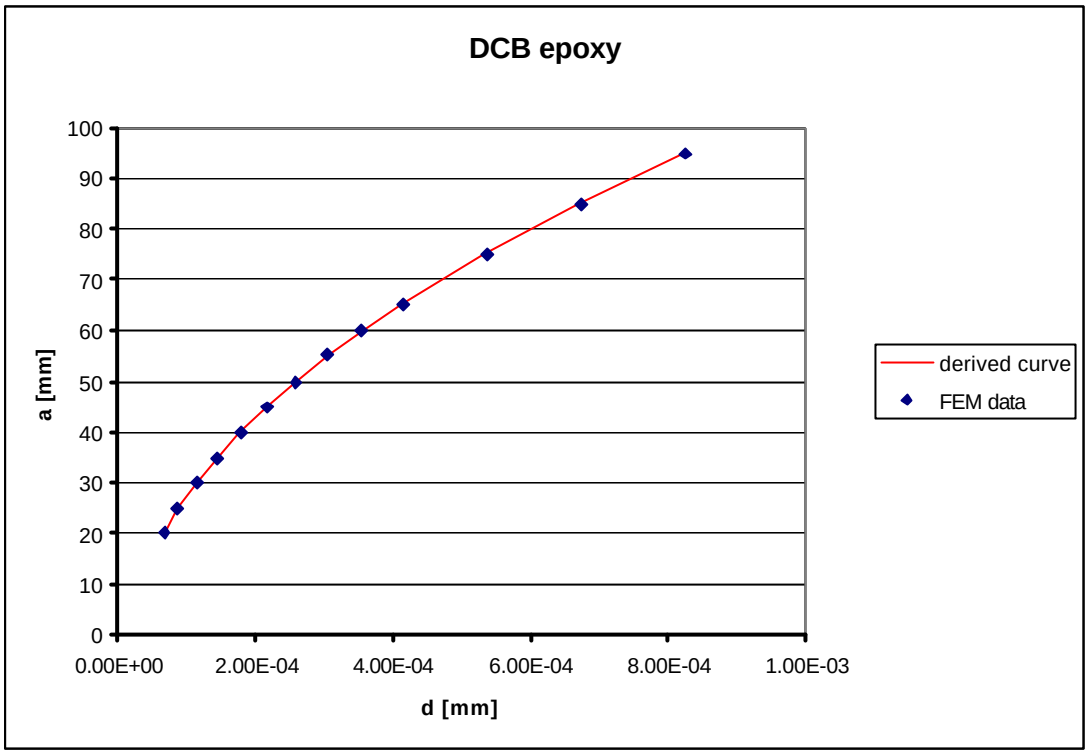

Figure 1: a-d diagram; FEM data points and the derived curve for the DCB specimen for epoxy for a unit width and a unit load

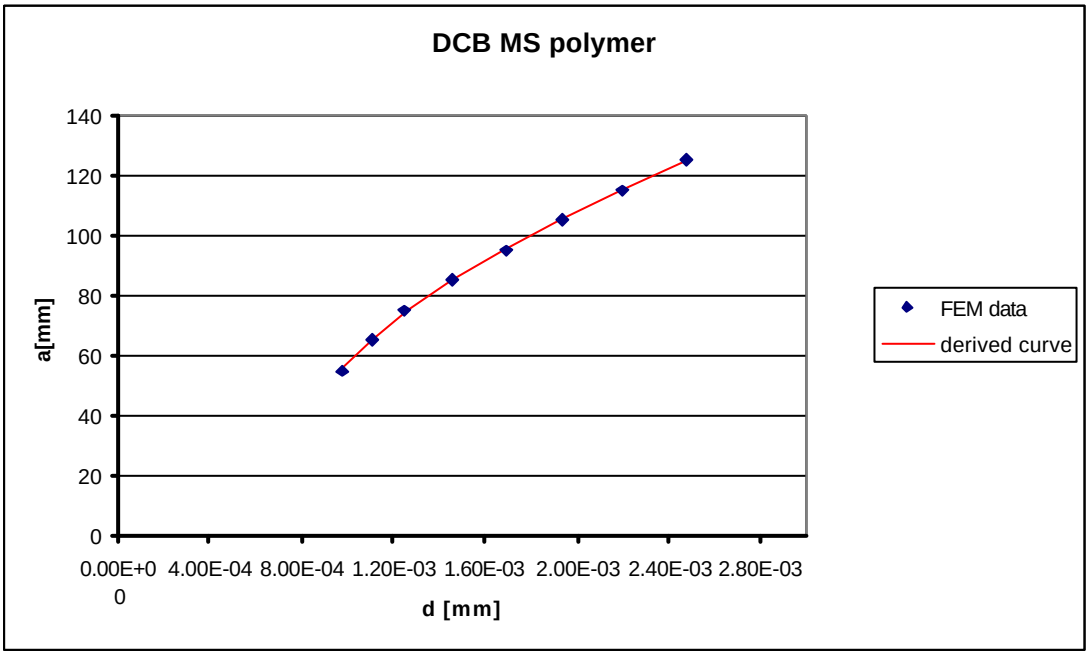

Figure 2: a-d diagram; FEM data points and the derived curve for the DCB specimen for MS polymer for a unit width and a unit load

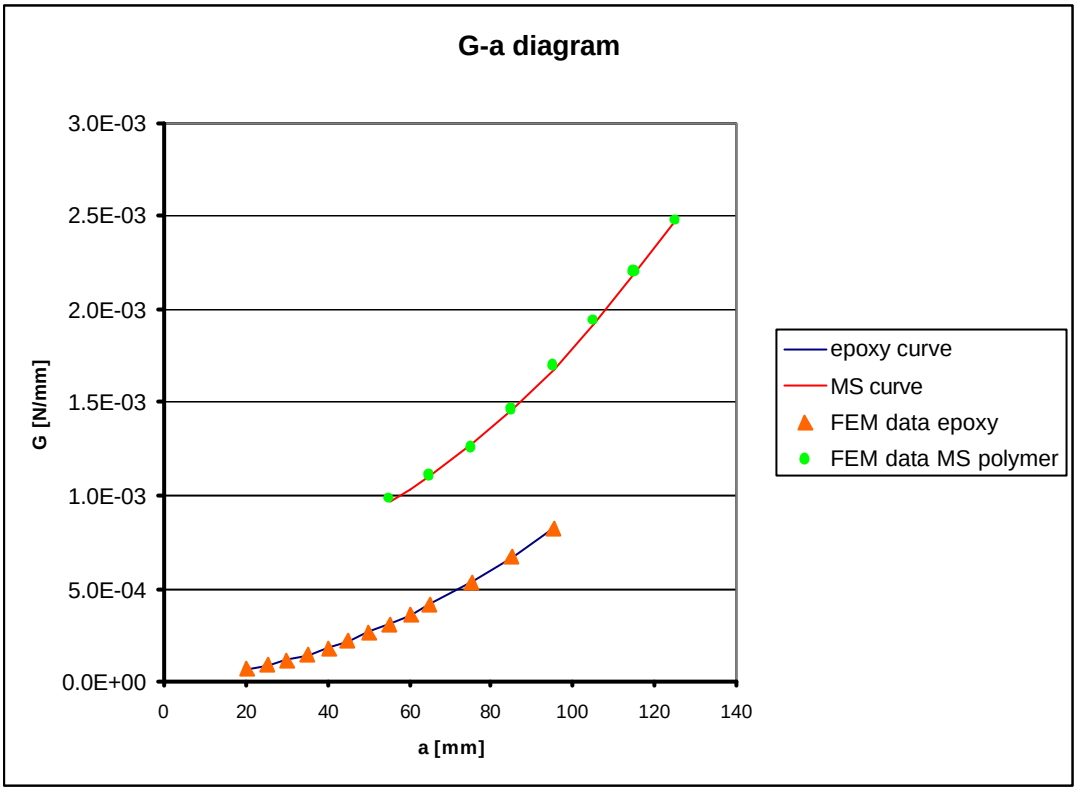

Figure 3: G-a diagram; FEM data points and the derived curve for the DCB specimen for epoxy and MS polymer for a unit width and a unit load

Double lap joint

Table 2: G-a curve coefficients for the double lap for epoxy and MS polymer

joint type	adhesive	lap length	side	b	c	f
double lap	epoxy	20	L	2.62E-07	0.58	3.60E-06
		20	R	2.68E-07	0.596	1.47E-06
		40	L	7.49E-10	0.551	1.58E-06
		40	R	1.13E-09	0.526	4.56E-07
	MS polymer	20	L	2.60E-05	0.372	-1.85E-05
		20	R	1.87E-05	0.426	-1.31E-05
		40	L	3.54E-06	0.239	7.81E-06
		40	R	1.95E-06	0.285	6.79E-06

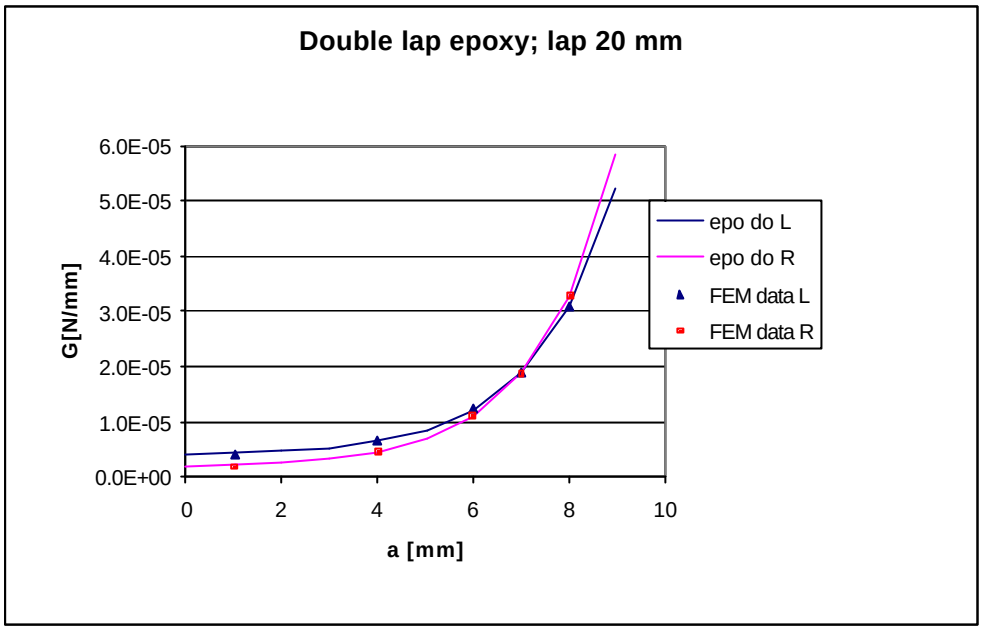

Figure 4: G-a diagram data points and the derived curve for the double lap joint, lap 20 mm for epoxy

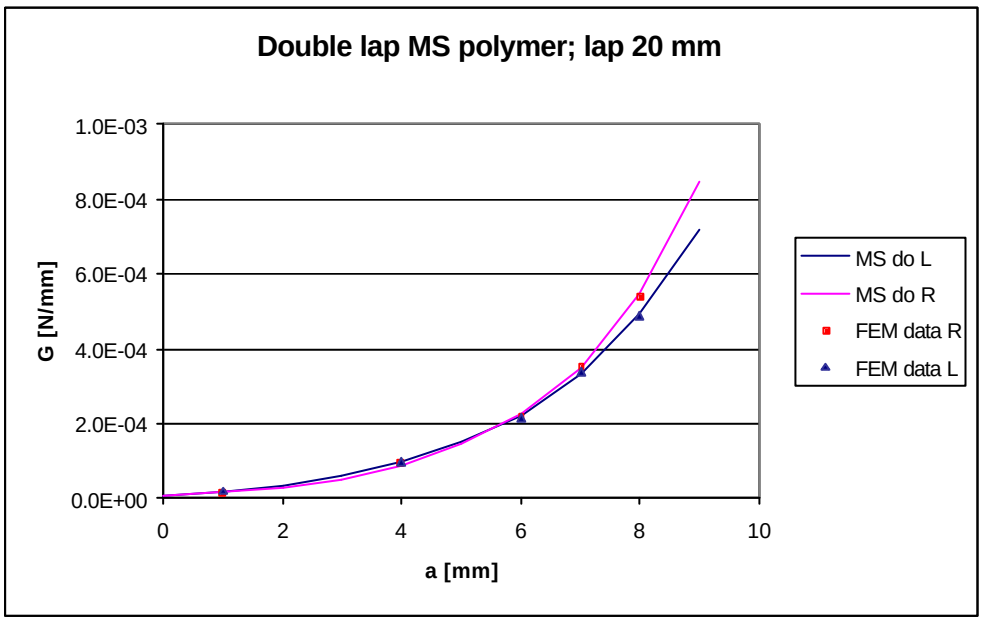

Figure 5: G-a diagram data points and the derived curve for the double lap joint, lap 20 mm for MS polymer

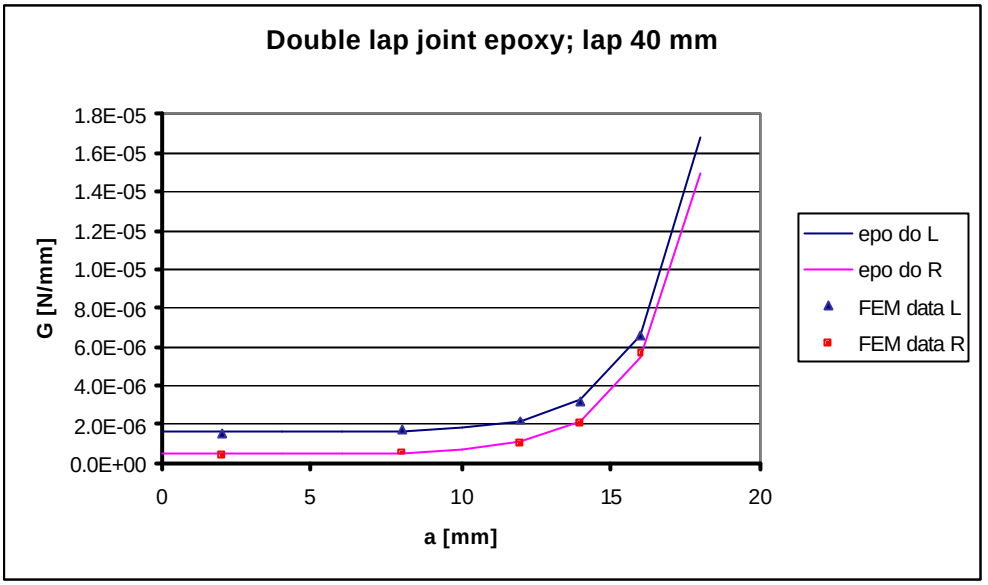

Figure 6: G-a diagram data points and the derived curve for the double lap joint, lap 40 mm for epoxy

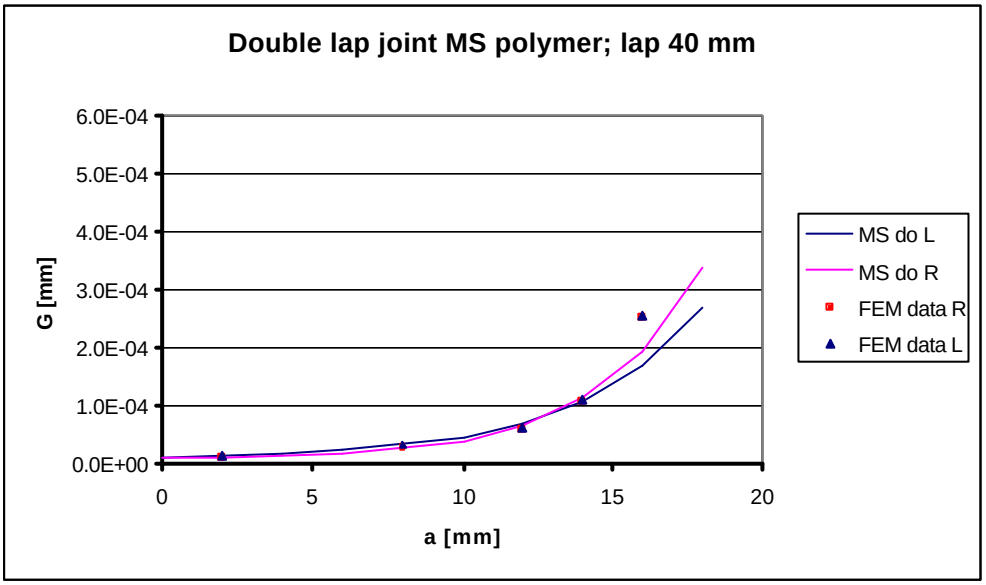

Figure 7: G-a diagram data points and the derived curve for the double lap joint, lap 40 mm for MS polymer

Tubular joint

Table 3: G-a curve coefficients for the tubular joint for epoxy

joint type	adhesive	lap length	side crack	b	c	f
Tubular	epoxy	15	L	1.48E-09	0.793	4.03E-08
		15	R	3.87E-10	1.039	3.19E-08
		20	L	7.89E-10	0.628	2.72E-08
		20	R	4.78E-10	0.703	1.85E-08
		40	L	1.96E-10	0.339	1.49E-08
		40	R	5.06E-10	0.281	9.36E-09

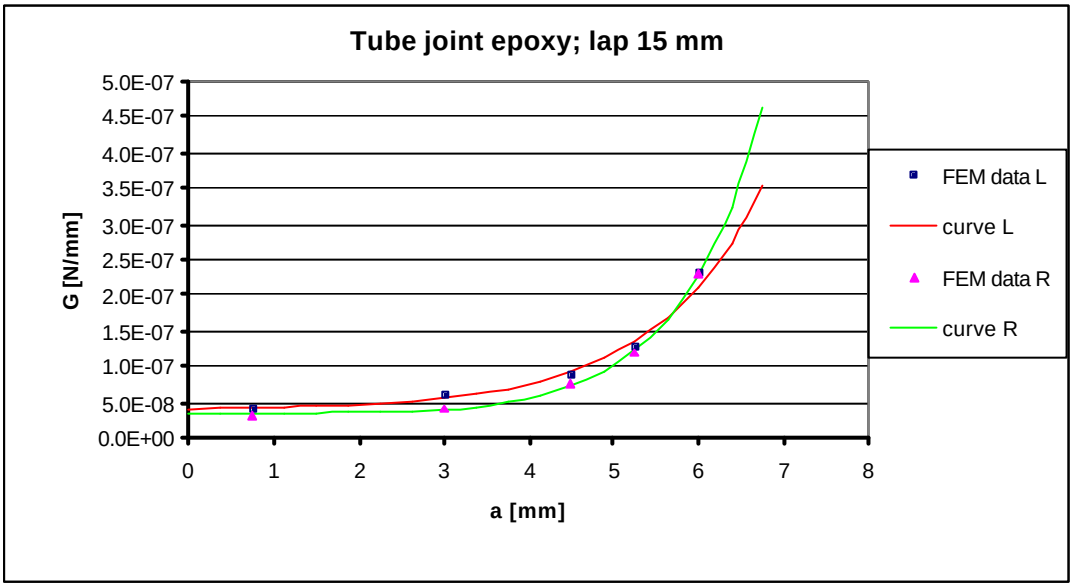

Figure 8: G-a diagram data points and the derived curve for the tubular joint, lap 15 mm for epoxy

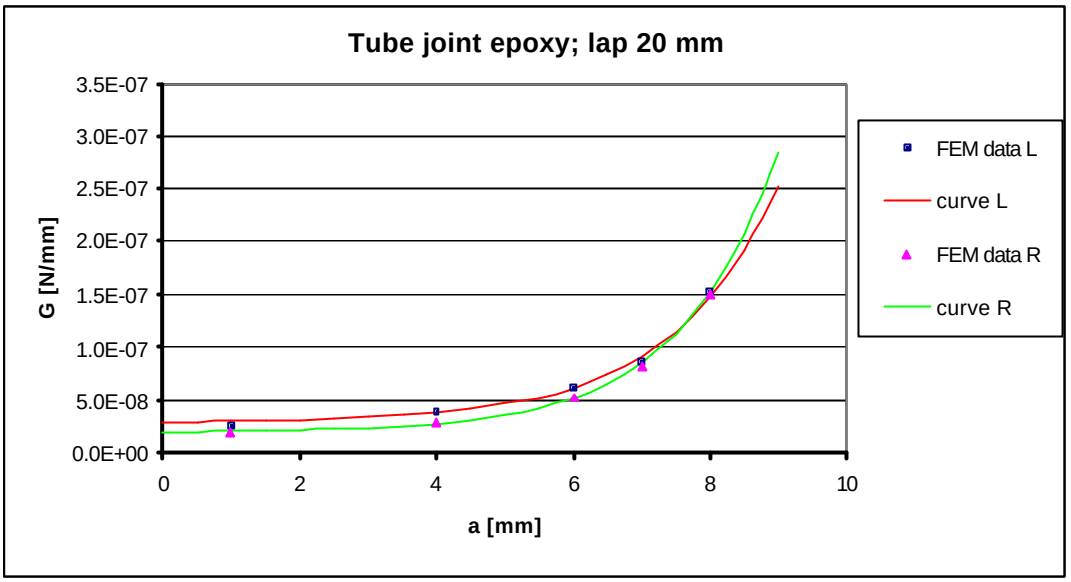

Figure 9: G-a diagram data points and the derived curve for the tubular joint, lap 20 mm for epoxy

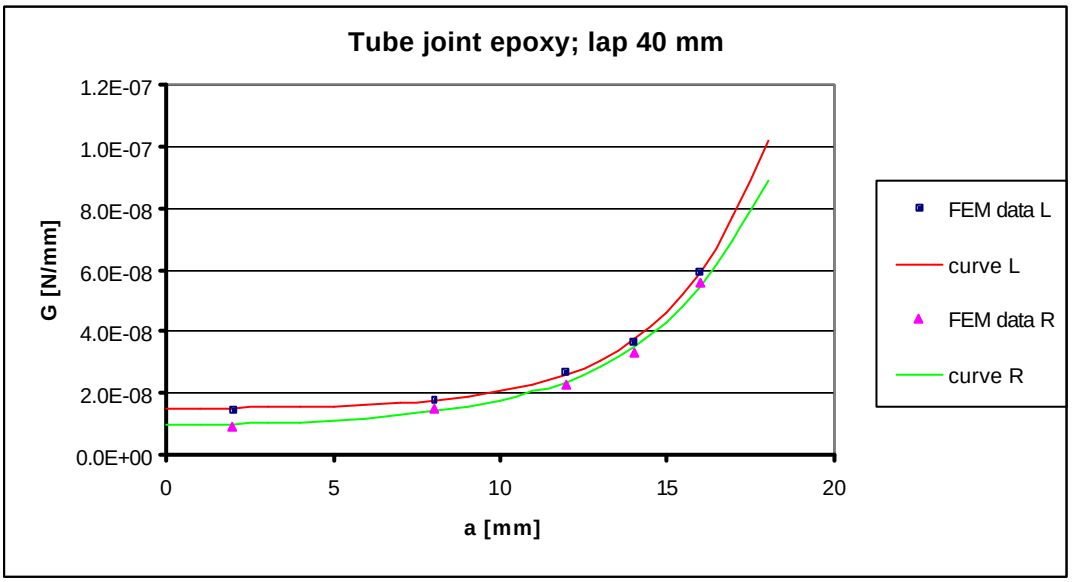

Figure 10: G-a diagram data points and the derived curve for the tubular joint, lap 40 mm for epoxy

Report of assembly of the specimen and measurement data

Jaap Strik
S448826

March 2005

Department of Structural Design
Faculty of Architecture, Building and Planning

A 2005-13
O 2005-09

1 Introduction

During the investigation, I have made three different specimens and four series of crack growth characteristics measurements. This report contains the pictures of the assembly and the measurement data.

2 Assembling specimen

2.1 DCB

2.1.1 Epoxy

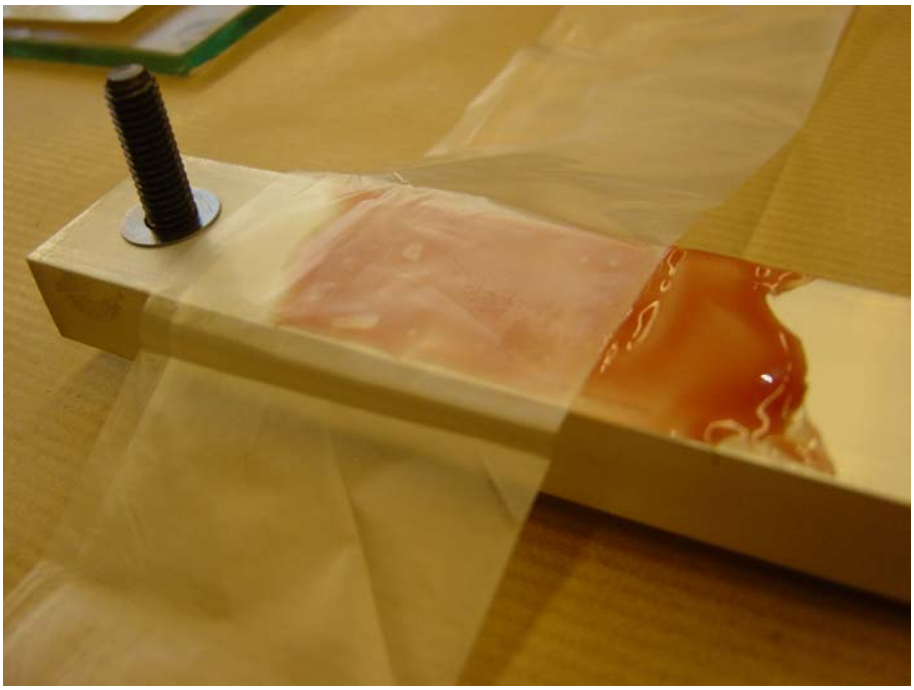

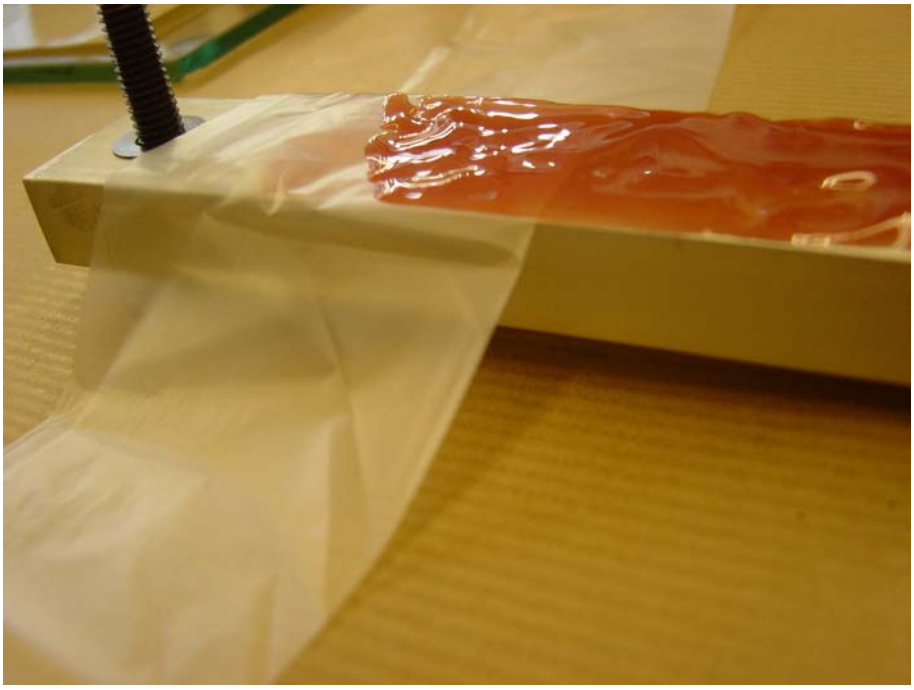

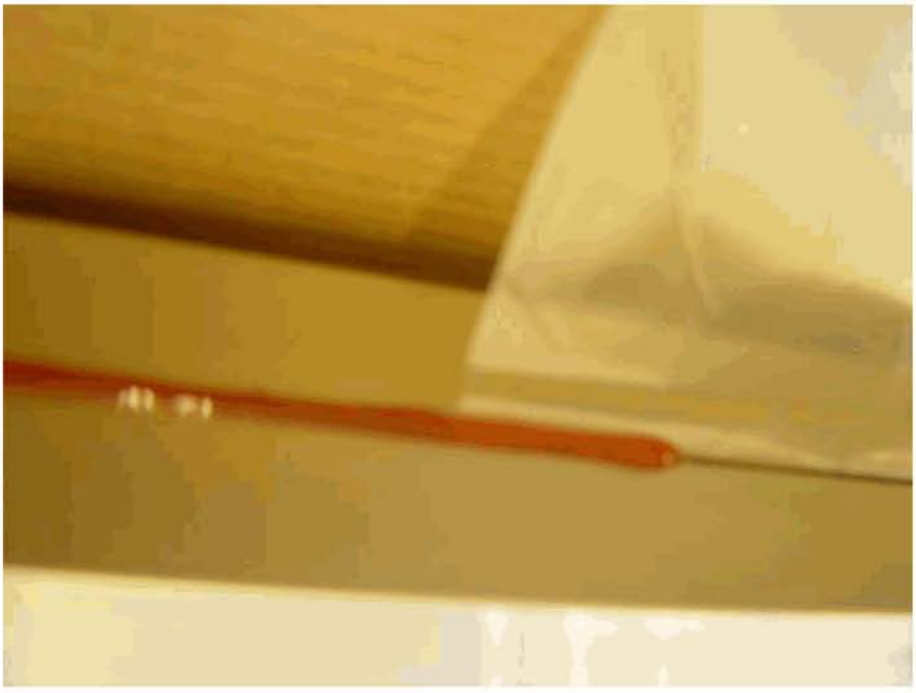

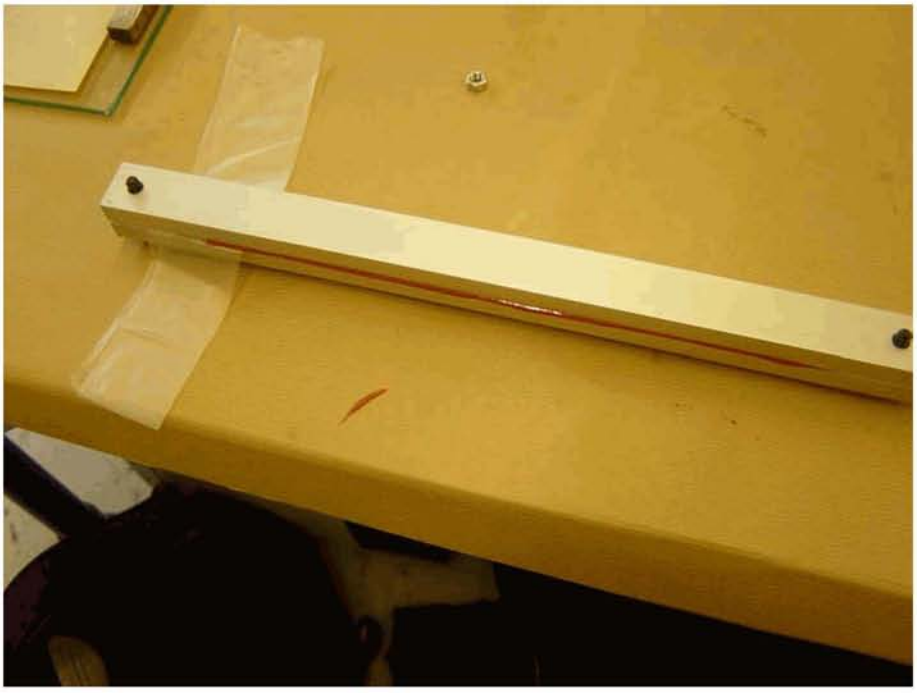

2.2 MS polymer

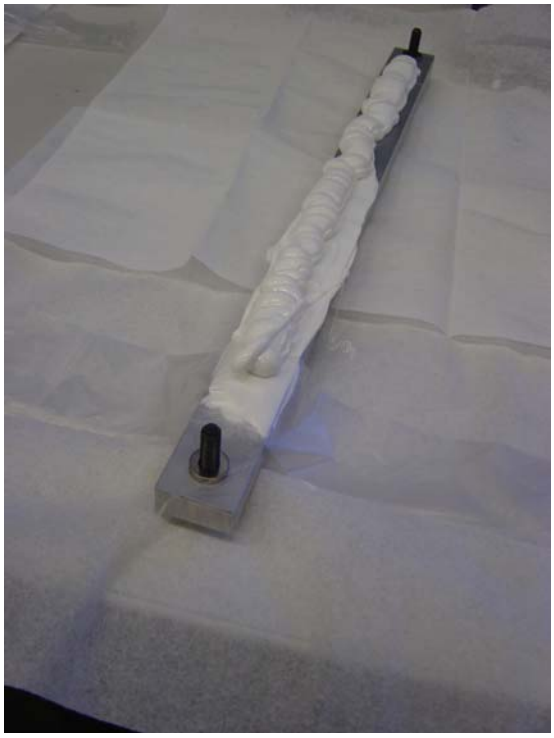

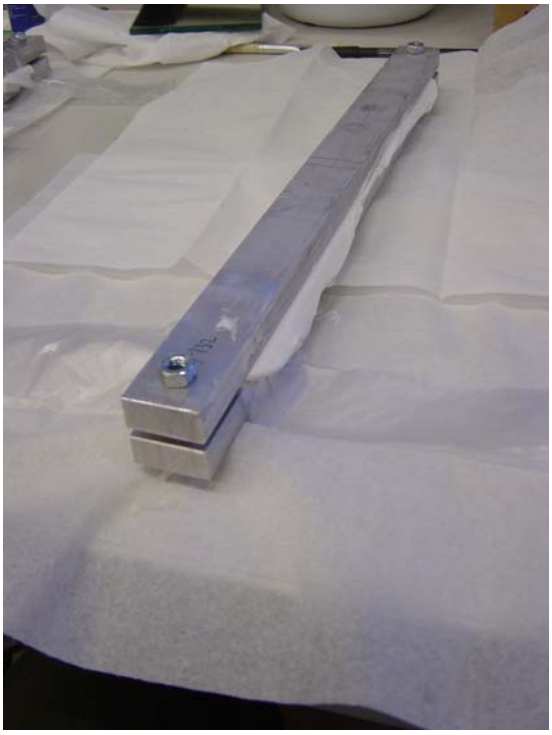

2.3 Tubular joint

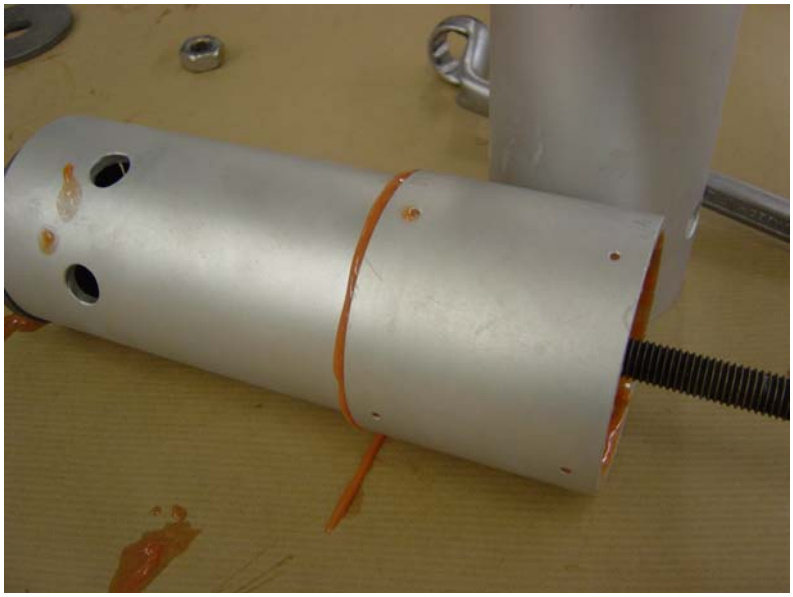

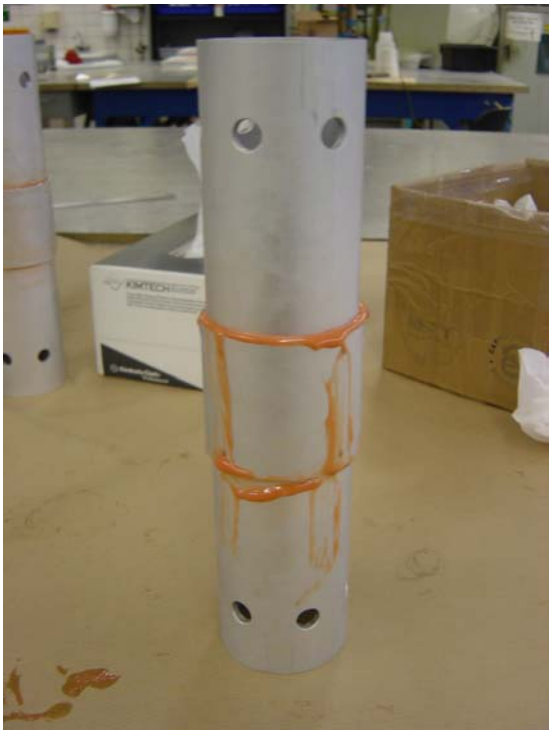

3 Crack growth data

3.1 Epoxy, R=0.1

specimen	date	time	f [Hz]	N [-]	P_{max} [N]	P_{min} [N]	d_{max} [mm]	a_{max} [mm]	E [N/mm²]	b [mm]	G_{max} [N/mm]	G_{min} [N/mm]	dG [N/mm]	da/dN
CV	3-jan	12:45	10	0	800	80	0.5550	38.222	70000	23.66				
		12:55	10	6000	800	80	0.7178	43.571			0.2125	0.0021	0.2103	8.91E-04
		13:05	10	12000	800	80	1.0007	51.236			0.2723	0.0027	0.2695	1.28E-03
		13:15	5	15000	800	80	1.9796	70.082			0.4237	0.0042	0.4194	6.28E-03
		13:20	3	16800	800	80	5.4828	108.159			0.8656	0.0087	0.8570	2.12E-02
WK	3-jan	13:38	10	0	600	60	0.6723	48.617		23.68				
		13:48	10	6000	600	60	0.8027	52.919			0.1713	0.0017	0.1695	7.17E-04
		13:58	8	10800	600	60	0.9822	58.156			0.2002	0.0020	0.1982	1.09E-03
		14:08	8	15600	600	60	1.4562	69.508			0.2571	0.0026	0.2546	2.37E-03
		14:18	4	17760	600	60	4.9461	116.685			0.5348	0.0053	0.5295	2.18E-02
OU	3-jan	15:32	10	0	400	40	0.2835	38.637		23.64				
		15:42	10	6000	400	40	0.2851	38.743			0.0485	0.0005	0.0480	1.78E-05
		15:52	10	12000	400	40	0.2866	38.850			0.0487	0.0005	0.0482	1.77E-05
		16:02	10	18000	400	40	0.2875	38.913			0.0489	0.0005	0.0484	1.06E-05
		16:12	10	24000	400	40	0.2881	38.956			0.0490	0.0005	0.0485	7.06E-06
		16:22	10	30000	420	42	0.3045	39.087						
		16:32	10	36000	420	42	0.3051	39.127			0.0544	0.0005	0.0538	6.69E-06
		16:42	10	42000	420	42	0.3072	39.267			0.0546	0.0005	0.0540	2.33E-05
		16:52	10	48000	420	42	0.3084	39.347			0.0548	0.0005	0.0543	1.33E-05
		17:02	10	54000	420	42	0.3102	39.466			0.0550	0.0006	0.0545	1.99E-05
		17:12	10	60000	440	44	0.3269	39.585						
		17:22	10	66000	440	44	0.3290	39.717			0.0610	0.0006	0.0604	2.20E-05
		17:32	10	72000	440	44	0.3315	39.867			0.0614	0.0006	0.0608	2.50E-05
		17:42	10	78000	440	44	0.3345	40.053			0.0618	0.0006	0.0612	3.11E-05
		17:52	10	84000	440	44	0.3378	40.257			0.0623	0.0006	0.0617	3.40E-05
	4-jan	8:46	10	86000	460	46	0.3406	39.513						
		8:56	10	92000	460	46	0.3436	39.693			0.0666	0.0007	0.0659	3.01E-05
		9:06	10	98000	460	46	0.3500	40.068			0.0673	0.0007	0.0667	6.26E-05
		9:16	10	104000	460	46	0.3539	40.299			0.0682	0.0007	0.0675	3.84E-05
		9:26	10	110000	460	46	0.3581	40.545			0.0688	0.0007	0.0681	4.10E-05
		9:36	10	116000	480	48	0.3800	40.889						
		9:46	10	122000	480	48	0.3863	41.236			0.0769	0.0008	0.0761	5.78E-05
		9:56	10	128000	480	48	0.3921	41.547			0.0779	0.0008	0.0771	5.18E-05
		10:06	10	134000	480	48	0.3982	41.870			0.0789	0.0008	0.0781	5.39E-05
		10:16	10	140000	480	48	0.4039	42.175			0.0799	0.0008	0.0791	5.08E-05
		10:26	10	146000	500	50	0.4309	42.684						
		10:36	10	152000	500	50	0.4397	43.119			0.0897	0.0009	0.0888	7.24E-05
		10:46	10	158000	500	50	0.4488	43.562			0.0912	0.0009	0.0903	7.39E-05
		10:56	10	164000	500	50	0.4579	44.000			0.0927	0.0009	0.0918	7.30E-05
		11:06	10	170000	500	50	0.4676	44.461			0.0943	0.0009	0.0934	7.68E-05
		11:16	10	176000	520	52	0.5028	45.200						
		11:26	10	182000	520	52	0.5204	45.972			0.1073	0.0011	0.1063	1.29E-04
		11:36	10	188000	520	52	0.5401	46.817			0.1106	0.0011	0.1094	1.41E-04
		11:46	10	194000	520	52	0.5601	47.655			0.1140	0.0011	0.1128	1.40E-04
		11:56	10	200000	520	52	0.5816	48.536			0.1175	0.0012	0.1163	1.47E-04
		12:06	10	206000	540	54	0.6371	49.802						
		12:16	10	212000	540	54	0.6763	51.243			0.1379	0.0014	0.1365	2.40E-04
		12:26	10	218000	540	54	0.7220	52.863			0.1451	0.0015	0.1437	2.70E-04
		12:36	10	224000	540	54	0.7879	55.079			0.1546	0.0015	0.1530	3.69E-04
		12:46	10	230000	540	54	0.8673	57.600			0.1666	0.0017	0.1649	4.20E-04
		12:49	7	231260	560	56	0.9677	59.577						
		12:52	7	232520	560	56	1.0032	60.569			0.2005	0.0020	0.1985	7.87E-04
		12:55	7	233780	560	56	1.0483	61.800			0.2071	0.0021	0.2051	9.77E-04
		12:58	7	235040	560	56	1.1026	63.234			0.2152	0.0022	0.2131	1.14E-03
		13:01	7	236300	560	56	1.1712	64.981			0.2251	0.0023	0.2228	1.39E-03
		13:04	7	237560	560	56	1.2485	66.875			0.2366	0.0024	0.2343	1.50E-03
		13:07	7	238820	560	56	1.3389	68.993			0.2497	0.0025	0.2472	1.68E-03
		13:10	7	240080	560	56	1.4489	71.453			0.2651	0.0027	0.2624	1.95E-03
		13:13	7	241340	560	56	1.5997	74.630			0.2846	0.0028	0.2818	2.52E-03
		13:16	5	242240	560	56	1.9354	81.069			0.3199	0.0032	0.3167	7.15E-03
		13:19	5	243140	560	56	2.4991	90.416			0.3821	0.0038	0.3783	1.04E-02
		13:22	5	244040	560	56	3.3106	101.717			0.4714	0.0047	0.4667	1.26E-02
		13:25	5	244340	560	56	5.3524	123.812			0.6382	0.0064	0.6318	7.36E-02
YQ	6-jan	10:40	15	0	350	35	0.2991	42.498		23.633				
		11:40	15	54000	350	35	0.3089	43.186			0.0439	0.0004	0.0434	1.27E-05
		12:40	15	108000	350	35	0.3204	43.984			0.0451	0.0005	0.0447	1.48E-05
		13:40	15	162000	350	35	0.3349	44.961			0.0467	0.0005	0.0462	1.81E-05
		14:43	15	216000	250	25	0.2610	46.926						
		15:43	15	270000	250	25	0.2633	47.134			0.0262	0.0003	0.0259	3.84E-06
		16:43	15	324000	250	25	0.2628	47.090			0.0262	0.0003	0.0260	-8.16E-07
		17:43	15	378000	250	25	0.2616	46.979			0.0262	0.0003	0.0259	-2.04E-06
		18:43	15	432000	250	25	0.2620	47.015			0.0261	0.0003	0.0259	6.55E-07
		19:43	15	486000	320	32	0.3359	47.051						
		20:43	15	540000	320	32	0.3418	47.452			0.0432	0.0004	0.0428	4.05E-06
		21:43	15	594000	320	32	0.3486	47.912			0.0439	0.0004	0.0434	8.53E-06
		22:43	15	648000	320	32	0.3581	48.543			0.0447	0.0004	0.0443	1.01E-05
		23:43	15	702000	310	31	0.3647	49.728						
	7-jan	0:43	15	756000	310	31	0.3735	50.295			0.0447	0.0004	0.0442	1.62E-05
		1:43	15	810000	310	31	0.3814	50.806			0.0455	0.0005	0.0450	9.46E-06

specimen	date	time	f [Hz]	N [-]	P_{max} [N]	P_{min} [N]	d_{max} [mm]	a_{max} [mm]	E [N/mm²]	b [mm]	G_{max} [N/mm]	Gmin [N/mm]	dG [N/mm]	da/dN
		2:43	15	864000	310	31	0.3893	51.303			0.0463	0.0005	0.0458	9.33E-06
		3:43	15	918000	310	31	0.3974	51.810			0.0471	0.0005	0.0466	9.38E-06
		4:43	15	972000	310	31	0.4084	52.485			0.0480	0.0005	0.0475	1.09E-05
		5:43	15	1026000	310	31	0.4174	53.028			0.0490	0.0005	0.0485	1.01E-05
		6:43	15	1080000	310	31	0.4295	53.751			0.0500	0.0005	0.0495	1.17E-05
		7:43	15	1134000	310	31	0.4402	54.379			0.0511	0.0005	0.0506	1.16E-05
		8:43	15	1188000	310	31	0.4518	55.043			0.0522	0.0005	0.0516	1.20E-05
		9:43	15	1242000	300	30	0.4527	55.946			0.0518	0.0005	0.0512	1.67E-05
		10:43	15	1296000	300	30	0.4625	56.508			0.0512	0.0005	0.0507	1.04E-05
		11:43	15	1350000	300	30	0.4840	57.714			0.0527	0.0005	0.0521	2.23E-05
		12:43	15	1404000	260	26	0.4346	58.668						
		13:43	15	1458000	260	26	0.4399	58.996			0.0417	0.0004	0.0413	6.08E-06
		14:43	15	1512000	260	26	0.4451	59.315			0.0421	0.0004	0.0417	5.92E-06
		14:46	15	1566000	200	20	0.3474	59.712						
		15:46	15	1620000	200	20	0.3493	59.859			0.0254	0.0003	0.0251	2.72E-06
		16:46	15	1674000	200	20	0.3510	59.997			0.0255	0.0003	0.0252	2.57E-06
		17:46	15	1728000	200	20	0.3522	60.092			0.0256	0.0003	0.0253	1.75E-06
		17:55		1728000	600	60	1.3355	66.818						
		17:56	7	1728420	600	60	1.4875	70.104			0.2909	0.0029	0.2880	7.82E-03
		17:57	7	1728840	600	60	1.6354	73.102			0.3154	0.0032	0.3122	7.14E-03
		17:58	7	1729260	600	60	1.8235	76.668			0.3421	0.0034	0.3386	8.49E-03
		17:59	7	1729680	600	60	2.0782	81.136			0.3762	0.0038	0.3725	1.06E-02
		18:00	7	1730100	600	60	2.4697	87.359			0.4244	0.0042	0.4201	1.48E-02
		18:01	7	1730520	600	60	2.9883	94.683			0.4893	0.0049	0.4844	1.74E-02
		18:02	6	1730880	600	60	3.9053	105.835			0.5858	0.0059	0.5800	3.10E-02
		18:03	5	1731180	600	60	5.1235	118.274			0.7205	0.0072	0.7133	4.15E-02

3.2 Epoxy, R=0.5

specimen	date	time	f [Hz]	N [-]	P_{max} [N]	P_{min} [N]	d_{max} [mm]	a_{max} [mm]	E [N/mm²]	b [mm]	G_{max} [N/mm]	G_{min} [N/mm]	dG [N/mm]	da dN
NF	10-jan	8:28	8	0	800	400	0.257159	24.81333	70000	23.62				
		8:32	8	1920	800	400	0.260495	25.00891			0.101159632	0.02528991	0.0758697	1.02E-04
		8:36	8	3840	800	400	0.262011	25.09728			0.101929037	0.02548226	0.0764468	4.60E-05
		8:40	8	5760	800	400	0.263528	25.18532			0.102409495	0.02560237	0.0768071	4.59E-05
		8:44	8	7680	800	400	0.264437	25.23798			0.102793692	0.02569842	0.0770953	2.74E-05
		8:48	8	9600	820	410	0.27869	25.66521						
		8:52	8	11520	820	410	0.2796	25.71556			0.110772627	0.02769316	0.0830795	2.62E-05
		8:56	8	13440	820	410	0.280207	25.74907			0.111017909	0.02775448	0.0832634	1.75E-05
		9:00	8	15360	820	410	0.28142	25.81595			0.111312136	0.02782803	0.0834841	3.48E-05
		9:05	8	17760	840	420	0.295066	26.17773						
		9:10	8	20160	840	420	0.295673	26.20982			0.119357837	0.02983946	0.0895184	1.34E-05
		9:15	8	22560	840	420	0.296279	26.24187			0.119558183	0.02988955	0.0896686	1.34E-05
		9:20	8	24960	840	420	0.296582	26.25787			0.119708419	0.0299271	0.0897813	6.67E-06
		9:25	8	27360	840	420	0.297492	26.30583			0.11990868	0.02997717	0.0899315	2.00E-05
		9:30	8	29760	840	420	0.298402	26.35369			0.120209006	0.03005225	0.0901568	1.99E-05
		9:35	8	32160	840	420	0.298705	26.36963			0.12040918	0.0301023	0.0903069	6.64E-06
		9:40	8	34560	840	420	0.299008	26.38555			0.120509246	0.03012731	0.0903819	6.63E-06
		9:45	8	36960	860	430	0.313261	26.74855						
		9:50	8	39360	860	430	0.314171	26.79446			0.128928519	0.03223213	0.0966964	1.91E-05
		9:55	8	41760	860	430	0.315384	26.85553			0.129286029	0.03232151	0.0969645	2.54E-05
		10:00	8	44160	860	430	0.315384	26.85553			0.129490288	0.03237257	0.0971177	0.00E+00
		10:05	8	46560	860	430	0.3169	26.93166			0.129745491	0.03243637	0.0973091	3.17E-05
		10:10	8	48960	860	430	0.317204	26.94686			0.130051717	0.03251293	0.0975388	6.33E-06
		10:15	8	51360	860	430	0.318113	26.9924			0.130255782	0.03256395	0.0976918	1.90E-05
		10:20	8	53760	880	440	0.332973	27.35437						
		10:25	8	56160	880	440	0.333579	27.38356			0.139214022	0.03480351	0.1044105	1.22E-05
		10:30	8	58560	880	440	0.334792	27.44184			0.139526277	0.03488157	0.1046447	2.43E-05
		10:35	8	60960	880	440	0.336005	27.49999			0.139942486	0.03498562	0.1049569	2.42E-05
		10:40	8	63360	880	440	0.336915	27.54351			0.140306537	0.03507663	0.1052299	1.81E-05
		10:45	8	65760	880	440	0.337825	27.58695			0.140618467	0.03515462	0.1054639	1.81E-05
		10:50	8	68160	880	440	0.339341	27.65918			0.141034201	0.03525855	0.1057757	3.01E-05
		10:55	8	70560	880	440	0.341464	27.75996			0.141657478	0.03541437	0.1062431	4.20E-05
		11:00	8	72960	900	450	0.356323	28.08668						
		11:05	8	75360	900	450	0.358143	28.16975			0.151349971	0.03783749	0.1135125	3.46E-05
		11:10	8	77760	900	450	0.360266	28.26631			0.152038007	0.0380095	0.1140285	4.02E-05
		11:15	8	80160	900	450	0.362388	28.3625			0.152778479	0.03819462	0.1145839	4.01E-05
		11:20	8	82560	900	450	0.363601	28.4173			0.153359953	0.03833999	0.11502	2.28E-05
		11:25	8	84960	930	465	0.388165	28.95505						
		11:30	8	87360	930	465	0.391804	29.11019			0.169103352	0.04227584	0.1268275	6.46E-05
		11:35	8	89760	930	465	0.394837	29.23877			0.170298265	0.04257457	0.1277237	5.36E-05
		11:40	8	92160	930	465	0.398476	29.39222			0.171491771	0.04287294	0.1286188	6.39E-05
		11:45	8	94560	930	465	0.402721	29.5701			0.172900621	0.04322516	0.1296755	7.41E-05
		11:50	8	96960	960	480	0.43244	30.2381						
		11:55	8	99360	960	480	0.440325	30.54716			0.192633343	0.04815834	0.144475	1.29E-04
		12:00	8	101760	960	480	0.447906	30.84097			0.195460778	0.04886519	0.1465956	1.22E-04
		12:05	8	104160	960	480	0.457307	31.20086			0.198557138	0.04963928	0.1489179	1.50E-04
		12:10	8	106560	960	480	0.467921	31.60146			0.202196235	0.05054906	0.1516472	1.67E-04
		12:15	8	108960	980	490	0.499156	32.37881						
		12:20	8	111360	980	490	0.515532	32.95681			0.223647227	0.05591181	0.1677354	2.41E-04
		12:25	8	113760	980	490	0.532514	33.54378			0.229750765	0.05743769	0.1723131	2.45E-04
		12:30	8	116160	980	490	0.551922	34.19994			0.236374785	0.0590937	0.1772811	2.73E-04
		12:35	8	118560	980	490	0.570117	34.80164			0.243185287	0.06079632	0.182389	2.51E-04
		12:40	8	120960	990	495	0.602565	35.65171						
		12:45	8	123360	990	495	0.626219	36.38657			0.265444781	0.0663612	0.1990836	3.06E-04
		12:50	8	125760	990	495	0.648357	37.0582			0.273667117	0.06841678	0.2052503	2.80E-04
		12:55	8	128160	990	495	0.67383	37.8129			0.28216089	0.07054022	0.2116207	3.14E-04
		13:33	8	128160	1000	500	0.714466	38.77752						
		13:35	8	129120	1000	500	0.726596	39.11618			0.306729536	0.07668238	0.2300472	3.53E-04
		13:37	8	130080	1000	500	0.737817	39.4262			0.310864148	0.07771604	0.2331481	3.23E-04
		13:39	8	131040	1000	500	0.748127	39.70839			0.314666149	0.07866654	0.2359996	2.94E-04
		13:41	8	132000	1000	500	0.759651	40.02082			0.318511104	0.07962778	0.2388833	3.25E-04
		13:43	8	132960	1000	500	0.771781	40.3464			0.322665277	0.08066632	0.241999	3.39E-04
		13:45	8	133920	1000	500	0.783305	40.65263			0.326808082	0.08170202	0.2451061	3.19E-04
		13:47	8	134880	1000	500	0.795435	40.97185			0.330939062	0.08273477	0.2482043	3.33E-04
		13:49	8	135840	1020	510	0.83789	41.64626						
		13:51	8	136800	1020	510	0.858815	42.16815			0.359599896	0.08989997	0.2696999	5.44E-04
		13:53	8	137760	1020	510	0.879739	42.68186			0.36695565	0.09173891	0.2752167	5.35E-04
		13:55	8	138720	1020	510	0.90218	43.22407			0.374541938	0.09363548	0.2809065	5.65E-04
		13:57	8	139680	1020	510	0.926744	43.80764			0.382724793	0.0956812	0.2870436	6.08E-04
		13:59	8	140640	1020	510	0.95525	44.47244			0.391914002	0.0979785	0.2939355	6.93E-04
		14:01	8	141600	1020	510	0.988608	45.23427			0.402562037	0.10064051	0.3019215	7.94E-04
		14:03	8	142560	1020	510	1.025605	46.05998			0.414591561	0.10364789	0.3109437	8.60E-04
		14:05	8	143520	1050	525	1.130834	47.63256						
		14:07	8	144480	1050	525	1.205131	49.1238			0.48479781	0.12119945	0.3635984	1.55E-03
		14:09	8	145440	1050	525	1.287009	50.69972			0.511351982	0.127838	0.383514	1.64E-03
		14:11	8	146400	1050	525	1.387083	52.53998			0.541839312	0.13545983	0.4063795	1.92E-03
		14:13	8	147360	1050	525	1.519605	54.849			0.580155766	0.14503894	0.4351168	2.41E-03
		14:15	8	148320	1050	525	1.671838	57.34569			0.626191912	0.15654798	0.4696439	2.60E-03

specimen	date	time	f [Hz]	N [-]	P_{max} [N]	P_{min} [N]	d_{max} [mm]	a_{max} [mm]	E [N/mm²]	b [mm]	G_{max} [N/mm]	G_{min} [N/mm]	dG [N/mm]	da dN
		14:17	8	149280	1050	525	1.854701	60.15701			0.67919381	0.16979845	0.5093954	2.93E-03
		14:19	8	150240	1050	525	2.130055	64.06959			0.749733283	0.18743332	0.5623	4.08E-03
		14:21	8	151200	1050	525	2.652865	70.67791			0.867875823	0.21696896	0.6509069	6.88E-03
		14:23	5	151800	1050	525	3.784608	82.51869			1.0976253	0.27440633	0.823219	1.97E-02
		14:25	5	152100	1050	525	5.695107	98.10114			1.485870638	0.37146766	1.114403	5.19E-02
IM	11-jan	8:59	10	0	600	300	0.739721	50.84083		23.62				
		9:29	10	18000	600	300	0.747886	51.10812			0.173091123	0.04327278	0.1298183	1.48E-05
		9:59	10	36000	600	300	0.753934	51.3049			0.174449319	0.04361233	0.130837	1.09E-05
		10:29	10	54000	600	300	0.762048	51.56731			0.175799573	0.04394989	0.1318497	1.46E-05
		10:59	10	72000	600	300	0.773842	51.94549			0.177692857	0.04442321	0.1332696	2.10E-05
		11:31	12	95040	400	200	0.51539	51.92136						
		12:01	12	116640	400	200	0.515491	51.92619			0.079415157	0.01985379	0.0595614	2.23E-07
		12:31	12	138240	400	200	0.517104	52.00334			0.079523483	0.01988087	0.0596426	3.57E-06
		13:01	12	159840	400	200	0.518918	52.08995			0.079740049	0.01993501	0.059805	4.01E-06
		13:31	12	181440	400	200	0.518011	52.04667			0.079797367	0.01994934	0.059848	-2.00E-06
		14:01	12	203040	400	200	0.517961	52.04426			0.079736887	0.01993422	0.0598027	-1.11E-07
		14:02	12	203760	460	230	0.591948	51.89007						
		14:32	12	225360	460	230	0.591142	51.85645			0.104850206	0.02621255	0.0786377	-1.56E-06
		15:39	12	246960	460	230	0.588218	51.73431						
		16:09	12	268560	460	230	0.597492	52.12045			0.105040272	0.02626007	0.0787802	1.79E-05
		16:39	12	290160	460	230	0.599357	52.19763			0.105849982	0.0264625	0.0793875	3.57E-06
		17:09	12	311760	460	230	0.597542	52.12254			0.105853641	0.02646341	0.0793902	-3.48E-06
		17:39	12	333360	460	230	0.597946	52.13923			0.105751234	0.02643781	0.0793134	7.73E-07
		17:40	12	354960	520	260	0.668002	51.84739						
		18:10	12	376560	520	260	0.670118	51.92545			0.134044999	0.03351125	0.1005337	3.61E-06
		18:40	12	398160	520	260	0.672941	52.02927			0.134450988	0.03361275	0.1008382	4.81E-06
		19:10	12	419760	520	260	0.673747	52.05888			0.134749126	0.03368728	0.1010618	1.37E-06
	12-jan	8:37	12	419760	400	200	0.491249	50.74716						
		9:07	12	441360	400	200	0.498002	51.07934			0.076770697	0.01919267	0.057578	1.54E-05
		9:37	12	462960	400	200	0.507125	51.52343			0.077781562	0.01944539	0.0583362	2.06E-05
		10:07	12	484560	400	200	0.510653	51.69379			0.078585283	0.01964632	0.058939	7.89E-06
		10:37	12	506160	400	200	0.50274	51.31062			0.078306775	0.01957669	0.0587301	-1.77E-05
		11:07	12	527760	400	200	0.504605	51.40127			0.077923063	0.01948077	0.0584423	4.20E-06
		11:37	12	549360	400	200	0.504454	51.39393			0.078031967	0.01950799	0.058524	-3.40E-07
		11:38	12	570960	460	230	0.577735	51.29302						
		12:08	12	592560	460	230	0.575417	51.19473			0.102666117	0.02566653	0.0769996	-4.55E-06
		12:38	12	614160	460	230	0.577735	51.29302			0.102666117	0.02566653	0.0769996	4.55E-06
		13:08	12	635760	460	230	0.581263	51.44211			0.10309353	0.02577338	0.0773201	6.90E-06
		13:38	12	657360	460	230	0.581666	51.45911			0.103380784	0.0258452	0.0775356	7.87E-07
		14:08	12	678960	460	230	0.582876	51.51007			0.103498529	0.02587463	0.0776239	2.36E-06
		14:38	12	700560	460	230	0.583027	51.51643			0.103597866	0.02589947	0.0776984	2.95E-07
		14:42	12	722160	500	250	0.633326	51.50098						
		15:12	12	743760	500	250	0.635494	51.58485			0.122519872	0.03062997	0.0918899	3.88E-06
		15:42	12	765360	500	250	0.637711	51.67047			0.122867495	0.03071687	0.0921506	3.96E-06
		16:12	12	786960	500	250	0.638669	51.70738			0.123119089	0.03077977	0.0923393	1.71E-06
		16:42	12	808560	500	250	0.641491	51.81598			0.123418353	0.03085459	0.0925638	5.03E-06
		17:12	12	830160	500	250	0.643306	51.88562			0.12378528	0.03094632	0.092839	3.22E-06
DZ		17:34	15	0	360	180	0.267473	39.55922		23.61				
		19:34	15	108000	360	180	0.267624	39.57072			0.040811014	0.01020275	0.0306083	1.06E-07
		21:34	15	216000	360	180	0.266162	39.45946			0.040727748	0.01018194	0.0305458	-1.03E-06
		23:34	15	324000	360	180	0.265154	39.3825			0.040570778	0.01014269	0.0304281	-7.13E-07
	13-jan	1:34	15	432000	360	180	0.264247	39.31307			0.040448949	0.01011224	0.0303367	-6.43E-07
		3:34	15	540000	360	180	0.254369	38.54689			0.03976031	0.00994008	0.0298202	-7.09E-06
		5:34	15	648000	360	180	0.230227	36.58954			0.037569076	0.00939227	0.0281768	-1.81E-05
		7:34	15	756000	360	180	0.216367	35.40505			0.035100558	0.00877514	0.0263254	-1.10E-05
		9:34	15	864000	380	190	0.221306	34.81403			0.035651145	0.00891279	0.0267384	-5.47E-06
		11:34	15	972000	380	190	0.216518	34.40742					0	-3.76E-06
		12:22	15	981000	900	450	0.669281	39.57744			0.145819366	0.03645484		
		12:32	8	985800	900	450	0.682624	39.98032			0.257313704	0.06432843	0.1929853	8.39E-05
		12:42	8	990600	900	450	0.689903	40.19792			0.26057855	0.06514464	0.1954339	4.53E-05
		12:52	8	995400	900	450	0.696271	40.38711			0.262733463	0.06568337	0.1970501	3.94E-05
		13:02	8	1000200	900	450	0.702033	40.55732			0.264645655	0.06616141	0.1984842	3.55E-05
		13:03	8	1005000	930	465	0.726899	40.59908						
		13:13	8	1009800	930	465	0.736907	40.88277			0.285653362	0.07141334	0.21424	5.91E-05
		13:23	8	1014600	930	465	0.745095	41.11302			0.2886047	0.07215117	0.2164535	4.80E-05
		13:33	8	1019400	930	465	0.754192	41.36695			0.291401791	0.07285045	0.2185513	5.29E-05
		13:43	8	1024200	930	465	0.765413	41.6774			0.294681711	0.07367043	0.2210113	6.47E-05
		13:44	8	1029000	960	480	0.790583	41.69019						
		13:54	8	1033800	960	480	0.807868	42.1479			0.318954315	0.07973858	0.2392157	9.54E-05
		14:04	8	1038600	960	480	0.827277	42.65431			0.325026682	0.08125667	0.24377	1.06E-04
		14:14	8	1043400	960	480	0.847291	43.16855			0.33152257	0.08288064	0.2486419	1.07E-04
		14:24	8	1048200	960	480	0.867306	43.67498			0.338088757	0.08452219	0.2535666	1.06E-04
		14:26	8	1053000	980	490	0.892476	43.84922						
		14:36	8	1057800	980	490	0.924924	44.63416			0.363483458	0.09087086	0.2726126	1.64E-04
		14:46	8	1062600	980	490	0.961011	45.48644			0.374807088	0.09370177	0.2811053	1.78E-04
		14:56	8	1067400	980	490	1.000738	46.40102			0.387238961	0.09680974	0.2904292	1.91E-04
		15:06	8	1072200	980	490	1.046529	47.42649			0.401145688	0.10028642	0.3008593	2.14E-04
		15:07	8	1074600	1000	500	1.070789	47.48922						
		15:12	8	1077000	1000	500	1.105664	48.2345			0.432079194	0.1080198	0.3240594	3.11E-04

specimen	date	time	f [Hz]	N [-]	P_{max} [N]	P_{min} [N]	d_{max} [mm]	a_{max} [mm]	E [N/mm²]	b [mm]	G_{max} [N/mm]	G_{min} [N/mm]	dG [N/mm]	da dN
		15:17	8	1079400	1000	500	1.14539	49.06514			0.444260755	0.11106519	0.3331956	3.46E-04
		15:22	8	1081800	1000	500	1.186026	49.8957			0.457292337	0.11432308	0.3429693	3.46E-04
		15:27	8	1084200	1000	500	1.225449	50.68403			0.470182754	0.11754569	0.3526371	3.28E-04
		15:32	8	1086600	1000	500	1.277608	51.70218			0.484809543	0.12120239	0.3636072	4.24E-04
		15:37	8	1089000	1000	500	1.334317	52.77902			0.502055771	0.12551394	0.3765418	4.49E-04
		15:42	8	1091400	1000	500	1.406795	54.11296			0.522312159	0.13057804	0.3917341	5.56E-04
		15:47	8	1093800	1000	500	1.502926	55.81523			0.548433361	0.13710834	0.411325	7.09E-04
		15:52	8	1096200	1000	500	1.629686	57.95525			0.5824512	0.1456128	0.4368384	8.92E-04
		15:57	8	1098600	1000	500	1.841357	61.30017			0.633000091	0.15825002	0.4747501	1.39E-03
		15:58	8	1099080	1000	500	1.881387	61.90429			0.670170901	0.16754273	0.5026282	1.26E-03
		16:00	8	1100040	1000	500	2.057577	64.46869			0.701331692	0.17533292	0.5259988	2.67E-03
		16:02	8	1101000	1000	500	2.329293	68.15804			0.764742584	0.19118565	0.5735569	3.84E-03
		16:04	8	1101960	1000	500	2.940956	75.54503			0.884848979	0.22121224	0.6636367	7.69E-03
		16:06	5	1102740	1000	500	5.767888	100.6281			1.302116049	0.32552901	0.976587	3.22E-02
IM		16:20	12	0	360	180	0.412877	49.10596		23.62				
		17:20	12	43200	360	180	0.293832	41.51106			0.051273357	0.01281834	0.038455	-1.76E-04
		18:20	12	86400	360	180	0.298368	41.83392			0.04438166	0.01109541	0.0332862	7.47E-06
		19:20	12	129600	360	180	0.30109	42.02612			0.044833485	0.01120837	0.0336251	4.45E-06
		20:20	12	172800	360	180	0.30114	42.02967			0.045005808	0.01125145	0.0337544	8.21E-08
		21:20	12	216000	360	180	0.301342	42.04386			0.045021459	0.01125536	0.0337661	3.28E-07
		22:20	12	259200	360	180	0.301644	42.06513			0.045052759	0.01126319	0.0337896	4.92E-07
		23:20	12	302400	360	180	0.302098	42.09702			0.045099698	0.01127492	0.0338248	7.38E-07
		0:20	12	345600	360	180	0.302702	42.13948			0.045165394	0.01129135	0.033874	9.83E-07
		1:20	12	388800	360	180	0.30371	42.21013			0.045265458	0.01131636	0.0339491	1.64E-06
		2:20	12	432000	360	180	0.306029	42.37206			0.04547165	0.01136791	0.0341037	3.75E-06
		3:20	12	475200	360	180	0.309355	42.60301			0.045821083	0.01145527	0.0343658	5.35E-06
		4:20	12	518400	360	180	0.320393	43.35799			0.046706634	0.01167666	0.03503	1.75E-05
		5:20	12	561600	360	180	0.321754	43.4499			0.047469912	0.01186748	0.0356024	2.13E-06
		6:20	12	604800	360	180	0.322006	43.46689			0.047568861	0.01189222	0.0356766	3.93E-07
		7:20	12	648000	360	180	0.322711	43.51442			0.047627576	0.01190689	0.0357207	1.10E-06
		8:20	12	691200	360	180	0.323719	43.58221			0.047732604	0.01193315	0.0357995	1.57E-06
		8:50	12	734400	400	200	0.325584	41.45333						
		9:35	12	766800	400	200	0.348062	42.8718			0.055868373	0.01396709	0.0419013	4.38E-05
		10:20	12	799200	400	200	0.34897	42.92779			0.057479904	0.01436998	0.0431099	1.73E-06
		11:05	12	831600	400	200	0.348617	42.90603			0.057517873	0.01437947	0.0431384	-6.72E-07
		11:50	12	864000	400	200	0.348214	42.88114			0.057466104	0.01436653	0.0430996	-7.68E-07
		12:35	12	896400	400	200	0.347861	42.85935			0.057414324	0.01435358	0.0430607	-6.73E-07
		12:48	8	901200	640	320	0.887624	53.76228						
		12:58	8	906000	640	320	0.896418	54.01245			0.216807776	0.05420194	0.1626058	5.21E-05
		13:08	8	910800	640	320	0.899451	54.09835			0.217983771	0.05449594	0.1634878	1.79E-05
		13:18	8	915600	640	320	0.900967	54.14123			0.218435506	0.05460888	0.1638266	8.93E-06
		13:28	8	920400	640	320	0.90218	54.1755			0.218706407	0.0546766	0.1640298	7.14E-06
		13:29	8	925200	720	360	1.007106	53.97804						
		13:39	8	930000	720	360	1.009229	54.03155			0.275436661	0.06885917	0.2065775	1.11E-05
		13:49	8	934800	720	360	1.014081	54.1536			0.276215978	0.06905399	0.207162	2.54E-05
		13:59	8	939600	720	360	1.01681	54.22209			0.277062616	0.06926565	0.207797	1.43E-05
		14:09	8	944400	720	360	1.021965	54.35113			0.277942168	0.06948554	0.2084566	2.69E-05
		14:10	8	946800	800	400	1.132956	54.29349						
		14:15	8	949200	800	400	1.145693	54.57933			0.344790007	0.0861975	0.2585925	1.19E-04
		14:20	8	951600	800	400	1.153578	54.75524			0.347339984	0.086835	0.260505	7.33E-05
		14:25	8	954000	800	400	1.161462	54.93038			0.349286106	0.08732153	0.2619646	7.30E-05
		14:30	8	956400	800	400	1.169044	55.09806			0.351191989	0.087798	0.263394	6.99E-05
		14:35	8	958800	800	400	1.175109	55.23169			0.352871423	0.08821786	0.2646536	5.57E-05
		14:36	8	961200	880	440	1.292771	55.23472						
		14:41	8	963600	880	440	1.331284	55.9975			0.433107758	0.10827694	0.3248308	3.18E-04
		14:46	8	966000	880	440	1.38769	57.08924			0.445838427	0.11145961	0.3343788	4.55E-04
		14:51	8	968400	880	440	1.453799	58.3328			0.462130237	0.11553256	0.3465977	5.18E-04
		14:56	8	970800	880	440	1.527186	59.67108			0.480490345	0.12012259	0.3603678	5.58E-04
		15:01	8	973200	880	440	1.61695	61.25248			0.501709997	0.1254275	0.3762825	6.59E-04
		15:02	8	974160	920	460	1.710352	61.58054						
		15:04	8	975120	920	460	1.777068	62.66243			0.575285831	0.14382146	0.4314644	1.13E-03
		15:06	8	976080	920	460	1.860766	63.9831			0.595238018	0.1488095	0.4464285	1.38E-03
		15:08	8	977040	920	460	1.947193	65.30704			0.617583387	0.15439585	0.4631875	1.38E-03
		15:10	8	978000	920	460	2.060913	66.99228						
		15:11	8	978960	960	480	2.149767	66.9818			0.687370386	0.1718426	0.5155278	-1.09E-05
		15:13	8	979920	960	480	2.402984	70.38691			0.749927356	0.18748184	0.5624455	3.55E-03
		15:15	8	980880	960	480	2.802672	75.31709			0.834394324	0.20859858	0.6257957	5.14E-03
		15:17	8	981840	960	480	5.179576	97.88551			1.158936312	0.28973408	0.8692022	2.35E-02

3.3 MS polymer, R=0.1

specimen	date	time	f [Hz]	N [-]	P_{max} [N]	P_{min} [N]	d_{max} [mm]	a_{max} [mm]	E [N/mm²]	b [mm]	G_{max} [N/mm	G_{min} [N/mm	dG [N/mm]	da dN
TEST1	13-dec	9:23	10	6200	150	15	0.282329334	29.006	70000	21.27				
		9:38	10	15200	200	20	0.38604215	29.448						
		9:53	10	24200	200	20	0.391803974	29.711			0.063345	0.000633	0.062711	2.92E-05
		10:23	10	33200	250	25	0.514925036	30.618			0.081685	0.000817	0.080868	
		10:38	10	42200	250	25	0.515834798	30.650			0.099964	0.001	0.098964	3.61E-06
		10:53	10	51200	250	25	0.518867337	30.758			0.100031	0.001	0.099031	1.20E-05
		11:08	10	60200	250	25	0.520080352	30.801			0.100103	0.001001	0.099102	4.79E-06
		11:23	10	69200	250	25	0.520990113	30.834			0.10014	0.001001	0.099138	3.59E-06
		11:38	10	78200	250	25	0.522203129	30.877			0.100176	0.001002	0.099174	4.78E-06
		11:53	10	87200	300	30	0.637136338	31.186						
		12:08	10	96200	300	30	0.640168876	31.275			0.144776	0.001448	0.143328	9.89E-06
		12:23	10	105200	300	30	0.644717684	31.408			0.144932	0.001449	0.143483	1.48E-05
		12:38	10	114200	300	30	0.647446969	31.488			0.145082	0.001451	0.143631	8.86E-06
		12:53	10	123200	300	30	0.650176253	31.567			0.145195	0.001452	0.143743	8.84E-06
		13:02	10	128600	400	40	0.919768926	32.709						
		13:12	10	134600	400	40	0.940693441	33.153			0.261744	0.002617	0.259126	7.41E-05
		13:22	10	140600	400	40	0.954339864	33.441			0.262714	0.002627	0.260087	4.80E-05
		13:32	10	146600	400	40	0.968289541	33.733			0.263492	0.002635	0.260857	4.87E-05
		13:42	10	152600	400	40	0.978600172	33.948			0.264177	0.002642	0.261536	3.58E-05
		13:52	10	158600	400	40	0.983755488	34.055			0.264616	0.002646	0.261969	1.79E-05
		14:02	10	164600	400	40	0.989820565	34.181			0.264934	0.002649	0.262285	2.10E-05
		14:12	10	170600	400	40	0.995582388	34.301			0.26527	0.002653	0.262618	1.99E-05
		14:22	10	176600	500	50	1.337349476	35.814						
		14:32	10	182600	500	50	1.377682238	36.458			0.422875	0.004229	0.418646	1.07E-04
		14:36	10	185000	600	60	1.772822004	38.019			0.522972	0.00523	0.517743	6.50E-04
		14:41	10	188000	600	60	1.855610305	39.074			0.625308	0.006253	0.619055	3.52E-04
		14:46	10	191000	600	60	1.908073221	39.733			0.631379	0.006314	0.625065	2.20E-04
		14:51	10	194000	600	60	1.975395576	40.569			0.636807	0.006368	0.630439	2.78E-04
		14:56	10	197000	600	60	2.028161746	41.216			0.642284	0.006423	0.635861	2.16E-04
	14-dec	9:39	7	197000	600	60	2.028161746	41.216						
		9:44	7	199100	600	60	2.066978238	41.687			0.646488	0.006465	0.640023	2.25E-04
		9:54	7	203300	600	60	2.180091924	43.041			0.653528	0.006535	0.646993	3.22E-04
		10:04	5	206300	600	60	2.334751387	44.848			0.66607	0.006661	0.65941	6.02E-04
		10:05	5	206600	600	60	2.347184795	44.991			0.67395	0.006739	0.66721	4.77E-04
		10:10	5	208100	600	60	2.411474611	45.727			0.677609	0.006776	0.670833	4.90E-04
		10:15	5	209600	600	60	2.52640782	47.022			0.68621	0.006862	0.679348	8.64E-04
		10:20	5	211100	600	60	2.617383975	48.031			0.696166	0.006962	0.689204	6.73E-04
		10:25	5	212600	600	60	2.694107199	48.871			0.704347	0.007043	0.697304	5.60E-04
		10:30	5	214100	600	60	2.778411769	49.783			0.712265	0.007123	0.705142	6.08E-04
		10:35	5	215600	600	60	2.874846493	50.812			0.721219	0.007212	0.714007	6.86E-04
		10:40	5	217100	600	60	2.976133279	51.879			0.731092	0.007311	0.723781	7.11E-04
		10:45	3	218000	600	60	3.166273443	53.843			0.745812	0.007458	0.738354	2.18E-03
		10:50	3	218900	600	60	3.253913805	54.732			0.759947	0.007599	0.752347	9.88E-04
		10:55	3	219800	600	60	3.352168052	55.718			0.769509	0.007695	0.761814	1.10E-03
		11:00	3	220700	600	60	3.490755062	57.089			0.781791	0.007818	0.773973	1.52E-03
		11:05	3	221600	600	60	3.604778509	58.201			0.794988	0.00795	0.787038	1.24E-03
		11:10	3	222500	600	60	3.72850608	59.391			0.807518	0.008075	0.799443	1.32E-03
		11:15	3	223400	600	60	3.847684843	60.523			0.820418	0.008204	0.812214	1.26E-03
		11:20	3	224300	600	60	3.971715667	61.686			0.833435	0.008334	0.825101	1.29E-03
		11:25	3	225200	600	60	4.087255384	62.757			0.846349	0.008463	0.837886	1.19E-03
		11:30	3	226100	600	60	4.198549546	63.776			0.858663	0.008587	0.850076	1.13E-03
		11:35	2	226700	650	65	4.946070285	67.065						
		11:40	2	227300	650	65	5.303909828	69.936			1.084199	0.010842	1.073357	4.78E-03
		11:45	2	227900	650	65	5.53256323	71.730			1.120102	0.011201	1.108901	2.99E-03
								#DEEL/0!						
TEST 2	14-dec	12:44	3	0	700	70	1.511417186	31.496		24.03				
		12:49	3	1700	700	70	1.609974687	32.713			0.795048	0.00795	0.787098	7.16E-04
		12:52	3	2700	700	70	1.670018949	33.440			0.80278	0.008028	0.794753	7.27E-04
		12:58	4	3800	700	70	1.732185988	34.181			0.808809	0.008088	0.800721	6.74E-04
		13:08	4	6200	700	70	1.864101413	35.720			0.818511	0.008185	0.810325	6.41E-04
		13:18	4	8600	700	70	1.949012491	36.688			0.829455	0.008295	0.82116	4.03E-04
		13:28	4	11000	700	70	2.012695799	37.402			0.837049	0.00837	0.828678	2.98E-04
		13:38	4	13400	700	70	2.063339192	37.964			0.842939	0.008429	0.83451	2.34E-04
		13:48	4	15800	700	70	2.107614254	38.451			0.847861	0.008479	0.839383	2.03E-04
		13:58	4	18200	700	70	2.143094954	38.838			0.852017	0.00852	0.843497	1.61E-04
		14:08	4	20600	700	70	2.184640732	39.288			0.856051	0.008561	0.84749	1.88E-04
		14:18	4	23000	700	70	2.227399525	39.748			0.860484	0.008605	0.851879	1.91E-04
		14:28	4	25400	700	70	2.266822525	40.168			0.864825	0.008648	0.856177	1.75E-04
		14:38	4	27800	700	70	2.316252903	40.691			0.869541	0.008695	0.860845	2.18E-04
		14:48	4	30200	700	70	2.357192172	41.121			0.874358	0.008744	0.865614	1.79E-04
		14:58	4	32600	700	70	2.409655088	41.668			0.879362	0.008794	0.870568	2.28E-04
		15:08	4	35000	700	70	2.464847289	42.238			0.885157	0.008852	0.876306	2.38E-04
		15:18	4	37400	700	70	2.523981789	42.843			0.891346	0.008913	0.882432	2.52E-04
		15:28	4	39800	700	70	2.571592644	43.326			0.897152	0.008972	0.888181	2.01E-04
		15:38	4	42200	700	70	2.665904591	44.273			0.904928	0.009049	0.895878	3.94E-04
		15:48	4	44400	800	80	3.831915642	50.803						
		15:58	3	46200	800	80	4.325916163	54.637			1.3239	0.013239	1.310661	2.13E-03
		16:08	3	48000	800	80	5.039169217	59.876			1.407059	0.014071	1.392988	2.91E-03

specimen	date	time	f [Hz]	N [-]	P_{max} [N]	P_{min} [N]	d_{max} [mm]	a_{max} [mm]	E [N/mm^2]	b [mm]	G_{max} [N/mm	G_{min} [N/mm	dG [N/mm]	da dN
		16:11	3	48600	800	80	5.339390528	61.991			1.478327	0.014783	1.463544	3.53E-03
		16:21	2	50400	800	80	7.193484564	74.131			1.638474	0.016385	1.622089	6.74E-03
		16:24	2	50760	800	80	8.096271274	79.581			1.847977	0.01848	1.829497	1.51E-02
		16:26	2	51000	800	80	8.91050786	84.290			1.984345	0.019843	1.964502	1.96E-02
		16:28	2	51240	800	80	10.1226135	90.994			2.15008	0.021501	2.128579	2.79E-02
								#DEEL/0!						
MS11	15-dec	16:58	5	0				#DEEL/0!		24.14				
		17:01	5	5200	650	65	1.780706604	36.333						
		17:03	5	9700	650	65	1.979337876	38.713			0.725685	0.007257	0.718428	5.29E-04
		17:18	5	14200	650	65	2.081231169	39.896			0.740185	0.007402	0.732783	2.63E-04
		17:33	5	18700	650	65	2.136726624	40.531			0.747896	0.007479	0.740417	1.41E-04
		17:39	5	20500	650	65	2.18918954	41.126			0.753232	0.007532	0.7457	3.30E-04
		17:54	5	25000	650	65	2.353249872	42.948			0.764062	0.007641	0.756422	4.05E-04
		18:09	5	29500	650	65	2.577051213	45.354			0.783739	0.007837	0.775901	5.35E-04
		18:24	5	34000	650	65	2.761429554	47.274			0.804797	0.008048	0.796749	4.27E-04
		18:39	4	37600	600	60	2.695016961	48.881			0.761302	0.007613	0.753689	4.46E-04
		18:54	4	41200	600	60	2.84148857	50.458			0.715442	0.007154	0.708287	4.38E-04
		19:09	4	44800	500	50	2.364470265	50.414			0.612135	0.006121	0.606014	
		19:41	4	40000	500	50	2.422998258	51.159			0.504016	0.00504	0.498976	-1.55E-04
		19:56	4	43600	500	50	2.41056485	51.001			0.505932	0.005059	0.500873	-4.38E-05
		20:11	4	47200	500	50	2.474248158	51.805			0.508076	0.005081	0.502995	2.23E-04
		20:26	4	50800	500	50	2.458175704	51.603			0.510064	0.005101	0.504963	-5.62E-05
		20:41	4	54400	500	50	2.536718451	52.586			0.512691	0.005127	0.507564	2.73E-04
		20:56	4	58000	500	50	2.565224313	52.940			0.517195	0.005172	0.512023	9.83E-05
		21:11	4	61600	500	50	2.540357497	52.631			0.517348	0.005173	0.512175	-8.57E-05
		21:26	4	65200	500	50	2.518826474	52.363			0.51539	0.005154	0.510236	-7.45E-05
		21:41	4	68800	500	50	2.616777467	53.576			0.518626	0.005186	0.51344	3.37E-04
		21:56	4	72400	500	50	2.798729777	55.781			0.530562	0.005306	0.525257	6.13E-04
		22:11	4	76000	500	50	2.86120007	56.525			0.54106	0.005411	0.53565	2.07E-04
		22:26	4	79600	500	50	2.989779702	58.035			0.549374	0.005494	0.543881	4.20E-04
	15-dec	14:14	4	81000	500	50	2.957634794	57.660						
		14:29	4	84600	500	50	3.081059111	59.092			0.557594	0.005576	0.552018	3.98E-04
		14:44	3	87300	400	40	3.136857819	68.289						
		14:59	3	90000	400	40	3.318203621	70.631			0.416112	0.004161	0.41195	8.67E-04
		15:14	3	92700	400	40	3.349742022	71.033			0.424143	0.004241	0.419902	1.49E-04
		15:29	3	95400	400	40	3.476198877	72.630			0.43017	0.004302	0.425869	5.91E-04
		15:44	3	98100	400	40	3.652995871	74.825			0.441822	0.004418	0.437404	8.13E-04
		15:59	3	100800	400	40	3.684231018	75.208			0.449858	0.004499	0.445359	1.42E-04
		16:14	3	103500	400	40	3.941693536	78.318			0.461167	0.004612	0.456555	1.15E-03
		16:29	3	106200	400	40	4.157610277	80.865			0.479851	0.004799	0.475053	9.43E-04
		16:44	3	108900	400	40	4.410220733	83.778			0.498624	0.004986	0.493638	1.08E-03
MS8	16-dec	10:12	10	0	280	28		0.000		24.18				
		10:13	10	600	280	28	0.872158071	39.242						
		10:43	10	18600	280	28	0.895508618	39.869			0.137738	0.001377	0.136361	3.48E-05
		11:13	10	36600	280	28	0.91067131	40.273			0.138552	0.001386	0.137166	2.24E-05
		11:43	10	54600	280	28	0.924317733	40.634			0.139164	0.001392	0.137772	2.01E-05
		12:13	10	72600	280	28	0.928260033	40.738			0.139538	0.001395	0.138143	5.77E-06
		12:43	10	90600	280	28	0.932505587	40.849			0.139713	0.001397	0.138316	6.21E-06
		13:13	10	108600	280	28	0.941603203	41.088			0.139998	0.0014	0.138598	1.33E-05
		13:43	10	126600	280	28	0.94766828	41.247			0.140323	0.001403	0.138919	8.81E-06
		14:13	10	144600	280	28	0.95555288	41.452			0.140622	0.001406	0.139216	1.14E-05
		14:43	10	162600	280	28	0.95949518	41.555			0.140876	0.001409	0.139467	5.70E-06
		15:13	10	180600	200	20	0.720227893	42.811						
		15:43	10	198600	200	20	0.720227893	42.811			0.072997	0.00073	0.072267	3.49E-05
		16:13	10	216600	200	20	0.721137654	42.843						
		16:43	10	234600	200	20	0.721744162	42.865			0.073034	0.00073	0.072304	1.50E-06
		17:13	10	252600	200	20	0.721744162	42.865						
		17:43	10	270600	200	20	0.728415747	43.102			0.073148	0.000731	0.072416	6.59E-06
		18:13	10	288600	200	20	0.725383208	42.995			0.073204	0.000732	0.072472	
		18:43	10	306600	200	20	0.729932016	43.156			0.073228	0.000732	0.072496	1.49E-06
		19:13	10	324600	200	20	0.729932016	43.156						
		19:43	10	342600	200	20	0.732054793	43.231			0.073332	0.000733	0.072599	2.09E-06
		20:13	10	360600	200	20	0.729628762	43.145			0.073327	0.000733	0.072594	-4.78E-06
		20:16	7	361860	350	35	1.232726898	42.244			0.14767	0.001477	0.146193	
		20:26	7	366060	350	35	1.253044906	42.661			0.222601	0.002226	0.220375	9.91E-05
		20:36	7	370260	350	35	1.260322999	42.809			0.22335	0.002234	0.221117	3.54E-05
		20:46	7	374460	350	35	1.266994583	42.945			0.22373	0.002237	0.221492	3.23E-05
		20:56	7	378660	350	35	1.275182437	43.111			0.224134	0.002241	0.221893	3.96E-05
		21:06	7	382860	350	35	1.274575929	43.099			0.224341	0.002243	0.222098	-2.93E-06
		21:16	7	387060	350	35	1.280034499	43.210			0.224474	0.002245	0.222229	2.63E-05
		21:26	7	391260	350	35	1.290041876	43.412			0.224896	0.002249	0.222647	4.82E-05
		21:36	7	395460	350	35	1.29428743	43.498			0.225286	0.002253	0.223033	2.04E-05
		21:42	7	397980	350	35	1.304598061	43.705			0.225684	0.002257	0.223428	8.24E-05
	17-dec	9:32	7	400500	360	36	1.297623222	42.835						
		9:42	7	404700	360	36	1.311572899	43.111			0.236968	0.00237	0.234598	6.56E-05
		9:52	7	408900	360	36	1.328555115	43.445			0.237836	0.002378	0.235458	7.95E-05
		10:02	7	413100	360	36	1.338259238	43.635			0.238587	0.002386	0.236201	4.53E-05
		10:12	7	417300	360	36	1.351602407	43.895			0.239237	0.002392	0.236844	6.20E-05
		10:22	7	421500	360	36	1.3628228	44.114			0.239931	0.002399	0.237532	5.20E-05

specimen	date	time	f [Hz]	N [-]	P_{max} [N]	P_{min} [N]	d_{max} [mm]	a_{max} [mm]	E [N/mm²]	b [mm]	G_{max} [N/mm	G_{min} [N/mm	dG [N/mm]	da dN
		10:32	7	425700	360	36	1.368584623	44.225			0.240411	0.002404	0.238007	2.66E-05
		10:42	7	429900	360	36	1.375559461	44.361			0.240773	0.002408	0.238365	3.22E-05
		10:52	7	434100	360	36	1.381018031	44.466			0.241125	0.002411	0.238714	2.51E-05
		11:02	7	438300	380	38	1.471994186	44.726						
		11:12	7	442500	380	38	1.484730847	44.958			0.270073	0.002701	0.267372	5.52E-05
		11:22	7	446700	380	38	1.484730847	44.958			0.270456	0.002705	0.267752	0.00E+00
		11:32	7	450900	380	38	1.507171632	45.365			0.271133	0.002711	0.268422	9.68E-05
		11:42	7	455100	380	38	1.515056232	45.507			0.272049	0.00272	0.269328	3.39E-05
		11:52	7	459300	380	38	1.526883132	45.720			0.272645	0.002726	0.269919	5.07E-05
		12:02	7	463500	400	40	1.618769049	45.916						
		12:12	7	467700	400	40	1.632718726	46.153			0.30368	0.003037	0.300643	5.64E-05
		12:22	7	471900	400	40	1.647881418	46.410			0.304612	0.003046	0.301566	6.11E-05
		12:32	7	476100	400	40	1.666076649	46.717			0.305684	0.003057	0.302627	7.30E-05
		12:42	7	480300	400	40	1.673961249	46.849			0.306522	0.003065	0.303457	3.16E-05
		12:52	6	483900	420	42	1.793443266	47.419						
		13:02	6	487500	420	42	1.810425482	47.688			0.341226	0.003412	0.337814	7.47E-05
		13:12	6	491100	420	42	1.824678412	47.913			0.342291	0.003423	0.338868	6.25E-05
		13:22	6	494700	420	42	1.840447613	48.161			0.343316	0.003433	0.339883	6.89E-05
		13:32	6	498300	420	42	1.845906182	48.247			0.344041	0.00344	0.340601	2.38E-05
		13:42	6	501900	420	42	1.86228189	48.503			0.344789	0.003448	0.341341	7.12E-05
		13:52	6	505500	460	46	2.077895377	49.047						
		14:02	6	509100	460	46	2.114589093	49.565			0.418533	0.004185	0.414347	1.44E-04
		14:12	6	512700	460	46	2.352036857	52.833			0.429037	0.00429	0.424746	9.08E-04
		14:22	6	516300	460	46	2.161593439	50.223			0.430823	0.004308	0.426514	-7.25E-04
		14:32	6	519900	480	48	2.309278064	50.937						
		14:42	6	523500	480	48	2.352036857	51.501			0.467114	0.004671	0.462442	1.57E-04
		14:52	6	527100	480	48	2.393885888	52.048			0.470511	0.004705	0.465806	1.52E-04
		14:55	6	528180	500	50	2.504270289	52.182						
		15:00	6	529980	500	50	2.54369329	52.673			0.514919	0.005149	0.509769	2.73E-04
		15:05	6	531780	500	50	2.574928436	53.060			0.517899	0.005179	0.51272	2.15E-04
		15:10	6	533580	500	50	2.607073344	53.456			0.520582	0.005206	0.515376	2.20E-04
		15:15	6	535380	500	50	2.627088098	53.702			0.522795	0.005228	0.517567	1.37E-04
		15:20	6	537180	500	50	2.660446022	54.110			0.525066	0.005251	0.519815	2.27E-04
		15:31	12	539000	180	18	1.101721235	58.853						
		17:31	12	625400	180	18	1.108089566	59.057			0.072832	0.000728	0.072103	2.36E-06

3.4 MS polymer, R=0.5

specimen	date	time	f [Hz]	N [-]	P_{max} [N]	P_{min} [N]	d_{max} [mm]	a_{max} [mm]	E [N/mm^2]	b [mm]	G_{max} [N/mm]	G_{min} [N/mm]	dG [N/mm]	da dN
MS10	20-dec	8:43	8	0	640	320	2.270461571	45.719	70000	24.09				
		8:53	8	4800	640	320	2.373264626	46.950			0.608352795	0.152088199	0.456264596	2.56E-04
		9:03	8	9600	640	320	2.414810404	47.441			0.614909304	0.153727326	0.461181978	1.02E-04
		9:13	8	14400	640	320	2.448774835	47.840			0.618362756	0.154590689	0.463772067	8.32E-05
		9:23	8	19200	640	320	2.465150543	48.032			0.620671629	0.155167907	0.465503722	3.99E-05
		9:33	8	24000	640	320	2.475461174	48.152			0.621898252	0.155474563	0.466423689	2.51E-05
		9:43	8	28800	680	340	2.675911968	48.653						
		9:53	8	33600	680	340	2.709269891	49.016			0.708722696	0.177180674	0.531542022	7.56E-05
		10:03	8	38400	680	340	2.735652976	49.302			0.711663838	0.17791596	0.533747879	5.95E-05
		10:13	8	43200	680	340	2.764765346	49.616			0.714403452	0.178600863	0.535802589	6.54E-05
		10:23	8	48000	680	340	2.785689862	49.841			0.71687867	0.179219668	0.537659003	4.69E-05
		10:33	7	52200	720	360	3.03375151	50.690						
		10:43	7	56400	720	360	3.079239588	51.144			0.816136875	0.204034219	0.612102656	1.08E-04
		10:53	7	60600	720	360	3.111384496	51.464			0.820251749	0.205062937	0.615188812	7.61E-05
		11:03	7	64800	720	360	3.145955435	51.806			0.823798903	0.205949726	0.617849177	8.15E-05
		11:13	7	69000	720	360	3.181739389	52.159			0.827549227	0.206887307	0.620661921	8.40E-05
		11:23	7	73200	720	360	3.210548505	52.442			0.831000651	0.207750163	0.623250488	6.73E-05
		11:33	6	76800	760	380	3.516228385	53.615						
		11:43	6	80400	760	380	3.580821455	54.204			0.945768883	0.236442221	0.709326662	1.64E-04
		11:53	6	84000	760	380	3.644504763	54.781			0.953116965	0.238279241	0.714837723	1.60E-04
		12:03	6	87600	760	380	3.686353795	55.157			0.959183518	0.23979588	0.719387639	1.05E-04
		12:13	6	91200	760	380	3.737906949	55.619			0.964572951	0.241143238	0.723429713	1.28E-04
		12:23	6	94800	760	380	3.790369865	56.086			0.970593004	0.242648251	0.727944753	1.30E-04
		12:33	6	98400	800	400	4.116671007	57.149						
		12:43	6	102000	800	400	4.224932631	58.046			1.101067071	0.275266768	0.825800303	2.49E-04
		12:53	6	105600	800	400	4.291951732	58.596			1.111915284	0.277978821	0.833936463	1.53E-04
		13:03	6	109200	800	400	4.36503591	59.193			1.120630613	0.280157653	0.84047296	1.66E-04
		13:13	6	112800	800	400	4.436603818	59.773			1.129663303	0.282415826	0.847247477	1.61E-04
		13:23	6	116400	800	400	4.508171727	60.350			1.138636407	0.284659102	0.853977305	1.60E-04
		13:36	4	119520	900	450	5.928612758	66.276						
		13:46	4	121920	900	450	6.215490899	68.182			1.591654417	0.397913604	1.193740812	7.94E-04
		13:56	4	124320	900	450	6.493574679	69.997			1.633628568	0.408407142	1.225221426	7.56E-04
		14:06	4	126720	900	450	6.723441097	71.473			1.671736079	0.41793402	1.253802059	6.15E-04
		14:08	2	126960	1000	500	8.430457016	76.850						
		14:13	2	127560	1000	500	10.75034897	88.917			2.456251921	0.61406298	1.842188941	2.01E-02
MS4	20-dec	14:58	12	0	400	200	0.718105116	30.381		24.17				
		15:28	12	21600	400	200	0.742668677	31.001			0.199612912	0.049903228	0.149709684	2.87E-05
		15:58	12	43200	400	200	0.751159785	31.213			0.200409023	0.050102256	0.150306767	9.82E-06
		16:28	12	64800	400	200	0.760257401	31.439			0.20083494	0.050208735	0.150626205	1.05E-05
		16:58	12	86400	400	200	0.769961524	31.679			0.201291539	0.050322885	0.150968654	1.11E-05
		17:28	12	108000	400	200	0.78148517	31.963			0.201808711	0.050452178	0.151356533	1.31E-05
		17:58	12	129600	400	200	0.785124216	32.052			0.20217888	0.05054472	0.15163416	4.13E-06
		18:10	12	138240	400	200	0.786640486	32.089			0.202304989	0.050576247	0.151728741	4.30E-06
	21-dec	8:29	12	141000	440	220	0.881558941	32.450						
		8:59	12	162600	440	220	0.844258717	31.619			0.244707541	0.061176885	0.183530656	-3.85E-05
		9:29	12	184200	440	220	0.833341578	31.373			0.24341194	0.060852985	0.182558955	-1.14E-05
		9:59	12	205800	440	220	0.854872602	31.857			0.243696515	0.060924129	0.182772386	2.24E-05
		10:29	12	227400	440	220	0.868519025	32.161			0.244640025	0.061160006	0.183480019	1.41E-05
		10:59	12	249000	440	220	0.884288225	32.510			0.245433086	0.061358272	0.184074815	1.62E-05
		11:29	12	270600	440	220	0.859724663	31.965			0.245196339	0.061299085	0.183897254	-2.52E-05
		11:59	12	292200	440	220	0.877313387	32.356			0.245007717	0.061251929	0.183755787	1.81E-05
		12:29	12	313800	500	250	1.083526004	34.014						
		12:59	12	335400	500	250	1.096262666	34.253			0.322765701	0.080691425	0.242074276	1.11E-05
		13:29	12	357000	500	250	1.12810432	34.847			0.324168565	0.081042141	0.243126424	2.75E-05
		13:59	12	378600	500	250	1.149938597	35.250			0.325863976	0.081465994	0.244397982	1.87E-05
		14:29	12	400200	560	280	1.387689615	36.863						
		14:59	12	421800	560	280	1.44318507	37.741			0.418813503	0.104703376	0.314110127	4.06E-05
		15:29	12	443400	560	280	1.483214578	38.366			0.422300857	0.105575214	0.316725643	2.89E-05
		15:59	12	465000	560	280	1.515359486	38.862			0.424954745	0.106238686	0.318716058	2.30E-05
		16:43	12	475080	560	280	1.717023296	41.888			0.433713208	0.108428302	0.325284906	3.00E-04
		16:58	12	485880	600	300	1.754626773	40.715						
		17:13	12	496680	600	300	1.800114851	41.345			0.501515435	0.125378859	0.376136576	5.83E-05
		17:28	12	507480	600	300	1.837718328	41.861			0.504888106	0.126222027	0.37866608	4.78E-05
		17:43	12	518280	600	300	1.883206405	42.480			0.508280949	0.127070237	0.381210712	5.73E-05
		17:58	12	529080	600	300	1.923842421	43.027			0.511815283	0.127953821	0.383861462	5.07E-05
		18:13	12	539880	600	300	1.966601214	43.598			0.515256591	0.128814148	0.386442443	5.29E-05
		18:15	4	540360	1000	500	4.927268547	55.680						
		18:18	4	541080	1000	500	6.106319514	63.329			1.768736549	0.442184137	1.326552412	1.06E-02
		18:21	4	541800	1000	500	7.955864742	74.224			2.0142728	0.5035682	1.5107046	1.51E-02
		18:24	4	542520	1000	500	9.640439876	83.289			2.314882477	0.578720619	1.736161858	1.26E-02
								#DEEL/0!						
MS5	22-dec	9:02	25	0	200	100	0.339947565	29.401		24.17				
		10:02	25	90000	200	100	0.356020019	30.227			0.049491888	0.012372972	0.037118916	9.18E-06
		11:02	25	180000	200	100	0.368756681	30.872			0.049835846	0.012458962	0.037376885	7.16E-06
		12:02	25	270000	200	100	0.372395727	31.054			0.050032649	0.012508162	0.037524487	2.03E-06
		13:02	25	360000	200	100	0.379067312	31.387			0.050157342	0.012539336	0.037618007	3.70E-06
		14:02	25	450000	200	100	0.383919373	31.627			0.050297081	0.01257427	0.037722811	2.67E-06
		15:02	25	540000	200	100	0.386648658	31.762			0.050389286	0.012597321	0.037791964	1.50E-06

specimen	date	time	f [Hz]	N [-]	P_{max} [N]	P_{min} [N]	d_{max} [mm]	a_{max} [mm]	E [N/mm^2]	b [mm]	G_{max} [N/mm]	G_{min} [N/mm]	dG [N/mm]	da dN
		16:22	30	648000	150	75	0.285665126	31.477						
		17:22	30	756000	150	75	0.291426949	31.856			0.028336411	0.007084103	0.021252308	3.51E-06
		18:22	30	864000	150	75	0.296279011	32.173			0.028433531	0.007108383	0.021325148	2.94E-06
		19:22	30	972000	150	75	0.296582265	32.193			0.028480821	0.007120205	0.021360616	1.83E-07
		20:22	30	1080000	150	75	0.296279011	32.173			0.028480821	0.007120205	0.021360616	-1.83E-07
		21:22	30	1188000	150	75	0.299311549	32.371			0.028505937	0.007126484	0.021379453	1.83E-06
		22:22	30	1296000	150	75	0.296885519	32.213			0.028511512	0.007127878	0.021383634	-1.46E-06
		23:22	30	1404000	150	75	0.296885519	32.213			0.028489184	0.007122296	0.021366888	0.00E+00
	23-dec	0:22	30	1512000	150	75	0.295369249	32.114			0.028475252	0.007118813	0.021356439	-9.15E-07
		1:22	30	1620000	150	75	0.295975757	32.154			0.02846689	0.007116722	0.021350167	3.66E-07
		2:22	30	1728000	150	75	0.295065996	32.094			0.028464105	0.007116026	0.021348079	-5.49E-07
		3:22	30	1836000	150	75	0.295975757	32.154			0.028464105	0.007116026	0.021348079	5.49E-07
		4:22	30	1944000	150	75	0.299614803	32.390			0.028505944	0.007126486	0.021379458	2.19E-06
		5:22	30	2052000	150	75	0.301434326	32.508			0.028556206	0.007139051	0.021417154	1.09E-06
		6:22	30	2160000	150	75	0.304466865	32.704			0.028601001	0.00715025	0.021450751	1.81E-06
		7:22	30	2268000	150	75	0.307802657	32.919			0.028659914	0.007164978	0.021494935	1.99E-06
		8:22	30	2376000	150	75	0.312048211	33.190			0.028730247	0.007182562	0.021547685	2.52E-06
		9:22	30	2484000	120	60	0.25442998	33.571			0.023626887	0.005906722	0.017720165	3.53E-06
		10:22	30	2592000	120	60	0.258069026	33.858			0.018511345	0.004627836	0.013883509	2.66E-06
		11:22	30	2700000	120	60	0.259888549	34.001			0.018552264	0.004638066	0.013914198	1.32E-06
		12:22	30	2808000	120	60	0.296582265	36.805			0.018846169	0.004711542	0.014134627	2.60E-05
		13:22	30	2916000	120	60	0.301434326	37.165			0.019164115	0.004791029	0.014373086	3.33E-06
		14:22	30	3024000	120	60	0.303860357	37.345			0.019220725	0.004805181	0.014415544	1.66E-06
		14:42	10	3036000	250	125	0.596197068	36.025						
		15:22	10	3060000	250	125	0.599836114	36.157			0.082374571	0.020593643	0.061780928	5.49E-06
		16:02	10	3084000	250	125	0.604688176	36.332			0.082510831	0.020627708	0.061883123	7.30E-06
	24-dec	9:14	10	3102000	250	125	0.507950198	32.724						
		9:44	10	3120000	250	125	0.520990113	33.225			0.079742323	0.019935581	0.059806742	2.79E-05
		10:14	10	3138000	250	125	0.529784475	33.560			0.080080716	0.020020179	0.060060537	1.86E-05
		10:44	10	3156000	250	125	0.529784475	33.560			0.080217421	0.020054355	0.060163066	0.00E+00
		11:14	10	3174000	250	125	0.536759314	33.825			0.080326228	0.020081557	0.060244671	1.47E-05
		11:30	10	3183600	280	140	0.601958891	33.851						
		11:45	10	3192600	280	140	0.603778414	33.913			0.100957168	0.025239292	0.075717876	6.82E-06
		12:00	10	3201600	280	140	0.607720714	34.045			0.101058141	0.025264535	0.075793606	1.47E-05
		12:15	10	3210600	280	140	0.609236984	34.096			0.101153863	0.025288466	0.075865397	5.66E-06
		12:30	10	3219600	280	140	0.612572776	34.208			0.10123907	0.025309768	0.075929303	1.24E-05
		12:40	10	3225600	300	150	0.655938076	34.196						
		12:50	10	3231600	300	150	0.658364107	34.272			0.116316606	0.029079152	0.087237455	1.26E-05
		13:00	10	3237600	300	150	0.659273869	34.300			0.116379459	0.029094865	0.087284594	4.73E-06
		13:10	10	3243600	300	150	0.660486884	34.338			0.116419483	0.029104871	0.087314612	6.31E-06
		13:20	10	3249600	300	150	0.6616999	34.376			0.116465242	0.02911631	0.087348931	6.30E-06
		13:30	10	3255600	300	150	0.664429184	34.461			0.116539653	0.029134913	0.08740474	1.42E-05
		13:40	10	3261600	300	150	0.667764977	34.565			0.116654225	0.029163556	0.087490668	1.73E-05
		13:50	10	3267600	340	170	0.756011847	34.543						
		14:00	10	3273600	340	170	0.758134624	34.601			0.149928556	0.037482139	0.112446417	9.69E-06
		14:10	10	3279600	340	170	0.761470416	34.693			0.150045618	0.037511404	0.112534213	1.52E-05
		14:20	10	3285600	340	170	0.765412716	34.800			0.150201849	0.037550462	0.112651386	1.79E-05
		14:30	10	3291600	340	170	0.766322478	34.825			0.150306072	0.037576518	0.112729554	4.14E-06
		14:40	10	3297600	380	190	0.86184744	34.956						
		14:50	10	3303600	380	190	0.866092994	35.059			0.188137401	0.04703435	0.14110305	1.72E-05
		15:00	10	3309600	380	190	0.872461325	35.214			0.188393157	0.047098289	0.141294868	2.57E-05
		15:10	10	3315600	380	190	0.875797117	35.294			0.188627235	0.047156809	0.141470426	1.35E-05
		15:20	10	3321600	380	190	0.87913291	35.375			0.188788377	0.047197094	0.141591283	1.34E-05
		15:30	10	3327600	460	230	1.098991951	36.064						
		15:40	10	3333600	460	230	1.119916466	36.474			0.279425595	0.069856399	0.209569196	6.84E-05
		15:50	10	3339600	460	230	1.143267013	36.929			0.28073748	0.07018437	0.21055311	7.57E-05
		16:00	10	3345600	460	230	1.160855736	37.269			0.281955462	0.070488866	0.211466597	5.66E-05